Identification of novel disease-causing genes in inherited retinal dystrophy

Solomon Sarpong Merepa



St Cross College

Nuffield Laboratory of Ophthalmology
Nuffield Department of Clinical Neurosciences
University of Oxford

A thesis submitted to the University of Oxford for the degree of Doctor of Philosophy (DPhil)

November 2021







Dedication

To my parents: Sampson and Gifty Tuffour

Despite having no formal education yourselves, you have sacrificed everything for me to pursue education to the highest level.

I love you!

Abstract

Over 270 genes underlying monogenic forms of inherited retinal dystrophies (IRDs) have been identified to date, enabling the development of new treatment regimens such as gene therapy. However, there are still IRD cases with underlying genetic causes yet to be identified, prompting the need for continued disease-gene identification studies. In this thesis, individuals from four families with dominant IRDs without a known genetic cause underwent whole-exome sequencing (WES). Rare pathogenic variants identified in each family were prioritised for segregation analysis using Sanger sequencing. Variants segregating with the condition in each family were considered as candidate genes and were further characterised for expression, localisation and potential function in the mammalian retina using techniques such as polymerase chain reaction (PCR), western immunoblotting (WB), immunohistochemistry (IHC), site-directed mutagenesis and gene transfection.

Together, four genes, *PARPBP*, *MYO5B*, *PIEZO1* and *MTSS1*, with rare variants were identified in three families with dominant RP (adRP). The expression and function of these candidate genes in the mammalian retina have not been previously described. We provide experimental evidence of the expression of *PARPBP*, *PIEZO1*, *MYO5B* and *MTSS1* in the human retina. We determined the sites of Parpbp and Mtss1 expression in the mouse retina using antibodies specific for human PARPBP and MTSS1. Parpbp localised to cells in the inner nuclear layer and ganglion cell layer of the mouse retina. Mtss1 localisation was identified in the inner and outer segment of rod photoreceptors, the synaptic layers and ganglion cells of the mouse retina. We also showed that MTSS1 colocalises with F-actin in the photoreceptor inner and outer segments and in the synaptic layers of the retina. By transfecting several *in vitro* models with wild-type and mutant constructs of *MTSS1*, we show that the *MTSS1* variant identified in one of the families, alters the expression and function of MTSS1 at the cellular level including altered subcellular localisation and ability to induce extensive cellular processes. Retinal tissue from a previously generated *Mtss1* knockout mouse model was examined for potential abnormalities in the eye that may be attributable to the lack of *Mtss1* expression. However, findings

were inconclusive due to extensive folding of the retinas examined and the identification of residual Mtss1 expression in the retina of these knockout mice.

Overall, the findings in this thesis demonstrate that combining modern gene sequencing technologies, such as next generation sequencing, with other molecular biology techniques enables the identification of candidate genes for IRDs. For the first time, this thesis describes the expression of MTSS1 in the retina and provides compelling evidence linking MTSS1 to IRD. This thesis also provides a list of other candidate genes for IRDs worth investigating further.

Declaration

I declare that this thesis submitted for Doctor of Philosophy (DPhil) degree in Clinical Neuroscience at the University of Oxford is the results of my own original research work unless otherwise stated. Figures and tables that have been adapted from studies previously published by others have been acknowledged and appropriately referenced. Bioinformatic analysis of whole exome sequencing data from participants included in this thesis was carried out by Dr Jing Yu as part of the UKIRDC study. DNA sequencing (WES and Sanger) was carried out by third party companies and have been mentioned in the relevant sections. Eye tissue from *Mtss1* knockout mice used in this thesis were obtained from the laboratory of Dr Pieta Mattila, Finland, who generated this transgenic mouse line previously. In all cases, sources of reagents used in this thesis, whether purchased from commercial sources or being kind gifts from other collaborators, have been declared. At the time of writing up this thesis, none of the results from this work have been published elsewhere. Some sections of the general introduction (Chapter 1) include information from a review paper I published in 2018 in collaboration with my supervisors titled “Genetics of the inherited retinal dystrophies”. I declare that no aspects of this thesis have been previously presented to the University of Oxford or any other university for an academic degree.

Acknowledgements

I would like to express profound gratitude to my supervisors, Dr Stephanie Halford, Dr Sumathi Sekaran and Dr Suzanne Broadgate, through whose tremendous support and mentorship this thesis has been possible. Steph, thank you for showing interest in me in the first place when I wrote to you to discuss DPhil opportunities. I would never have had the unrivalled privilege of pursuing a DPhil in Oxford had it not been the interest you took in me. Sum, thank you also for being part of my entry into Oxford and for teaching me immunohistochemistry among other things. Suze, I am grateful to have worked next to you in the lab on a daily basis. You taught me all the basic lab routines and techniques that enabled me to go on to develop more skills over the years. Thank you all for the time, patience and the tremendous efforts you put in to make a scientist out of an ordinary Ghanaian man. Outside the lab, you were also there to counsel, comfort and encourage me to ensure I fared well on all other fronts. I am grateful!

Many thanks to the Commonwealth Scholarships Commission (CSC) for funding my DPhil study in Oxford. Your generous support made my study in Oxford possible. Thanks to Retina UK and Fight for Sight for sponsoring the UKIRDC research of which my DPhil thesis forms part. I am grateful to members of the Oxford UKIRDC team, Prof Susan Downes, Dr Jing Yu, Clare Arnision-Newgass and Sophie Marlowe, for their help in recruiting participants for this project. Jing, thank you for all the Bioinformatic analysis you did to make this project possible. Many thanks also to other DPhil students in the Halford Lab, Saoud Al-Khuzaei and Ahmed Shalaby, for their support and always sharing of ideas at lab meetings and journal clubs.

I would like to also thank Dr Pieta Matilla and Mr Alexey Vladimirovich Sarapulov of the University of Turku, Finland, for generously making the *Mtss1* knockout mouse eye tissue available for this thesis. I am also thankful to members of the NLO especially Lewis, Caroline, Laurel, Ariel, Elena, Cristina, Michelle, and Ahmed for their support and friendship throughout my stay in the NLO as a DPhil student. Many thanks to Alex Davies, Ricardo P. Schnekenberg and Lucy McDermott of NDCN LL3 who

were there to provide various forms of support and friendship. Special thanks to Victor Mgbachi of the Oxford Autoimmune Neurology group. Thank you very much for being a special friend and brother to me throughout my stay in Oxford and in the NDCN. You and your family have been a blessing to me and mine. I am grateful to God for planting you in the NDCN for my sake.

I would also like to thank my wife Mrs Belinda Merepa, my little daughter Stephanie Joy and Baby No. 2 (who is due soon) for their unflinching support throughout this period of my DPhil. You have had to make a lot of sacrifices and adjustments, especially during the thesis writing period, and I am very grateful for that. Belinda, thank you for the encouragement, love, support and patience while this work was being completed. You made me a peaceful and lovely home that I always looked forward to. God bless you!

My special gratitude goes to my parents who, despite having no formal education, worked tirelessly to ensure that me and all my siblings had the privilege of obtaining formal education. Without your numerous sacrifices, I would not have had any education, talk less of attaining a DPhil degree from the best university in the world, Oxford. I am eternally grateful to you! Special thanks to my siblings (Mary, Diana (of blessed memory), Deborah, Lucy and Josephine) and my entire family for your support and contributions towards my education and success. I am also thankful to my British family, The Sorsbie Family of Sheffield, for their continued show of love and support for me and my family throughout our time here in the UK. Thank you for adopting us into your lovely family.

Many thanks to my Pastor in Oxford, Pastor Frank Addai, and the entire membership of the Oxford and North Oxford branches of Mustard Seed Chapel International for their massive support and friendship from the day I came into Oxford. You all have been a great blessing to me and my family in diverse ways. May the Lord show you all His goodness in the land of the living.

Finally, my utmost gratitude to my Lord and Saviour, Jesus Christ, who loved me and came to die for me that I will obtain everlasting life with God the Father. I am thankful to God for picking me up from the miry clay and setting my feet upon a solid rock that I can stand. I am thankful to the Holy Spirit for

His constant presence and companionship through the ordinary and difficult times I went through during the period of my DPhil. All that I am and ever hope to be, I owe it all to you my Lord!

Table of Contents

Dedication……i

Abstract……ii

Declaration……iv

Acknowledgement……v

Table of Contents……vii

List of Abbreviations……xiii

List of Figures……xix

List of Tables……xxi

1 General introduction 1

1.1 The mammalian retina 1

1.1.1 Retina structure and cell types 1

1.1.2 Rod and cone photoreceptors 4

1.1.3 Molecular steps involved in vision 7

1.1.4 Mouse versus human retina 13

1.1.5 Fovea and macular in the human retina 14

1.1.6 Retinal structure and function in humans 16

1.2 Inherited retinal dystrophies (IRDs) 17

1.2.1 Retinitis pigmentosa 18

1.2.2 Macular dystrophies 25

1.3 Approaches to identifying IRD genes (Past to present) 27

1.3.1 Linkage analysis 29

1.3.2 Positional cloning 30

1.3.3 Candidate gene approach 31

1.3.4 Functional candidate gene identification approach 32

1.3.5 Next generation sequencing 34

1.3.6 Establishing a variant as pathogenic 35
1.4 Therapeutic approaches for IRDs 40
1.4.1 Gene therapy 41
1.4.2 Gene editing 42
1.4.3 Antisense oligonucleotide therapy 43
1.4.4 Stem cell therapy 44
1.5 Thesis rationale 46
1.6 Aims 47
2 Materials and Methods 48
2.1 Materials 48
2.1.1 Reagents 48
2.1.2 Enzymes 48
2.1.3 Electrophoresis 48
2.1.4 DNA Sequencing 48
2.1.5 Bacterial Strains 48
2.1.6 Oligonucleotide primers 49
2.1.7 Equipment and Apparatus 49
2.2 Buffers, Solutions, Media and Kits 50
2.2.1 General stock reagents 50
2.2.2 Preparation of Plasmid DNA 50
2.2.3 Preparation of RNA 52
2.2.4 Preparation of cDNA 52
2.2.5 PCR purification and Gel extraction 52
2.2.6 Gel Electrophoresis 53
2.2.7 Immunohistochemistry / Immunocytochemistry 53
2.2.8 Western immunoblotting 54
2.2.9 Cell culture 55
2.2.10 Kits used 55
2.3 Methods 57

2.3.1 Patient cohort 57
2.3.2 DNA 57
2.3.3 RNA 73
2.3.4 Cell Culture 74
2.3.5 Protein 78
2.3.6 Mouse Lines and Animal Husbandry 80
2.3.7 Histology 81
2.3.8 Microscopy 82
2.3.9 Bioinformatic Methods 83
2.3.10 Web Resources (URLs) 83
3 Identification of candidate genes 85
3.1 Introduction 85
3.2 Aims 87
3.3 Methods 88
3.3.1 Participant recruitment 88
3.3.2 Whole-exome sequencing 88
3.3.3 Variant analysis 89
3.3.4 Preliminary analysis of genes with segregating variants 90
3.4 Results 92
3.4.1 Family 3004 92
3.4.2 Family 3013 106
3.4.3 Family 3027 116
3.3.4 Family 3032 126
3.5 Discussion 132
4 Characterisation of *MTSS1* expression in mammalian retina. 136
4.1 Introduction 136
4.2 Aims 143
4.3 Methods 143
4.3.1 5’ Rapid Amplification of cDNA Ends (5’ RACE) 143

4.4 Results 147
4.4.1 *MTSS1* gene expression 147
4.4.2 MTSS1 protein expression and localisation 162
4.5 Discussion 172
5 Functional characterisation of MTSS1 in mammalian retina and cells 179
5.1 Introduction 179
5.2 Aims 182
5.3 Methods 182
5.3.1 *In vitro* expression of *MTSS1* 182
5.3.2 Site directed mutagenesis 183
5.3.3 Mtss1 knockout mouse retina analysis 183
5.4 Results 187
5.4.1 Colocalization of MTSS1 with previously reported binding partners in wild type mouse retina 187
5.4.2 Functional characterisation of *MTSS1* p.(Glu213del) variant 192
5.4.3 Characterisation of *Mtss1* knockout mouse retina 208
5.5 Discussion 218
6 General discussion 225
6.1 Summary of key findings 225
6.2 Potential disease mechanism of the MTSS1 p.Glu213del variant 227
6.3 Relevance to candidate gene identification for IRDs 230
6.4 Future directions 233
6.4.1 Further characterisation of MTSS1 233
6.4.2 Characterisation of other prioritised candidate genes 236
6.4.3 Patient screening 237
6.5 Conclusions 237
6.6 Covid-19 pandemic impact statement 238
References 240
Appendices 269

Appendix A: List of genes on RP 111 Gene panel (RP and RP-associated genes) used in standard NHS genetic testing 269

Appendix B: Primers used for segregation analysis 270

Appendix C: Primers used for gene expression and 5' RACE 275

Appendix D: Summary of levels of expression of key candidate genes in the various retinal cell types as reported by scRNA-seq on the adult human retina 277

Appendix E: List of antibodies used for immunohistochemistry and western immunoblot 278

Appendix F: Antibody validation information 280

Appendix G: IRD patients with variants in *MTSS1* from Genomics England rare disease programme database 281

List of Abbreviations

AAV	Adeno-associated viral vector
ABCA4	ATP Binding Cassette Subfamily A Member 4
ACTB	Beta Actin
ACHM	Achromatopsia
AD	Autosomal Dominant
AMD	Age-related Macular Degeneration
ARB	Autosomal Recessive Bestrophinopathy
AR	Autosomal Recessive
atRDH	All-trans Retinol Dehydrogenase
ATP	Adenosine Triphosphate
BAR	Bin/Amphiphysin/Rvs
BCA	Bicinchoninic Acid Assay
BD	Best Disease
BE	Both Eyes
BP	Base Pair
BVMD	Best Vitelliform Macular Dystrophy
C-	Carboxyl Terminus
CADD	Combined Annotation Dependent Depletion
CDH	Cadherin
CC	Connecting Cilium
CAS9	CRISPR Associated Protein 9
cDNA	Complementary DNA
cGMP	Cyclic Guanosine Monophosphate
CHIP	Chromatin Immunoprecipitation

CHM	Choroideremia
CMO	Cystoid Macular Oedema
CRISPR	Clustered Regularly Interspaced Short Palindromic Repeats
CSNB	Congenital Stationary Night Blindness
CRD	Cone-Rod Dystrophy
DAAM1	Dishevelled Associated Activator of Morphogenesis 1
DAPI	4',6-Diamidino-2-Phenylindole
DNA	Deoxyribonucleic Acid
DSB	Double-Stranded Break
EGFP	Enhanced Green Fluorescence Protein
ERG	Electroretinogram
ESCS	Enhanced S-Cone Syndrome
EZ	Ellipsoid Zone
FAF	Fundus Autofluorescence
FEVR	Familial Exudative Vitreoretinopathy
FPKM	Fragments Per Kilobase Of Transcript Per Million Mapped Reads
FRMPD1	FERM And PDZ Domain Containing 1
GC	Guanylate Cyclase
GCL	Ganglion Cell Layer
GDP	Guanosine Diphosphate
GFP	Green Fluorescent Protein
GMP	Guanosine Monophosphate
gnomAD	Genome Aggregation Database
GPCR	G-Protein-Coupled Receptors
GTP	Guanosine Triphosphate
HEK293	Human Embryonic Kidney Cells 293

HDR	Homology Directed Repair
HGP	Human Genome Project
HPO	Human Phenotype Ontology
I-BAR	Inverse Bin/Amphiphysin/Rvs
IRBP	Interphotoreceptor Binding Proteins
IRD	Inherited Retinal Dystrophy
IFT	Intraflagellar Transport
IHC	Immunohistochemistry
ILM	Inner Limiting Membrane
IMD	IRSp53/MIM Homology Domain
INDEL	Insertion/Deletion
INL	Inner Nuclear Layer
IP	Immunoprecipitation
IPL	Inner Plexiform Layer
IRSp53	Insulin Receptor Substrate 53
IS	Inner Segment
kDa	Kilodalton
KLD	Kinase, Ligase, Dpn1
KO	Knockout
KPNA7	Karyopherin Subunit Alpha 7
LCA	Leber Congenital Amaurosis
LE	Left Eye
LOD	Logarithm Of Odds
LRAT	Lecithin Retinol Acyltransferase
MD	Macular Dystrophy
µ	Micrometer

MIM	Missing In Metastasis
mRNA	Messenger RNA
MTSS1	Metastasis Suppressor 1
MYO5B	Myosin VB
N-	Amino Terminus
NBL	Neuroblastic layer
NFL	Nerve Fibre Layer
NGS	Next Generation Sequencing
NHEJ	Non-Homologous End-Joining
NRL	Neural Retina Leucine Zipper
OCT	Optimal Cutting Temperature
OLM	Outer Limiting Membrane
OMIM	Online Mendelian Inheritance in Man
ONL	Outer Nuclear Layer
OPL	Outer Plexiform Layer
OS	Outer Segment
P	Postnatal Day
PARPBP	PARP1 Binding Protein
PBS	Phosphate-Buffered Saline
PCR	Polymerase Chain Reaction
PDE	Phosphodiesterase
PFA	Paraformaldehyde
PIEZO1	Piezo Type Mechanosensitive Ion Channel Component 1
PNA	Peanut Agglutinin
PKCA	Protein Kinase C Alpha
qPCR	Quantitative PCR

RACE	Rapid Amplification of cDNA Ends
RD1	Pde6b−/− Retinal Degeneration Model
rdCVF	Rod-derived Cone Viability Factors
RDH5	Retinol Dehydrogenase 5
RE	Right Eye
RFLP	Restriction Fragment Length Polymorphisms
RIPA	Radioimmunoprecipitation Assay Buffer
RGC	Retinal Ganglion Cell
RNA	Ribonucleic Acid
RP	Retinitis Pigmentosa
RPE	Retinal Pigment Epithelium
RPE65	Retinal Pigment Epithelium 65
S	Second
SAGE	Serial Analysis of Gene Expression
scRNA-seq	Single Cell RNA Sequence
SD-OCT	Spectral-Domain Optical Coherence Tomography
SIFT	Scale-Invariant Feature Transform
SHH	Sonic Hedgehog
SNP	Single Nucleotide Polymorphisms
SSCP	Single Strand Conformational Polymorphism Electrophoresis
STGD	Stargardt Disease
TALENs	Transcription Activator Like Effector Nucleases
TSS	Transcription Start Site
UTR	Untranslated Region
WES	Whole Exome Sequencing
WGS	Whole Genome Sequencing

WH2	Wiskott-Aldrich Syndrome (WASP) Protein Homology 2
WT	Wild Type
XL	X-linked
ZFN	Zinc-Finger Nucleases
g	Gravitational Force

List of Figures

Figure 1.1. Anatomy of the human eye and retina. 3
Figure 1.2. Morphology of the photoreceptors. 9
Figure 1.3. Phototransduction in rod photoreceptors. 10
Figure 1.4. The retinoid cycle. 12
Figure 1.5. The human fundus. 15
Figure 1.6. Venn diagram showing the genetic overlap between RP and other IRDs. 24
Figure 3.1. Pedigree of family 3004 diagnosed with adRP. 93
Figure 3.2. Retina imaging of proband in family 3004 with adRP. 95
Figure 3.3. Segregation analyses in 3004 family. 99
Figure 3.4. Expression of *KPNA7* and *PARPBP*. 102
Figure 3.5. Preliminary analysis of *PARPBP* transcripts in the human retina. 104
Figure 3.6. Immunohistochemical staining of wild type mouse retina with PARPBP antibody. 107
Figure 3.7. Parpbp protein expression in developing mouse retina. 108
Figure 3.8: Pedigree of family 3013 diagnosed with adRP. 109
Figure 3.9. Retina imaging of proband in family 3013 with adRP. 111
Figure 3.10. Segregation analyses in 3013 family. 114
Figure 3.11. *MYO5B* and *PIEZO1* expression and conservation across species. 117
Figure 3.12. Pedigree of family 3027 diagnosed with adRP. 118
Figure 3.13. Retina imaging of proband in family 3027 with adRP. 120
Figure 3.14. MTSS1 variant segregates with adRP in family 3027. 123
Figure 3.15. *MTSS1* gene expression and protein conservation. 125
Figure 3.16. Pedigree of family 3032 diagnosed with dominant macular dystrophy. 127
Figure 3.17. Retina imaging of proband in family 3032 with dominant macular dystrophy. 129
Figure 4.1. Genomic structures of *MTSS1* transcripts. 140
Figure 4.2. Comparison of human and mouse *MTSS1/Mtss1* protein sequence. 141
Figure 4.3. Schematic diagram of genomic structure of MTSS1 and corresponding protein domains. 142
Figure 4.4. *Mtss1* expression in mouse retina. 148
Figure 4.5. *Mtss1/MTSS1* expression in transgenic mice and human retina-derived cell lines. 150
Figure 4.6. Amplification of full length *MTSS1* sequence from human retina. 153
Figure 4.7. Alternate splicing of MTSS1 in human retina between exons 11 and 13. 155
Figure 4.8. Alternate exons and transcripts of *MTSS1*/*Mtss1* in retina. 157
Figure 4.9. Analysis of 5' UTR of Mtss1 in mouse brain and retina. 159
Figure 4.10. 5' RACE confirms retina-specific transcript of *Mtss1*. 161

Figure 4.11. MTSS1 protein expression in retina and brain assessed by western immunoblotting... 163
Figure 4.12. Immunohistochemical staining of wild type mouse retina with MTSS1 antibodies..... 166
Figure 4.13. Mtss1 protein is expressed in rod photoreceptor cells of the mouse retina..... 168
Figure 4.14. Mtss1 expression in synaptic layers and ganglion cell layer..... 170
Figure 4.15. Mtss1 protein expression in developing mouse retina..... 171
Figure 4.16. Schematic representation summarising the alternate splice variants of *MTSS1* identified in brain and retina..... 178
Figure 5.1. MTSS1 staining colocalises with F-actin in the photoreceptors and synaptic layers..... 190
Figure 5.2. DAAM1 protein expression in the mammalian retina. 191
Figure 5.3. *MTSS1* expression in HEK2938, MDCKII and RPE1 cell lines. 195
Figure 5.4. Wild-type and mutant MTSS1 overexpression in HEK293T cells. 200
Figure 5.5. Wild-type and mutant MTSS1 transfection in MDCKII cells..... 202
Figure 5.6. Wild-type MTSS1 overexpression in RPE1 cells induces formation of extensive cellular processes..... 205
Figure 5.7. Transfection of AK030533 transcript constructs in HEK293T cells. 207
Figure 5.8. Generation of the Mtss1 knockout mice. 209
Figure 5.9. Haematoxylin and eosin staining of retinas from *Mtss1* knockout mice..... 213
Figure 5.10. Immunohistochemical staining of Mtss1 knockout mouse retina..... 215
Figure 5.11. Residual expression of Mtss1 gene and protein in retina of *Mtss1* KO mice. 217

List of Tables

Table 1.1. Summary of common macular dystrophies. 28
Table 1.2. Tools and resources used in the analysis of WES and WGS data. 38
Table 3.1. Summary of clinical findings in Family 3004 with adRP 94
Table 3.2 Family 3004: Segregation analysis for variants with a gnomAD frequency of zero. 97
Table 3.3. Summary of clinical findings in Family 3013 with adRP 110
Table 3.4. Family 3013: Segregation analysis for variants with gnomAD frequency of zero. 113
Table 3.5. Summary of clinical findings in Family 3027 with adRP 119
Table 3.6. Family 3027: Segregation analysis for variants with gnomAD frequency of zero 122
Table 3.7. Summary of clinical findings in Family 3032 with dominant macular dystrophy 128
Table 3.8. Family 3032: Segregation analysis for variants with gnomAD frequency of 0 – $4.3E^{-5}$ 130
Table 5.1 Predicted protein-protein affinity Change (ΔΔG) upon mutation of p.(Glu213) of MTSS1. 193
Table 6.1. Summary of key candidate genes identified in families presented in order of the strength of evidence. 229

1 General introduction

1.1 The mammalian retina

The retina is the light-sensitive layer of tissue that lines the inside of the posterior segment of the eyeball. The detection of light begins with the photoreceptor cells whose main role is to absorb photons of light reaching the retina leading to an intracellular signalling cascade, ultimately converting light energy into an electrochemical signal. This information is processed within the retina via the retinal interneurons before transmission, via the retinal ganglion cells, to higher centres in the brain for further processing and interpretation. In this section, the cellular components and molecular events relevant for the normal function of the mammalian retina will be described with a particular emphasis on the photoreceptor cells.

1.1.1 Retina structure and cell types

The mammalian retina is composed of three distinct layers of neuronal cells, the first being the outer nuclear layer (ONL) consisting of cell bodies of photoreceptor cells (Rodieck, 1998). The second distinct layer of cells is the inner nuclear layer (INL), made up of cell bodies of bipolar, horizontal and amacrine cells. The third distinct cellular layer is the ganglion cell layer (GCL), made of retinal ganglion cells (RGCs) whose axons form the nerve fibre layer (NFL) which goes on to form the optic nerve, involved in transmitting visual information to the brain for central processing (Figure 1.1). Although ganglion cells reside mainly in the GCL, a smaller minority, known as displaced ganglion cells, can sometimes be found in the INL. The GCL is also known to contain cell bodies of displaced amacrine cells, which could represent up to 50% of the GCL cell population (Jeon et al., 1998). Two main synaptic/neuropil layers, known as plexiform layers, separate the three cellular layers of the neural retina. The outer plexiform layer (OPL), located in between the ONL and INL, comprise synapses formed by the photoreceptors in the ONL and cells in the INL. The inner plexiform layer (IPL), which lies between the INL and GCL, comprise synapses formed between cells in the INL and GCL neurons (Figure 1.1) (Rodieck, 1998).

For visual information to be transmitted to the brain for further processing, light photons are first detected by photoreceptors located at the outermost part of the neural retina, next to a monolayer of pigmented epithelial cells known as retinal pigment epithelium (RPE). The RPE sits on an acellular layer called the Bruch's membrane, which separates it from the vascular choroid beneath. Among other crucial functions, the RPE provides "biochemical" support to the photoreceptors (Strauss, 2005). In the direct pathway through the retina, electrochemical signals from the photoreceptors are transmitted to the retinal ganglion cells via the bipolar cell interneurons (Figure 1.1). Horizontal and amacrine cells located in the INL form lateral connections with bipolar and ganglion cells, respectively, to perform intermediate processing that enables integration of the enormous amount of visual information coming from over 100 million photoreceptors into about 1 million ganglion cells whose axons go on to form the optic nerve (Jeon et al., 1998). Another type of cell found in the neural retina are the Muller glial cells. These specialised glial cells provide structural and metabolic support for retinal neurons through projections that run perpendicularly in the retina, forming the inner and outer limiting membranes (ILM and OLM) with their inner and outer footplates, respectively (Hildebrand and Fielder, 2011).

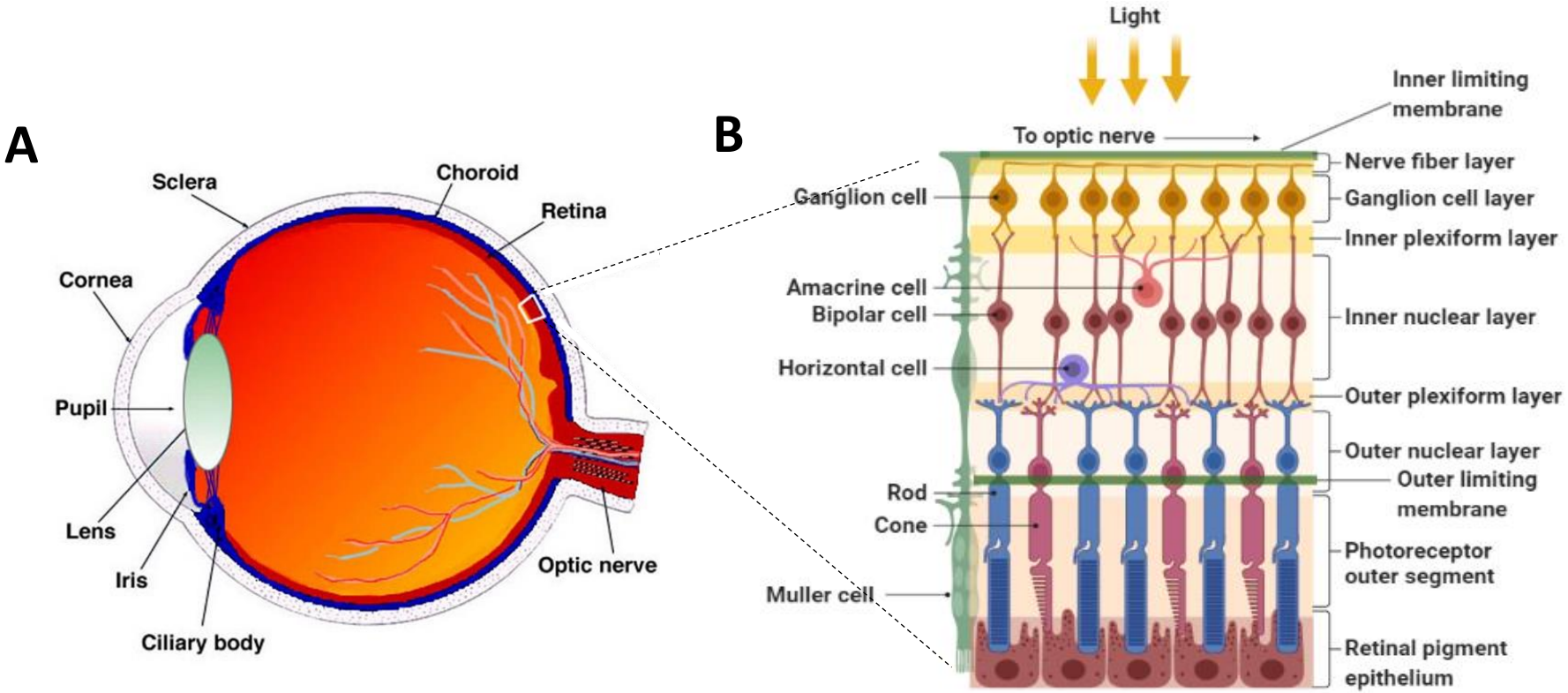


Figure 1.1. Anatomy of the human eye and retina. (A) Schematic of a section through the human eye ball (globe) with major structures indicated. Light enters the eye through the pupil and is refracted by the lens and cornea onto the retina. (Image source: Webvision [http://webvision.med.utah.edu/]). (B) Anatomy of the human retina which comprises three major cell layers (outer nuclear layer, inner nuclear layer and ganglion cell layer), two synaptic layers (outer and inner plexiform layers). Light reaching the retina travels through the layers of the retina to reach the outer segments of the rod and cone photoreceptors in the ONL where phototransduction occurs. Figure created from BioRender.com.

1.1.2 Rod and cone photoreceptors

Two main types of image forming photoreceptors with distinct functions exist in the mammalian retina: rods and cones. In the human retina, rod photoreceptors far outnumber cone photoreceptors, by approximately 20:1 (Curcio et al., 1990), and increase in density as you move from the centre of the retina towards the periphery. The rods are more sensitive to light and are responsible for vision in dim light, known as scotopic vision (Rodieck, 1998). Cones on the other hand, are more concentrated in the centre of the retina (called the fovea), decrease in density towards the retinal periphery, are less sensitive to light, and are responsible for high acuity and colour vision (Kolb, 1995). Rod and cone photoreceptors are highly specialised neurons with a polarized structure. These cells have specialised compartments including the outer segments (OS), inner segments (IS), cell bodies and synaptic terminals (Figure 1.2).

1.1.2.1 The photoreceptor outer segment (OS)

Rod and cone photoreceptors derive their names from the shapes of their outer segments which are in close contact with the RPE: rods have slender rod-shaped outer segments whereas cones have relatively thicker cone-shaped outer segments. Both are elongated structures oriented along the axis of incoming light and protrude into an area next to the underlying RPE called the sub-retinal space (Strauss, 2011). Apical processes from the RPE envelope the distal parts of the outer segments of both rods and cones, and function to increase the surface area of the RPE in their functional interaction with the photoreceptor outer segments (Strauss, 2011). The outer segments are densely packed with stacks of membranous discs containing the visual pigments necessary for phototransduction (Kolb, 1995). The photoreceptor outer segments are known to be elaborate primary non-motile cilia in which the ciliary plasma membranes have been extensively amplified to enable light reception (Goldberg et al., 2016). In cones, the discs remain attached and are continuous with the outer segment membrane. In rods, however, the discs are detached, stacked atop one another and are fully internalised by the outer segment membrane, except for a few discs at the base of the outer segments, which are continuous

with the OS membrane (Sjostrand, 1959) **(**Figure 1.2). The outer segments undergo a regular renewal process during which old discs in the distal parts are shed and phagocytosed by the RPE while new discs are formed at the basal parts through evagination and invagination of plasma membranes of the photoreceptor cells (Young, 1967). The extensive curvatures observed in outer segment disc membranes have attracted much research interest with the aim of understanding the underlining mechanisms for generating such membrane curvature (Goldberg et al., 2016). Though not definitive, a variety of mechanisms have been suggested including the role of membrane lipids in the phospholipid bilayer and most importantly specialised curvature-generating proteins such as BAR (Bin/Amphiphysin/Rvs) proteins (Peter et al., 2004, Graham and Kozlov, 2010). These membrane-bending mechanisms are deemed crucial to the morphology of photoreceptor outer segments, especially as it enables the dense stacking of the membranous discs, which increases the surface area of the outer segments to enable absorption of more photons of light in phototransduction (Kolb, 1995, Goldberg et al., 2016).

1.1.2.2 The photoreceptor inner segment (IS) and synaptic terminals

The inner segment of the photoreceptor cell is connected to the outer segment by the connecting cilium, a thin microtubular structure (see 1.1.2.3). The inner segment is the part of the photoreceptor cell that contains the cellular machinery necessary for the house-keeping functions of the cell. It has two main regions: (i) an outer ellipsoid region which is densely packed with mitochondria providing ATP for the cell through oxidative phosphorylation; and (ii) an inner myoid region which contains protein and lipid synthesis machinery such as the endoplasmic reticulum and Golgi apparatus, as well as a cytoskeletal network of microtubules and F-actin fibres necessary for intracellular transport (Hildebrand and Fielder, 2011). Below the myoid region of the inner segment, the diameter of the plasma membrane constricts at a band of adherens junctions formed between photoreceptors and processes from Muller glia cells called the outer limiting membrane (Figure 1.2). The inner segment is then continuous into the soma of the cell which widens to accommodate the nucleus (forming the ONL) before narrowing down to form an axon with presynaptic terminals which form synaptic

connections with horizontal and bipolar cells in the OPL in the outer plexiform layer (OPL) (Baker and Kerov, 2013). The rod synaptic terminal is called the spherule whiles the cone synaptic terminal is called the pedicle (Kolb, 1995). The presynaptic terminals have specialised plasma membrane ribbons containing synaptic vesicles which fuse with the pre-synaptic plasma membrane to release neurotransmitters such as glutamate into the synaptic cleft, under the control of voltage-gated calcium channels to enable transmission of electrical impulses generated by visual stimuli (Baker and Kerov, 2013) (see 1.1.3.1). The pre-synaptic terminals of the photoreceptors also contain scaffolding, adhesion and cytoskeletal proteins which play a crucial role in the formation of proper synaptic contacts with post-synaptic bipolar cells, signal transduction as well as synaptic remodelling of the synapsis in response to the exocytosis and endocytosis of synaptic vesicles (Aartsen et al., 2009, Aartsen et al., 2006, Vaughan and Fisher, 1987, Yamagata and Sanes, 2010).

1.1.2.3 The connecting cilium

Crucial to the development and maintenance of the photoreceptor outer segments and for photoreceptor viability is the transport of proteins and molecules between the inner segment and the outer segment. The connecting cilium linking the photoreceptor inner and outer segment (Figure 1.2) is organised around a microtubule axoneme, which is maintained in a polymerised state by acetylated tubulin subunits (Sale et al., 1988). Proteins such as RP1, Prominin-1 (PROM1) and actin filaments (F-actin) are known to associate with the microtubular axonemes in photoreceptor outer segments, and are known to play various roles in the function of the outer segments including the regulation of the cytoskeleton and formation of nascent discs at the basal OS (Liu et al., 2002, Williams et al., 1988, Yang et al., 2008). The essential roles of RP1 and PROM1 in the photoreceptor outer segments are emphasised by the implication of the genes encoding these proteins, and their binding partners in the retina, in various inherited retinal diseases (Maw et al., 2000, Bowne et al., 1999).

An active form of transport called intraflagellar transport (IFT), which occurs across the connecting cilium, is one of the main means of transporting proteins and molecules between the inner and outer segment (Goldberg et al., 2016). The photoreceptor outer segment relies greatly on IFT across the

connecting cilium to transport proteins, such as opsins, produced in the inner segment to the outer segment (Besharse and Wetzel, 1995). It is also involved in the redistribution of proteins, such as arrestin and transducin, from the outer segment to the inner segment depending on ambient light levels using cytoskeleton-associated motor proteins such as kinesin-2 and dynein-2 (Pearring et al., 2013, Marszalek et al., 2000). As such, transgenic mice lacking the *KIF3A* subunit of the kinesin-2 protein resulted in the accumulation of rhodopsin, arrestin and disc membranes within the photoreceptor inner segment due to impaired IFT (Marszalek et al., 2000, Jimeno et al., 2006). In another mouse deficient in the IFT protein IFT88, ectopic localisation of the outer segment protein Guanylate cyclase-1 was reported, emphasising the importance of IFT to outer segment development and function (Pazour et al., 2002).

1.1.3 Molecular steps involved in vision

1.1.3.1 Phototransduction

For vision to occur, photons of light entering the human eye are refracted by both the transparent cornea and lens onto the retina at the posterior end of the eye. Light photons reaching the photoreceptor outer segments of rods and cones are absorbed by rhodopsin and cone opsins, respectively. Each photon of light is absorbed by 11-*cis* retinal, a vitamin A derivative, sitting in the binding pocket of the opsin molecule. Absorption of a photon of light causes the conversion of 11-*cis* retinal into an all-*trans* isomer, an activated form. This activation results in a conformational change in the opsin protein resulting in the all-*trans* isomer detaching from the activated opsin protein (Lamb and Pugh, 2006, Arshavsky and Burns, 2012). The activated opsin then stimulates a G-protein called transducin comprising an alpha, beta and gamma (αβγ) subunit (Figure 1.3). Upon stimulation, the alpha subunit of transducin binds to guanosine triphosphate (GTP), forming a transducin-GTP complex that goes on to activate an enzyme called phosphodiesterase (PDE). In turn, activated PDE breaks down cyclic guanosine monophosphate (cGMP) to 5’ guanosine monophosphate (5’GMP). Reduction in cGMP levels in the disc membranes of the photoreceptor outer segment results in the closure of cGMP-

gated cation channels. This results in the hyperpolarisation of the photoreceptor cells, which further leads to the closure of voltage-gated calcium ion (Ca^{2+}) channels in the disc membrane (Molday and Moritz, 2015). Closure of Ca^{2+} channels inhibits the release of glutamate at the synaptic terminal of the photoreceptor (Arshavsky et al., 2002). The series of processes through which photons of light are converted to electrical impulses in the photoreceptors in order for vision to occur, as described above, is known as phototransduction (Figure 1.3). The importance of proteins such as rhodopsin and PDE in maintaining normal photoreceptor function can be seen in the identification of mutations in genes encoding these proteins in various IRDs (see 1.2.1.3).

Reduction in the release of glutamate at the photoreceptor – bipolar cell synapse causes activation (depolarization) of on-centre bipolar cells and deactivation (hyperpolarization) of off-centre bipolar cells leading to the passage of the visual stimulus impulses to the RGCs. The RGCs, subsequently, send the impulses along their axons, which form the optic nerve, to higher centres of the visual pathway (Rodieck, 1998).

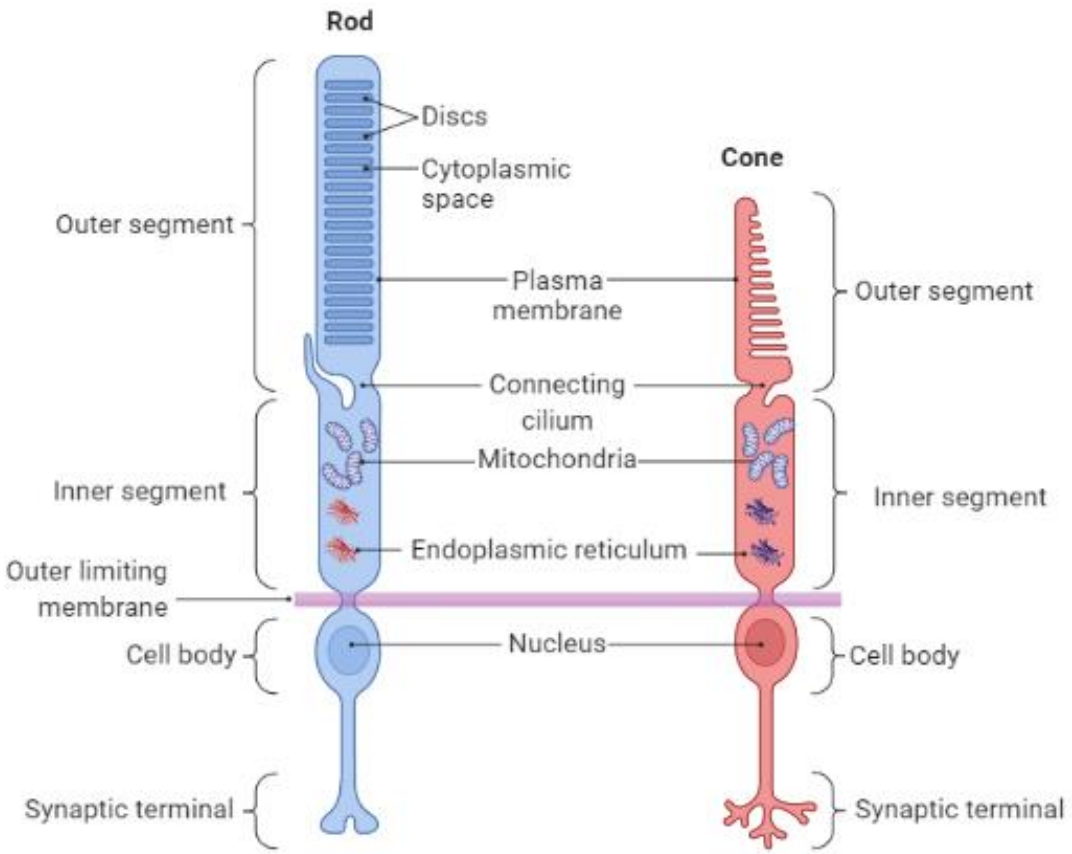


Figure 1.2. Morphology of the photoreceptors. Schematic of the morphology of rod and cone photoreceptor cells. The plasma membrane of both cells is divided into two compartments, the outer and inner segments which are connected by the connecting cilium. Other specific features of the photoreceptor cells are labelled. Figure created with BioRender.com**.**

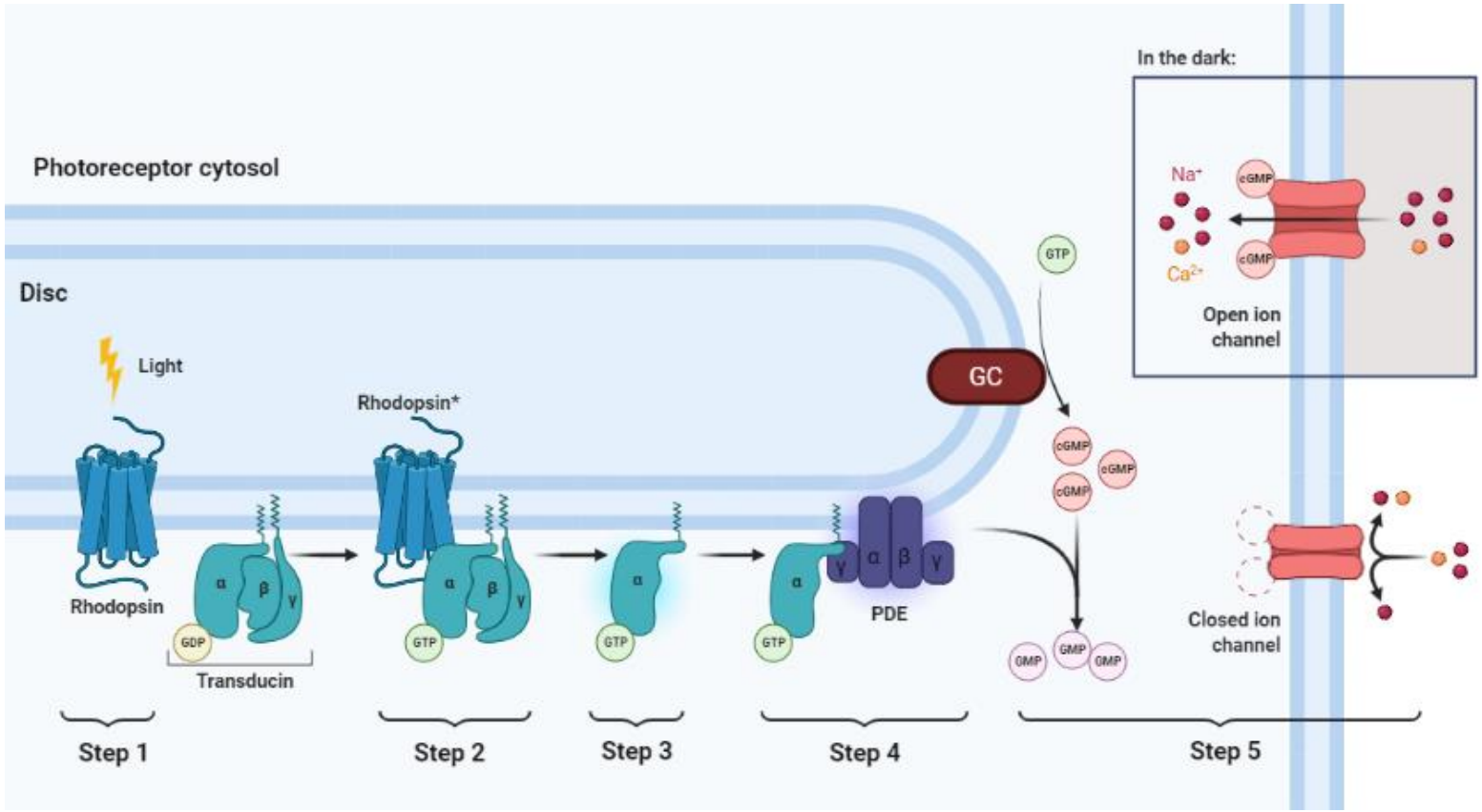


Figure 1.3. Phototransduction in rod photoreceptors. In the dark, the rod photoreceptor cell is polarised through cGMP-gated cation channels that allow influx of cations including calcium (Ca^{2+}). Light reaching the rod outer segment (OS) activates 11-*cis* retinal in rhodopsin into all-*trans* retinal which goes on to activate transducin. The α-subunit of transducin detaches upon activation and, upon attaching to GTP, goes on to activate the enzyme phosphodiesterase (PDE). cGMP which is synthesised by guanylate cyclase (GC) is hydrolysed by activated PDE leading to reduction in levels of cGMP levels inside the cell. Reduced levels cGMP leads to closure of cGMP-gated channel with resultant hyperpolarisation of the photoreceptor cell. Figure created from BioRender.com

1.1.3.2 The visual cycle

In order for another photon of light to be absorbed, the phototransduction cascade needs to be inactivated. Activated opsin is phosphorylated by opsin kinases (such as rhodopsin kinase in the case of rhodopsin) which enables it to be bound by an inactivating enzyme called arrestin (Burns et al., 2006, Gurevich et al., 2011). Transducin is deactivated by an intrinsic GTPase activity whilst reduced Ca^{2+} levels in the cell activates guanylate cyclase-activating protein, which in turn stimulates guanylate cyclase to increase cGMP production (Figure 1.3). After 11-*cis* retinal is activated and isomerised to all-*trans* retinal to begin the visual cascade, all-*trans* retinal needs to be converted back to its inactive isoform, 11-*cis* retinal (Lamb and Pugh, 2006). To do this, all-*trans* retinal in the photoreceptor outer segment is reduced by all-trans retinol dehydrogenase (atRDH) into all-*trans* retinol (Figure 1.4). It is then transported to the RPE, aided by proteins such as interphotoreceptor binding proteins (IRBP) and the ATP binding cassette subfamily A member 4 (ABCA4), where it undergoes a series of steps to be restored to 11-*cis* retinal by enzymes such as lecithin retinol acyltransferase (LRAT), the retinoid isomerohydrolase RPE65 and retinol dehydrogenase 5 (RDH5) (Lamb and Pugh, 2006). The 11-*cis* retinal in the RPE is then transported back to photoreceptor outer segment by IRBPs (Figure 1.4). To emphasize the importance of these steps in the physiology of the retina, mutations in genes that encode ABCA4, LRAT, RDH5 and RPE65 resulting in defective function of these proteins have been implicated in various forms of IRDs including Stargardt disease, fundus albipunctatus, Leber congenital amaurosis and retinitis pigmentosa (Cremers et al., 1998a, Cideciyan et al., 2000, Ruiz et al., 2001, Morimura et al., 1998).

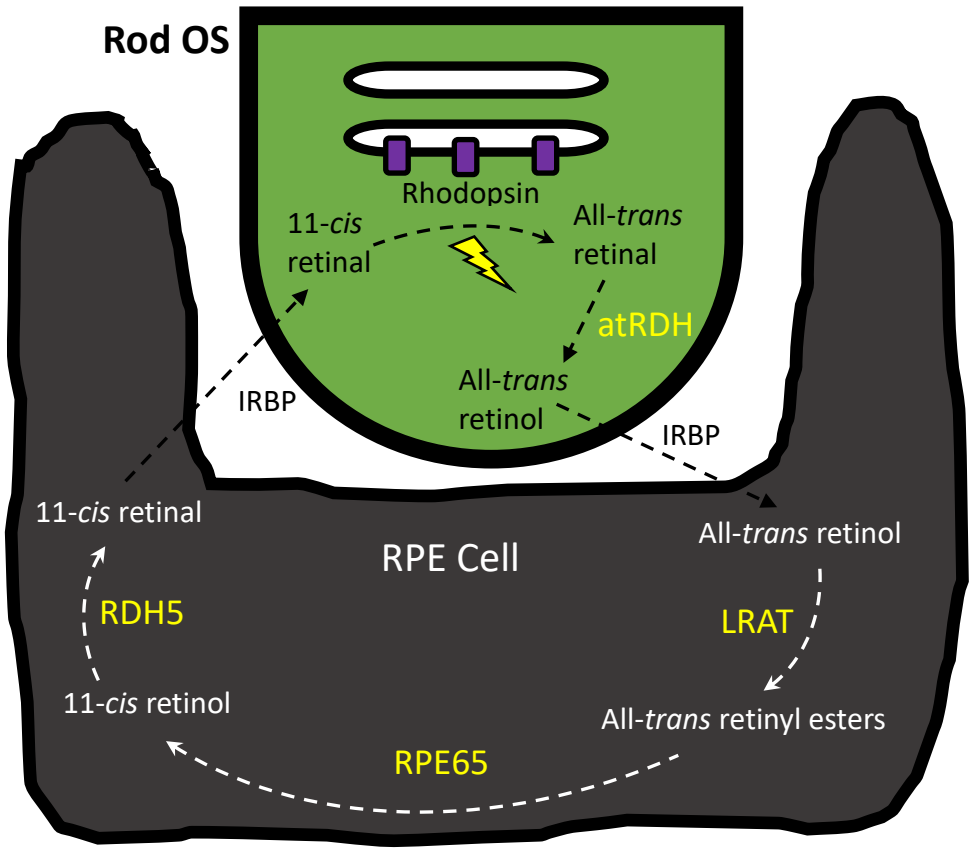


Figure 1.4. The retinoid cycle. Absorption of a light photon by rhodopsin causes the photoisomerization of the rhodopsin-bound 11-*cis* retinal into all-*trans* retinal in the rod outer segment (OS). The enzyme all-*trans* retinol dehydrogenase (atRDH) converts all-*trans* retinal to all-*trans* retinol. All-*trans* retinol is transported from the OS into the retinal pigment epithelium (RPE) facilitated by interphotoreceptor retinoid binding protein (IRBP) where it is converted into all-*trans* retinyl esters by the enzyme lecithin retinol acyltransferase (LRAT). The RPE65 enzyme converts the all-trans retinyl esters into 11-*cis* retinol which is eventually oxidised into 11-*cis* retinal by retinol dehydrogenase 5 (RDH5). 11-*cis* retinal in the RPE is then transported back into the photoreceptor OS by IRBP.

1.1.3.3 The opsins

Each photopigment in the mammalian retina consists of an opsin protein bound to a chromophore (11-*cis* retinal) (Rodieck, 1998). Opsins are 7-transmembrane G-protein-coupled receptors (GPCRs), which, depending on the type that is expressed, confers unique spectral properties to retinal cells (Terakita, 2005). Multiple cell types in the mammalian retina express opsins. However, a subset of opsins are exclusively expressed in photoreceptors. In the human retina, for instance, rhodopsin is the only opsin expressed by rod photoreceptors (Palczewski, 2006) whereas cone photoreceptors express three different opsins, giving rise to three cone subtypes. Based on their spectral sensitivities, there are; short-wavelength (S) cones which maximally absorb light in the blue range, medium-wavelength (M) cones which maximally absorb light in the green range and long-wavelength (L) cones which maximally absorb light in the red range of the spectrum. These three spectral sensitivities exhibited by cones make diverse colour vision possible (Imamoto and Shichida, 2014). A subset of RGCs express another opsin called melanopsin (Provencio et al., 1998, Provencio et al., 2000). This subset of RGCs are intrinsically photosensitive, unlike other RGCs, and are known to be crucial in the photo-entrainment of circadian rhythms among other functions (Do and Yau, 2010, Foster et al., 2020).

1.1.4 Mouse versus human retina

Histological studies in non-primate mammals, such as rodents, have been useful for our current knowledge and understanding of the mammalian retina. The retina of the domestic mouse (Mus musculus) has been a useful resource in understanding the cyto-architecture of the mammalian retina as well as serving a useful model for developing new therapeutic treatments for retinal disease (Chang, 2013). Though it remains an invaluable model, it is important to note that the mouse retina differs from the human retina in a number of ways. The mouse retina is smaller in size and number of cells compared to that of human, lacks a fovea and expresses only two of the three cone subtypes found in human retina. The mouse retina also has a centrally placed optic nerve and has a different distribution of rods and cones across the retina compared to the human retina (Volland et al., 2015). Despite these

differences, the similarities between the mouse and human retina, as well as genetic make-up, makes it an invaluable resource in studying the mammalian retina, especially as human retina tissue is not easily available (Veleri et al., 2015).

1.1.5 Fovea and macular in the human retina

Due to its accessibility, the mammalian retina is one of the most studied parts of the nervous system, and has served as the basis for much of the understanding we have of the central nervous system (London et al., 2013). Using non-invasive techniques such as funduscopy and fundus imaging, the macroscopic structure of the human retina can be visualised *in vivo*. In a fixated eye, light is directed to the fovea, a specialised nonvascular pit located within the area of the central retina called the macula (Figure 1.5). The macula is a centralised area of about 4.5-6mm diameter situated between the superior and inferior arcades at the posterior pole of the retina and approximately 3mm from the optic disc (Hildebrand and Fielder, 2011, Polyak, 1941). The centre of the fovea is densely packed with cone photoreceptors, is devoid of rods and is responsible for central high acuity daylight vision. The cell bodies of cones in the fovea are outwardly displaced, leading to the formation of a pit in cross-section known as the fovea pit which is responsible for a bright reflection commonly called the foveal reflex seen when light is fixated at the fovea. The density of cones reduce as you move from the centre of the fovea towards the peri-foveal retina whilst the density of rods increases as you move from the fovea towards the peripheral retina, reaching a maximum at the mid-periphery before declining with increasing eccentricity (Curcio et al., 1990).

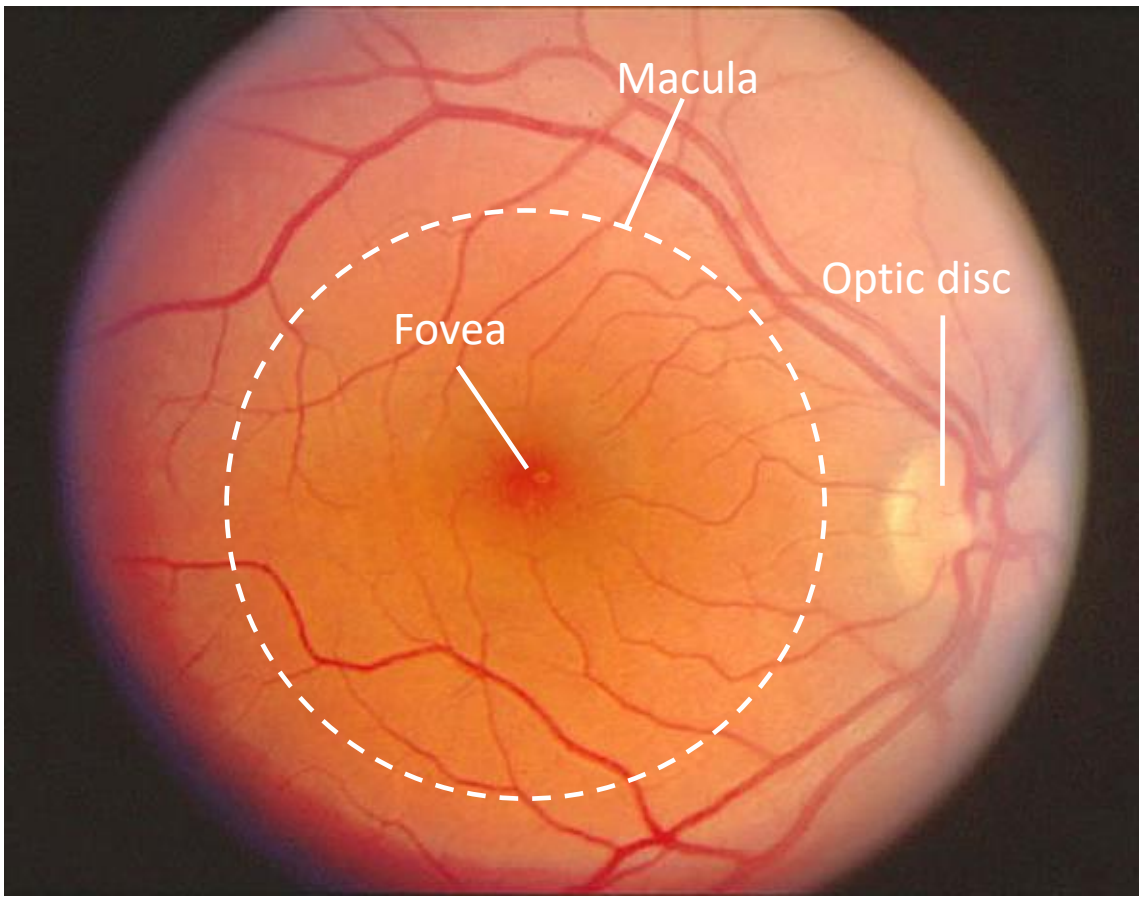


Figure 1.5. The human fundus. A colour photograph of the human fundus from the right eye as seen with an ophthalmoscope. The optic nerve head, macula area and the fovea are indicated. Image was adapted from Webvision (http://webvision.med.utah.edu/).

1.1.6 Retinal structure and function in humans

1.1.6.1 Assessing retina structure

To assess the retina structure in health and disease, clinicians have employed non-invasive imaging techniques such as scanning laser ophthalmoscopy to measure fundus autofluorescence (FAF) (Delori et al., 1995) and spectral-domain optical coherence tomography (SD-OCT) (Hee et al., 1995), with each having unique clinical advantages. Fundus autofluorescence, resulting from accumulation of retinoid by-products in the RPE and photoreceptors (Flynn et al., 2014), serves as a measure of the age and state of health of the retina, with reduced FAF being reportedly associated with retinal disease such as Stargardt disease and age-related macular degeneration (AMD) (von Rückmann et al., 1995, Ach et al., 2014). As a more recent technique, SD-OCT uses infrared interferometry to take high-resolution cross-sectional images of the layers of the retina *in vivo* corresponding to the layers of the retina seen in *in vitro* histological studies, and has been used to measure structural changes related to retinal disease and therapeutic interventions (Jaffe and Caprioli, 2004, Murthy et al., 2016).

1.1.6.2 Assessing retina function

To assess retinal function, Ophthalmologists have often used both subjective and objective techniques in humans. Subjective methods include using reading charts to measure central visual acuity (VA) and contrast sensitivity. Objective tests include static and dynamic perimetry, which map the extent of visual fields and sensitivity, and electroretinography (ERG) which measures differences in electrical responses in photoreceptor cells after exposure to light (Gabriel et al., 2012). These tests are often used, in combination with structural measures like funduscopy and SD-OCT, to take quantitative measures of retinal function. Particularly, ERGs have been useful in diagnosing retinal dystrophies that involve the photoreceptors due to the ability to measure cone and rod responses separately, as well as distinguishing outer retina responses from that of the inner retina (Robson et al., 2003). In addition, ERG is used as the preferred and appropriate objective technique to measure photoreceptor function in animal models of retinal dystrophies to monitor disease progression and/or response to therapeutic interventions (Collin et al., 2020a).

1.2 Inherited retinal dystrophies (IRDs)

Inherited retinal dystrophies (IRDs) are a heterogeneous group of disorders that affect the human retina, resulting in varying consequences on the vision and lives of those affected. Collectively, IRDs are known to affect 1 in 2000-3000 individuals and are estimated to affect over 2 million people worldwide, despite being individually classified as rare conditions (Hartong et al., 2006). Most IRDs result from dysfunction in the photoreceptor cells, leading to slow but progressive degeneration of these cells and accompanying visual deficits. Presently, most IRDs do not have a cure and as many manifest bilaterally in affected individuals, the resultant impact is not only limited to compromised visual function but also a low quality of life (Yioti et al., 2017). Currently, data on the economic burden of IRDs worldwide is lacking. However, recent reviews into the cost implications of IRDs on affected individuals, their families, friends and wider society, reported them to be an estimated £42.6 million and £523.3 million for the Republic of Ireland (ROI) and the United Kingdom (UK), respectively, in the year 2019 (Galvin et al., 2020).

IRDs can be classified in several ways, including by their mode of inheritance, whether they are accompanied by extraocular manifestations or by the cells they primarily affect in the retina. Based on mode of inheritance, IRDs can be autosomal dominant in which affected individuals inherit a mutation in one copy of the disease-causing gene, autosomal recessive in which affected individuals inherit mutations in both copies of the disease-causing gene, or X-linked in which the defective gene is located on the X-chromosome. Other non-Mendelian forms of inheritance such as mitochondrial inheritance (Jarrett et al., 2010) and digenism (Kajiwara et al., 1994) have also been reported in some IRDs. However, reduced penetrance, *de novo* mutations and other disease-modifying factors can make the inheritance patterns of some IRD cases not clearly deducible (Cooper et al., 2013, Acuna-Hidalgo et al., 2016). On the basis of whether they elicit only visual symptoms or visual with extraocular manifestations, IRDs can be either syndromic or non-syndromic. Non-syndromic IRDs, such as retinitis pigmentosa (RP), constitute the majority of IRDs and disease manifestation is usually restricted to the retina. Syndromic IRDs include Usher syndrome, which affects hearing and vision, and Bardet-Biedl

syndrome, which affects vision, metabolic systems, central nervous systems and causes congenital physical malformations such as polydactyly (Werdich et al., 2014). On the basis of the retinal cell type affected, IRDs can be broadly grouped into the following: those where rod photoreceptors are primarily affected such as RP; those where cone photoreceptors are the first cells to show dysfunction such as achromatopsia; those that are generalised diseases of the photoreceptors and/or retinal pigment epithelium (RPE) such as Leber congenital amaurosis (LCA) and choroideremia, and those that primarily affect specific areas of the retina, for example Stargardt disease which affects the macula.

Recent advances in clinical and molecular genetic techniques have enabled the unravelling of the genetic factors underpinning some of these conditions. To date, RetNet (a web-based database for genes involved in IRDs) lists over 270 genes and over 300 genetic loci identified to be associated with various forms of IRDs (RetNet; https://sph.uth.edu/retnet/home.htm). The majority of IRDs, such as RP, have been found to be monogenic, where the condition is caused by mutations in a single gene, whereas other complex forms , such as age-related macular degeneration (AMD) are caused by a combination of genetic, lifestyle and environmental factors (Haddad et al., 2006). However, monogenic forms of IRDs exhibit a high level of both genetic and phenotypic heterogeneity. Thus, mutations in different genes could present the same phenotype while mutations in the same gene could elicit different phenotypes in different individuals (Berger et al., 2010). These factors result in significant overlaps between different disorders, often making clear-cut diagnosis difficult.

For the purpose of this thesis, further discussion on specific IRDs will be limited to Retinitis pigmentosa and Macular dystrophies which are the conditions found in the families recruited in the present study.

1.2.1 Retinitis pigmentosa

Retinitis pigmentosa (RP; MIM #268000) refers to a group of heterogeneous IRDs characterised by the gradual but progressive dysfunction of rod photoreceptors in the retina. The term was first used by the Dutch ophthalmologist Franciscus Cornelius Donders in 1857 (Donders, 1857). RP patients often report, as an early symptom, reduction in ability to see in dim light (especially at night), a symptom

commonly referred to as nyctalopia. Nyctalopia in RP patients is often accompanied by the progressive loss of peripheral vision, which results in tunnel vision and can lead to complete loss of vision overtime. Deriving its name from the classical presentation of pigmentary deposits on fundus examination, the term 'retinitis pigmentosa' often gives an indication that the condition has more of an inflammatory origin than degenerative. RP cases are typically characterised by degeneration of rods in the early years of the condition followed by degeneration of cones. Notwithstanding, there is growing evidence of the role of inflammatory mechanisms in the pathogenesis of RP (de Hoz et al., 2016, Yoshida et al., 2013, Noailles et al., 2016).

1.2.1.1 Epidemiology and inheritance

RP is the most common form of the IRDs with an estimated 1.5 million affected individuals worldwide (Verbakel et al., 2018). A prevalence rate of 1 in 3500 has reported (Hartong et al., 2006), although this is highly variable depending on the geographical location of the population being described, with some reports predicting a frequency from as low as 1 in 9000 in Korean populations (Na et al., 2017) to as high as 1 in 750 in Indian populations (Nangia et al., 2012). Most RP cases are non-syndromic with only 20-30% being syndromic. RP is inherited as dominant, recessive and X-linked fashion with approximately 15-25% being autosomal dominant (adRP), 15-20% being recessive (arRP) and 5-15% as X-linked (xlRP). A proportion of RP cases (40-50%) are of unknown inheritance patterns, largely attributable to single isolated cases or the lack of documented/appropriate family history (Dias et al., 2018).

1.2.1.2 Symptoms, diagnosis and management

The clinical presentation of RP is highly variable with varying ages of onset, severity and disease progression. This variable expressivity emanates mainly from the vast number of genes that cause the same disease in different people. Some patients with RP experience symptoms in early childhood whereas others may not have any symptoms until adulthood (Hartong et al., 2006). Typically, night blindness and dysfunction in dark adaptation begin in early adolescence in classical forms of RP. Onset

of mid-peripheral visual field scotomas vary from early childhood to young adulthood, depending on the inheritance pattern and genes involved. For instance, in xlRP cases with mutations in the *RPGR* gene, severe mid-peripheral degeneration may be present in early childhood with or without macula involvement (Sharon et al., 2003), compared to adRP forms resulting from mutations in the *TOPORS* gene in which degenerations is not present until adulthood (Latasiewicz et al., 2017). Except in a minority of cases such as arRP cases with *PROM1* mutations (Zhang et al., 2007), visual acuity, a quantitative measure of central retina and macular, is usually preserved until the late stages of the condition when secondary cone degeneration occurs, resulting in a decline in visual acuity. Symptoms such as photopsia, photophobia and dyschromatopsia may also be experienced by individuals with advanced forms of RP (Verbakel et al., 2018).

At onset, many RP cases may not present observable pathologies upon fundus examinations despite the presence of symptoms like difficulty with dark adaptation. However, in established cases, fundus examination may reveal classical abnormalities typical of the condition, although there is usually variability in the pattern and extent due to duration and the genetic mutations involved. These classical features include: thinning of the neural retina resulting from the loss of photoreceptors, with accompanying loss of the OLM and ellipsoid zone (EZ) bands upon SD-OCT imaging (Liu et al., 2016); pigmentary deposits called 'bone spicules' in the mid-periphery resulting from invasion of perivascular sites in the inner retina by RPE cells following photoreceptor degeneration (Li et al., 1995); attenuated retinal blood vessels which may result from, among other factors, autoregulated vasoconstriction in response to a hyperoxic environment due to death of the oxygen-consuming photoreceptor cells (Padnick-Silver et al., 2006, Penn et al., 2000); and a waxy pallor optic disc possibly resulting from increased light reflectance caused by glial cell formation in and on top of the optic disc (Hwang et al., 2012, Szamier, 1981).

Management of RP cases currently involves genetic counselling and testing, clinical monitoring, visual rehabilitation, and social support. Current genetic testing procedures seek to provide a molecular diagnosis. Although obtaining a genetic diagnosis could be crucial in predicting visual prognosis and to

determine heritability, this is not possible in all cases. Frequent follow-up by clinicians is recommended, as serial fundus examination and imaging are useful in determining the rate of visual decline and effects of disease modifying factors. Occasionally, cases of RP have associated ocular conditions such as cataracts, refractive errors or cystoid macular oedema (CMO), some of which are often amenable to treatment and could be identified and remedied during continuous clinical monitoring (Verbakel et al., 2018). In advanced forms of RP where visual loss is profound, low vision and social support services are useful in enabling patients to make optimal use of their residual vision.

1.2.1.3 Molecular basis of RP

Since the first genetic cause of RP was reported in 1990 (Dryja et al., 1990a) to now, more than 80 genes have been identified as responsible for non-syndromic RP (RetNet; https://sph.uth.edu/retnet/home.htm). The increasing list of genes implicated in RP is indicative of the heterogeneous nature of the condition, in common with other IRDs. Proteins encoded by genes implicated in RP can be broadly grouped into those involved in the normal function of the phototransduction cascade or visual cycle, those required for retina cell or tissue development and integrity, transcription factors or those that are part of the splicing machinery. Examples of genes directly involved in the phototransduction cascade (Figure 1.3) implicated in RP include rhodopsin (*RHO*) (Dryja et al., 1990a), subunits of rod cGMP phosphodiesterase (*PDE6A*, *PDE6B* and *PDE6G*) (Tsang et al., 2008, Dvir et al., 2010), subunits of the cyclic nucleotide-gated (CNG) channels in rods (*CNGA1* and *CNGB1*) (Katagiri et al., 2014, Bareil et al., 2001), a subunit of transducin (*GNAT1*) (Méjécase et al., 2016) and the gene encoding rod arrestin (*SAG*) (Nakazawa et al., 1998). Genes involved in the visual cycle have been implicated in RP including *RPE65* (Morimura et al., 1998, Bowne et al., 2011) and *LRAT* (Ruiz et al., 2001), which are crucial in re-isomerising all-*trans* retinal to 11-*cis* retinal in order to enable phototransduction to recur (see Figure 1.3 and Figure 1.4). The ability to transport proteins and molecules across the connecting cilium of rod and cone photoreceptors and the maintenance of outer segment structural integrity are also crucial in the normal functioning of the retina. Approximately 30 genes involved in intraflagellar transport (IFT) across the connecting cilium

(see 1.1.2.3) have been implicated in RP (Verbakel et al., 2018) and include *IFT40* (Xu et al., 2015) and *IFT172* (Bujakowska et al., 2015) which are involved in forming complexes A and B, respectively, necessary for transporting ciliary cargo (Bhogaraju et al., 2013). Proteins linked to the maintenance of photoreceptor outer segment implicated in RP include the fascin homolog 2 (FSCN2) protein (encoded by the *FSCN2* gene) and TUB like protein 1 (TULP1 – encoded by the *TULP1* gene) which are involved in bundling and crosslinking of F-actin filaments necessary for the formation of nascent discs at the base of the outer segments (Saishin et al., 2000, Xi et al., 2005). Other genes involved in outer segment and disc morphogenesis implicated in RP include *PRPH2* (peripherin-2), *PROM1* (prominin-1), *CDHCR1* (Cadherin-related family member 1) and *RP1* (Goldberg et al., 2016).

Many of the genes implicated in RP are expressed exclusively in the photoreceptors. Although there are some that have been found to be expressed in other tissues outside the eye, but mutations in them only lead to classical RP. Typical examples are the ubiquitously expressed pre-mRNA processing factors 3, 4, 6, 8 and 31 (*PRPF3, PRPF4, PRPF6*, *PRPF8* and *PRPF31*) genes which encode components of spliceosomes but mutations in them lead to cases of non-syndromic RP (Tanackovic et al., 2011). It is interesting how mutations in ubiquitously expressed genes such as *PRPF31* only result in retinal disease. A possible explanation is the stressful demands placed on the retinal cell machinery by photoreceptor outer segment turnover rate (Tanackovic et al., 2011, Mordes et al., 2006).

RP cases are genetically and phenotypically heterogeneous. Mutations in the same gene can cause different phenotypes. For example, mutations in *RHO* can cause both autosomal dominant and autosomal recessive forms of RP (Rosenfeld et al., 1992, Dryja et al., 1990b) as well as autosomal dominant congenital stationary night blindness (CSNB) (Dryja et al., 1993). Figure 1.6 provides a summary of the genetic heterogeneity in RP and other IRDs.

Although RP is known to be a rod-dominant disorder, where cell dysfunction and death occur primarily in rods, the condition is known to result in the secondary loss of cone photoreceptors, evidenced by the eventual reduction in central visual acuity and loss of central visual field in RP patients. Understanding the exact mechanisms by which cone cells die in RP could be a good avenue for

developing cone-preserving therapies for treating RP. As such, various theories have been explored in attempts to explain the mechanism by which this secondary loss of cones occur (Narayan et al., 2016). These include the proposition that degenerating rods produce toxins (rod-derived toxins), which are released into the extracellular space between photoreceptors or across the gap junctions between them (Ripps, 2002). Another proposed theory suggests that the absence of trophic factors, such as rod-derived cone viability factors (rdCVF), whose availability in the neural retina becomes depleted due to continuous death of rod photoreceptors during RP may account for cone cell loss (Léveillard et al., 2004). Other hypotheses include starvation in cones (Punzo et al., 2009) and oxidative stress (Shen et al., 2005). However, further investigations to elucidate the exact mechanisms involved in the secondary cone cell death seen in RP is required.

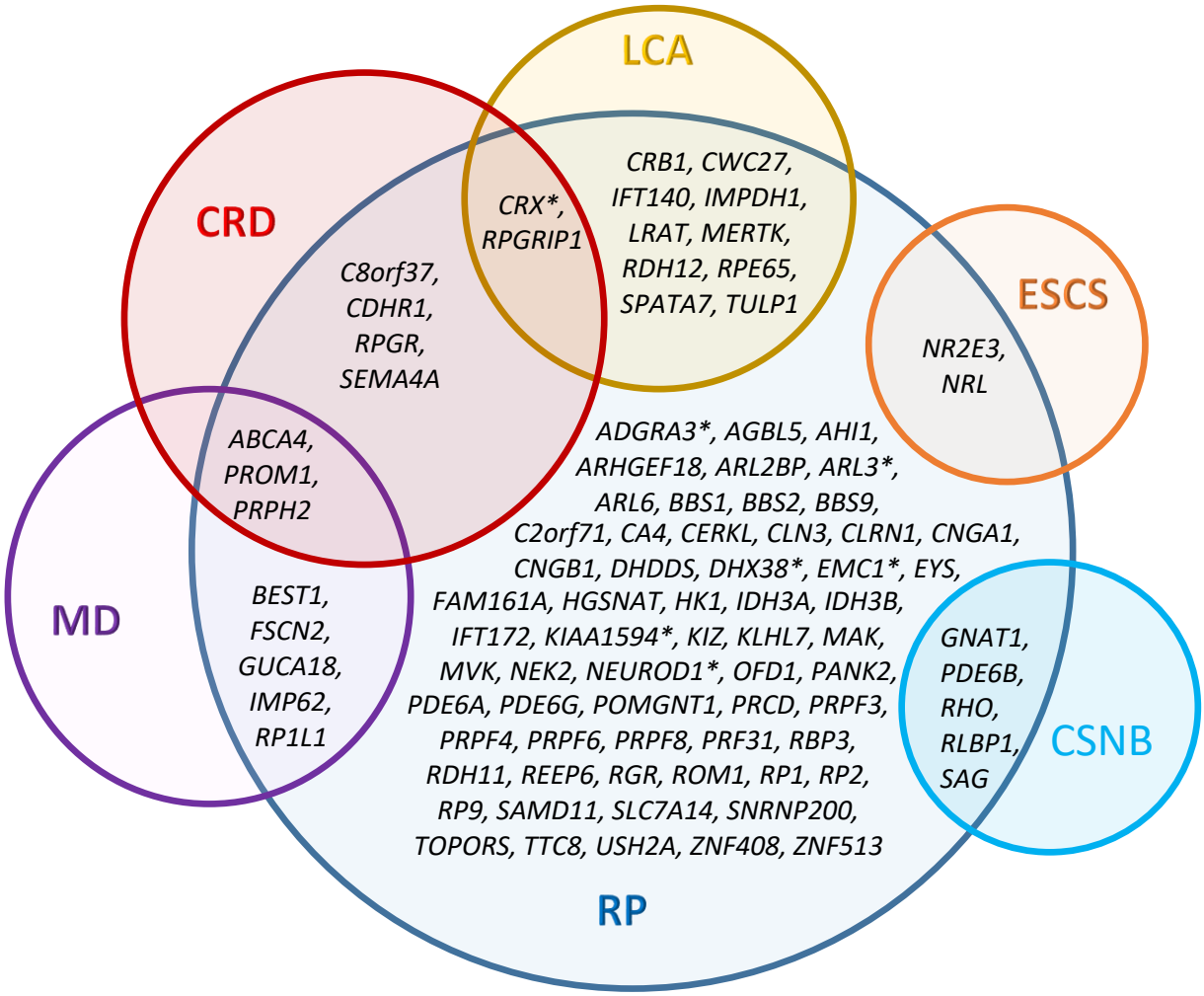


Figure 1.6. Venn diagram showing the genetic overlap between RP and other IRDs. Adapted from (Verbakel et al., 2018). Genes shown in overlapping areas of diagram indicate are genes with mutations that cause those different phenotypes. Gens with asterisk represent candidate genes for non-syndromic RP. CRD = cone-rod dystrophy; CSNB = congenital stationary night blindness; ESCS = enhanced S-cone syndrome; LCA = Leber congenital amaurosis; MD = macular dystrophy; RP = retinitis pigmentosa.

1.2.2 Macular dystrophies

Macular dystrophies (MDs) refer to a group of heterogeneous IRDs primarily characterised by bilateral dysfunction in the photoreceptor cells in the central retina (Figure 1.5) leading to reduction or complete loss of central vision. Effects of most MDs are bilateral, relatively symmetrical and often have profound impact on patients as they primarily affect their central vision at the onset. Although atrophy from most MDs is localised to the macular, there have been suggestion of more widespread retinal involvement due to psychophysical, electrophysiological and/or histopathological changes recorded from other parts of the retina (Rahman et al., 2020). The term 'macular dystrophies' is often confused with the more common age-related macular degeneration (AMD). Although they often present with similar symptoms such as reduced visual acuity and eventual loss of central vision, MDs more appropriately refer to macular abnormalities resulting from genetic mutations whereas AMD refers to reduction or loss in central vision resulting from age-related abnormalities in the macular (Lim et al., 2012). In spite of the clear genetic involvement in MDs, recent studies have also identified various genes believed to work together with environmental and lifestyle factors to increase susceptibility to AMD in a polygenic multi-factorial fashion (Haddad et al., 2006). How these factors work together to cause AMD are still being investigated. Typically, MDs have ages of onset ranging from early childhood to early adulthood whereas AMD is usually diagnosed in late adulthood. However, there are recent reports of late onset MD cases (Westeneng-van Haaften et al., 2012), further indicating the underlying complexities of IRDs.

The most common forms of MDs include Stargardt disease (OMIM #248200), Best disease (OMIM #607854) and Sorsby fundus dystrophy (OMIM #136900). Stargardt disease (STGD1) is the commonest form of macular dystrophy with juvenile onset, and has a reported incidence of 1 in 8,000 to 10,000 (Blacharski, 1988). It is progressive and is normally diagnosed in late childhood or early adulthood. There have been, however, recent reports of late onset forms with a better visual prognosis compared to the early onset forms (Westeneng-van Haaften et al., 2012). STGD1 symptoms usually include bilateral reduction in central vision, colour deficiency (dyschromatopsia) and central scotomas

resulting from progressive central vision loss often in the first two decades (Fujinami et al., 2013a), though some forms can present with foveal-sparing (Fujinami et al., 2013b). Fundus examination in patients with early STGD1 might reveal a near-normal fundus. As such, examination with advanced imaging modalities such as FAF and OCT (see 1.1.6.1) are useful in revealing macular atrophy with characteristic accumulation of lipofuscin in the RPE and photoreceptor inner segments around the macula (commonly called retinal flecks), atrophy of the RPE and choroidal vasculature, and macular photoreceptor loss (Mellough et al., 2009). Best disease (BD), also referred to as Best vitelliform macular dystrophy (BVMD), is the second most common MD with an incidence of 1 in 10,000 usually inherited in an autosomal dominant fashion (Schachat et al., 2017). Although BVMD usually has childhood to early adolescence onset, there is often no manifest atrophy and visual acuity could remain preserved until the fifth decade, usually leading to late diagnosis. The early stage is characterised by the classical bilateral symmetrical yolk-like appearance (vitelliform) of the fovea and the late stage usually presents with atrophic maculopathy or choroidal neovascularisation (Rahman et al., 2020). BVMD is mostly bilateral, with the exception of a few reported cases of unilateral maculopathy (Arora et al., 2016). Other common forms of MDs can be found in Table 1.1.

1.2.2.1 Molecular basis of the Macular dystrophies

Stargardt disease (STGD1) is inherited in an autosomal recessive manner and is caused by mutations associated in the *ABCA4* gene, which encodes the ABCR protein. ABCR plays a crucial role in the translocation of all-*trans* retinal from photoreceptor OS into neighbouring RPE cells to be converted into 11-*cis* retina during the visual cycle (see 1.1.3.2). Many of the mutations in the *ABCA4* gene result in the impaired translocation of all-*trans* retinal and its derivatives out of the photoreceptor OS, leading to the formation of bisretinoids which become deposited as lipofuscin in RPE cells during phagocytosis of photoreceptor outer segment discs (Sparrow et al., 2012). Accumulation of lipofuscin in RPE cells leads to their dysfunction and ultimate death followed by dysfunction and death of adjacent photoreceptor cells (Westeneng-van Haaften et al., 2012). Beside ABCA4-associated autosomal recessive STGD1, there have been reports of 'STGD-like' autosomal dominant forms caused

by mutations in *ELOVL4* (STGD3, OMIM #600110) and *PROM1* (STGD4, OMIM #603786) genes (Zhang et al., 2001, Yang et al., 2008). As an indication of the heterogeneous nature of the IRDs, mutations in *ABCA4* and *PROM1* have also been reported to cause cone-rod dystrophy and RP (Cremers et al., 1998b, Martínez Mir et al., 1998) (Figure 1.6). To date, all BVMD cases have been associated with mutations in the *BEST1* gene which encodes the bestrophin 1 protein that functions as a transmembrane oligmeric chloride channel in RPE cells (Petrukhin et al., 1998). In common with other IRD genes, mutations in *BEST1* have been found to be responsible for other IRD phenotypes including adult vitelliform MD (Krämer et al., 2000), autosomal dominant vitreoretinochoroidopathy (Yardley et al., 2004) and autosomal recessive bestrophinopathy (ARB) (Burgess et al., 2008). Other genes implicated in in MDs are listed in Table 1.1.

1.3 Approaches to identifying IRD genes (Past to present)

In common with other inherited disorders, various genetic approaches have been used to identify the underlining causative genes in IRDs. The techniques involved have evolved over the years from traditional linkage mapping and positional cloning of disease genes through candidate gene analysis to more recent high throughput technologies such as whole genome and whole exome sequencing. In this section, the discussion will focus on how approaches such as linkage analysis, positional cloning, candidate gene analysis, functional gene identification approach and next generation sequencing have been employed, either individually or in combination, to identify disease loci and causative genes for various IRDs.

Table 1.1. Summary of common macular dystrophies.

Disease name	OMIM #	Genes	Inheritance
Stargardt disease (STGD1)	248200	*ABCA4*	AR
Stargardt-like dominant macular dystrophy (STGD3)	600110	*ELOVL4*	AD
Stargardt-like dominant macular dystrophy (STGD4)	603786	*PROM1*	AD
Best disease	607854	*BEST1*	AD
Retinoschicis	312700	*RS1*	XL
Pattern dystrophy	169150	*PRPH2, BEST1, CTNNA1*	AD
Sorsby fundus dystrophy	136900	*TIMP3*	AD
Autosomal dominant drusen	601548	*EFEMP1*	AD

AR = autosomal recessive; AD = autosomal dominant; XL = x-linked

1.3.1 Linkage analysis

Genetic linkage analysis is a technique used to determine the location of a disease gene on a particular chromosome. The technique makes use of the physical distance (recombination fraction) between specific genome-wide markers to calculate the probability that two markers that are close to each other in the genome will remain together during meiosis. Genetic markers are specific DNA sequences whose position and inheritance pattern in the genome can be tracked. Common examples used include restriction fragment length polymorphisms (RFLPs), polymorphic short interspersed tandem repeats (microsatellite markers) and single nucleotide polymorphisms (SNPs) (Vignal et al., 2002). The probability that two markers are linked is determined by a logarithm of odds (LOD) score, calculated as the Log_{10} ratio of the likelihood that a disease locus and a given genomic marker are linked versus the likelihood that they are not linked. Generally, a LOD score of 3 or more is considered a significant prediction of genetic linkage between two loci on the same chromosome. This technique is especially useful in determining shared chromosomal loci that segregate with a condition in families with multiple affected and unaffected members from multiple generations. Linkage analysis was used as the main technique in the second half of the twentieth century to determine the chromosomal location of traits that had no known chromosomal locations. It was used to successfully map the chromosomal loci of several IRDs including the RP1 locus on chromosome 8 (Blanton et al., 1991) and the RP11 locus on chromosome 19 (Al-Maghtheh et al., 1994). The identification of a disease locus by linkage analysis was then followed by examination of the DNA sequence at that locus for markers, genes or mutations that could account for the disease using positional cloning. More recently, however, the mapping of the human genome through the Human Genome Project (HGP) (Collins and Galas, 1993, International Human Genome Sequencing, 2004) has made it easy to identify the genes that lie in an already mapped disease locus. An example is the identification of the RP1-like (*RP1L1*) gene responsible for macular dystrophy following high throughput linkage mapping that mapped the disease locus to chromosome 8p22-p23 (Akahori et al., 2010). It is, however, not always possible that the causative gene in the

mapped disease locus can be identified, as there remain a number of IRD disease loci for which the causative genes are yet to be identified. Examples of such include the adRP RP22 locus which maps to chromosome 16p12.1 – p12.3 (Finckh et al., 1998), RP29 locus which maps to chromosome 4q32-q34 (Hameed et al., 2001) and the RP63 locus that maps to chromosome 6q23 (Kannabiran et al., 2012), for which the causative genes have yet to identified. Although this technique has proved useful over the years, the occurrence of phenocopies (affected relatives with the same phenotype but different genetic cause) and non-penetrance (individuals with the genetic mutation but not showing the phenotype) can interfere with the linkage analysis process (Khan et al., 2019).

1.3.2 Positional cloning

Positional cloning, also called "reverse genetics", is a technique used to identify disease-causing genes based solely on their location in the genome. Having successfully linked a disease trait in a family or a set of families to a particular genetic locus, specific markers within the disease locus were identified and the DNA sequence around these markers were closely examined, with the aim of identifying the causative gene without prior knowledge of what sort of gene or protein they are looking for. This technique was used to successfully identify the choroideremia (*CHM*) gene (Cremers et al., 1990) five years after the disease locus had been linked to a marker (DXYS1) on the X chromosome at Xq13-21 (Nussbaum et al., 1985). The years in-between the mapping of the disease locus and the discovery of the *CHM* gene involved a large body of work that led to the identification of a specific marker, DXS165, that was deleted in choroideremia patients, around which was found the causative gene (Cremers et al., 1987). This technique was very laborious and required several years of work, especially as an identified disease locus could contain over 100 genes and often required further studies and/or families with the same condition to either enable the further refinement of the locus to a smaller area on the chromosome or to more specific markers within the mapped locus. This was exacerbated by the fact there was little knowledge of the genetic map of the human genome in the era prior to the

human genome project during which the entire human genome was mapped (Collins and Galas, 1993, Collins et al., 1998).

1.3.3 Candidate gene approach

The candidate gene approach of identifying disease-causing genes, also called "forward genetics", refers to a relatively recent approach in which geneticists prioritise a gene as a candidate for a disease based on its known function and screen individuals and families with a common trait for potential mutations. The inception of the HGP came with the development of more detailed genetic maps and tools that made it possible for geneticists to know the sequence of genes, which previously, were very difficult to find. As such, scientists used factors such a gene's position in the genome, where the gene product is expressed, the potential biological pathway(s) it could be involved in, and the physiology of the disease to prioritise a gene or a set of genes as good candidates for particular conditions. The use of the candidate gene approach in IRD gene identification was proposed by Ted Dryja in 1990 (Dryja, 1990) as a better alternative to the then conventional positional cloning approach using the following observations he had made: that missense mutations had been identified in the rod opsin gene in some patients with adRP (Dryja et al., 1990b); that the gene that was responsible for the *rds* (retinal degeneration slow) mouse model encoded the rod disc protein, peripherin (PRPH2) (Connell et al., 1991); and the fact that the β subunit of rod cGMP-phosphodiesterase was responsible for the autosomal recessive retinal degeneration found in the *rd* mouse (Bowes et al., 1990). He, therefore, reasoned that genes known to be involved in the phototransduction pathway, vitamin A metabolism and the structure of the disk membrane could be good candidates for IRDs and suggested screening for mutations in these genes in various IRD patients.

Although this approach had been, unconventionally, used earlier by a group who identified the cone opsin genes (Nathans et al., 1986b) and further demonstrated that mutations found in these genes were responsible for some forms of colour blindness in Caucasian males (Nathans et al., 1986a), the approach gained prominence as the main method for identifying many IRD genes during the human

genome project era. The increased use of the candidate gene methodology between the time when rhodopsin was identified as causative for adRP and the completion of the HGP in 2003 is evidenced by the fact that the majority of the IRD genes (40 out of the 48) identified during this period employed this approach (Broadgate et al., 2017). By screening for mutations in genes known to be involved in photoreceptor structure and function in large numbers of unrelated patients with a common phenotype, using PCR and sequencing methods like Single Strand Conformational Polymorphism Electrophoresis (SSCP) and Sanger sequencing, scientists were able to identify several causative genes for IRDs. Typical among these include the screening of the gene encoding the alpha subunit of rod-cGMP channel (*CNGA1*) in 173 unrelated patients with arRP, which identified five mutations responsible for the arRP in four unrelated families (Dryja et al., 1995)

1.3.4 Functional candidate gene identification approach

The use of the candidate gene methodology led to the identification of genes whose involvement in the retina and photoreceptors were already known. To identify other genes with no known functional roles in the retina but could be potential candidate for IRDs, methods such as the study and generation of animal models of IRDs, microarrays and serial analysis of gene expression (SAGE) experiments were used. These varying and unconventional approaches led to the identification of several genes which, otherwise, would not have been obvious candidates for IRDs. Given the fact that there are many naturally occurring mouse models of IRDs and the relative ease of being able to manipulate the genome of the mouse to produce transgenic mice, scientists have extensively used mouse models of IRDs to identify genes that are involved in the development, maintenance and function of the retina. The identification of the β subunit of the rod cGMP phosphodiesterase (*PDE*) and *PRPH2* as functional genes in the rod photoreceptor was made possible through studies in the naturally occurring *rd* mouse (Bowes et al., 1990) and *rds* mouse (Travis et al., 1989, Connell et al., 1991), respectively. The HGP, which also mapped the genome of other organisms, made it easy to identify human orthologues of genes from mutant animals that could also be of importance in humans. An example is how the *Myo7a*

gene responsible for the shaker-1 (*sh-1*) mouse model with hearing impairment (Gibson et al., 1995) led to the mapping of the *MYO7A* gene in humans to a locus on chromosome 11 that had been linked to Usher syndrome (USH1B). This led to the screening and identification of *MYO7A* mutations in nine families with USH1B (Weil et al., 1995).

At the same time, microarray analysis has been used to study the patterns of gene expression in wild type mice and naturally occurring or transgenic mouse models of retinal diseases with the aim of identifying novel genes and pathways that are down regulated or upregulated and could be crucial in normal retinal function (Holt et al., 2015). Comparing retinal gene expression to gene expression in brain and liver of wild type mice using microarrays, Hackam and colleagues identified 733 genes that were preferentially expressed in the retina (Hackam et al., 2004). Another study that compared retinal gene expression between $Rho^{-/-}$ mice and their wild type littermates identified a group of genes that were differentially expressed in the retina, one of which was the *Impdh1* gene (Kennan et al., 2002). This led to the identification of the human *IMPDH1* gene, which mapped to an already identified adRP locus (retinitis pigmentosa 10 – RP10), as a functional candidate gene for RP. Screening of the gene in four different RP10 families, including the original family used mapping the RP10 locus, revealed mutations in the gene which segregated with the adRP in these families (Bowne et al., 2002, Kennan et al., 2002). In addition, the SAGE technique, a technique that uses small tags to obtain a snapshot of the total messenger RNA (mRNA) population of a gene of interest in a tissue, has been used to quantify the expression of particular genes or their transcripts at different developmental time points in the retina. Notable among these is a study by Blackshaw and colleagues (2001) in which they used SAGE analysis on developing mice retinae from embryonic day 12.5 (E12.5) to postnatal day 6.5 (P6.5) and adult mice retina to identify numerous rod-specific genes out which 264 were uncharacterised (Blackshaw et al., 2001). A similar SAGE study on human retina identified 89 retina-specific genes of which 14 had already been implicated in retinal disease (Sharon et al., 2002). Together, these approaches used over the years in identifying functional retinal genes have made available a database of retina-specific genes which serve as a good resource for identifying candidate genes for IRDs (Holt et al., 2015).

1.3.5 Next generation sequencing

Next generation sequencing (NGS), a massively parallel sequencing technology (Behjati and Tarpey, 2013), is probably the most revolutionary molecular biology technique developed in the twentieth century. Compared to Sanger sequencing (Sanger et al., 1977), which is considered the gold standard for DNA sequencing and was used for the HGP (International Human Genome Sequencing, 2004), NGS technology is cost effective and allows the sequencing of many samples at the same time. Developed in 2007, the technology can be used to sequence both coding and non-coding regions of the genome, known as whole genome sequencing (WGS) or to target and sequence only the coding regions of the genome, known as whole exome sequencing (WES). NGS technology has been employed in the identification of disease-causing genes across a wide range of diseases including IRDs. Across all diseases, the application of NGS as a tool for disease gene identification has been described as a powerful resource for identifying genes which, otherwise, would not have been linked to those diseases (Broadgate et al., 2017). The large amount of data generated during NGS and the high level of bioinformatic analysis required have often posed a challenge in applying this technology to disease gene identification. However, there has been a growing number of bioinformatic tools and sequencing databases that enable the effective analysis of the numerous variants generated during NGS. Table 1.2 summarises a list of tools and resources used in analysing NGS data.

The first application of NGS to identify a novel IRD gene was reported in 2010 in a study investigating two Dutch families with familial exudative vitreoretinopathy (FEVR [OMIM #133780]) in whom linkage analysis had mapped the disease locus to a region on chromosome 7 (Nikopoulos et al., 2010). Family one had been mapped to a 40Mb region whereas family two had been mapped to a smaller 17Mb region that was located within the 40Mb region of family one. NGS was used to examine 338 genes in the 40Mb linkage region in family one and three genes were prioritised as candidates in this family. Of these three prioritised candidates, two of them (*PTCD1* and *ZAN*) were found to be located outside the smaller linkage region of family two, leaving only one gene *TSPAN2* (tetraspanin 2) with a variant shared between the two families. Using Sanger sequencing, this variant (c.709G > C; p.(Ala237Pro))

was found to be present in all affected individuals in these two families but not in the unaffected family members. In this same study, Nikopoulus and colleagues found the p.Ala237Pro variant in two other FEVR families and identified a second variant (p.(Gly188Arg)) in a fifth family (Nikopoulos et al., 2010). Although this was the first time *TSPAN2* was reported as a novel causative gene for FEVR, the findings were corroborated by another study (Poulter et al., 2010) while a previous study had predicted *TSPAN2* to be involved in the same pathway as previously identified FEVR genes (Junge et al., 2009).

Since the pioneering study by Nikopoulus and colleagues (Nikopoulos et al., 2010), several groups involved in identifying novel genes for IRDs have applied NGS in their studies. So far, over 64 novel IRD genes have been identified using both WGS and WES (source: RetNet: https://sph.uth.edu/retnet/home.htm). Another useful application of NGS in IRDs has been the identification of multiple novel causative variants in various IRD genes, as it offers the opportunity of sequencing the genomes of large cohorts of patients in parallel as well as covering areas of the genome such as intronic and intergenic regions which could not be easily done using previous methods (Carss et al., 2017). These findings and the increasing application of the NGS technology in IRDs is indicative of its unrivalled potential in the quest to identify novel IRD genes.

1.3.6 Establishing a variant as pathogenic

With the advent of high throughput sequencing methods such as NGS and their application in genetic testing and candidate gene identification, it is common to identify several genetic variants in every patient tested. This makes it difficult to distinguish pathogenic variants from non-pathogenic (benign) variants. Although guidelines published by the American College of Medical Genetics and Genomics (ACMG) and Association for Molecular Pathology (AMP) (Richards et al., 2015) and the Association of Clinical Genetics Scientists (ACGS) (Ellard et al., 2020) have been widely accepted, the lack a standardised methods of determining the pathogenicity of variants have prompted different labs or groups involved in such studies to employ a combination of methods, experience and clinical judgements in their assessments. The following are key considerations commonly employed in classifying a variant as pathogenic (Zhang et al., 2020, McCarthy and Mendelsohn, 2016):

1. The effect of the variant on protein structure or function

The likelihood of a variant to be pathogenic is higher if identified in protein coding regions of genes compared to non-coding regions. Variants that result in stop-gain, stop-lost, frameshift insertion/deletion and splice site disruption, collectively called 'loss of function' (LOF) variants, are considered more likely to be pathogenic (McCarthy and Mendelsohn, 2016). Various bioinformatic programs have been developed which use information such as protein function, conservation, structure and location of the variant to estimate the effect variants may have on the structure and function of proteins. Such programs include CADD, PhyloP, Polyphen, SIFT, MutationTaster, AlphaFold, mCSM and many others (see Table 1.2). Although these algorithms are only predictive and require experimental validation, they are increasingly becoming more useful in determining pathogenicity of genetic variants (Ganakammal and Alexov, 2019).

2. The allele frequency of the variant in the diseased and non-diseased populations

The presence of a variant in multiple unrelated individuals with a similar disease phenotype and its absence in an unaffected population is a valuable resource in determining the pathogenicity of variants. As such, a variant identified to be present in an unaffected population, especially for a disease that is known to be fully penetrant, is considered less likely to be pathogenic. Variants considered as rare variants with allele frequency less than the disease frequency, the allelic heterogeneity and mode of inheritance, are considered to be more pathogenic. In IRDs for instance, variants with less than 1% allele frequency in conditions with dominant mode of inheritance are considered to be more likely to be pathogenic. Publicly available genomic databases such as gnomAD (gnomad.broadinstitute.org/) are therefore useful in determining the allele frequencies of variants to help estimate the likelihood of their pathogenicity (Zhang et al., 2020).

3. Evidence from genetic linkage or co-segregation studies

One of the direct and important ways of determining the pathogenicity of a variant is identifying that a variant that is inherited with a specific disease phenotype among members of a family (co-

segregation) or is present in unrelated individuals with a common phenotype (association). However, obtaining family information is not always possible, prompting many variants to re-evaluated when data from more family members become available (McCarthy and Mendelsohn, 2016).

4. Effect of variant from *in vitro* and *in vivo* experimental studies

Whereas bioinformatic or *in silico* programs are useful in predicting the effect a variant could have on the structure and/or function of a protein, obtaining an observable phenotype from *in vitro*, *ex vivo*, or *in vivo* experiments consistent with the disease under investigation is the best way to confirm the pathogenicity of a particular variant. Experiments involving cell-based assays and animal models bearing the variant in question could provide excellent evidence in support of a variant being pathogenic.

5. Previous classification or report of variant as pathogenic

With several genetic studies ongoing around the world, various databases or platforms have been created as a repository for variants identified in various studies. These publicly/commercially available repositories enable the curation and sharing of pathogenic variants which can be accessed by other clinicians and researchers. Examples of such databases are the Human Gene Mutation Database (HGMD; http://www.hgmd.cf.ac.uk/ac/index.php) and ClinVar (https://www.ncbi.nlm.nih.gov/clinvar).

Table 1.2. Tools and resources used in the analysis of WES and WGS data. Table adapted from (Broadgate et al., 2017).

Tool/resource	Type	Description	URL	Reference
HPO	*Literature support*	The **H**uman **P**henotype **O**ntology (HPO) aims to provide a standardized vocabulary of phenotypic abnormalities encountered in human disease.	http://human-phenotype-ontology.github.io/	(Köhler et al., 2013)
OMIM	*Literature support*	**O**nline **M**endelian **I**nheritance in **M**an (OMIM) contains human genes and genetic disorders and traits, with particular focus on the molecular relationship between genetic variation and phenotypic expression	http://omim.org/	
PubMed	*Literature support*	A free search engine accessing a comprehensive list of references and abstracts on life sciences and biomedical topics	www.ncbi.nlm.nih.gov/pubmed	
RetNet	*Literature support*	Connects causative genes and loci to inherited retinal diseases using published reports	https://sph.uth.edu/retnet/	
dbSNP	*Allele frequency*	Contains polymorphisms including SNPs, small-scale multi-base deletions or insertions and short tandem repeats or STRs.	http://www.ncbi.nlm.nih.gov/snp/	
gnomAD (formerly ExAC)	*Allele frequency*	Contains 125,748 WES and 15,708 WGS data from unrelated individuals sequenced as part of various disease-specific and population genetic studies.	https://gnomad.broadinstitute.org/	
ENSEMBL	*Allele frequency and variant consequence*	Contains annotated genes, computes multiple alignments, predicts regulatory function and collects disease data	http://www.ensembl.org/index.html	(Yates et al., 2015)
Kaviar	*Allele frequency*	Contains both WGS and WES data from over 70,000 individuals (13.2K WGS, 64.6K WES). It excludes cancer genomes but includes some data from cell lines and individuals affected by disease. Relatedness in the data has not been removed yet	http://db.systemsbiology.net/kaviar/	(Glusman et al., 2011)

UCSC	*Allele frequency and variant consequence*	A genome browser that displays tracks from assembly contigs and gaps, mRNA and EST alignments, multiple gene predictions, cross-species homologies, single nucleotide polymorphisms, sequence-tagged sites, radiation hybrid data and transposon repeats. It also includes data from The Encyclopedia of DNA Elements (ENCODE) that focuses on functions of non-coding regions.	https://genome.ucsc.edu/index.html	(Kent et al., 2002)
1000 Genomes	*Allele frequency*	Contains WGS data from over 1000 individuals. Due to poor depth, it only considers variants of at least 1% in the populations studied	http://www.1000genomes.org/	(Auton et al., 2015)
CADD	*Variant consequence*	Score variants based on simulated evolutionary changes. It takes annotations from the Ensembl Variant Effect Predictor, ENCODE, UCSC that span a wide range of data types including conservation metrics like GERP, phastCons, and phyloP; functional genomic data like DNase hypersensitivity and transcription factor binding; transcript information like distance to exon-intron boundaries or expression levels in commonly studied cell lines; and protein-level scores like Grantham, SIFT, and PolyPhen.	http://cadd.gs.washington.edu/	(Kircher et al., 2014)
pMut	*Variant consequence*	Predicts possible impact of an amino acid substitution based on the use of different kinds of sequence information to label mutations, and neural networks to process this information	http://mmb.pcb.ub.es/PMut/	(Ferrer-Costa et al., 2005)
Polyphen	*Variant consequence*	Predicts possible impact of an amino acid substitution on the structure and function of a human protein using straightforward physical and comparative considerations. It is now superseded by Polyphen-2	http://genetics.bwh.harvard.edu/pph2/	(Adzhubei et al., 2010)
SIFT	*Variant consequence*	Predicts whether an amino acid substitution affects protein function based on sequence homology and the physical properties of amino acids.	http://sift.bii.a-star.edu.sg/	(Kumar et al., 2009)
MutationTaster	*Variant consequence*	Predicts disease-causing potential of variants based on evolutionary conservation, splice-site changes, loss of protein features and changes that might affect the amount of mRNA. Unlike Polyphen, SIFT and CADD, it also evaluates indel changes.	http://www.mutationtaster.org/	(Schwarz et al., 2010)

1.4 Therapeutic approaches for IRDs

The eye has several advantages over other organs or systems in the human body when it comes to clinical trials for new therapeutics. First, the eye can be accessed easily due to its location, has clearly defined anatomical compartments and is immune-privileged (ability to tolerate antigens with limited immune or inflammatory response) (Zhou and Caspi, 2010). Due to the bilateral nature of the eyes, they enable intra-subject control during therapeutic trials as one eye receives the treatment while the other eye serves as a control. In addition, there is relative ease in monitoring and measuring outcomes of interventions with non-invasive techniques such as ERG, visual acuity and other visual tasks. Finally, the relative closeness of the retinal anatomy and physiology between model organisms like mouse and dogs to humans and the existence of several IRD models, offers a great resource for preclinical testing in such disease models before their subsequent application in human subjects (Veleri et al., 2015, Beltran, 2009).

The complex and heterogeneous nature of IRDs has posed a major challenge to the development of treatments that will be effective across a range of IRDs or a range of patients with a common phenotype. However, scientific advances in the understanding of the retina in health and disease have enabled IRDs to receive a considerable amount of attention from clinicians and researchers aiming to develop therapies that halt the disease, slowing down their rate of progression or rescue photoreceptor function in affected individuals. Current avenues being explored in developing therapeutic interventions for the various IRDs include gene therapy, gene editing, RNA-based therapies, optogenetic, neuroprotective, cell replacement and pharmacological approaches (Georgiou et al., 2021, Vázquez-Domínguez et al., 2019). The principles and current applications of the three main gene-based therapeutic approaches, gene therapy, gene-editing and antisense oligonucleotides, as well as stem cell therapy are described below.

1.4.1 Gene therapy

Gene therapy, also referred to as gene replacement therapy, is an approach that involves the use of viral and non-viral shuttles to deliver wild-type copies of the defective genes into cells with the aim that they will produce normal copies of the proteins whose absence leads to disease. The basic principles of gene therapy were conceptualised in the early 1980s (Anderson, 1984) and have since been applied in a wide range of diseases including IRDs. The reported success of gene therapy in the naturally occurring canine model of Leber congenital amaurosis 2 (LCA2; *RPE65*$^{-/-}$), in which visual restoration was seen in the long term (Acland et al., 2001), led to a pioneering human trial. In the first human trial reported by Bainbridge and colleagues in 2008, wild-type copies of the human *RPE65* gene (*hRPE65*) were introduced, through sub-retinal injection, into the retina of three RPE65-associated LCA2 patients using adeno-associated viral vectors (AAV) serotype 2 (AAV2). Visual assessment in patients who received the treatment indicated improvement in visual acuity in the treated eye six months post-treatment (Bainbridge et al., 2008). A similar study looking at the long-term effect of AAV2-hRPE65 treatment in LCA2 patients reported improvement in visual function and retinal sensitivity in the eye that received the treatment compared to the untreated eye three years post-treatment, though not all participants saw these improvements (Testa et al., 2013). These were followed by effective phase 3 trials (Russell et al., 2017) leading to approval of one such treatment called Voretigene neparvovec marketed by Spark Therapeutics with the trade name Luxturna™, for the treatment of LCA2 in the USA.

Development and trials of another gene therapy treatment, NSR-REP1, for REP-1 associated choroideremia, led by Nightstar Therapeutics, has also reached an advanced stage (MacLaren et al., 2014, Edwards et al., 2016, Xue et al., 2018). Presently, over 30 gene therapy trials for various IRDs including RP, Stargardt disease and achromatopsia, ongoing across the globe (www.clinicaltrials.gov). This demonstrates the potential of this therapeutic approach for IRDs. Although the results are promising, gene therapy for IRDs is plagued with various challenges. These include vector choices for the optimal expression of target genes, limited duration of gene expression and continued

degeneration of photoreceptors after treatment (Jacobson et al., 2015). Again, the current gene therapy approaches are more applicable to autosomal recessive conditions resulting from biallelic null or nonsense mutations. Application to autosomal dominant conditions would require different methods, involving inactivation of the mutated version of the gene to avoid interference with the normal copy (Wilson and Wensel, 2003, Farrar et al., 2012).

1.4.2 Gene editing

The potential to precisely edit genomic DNA, made possible by recent advancements in molecular biology, has been explored as a therapeutic avenue for many genetic diseases including IRDs. Current techniques involve targeting and correcting disease-causing mutations into wild-type sequences in the genome to enable cells to produce their own functional protein naturally and permanently. Two approaches currently being explored are correcting the disease-causing mutation directly in the patient's retina or an *ex vivo* approach in which the mutation is corrected in patient-derived cells which are then transplanted back into the retina of the patient (Sanjurjo-Soriano and Kalatzis, 2018). Gene editing techniques are based on the discovery that cells, aided by specific endonucleases, are able to repair double-stranded breaks (DSB) in their DNA either by joining the two ends of the DNA molecule together using a mechanism called nonhomologous end-joining (NHEJ) or by using the sister chromatid as template, a process called homology directed repair (HDR). Endonuclease molecules that have been explored in gene editing for IRDs include Zinc-finger nucleases (ZFNs), transcription activator like effector nucleases (TALENs), and the clustered regularly interspaced short palindromic repeats/CRISPR-associated protein 9 (CRISPR/Cas9) system (Gaj et al., 2013). ZFNs and TALENS were mostly used in pioneering works (Schierling et al., 2012, Greenwald et al., 2010), whereas the CRISPR/Cas9 system is currently seen to be more advantageous due to its relative simplicity, higher efficacy and the ability to edit multiple genes at the same time when combined with guide RNAs (gRNAs) (Hsu et al., 2013, Peddle and MacLaren, 2017).

Presently, several studies have shown the potential of applying gene-editing technologies in various models of IRDs (Quinn et al., 2021). In fact, more recently, EDIT-101, a candidate genome-editing therapeutic for *CEP290*-associated Leber congenital amaurosis 10 (LCA10) was shown to be safe and effective in animal models of the disease (Maeder et al., 2019) and has since received approval from the FDA for phase 1 and 2 human clinical trials (NCT03872479; www.clinicaltrials.gov). In another study evaluating the effect of subretinal application of the CRISPR/Cas9 system on a rat model of adRP carrying a mutation in *Rho*, specific disruption of the mutation with associated halt in the progression of the condition as well as improved visual function in the rat was reported (Bakondi et al., 2016). These and several other preclinical studies (Zhu et al., 2017, Suzuki et al., 2016, Cai et al., 2019) illustrate the potential of gene editing tools in treating several forms of IRDs. Especially, the ability of gene editing to effect permanent ablation of mutations and to be applied on large gene fragments, which are major challenges of the current gene replacement therapy, makes it a promising technology. However, the ethics surrounding editing the human genome and the adverse effects that may result from potential off-target effects of the gene editing tools need to be fully understood (Smith et al., 2017, Quinn et al., 2021).

1.4.3 Antisense oligonucleotide therapy

Antisense oligonucleotides (ASOs), discovered over four decades ago, are oligodeoxynuleotides that bind to target mRNA sequences through complementary base pairing to directly regulate protein expression (Stephenson and Zamecnik, 1978). Advances in molecular biology have led to the design of synthetic ASO molecules which work by a range of mechanisms to regulate protein expression including endonuclease-mediated transcript knockdown, alteration of pre-mRNA splicing by sterically blocking splicing factors, and blocking of mRNA translation by inhibiting ribosome recruitment (Bennett and Swayze, 2010, Crooke, 2017). Consisting of a short, single-stranded oligodeoxynucleotides of typically 8-50 nucleotides, several studies have explored the therapeutic potential of ASOs that target disease-related genes in various disease areas including inflammatory diseases, neurological and ophthalmic diseases (Rinaldi and Wood, 2018, Scoles et al., 2019, Ferenchak

et al., 2021). Effective outcomes from clinical trials led to the first FDA-approved 21-mer ASO therapy (Formivirsen) for treatment of cytomegalovirus retinitis in patients with HIV/AIDS (Vitravene Study Group, 2002). Since then, several other therapies have received approval for clinical application in conditions such as spinal muscular atrophy and Duchenne muscular dystrophy (Doxakis, 2021).

The therapeutic potential of ASOs have also been explored in various inherited retinal diseases, with some promising results. One of such is the QR-110 ASO therapy for *CEP290*-associated LCA10 targeting the c.2991+1655A>G mutation (p.Cys998X). Following feasibility studies in humanised Cep290 mouse models (Garanto et al., 2016, Dulla et al., 2018) and in patient IPSC-derived retinal organoids (Parfitt et al., 2016), the QR-110 compound (also called Sepofarsen) is currently undergoing phase I/II clinical trials (Trail ID: NCT03140969 and NCT03913130; clinicaltrials.gov). Reports of effective patient outcomes upon intravitreal administration in the phase I/II trails (Cideciyan et al., 2021, Cideciyan et al., 2019) have led to an ongoing phase II/III trail (Trail ID: NCT03913143; clinicaltrials.gov). Other ASO therapies for IRDs are also undergoing clinical trials including the QR-1123 for *RHO*-associated dominant RP (Trial ID: NCT04123626; clinicaltrials.gov) and the QR-421a for RP due to mutations in the Usher syndrome type 2 (USH2A) gene (Trial ID: NCT03780257; clinicaltrials.gov). Although these therapies are yet to receive FDA approval for clinical use in IRDs, the promising results reported so far indicate ASOs have promising therapeutic potential in treating IRDs (Xue and MacLaren, 2020).

1.4.4 Stem cell therapy

Most IRDs result from the progressive loss of retinal cells, mainly the photoreceptors and RPEs. With cells of the adult retina lacking regenerative ability, several efforts aimed at transplantation of stem cells into the diseased retina with the hope of regenerating the retinal tissue and to restore visual have been explored. Cells used in most of the retinal disease studies include retinal progenitor cells (RPCs) derived from human embryonic stem cells (hESCs), induced pluripotent stem cells (iPSCs) and mesenchymal cells (Sharma and Jaganathan, 2021). In a preclinical study exploring the use of stem cells in treating dry forms of AMD, subretinal transplantation of hESC-derived RPE cells into mouse models of AMD led to development of a new RPE monolayer on top of the native RPE layer after

treatment (Petrus-Reurer et al., 2020, Mazzilli et al., 2020). Other preclinical studies involving hESCs in retinal organoids and non-human primates showed integration of injected cells into the RGC layers with transplanted cells having RGC markers (Wang et al., 2019), and reported increase in ONLs (Wang et al., 2020), respectively. Similarly, preclinical studies involving subretinal transplantation of iPSC-derived retinal cells in animal models of RP have reported promising outcomes, including establishment of new connections between transplanted cells and bipolar cells, delayed thinning of ONL and improved ERGs (Tu et al., 2019, Zhu et al., 2020). Presently, there are several ongoing clinical trials involving the use of stem cells in treating retinal diseases in humans. One of such trials (ID: NCT02286089; clinicaltrials.gov), is a phase I/II trial involving the use of hESC-derived RPE cells in treating patients with dry AMD and geographic atrophy in which long-term survival of transplanted cells as well as improvement in RPE layers have been reported (Riemann et al., 2020, Banin et al., 2019). Two other clinical trials for AMD (ID: NCT01344993; clinicaltrials.gov) and Stargardt's disease (ID: NCT01345006; clinicaltrials.gov) have also reported improvement in visual acuity of patients receiving the treatment without any evidence of adverse proliferation (Schwartz et al., 2015). Outcomes, challenges and prospects of currently ongoing stem cell therapy clinical trials for retinal disorders have been extensively reviewed elsewhere (Sharma and Jaganathan, 2021, Hinkle et al., 2021).

1.5 Thesis rationale

Taken together the IRDs affect a significant number of people worldwide, have an undesirable impact on the quality of life of those affected and their families and pose huge economic burdens to society. As discussed above (see 1.3), recent advancements in clinical and molecular biology techniques have enabled the identification and characterisation of the majority of genes underlying these conditions. Identifying the genetic underpinnings of IRDs is important in several ways: (i) it enables clinicians to offer tailored genetic counselling to patients and their families; (ii) it enables the prediction of the course of some disease phenotypes; (iii) and it enables patients to be educated on any disease-modifying habits. The identification of novel IRD genes, which previously had no known functions in the retina, have also led to better understanding of retina function. Importantly, the identification of underlying genetic causes of IRDs have enabled the elucidation of the disease mechanisms involved in many IRDs and has directed the therapeutic approach for developing treatments for these conditions.

Currently, most of the treatments being developed for various IRDs are based on their underlying genetic/molecular diagnosis. However, the advent of genetic testing for IRDs has revealed that there are many existing cases and families with IRDs that do not have variants in the currently known IRD genes, an indication that there are other genetic causes yet to be identified. The argument that there are other causative genes of IRDs yet to be identified is further supported by the current existing gap between identified genes and mapped loci for IRDs as documented by RetNet (https://sph.uth.edu/retnet/sum-dis.htm). Moreover, it is known that in spite of the high number of genes identified to be responsible for RP, for instance, these genes are responsible for only 50-60% of all RP cases (Wang et al., 2014), underlining that there are novel genetic loci that are yet to be identified.

The need for studies seeking to identify novel disease genes for IRDs has never been more important than present because without a genetic diagnosis, these individuals and their families cannot benefit from the gene-based treatments currently being developed. Therefore, in this project, we seek to use NGS to analyse the genomes of individuals with IRDs of unknown genetic causes with the aim of

identifying novel candidate genes for IRDs. We will use a range of molecular biology techniques to examine the expression and potential role of these genes in the retina and how their dysfunction may influence retinal disease.

1.6 Aims

Aim 1: To identify candidate genes in patients with IRDs

Selected individuals from families with dominant forms of IRDs whose conditions have no known genetic cause yet will undergo whole exome sequencing (WES) and will be followed by analysis of WES data using bioinformatic tools and gene sequencing databases. Rare variants will be prioritised for each family and examined for co-segregation with the condition in each of the families using DNA samples from other affected and unaffected family members. Genes with variants segregating with the condition in each family that are expressed in the mammalian retina, upon examination, will be considered as candidate gene(s) and prioritised for further examination.

Aim 2: To determine expression, localisation and binding partners of candidate genes in the retina

The candidate genes identified in Aim 1 will be examined further for their expression in the mammalian retina, including identifying which transcripts are present in the retina, investigating protein localisation in the mouse retina using appropriate antibodies, and examining co-localisation of the proteins with their reported binding partners in the mouse retina using immunohistochemistry.

Aim 3: To examine the effect of the mutations in the candidate genes on protein expression and function using *in vitro* and *in vivo* models

Wild-type and mutant expression constructs carrying the variant identified in candidate genes will be transfected into *in vitro* cell models to examine the potential effect on the expression and subcellular localisation of the related proteins. Retina from transgenic mice lacking the candidate gene will be examined for potential retinal phenotypes that may be attributable to the loss of the candidate gene.

2 Materials and Methods

2.1 Materials

2.1.1 Reagents

The majority of reagents used were supplied by Sigma (UK), Bioline (UK), Invitrogen (UK) and Qiagen (UK).

2.1.2 Enzymes

All restriction enzymes were supplied along with the appropriate buffer by Invitrogen (UK) and New England Biolab (UK) Ltd.

2.1.3 Electrophoresis

Agarose was supplied by Geneflow (UK). The ethidium bromide and the 1kb plus ladder used as size marker were from Invitrogen (UK).

2.1.4 DNA Sequencing

Sanger sequencing was carried out by Source Bioscience (UK) and Next Generation sequencing was carried out by Sequencing Facility, University of Leeds (UK) (http://dna2.leeds.ac.uk/genomics/).

2.1.5 Bacterial Strains

The DH5α and JM109 bacterial strain competent cells for transformation reactions were supplied by Invitrogen (UK) and Promega (UK), respectively.

2.1.6 Oligonucleotide primers

All custom-designed oligonucleotide primers were obtained from Sigma, UK.

2.1.7 Equipment and Apparatus

2.1.7.1 Pipettes

Pipettes were supplied by Gilson (UK).

2.1.7.2 Spectrophotometry equipment

Nanodrop spectrophotometer (ND1000) was supplied by (Thermo Fisher Scientific, USA).

2.1.7.3 Thermal Cycler

The T-100 Thermocycler was supplied by BioRad (UK).

2.1.7.4 Electrophoresis

Electrophoresis Tanks were supplied by Geneflow (UK). The U:Genius UV Transilluminator was supplied by Syngene (UK).

2.1.7.5 Cell Culture

Flow hood (Mars, LaboGene, Denmark). Incubator (Thermo Fisher Scientific, USA)

2.1.7.6 Tissue Preparation

Dissection microscope and Cryostat were supplied by Leica Biosystems (UK).

2.1.7.7 *Imaging*

LSM-710 confocal microscope was supplied by Zeiss (Germany). The EVOS FL Auto 2 Cell Imaging System was supplied by Thermo Fisher Scientific (UK). Odyssey Fc imaging system was supplied by LI-COR Inc. (USA).

2.1.7.8 *Software*

ImageJ software used for image processing was obtained from the National Institute of Health (USA). Image Studio software used for capturing and analysing western blot images was obtained from LI-COR Inc. (USA).

2.2 Buffers, Solutions, Media and Kits

2.2.1 General stock reagents

Molecular grade water was supplied by VWR (UK). 100% ethanol was supplied by Thermo Fisher, USA. 50X Tris/acetate/ETDA (TAE) buffer was supplied by Thermo Fisher, USA.

2.2.2 Preparation of Plasmid DNA

LB Broth

Luria-Bertani (LB) Broth was prepared by dissolving 25g of LB powder (Sigma, UK) in 1L of distilled water, which was then autoclaved. Each litre of LB broth contains 10g Bactotryptone, 10g NaCl and 5g Yeast Extract. Appropriate volume of antibiotic was added to the autoclaved LB Broth once cooled.

LB-agar plates

LB-agar plates (1.5% (w/v)) were prepared by dissolving 15g of bacteriological agar (Sigma, UK) in 1L of LB Broth, which was then autoclaved. The LB-agar was then cooled to approximately 55°C before adding the appropriate volume of antibiotic and, X-gal and IPTG where required. Approximately 20mL

of LB-agar was then poured into 10cm petri dishes. Plates were allowed to cool and solidify for 30-60mins before inverting and storing in sealed plastic bags at 4°C until required.

Ampicillin (100mg/mL)

Ampicillin sodium salt (Sigma, UK) was dissolved to 100mg/mL stock in distilled water, filter sterilised through a 0.22µm filter and stored at -20°C in 1mL aliquots. Stock was used at a final concentration of 100µg/mL (i.e. 1µl per mL media).

Kanamycin (50mg/mL)

Kanamycin sulphate (Sigma, UK) was dissolved to 50mg/mL stock in sterile distilled water, filter sterilised through a 0.22µm filter and stored at -20°C in 1mL aliquots. Stock was used at a final concentration of 15µg/mL (i.e. 1µl per mL media). Stored at -20°C in 1mL aliquots.

IPTG (Isopropylthio-ß-D-galactopyranoside)

Isopropylthio-ß-D-galactopyranoside (Bioline, UK) was dissolved to 25mg/mL stock in distilled water, filter sterilised through a 0.22µm filter and stored at -20°C in 1mL aliquots. Stock was used at a final concentration of 25µg/mL (i.e. 1µl per mL media). Stored at -20°C in 1mL aliquots.

X-Gal (5-Bromo-4-chloro-3-indolyl-β-D-galactopyranoside)

5-Bromo-4-chloro-3-indolyl-β-D-galactopyranoside (Bioline, UK) was dissolved to 20mg/mL stock in dimethyl formamide (DMF), was NOT filter sterilised and stored at -20°C in 1mL aliquots. Stock was used at final concentration of 20µg/mL (i.e. 1µl per mL media). Stored at -20°C in 1mL aliquots under dark room conditions (foil-wrapped).

SOC Media

SOC (super optimal broth with catabolite repression) media was supplied by Life Technologies (UK), and has the following composition: 2% tryptone, 0.5% yeast extract, 10mM NaCl, 2.5mM KCl, 10mM MgCl2, 10mM $MgSO_4$, and 20mM glucose

QIAGEN Buffer P1, Resuspension Buffer

50mM Tris·Cl, pH 8.0, 10mM EDTA, 100µg/mL RNase A.

QIAGEN Buffer P2, Lysis Buffer

200mM NaOH, 1% SDS.

QIAGEN Buffer N3, Neutralisation Buffer

3M potassium acetate, pH 5.5.

QIAGEN Buffer EB, Elution Buffer

10mM Tris·Cl, pH 8.5.

2.2.3 Preparation of RNA

TRIzol™

Trizol used for RNA extraction from animal tissue was supplied by Invitrogen (UK).

QIAGEN Buffer RLT, Lysis Buffer

Company keeps the composition confidential.

2.2.4 Preparation of cDNA

qScript cDNA Synthesis kit, QuantaBio (USA)

Components: 5X concentrated master mix containing: titered primer blend (oligo dT(20) and random hexamer), qPCR-optimized dNTP blend and flexible magnesium titration**;** 20X concentrated qScript reverse transcriptase**;** Nuclease-free water.

2.2.5 PCR purification and Gel extraction

Buffer PE

PE Buffer concentrates in QIAquick PCR purification and QIAquick Gel extraction kits were diluted with 100% ethanol before use, following manufacturer's instructions (48mL of was added for every 6mL of Buffer PE concentrate).

2.2.6 Gel Electrophoresis

TAE buffer

Tris-acetate-EDTA (TAE) buffer was prepared by diluting 50X TAE Buffer (Thermo Fisher, UK) in double distilled H_2O (ddH_2O) in a 1:50 dilution, with final concentration (1X TAE) being 40mM Tris, 20mM acetic acid, 1mM EDTA.

Orange G Dye

15% (*w*/v) ficoll, 0.25% (*w*/*v*) Orange G dissolved in 1X TAE.

2.2.7 Immunohistochemistry / Immunocytochemistry

Phosphate-Buffered Saline (PBS)

To make 1X Phosphate-Buffered saline (PBS) solution, one tablet (1g) of PBS (Sigma, UK) was dissolved in 200mL of ddH_2O to yield 0.01M phosphate buffer, 0.0027M Potassium chloride and 0.137 M sodium chloride, pH 7.4 at room temperature, and autoclaved.

PBST

0.1% PBST - 0.1% Triton X-100 in PBS

0.3% PBST - 0.3% Triton X-100 in PBS

4% Paraformaldehyde (PFA)

4% (*w*/*v*) paraformaldehyde (PFA) solution in PBS was prepared from a 16% PFA stock solution (Sigma, UK). Preparation was carried out in the fume hood for immediate use and waste disposed appropriately.

30% Sucrose solution (for cryopreservation)

30% sucrose solution (*w*/*v*) was prepared by dissolving 15g of sucrose (Sigma, UK) in 50mL of PBS and placed on a heated magnetic stirrer until fully dissolved. The solution was stored at 4°C.

Normal Goat and Donkey Serum (NDS/NGS)

2% or 10% Normal Donkey Serum and Normal Goat Serum (Abcam, UK) (*v*/*v*) was diluted in 0.1% PBST, aliquoted and stored at -20°C until required.

2.2.8 Western immunoblotting

Radioimmunoprecipitation Assay (RIPA) Buffer

Radioimmunoprecipitation Assay (RIPA) Buffer was supplied by Sigma (UK) as ready-to-use solution containing 150mM NaCl, 1.0% IGEPAL CA-630, 0.5% sodium deoxycholate, 0.1% SDS, 50 mM Tris, pH 8.0.

Laemmli Buffer

2X Laemmli Buffer was supplied by Sigma (UK) comprising 4% SDS, 20% glycerol, 10% 2-mercaptoethanol, 0.004% bromphenol blue and 0.125 M Tris HCl, pH approx. 6.8.

1X Tris Buffered Saline (TBS)

1X Tris Buffered Saline (TBS) was made by diluting 10X TBS Concentrate (Sigma) with appropriate amounts of ddH_20. 1X TBS contained 20mM Tris, 0.9% NaCl and pH approximately 7.4

Wash Buffer - TBS-Tween-20 (0.1%)

1mL Tween 20 was added to 1L of 1X TBS to prepare 0.1% TBST to be used as wash buffer.

Blocking Buffer (3% BSA in 0.1% TBST)

Blocking buffer containing 3% Bovine Serum Albumin (BSA) was made by dissolving 30g of BSA powder (Sigma, UK) in 1L of 0.1% TBST. Blocking buffer was filtered using a 0.22µm polyethersulfone membrane in 500 mL Stericup (Sigma, UK). Buffer was stored at -20°C in 50mL aliquots until required.

1X Running Buffer for SDS-PAGE

1x Running Buffer was made by diluting 100mL of Ultrapure 10x Tris/Glycine/SDS (Geneflow, UK) with 900mL of ddH_2O. Each bottle of Tris-Glycine-SDS PAGE Buffer (10X) contains 0.25M Tris base, 1.92M glycine, and 1% (*w*/*v*) SDS.

2.2.9 Cell culture

Complete Cell Culture medium for MDCK II and HEK239T Cells

500mL Dulbecco's Modified Eagle Medium – High glucose (DMEM HG, Sigma, UK)

10% (*v*/*v*) Fetal Bovine Serum (FBS; Gibco, UK),

1% (*v*/*v*) Penicillin/Streptomycin (Sigma, UK)

1% (*v*/*v*) L-glutamine (Sigma, UK)

1% (*v*/*v*) Non-essential amino acids (NEAA; Gibco, UK).

2.2.10 Kits used

QIAprep Miniprep Spin Kit	Qiagen, UK
QIAquick PCR Purification Kit	Qiagen, UK
QIAquick Gel Extraction Kit	Qiagen, UK
Qiagen RNeasy Mini Kit	Qiagen, UK
pGEM-T Easy Vector System	Promega, UK
SMARTer RACE 5'/3' kit	Takara Bio Inc., USA

qScript cDNA synthesis kit	QuantaBio, USA
ZymoPURE II Plasmid Midiprep kit	Zymo Research, USA
Pierce BCA Protein Assay Kit	Thermo Fisher Scientific, USA
Hematoxylin &Eosin Stain kit	Abcam, UK
Q5 Site-directed mutagenesis kit	New England Biolabs, UK

2.3 Methods

This section contains a general description of the principles and protocols for all techniques used in this thesis. Specific details of protocols are provided in the relevant Methods section of each experimental chapter.

2.3.1 Patient cohort

Patients used in this study were recruited by Prof. Susan Downes in the Oxford Eye Hospital as part of an on-going multi-site study into retinal dystrophies by the United Kingdom Inherited Retinal Dystrophy Consortium (UKIRDC). All patients gave written informed consent and the study protocols adhered to the tenets of the Declaration of Helsinki, with ethics approval from the Local Ethics Committee of the Oxford Eye Hospital. Patients included in this study were diagnosed with either autosomal dominant retinitis pigmentosa or autosomal dominant macular dystrophy and had previously undergone standard NHS genetic testing on the appropriate disease panel but were found not to have mutations in genes on the panels. Probands and relatives (affected and unaffected) for each participating family underwent extensive clinical examination including best-corrected visual acuity (BCVA), dilated fundus examination, fundus autofluorescence (FAF) imaging (Spectralis, Heidelberg Engineering Inc., Carlsbad, CA), electroretinography (ERG), and spectral-domain optical coherence tomography (SD-OCT; Spectralis, Heidelberg Engineering Inc.).

2.3.2 DNA

2.3.2.1 Genomic DNA extraction

Genomic DNA extraction was performed by the Oxford Regional Genetics Laboratory (ORGL) using Qiagen Autopure LS and EZ1 systems (Qiagen (UK) from peripheral blood samples from each participant. DNA samples obtained from the ORGL were diluted in Tris-EDTA (TE) buffer to desired

working concentrations, quantified using a Nanodrop spectrophotometer (Section 2.3.2.4) and stored at -20^{o}C until needed.

2.3.2.2 Preparation of Plasmid DNA (Miniprep)

Individual bacterial colonies (Section 2.3.2.13) were carefully picked with sterile inoculating loops (BD Diagnostics) and used to inoculate 7.5mL of autoclaved Luria-Bertani (LB) media with appropriate antibiotics (100µg/mL Ampicillin or 50µg/mL Kanamycin) in a 15mL polypropylene Falcon tube. This starter culture was incubated overnight in a 37°C shaker at 250 rpm. Minipreps were carried out using QIAprep Spin Miniprep kit following the manufacturer's instructions (Qiagen, UK). A total of 3mL of the overnight culture was used for plasmid minipreps by spinning down 1.5mL of the culture in 2mL Eppendorf tubes twice at 13,000 rpm for 3 minutes. After each spin, the clear LB supernatant was carefully discarded leaving the cell pellet, which was then suspended in 250µl of Buffer P1. After resuspension, 250µl of Buffer P2 was added to each tube, covered and inverted several times to ensure complete lysis of cells. Buffer N3 (350µl) was then added to each tube and thoroughly mixed by inverting the tubes before spinning at 13,000 rpm for 10 minutes. The supernatant was applied to the QIAprep 2.0 spin column and spun for 1 minute at 13,000 rpm to bind the plasmid DNA. The flow-through was discarded and the column was washed with 500µl of Buffer PB to remove any traces of nuclease activity by spinning for 1 minute. Buffer PE (750µl) was then applied to the column and spun for 1 minute. The flow-through was discarded and the column was spun for a second time to remove any residual ethanol present from washing with Buffer PE. The column was then transferred into a clean 1.5mL Eppendorf tube for DNA elution. In all instances 30µl of molecular grade water was applied directly to the column membrane, left to incubate at room temperature for 1 minute before being centrifuged at 13,000 rpm to elute plasmid DNA. The eluted plasmid DNA was then stored at -20°C until required.

2.3.2.3 Preparation of Plasmid DNA (Midiprep)

For experiments requiring a higher plasmid DNA yield, the ZymoPURE II Plasmid Midiprep kit (Zymo Research, USA) was used, following the manufacturer's instructions. Starter cultures were made as described in (section 2.3.2.2). 100µl of the turbid overnight starter culture was used to inoculate 50mL of autoclaved LB media containing appropriate antibiotic (100µg/mL Ampicillin or 50µg/mL Kanamycin) and incubated overnight in a 37°C shaker at 250 rpm. The entire 50mL culture was centrifuged at 6000 x *g* for 10 minutes and the supernatant discarded. The cell pellet was resuspended in 8mL of Buffer P1 by vortexing. Buffer P2 (8mL) was added to the cell suspension and immediately mixed by inverting the tube 6 times and was allowed to sit at room temperature for 3 minutes to ensure complete cell lysis. Buffer P3 (8mL) was then added and mixed gently but thoroughly by inversion. The entire lysate was transferred into the ZymoPURE Syringe Filter with a plug attached to the Luer Lock at the bottom and left to stand upright for 8 minutes for any precipitate to float to the top. With the Luer Lock plug removed, the syringe was placed in a clean 50mL conical flask and a syringe plunger used to push the cell lysate through the ZymoPURE Syringe Filter until about 20mL of clear lysate had been recovered. The syringe with the precipitate was discarded. To bind plasmid DNA, 8mL ZymoPURE Binding Buffer was added to the clear lysate, mixed thoroughly by inverting the capped tube 8 times and the entire mixture transferred into the Zymo-Spin III-P Column Assembly fitted onto a Vacuum pump (Zymo Research, USA). The vacuum pump was switched on and all the liquid in the mixture allowed to pass through the column. The column was washed once with 2mL of ZymoPURE Wash 1 Buffer and then washed twice with 2mL of ZymoPURE Wash 2 Buffer. The ZymoPURE III-P Column was then placed in a collection tube and spun at 13,000 rpm for 1 minute in a microcentrifuge to remove any residual wash buffer. To elute the DNA, the column was transferred into a clean 1.5mL microcentrifuge tube, 200µl of ZymoPURE Elution Buffer was added directly to the column matrix and allowed to incubate at room temperature for 2 minutes before spinning at 13,000 rpm for 1 minute. As an additional step to ensure eluted plasmid DNA was free of endotoxins, the EndoZero II Spin-Column supplied by the manufacturer was used. The entire eluate was applied to the EndoZero II Spin-

Column placed in a clean 1.5mL microcentrifuge tube, and was allowed to incubate at room temperature for 2 minutes and then spun at 13,000 rpm. The eluted plasmid DNA was then stored at -20°C until required.

2.3.2.4 DNA and RNA Quantification

The concentration of DNA and RNA, and their purity, was routinely determined using the Nanodrop spectrophotometer (ND1000, Thermo Fisher Scientific, USA). The Nanodrop spectrophotometer uses the property of nucleic acids to absorb ultra-violet (UV) light at 260nm and 280nm to estimate the amount and purity of nucleic acids present in a sample under measurement. The total absorbance at 260nm usually includes free nucleotides, RNA, double stranded DNA (dsDNA) and single stranded DNA (ssDNA), whereas absorbance at 280nm determines the purity of the sample. As such, ratios of absorbance at 260nm/280nm are recorded as measures of sample purity. Generally, 260nm/280nm ratios considered to be of acceptable purity are 1.7-1.9 for DNA and 1.9-2.0 for RNA samples.

2.3.2.5 Primer Design and Optimisation

Custom forward and reverse primers were designed in the flanking genomic regions of interest. Generally, primers were designed to be ~20 nucleotides long with 50-60% GC content and 55-65°C melting temperature (T_m) and ordered from Sigma-Aldrich, UK. A list of primers is provided in Appendix B and C and will be referenced by number throughout this thesis. Genomic reference sequences for genes were retrieved from NCBI (https://www.ncbi.nlm.nih.gov/) and Ensembl (https://www.ensembl.org/index.html) databases.

2.3.2.6 Polymerase Chain Reaction (PCR)

Polymerase Chain Reaction (PCR) is a technique that enables the amplification and isolation of specific DNA sequences. The region to be amplified is defined by custom-made oligonucleotide primers that hybridise to specific sequences on opposite strands of DNA, flanking the target region. PCR consists of three main steps: denaturation, annealing and extension. First, a high temperature incubation step

(usually 95°C) during which the double-stranded DNA molecule is denatured and separated into single strands. The second step involves annealing the oligonucleotide primers to the corresponding regions on each DNA strand at optimal temperatures specific to primers. Lower annealing temperatures increase the probability of non-specific binding of primers to other regions whereas higher annealing temperatures decrease the probability of the primers annealing. The final step is an elongation step, usually termed 'extension' during which the DNA sequence is extended from the primer in a 5' to 3' direction by a heat-stable DNA polymerase enzyme using all four deoxynucleoside triphosphates (dNTPs) present in the reaction mixture. Optimal extension temperatures are dependent on the DNA polymerase enzyme used. Incubation at these three temperatures represents a complete PCR cycle and result in double-stranded copies of the target DNA sequence. After the first round of thermal cycling, there is double the amount of target DNA (the original and the copy), both of which will serve as templates for the next cycle leading to four times the original quantity of target DNA. There is an exponential increase in the amount of target DNA with each round of thermal cycling, with the target amplified 2^n-fold, where n = number of cycles.

Generally, PCR amplification was performed using Taq-DNA polymerase (Bioline, UK) following manufacturer's instructions. PCR reactions were set up in 200µl PCR tubes to a final volume of either 25µl or 50µl using MyTaq PCR mix or MyTaq HS PCR mix, respectively, and other components as indicated in below:

25µl reactions		**50µl reactions**	
DNA Template (20ng)	1µl	DNA Template (20ng)	1µl
Forward primer (10µM)	0.5µl	Forward primer (20µM)	1µl
Reverse primer (10µM)	0.5µl	Reverse primer (20µM)	1µl
MyTaq 2X mix	12.5µl	MyTaq HS 2X mix	25µl
dH_20	10.5µl	dH_20	22µl
Total	**25µl**	**Total**	**50µl**

A negative control, in which molecular grade water was added instead of the DNA template, was run in parallel with the samples to exclude any possible reagent contamination. Thermal cycling was carried out on T100 Thermal cycler (BioRad, UK), under the following conditions;

Cycles	**Step**	**Temperature (°C)**	**Duration**	
			25 µl (MyTaq)	**50 µl (MyTaq HS)**
1	Initial denaturation	95	5 m	5 m
35-40	Denaturation	95	30 s	15 s
	Annealing	variable	15 s	15 s
	Extension	72	30 s / Kb	15 s / Kb
1	Final extension	72	5 m	5 m

2.3.2.7 Agarose Gels and Visualisation

Agarose gel electrophoresis is a technique used to separate DNA, for example PCR amplicons, based on their sizes. It is based on the principle that, when an electric current is passed through an agarose gel containing DNA, shorter fragments of the negatively charged DNA will be carried further along the agarose gel compared to longer fragments over the same amount of time. To determine the sizes of the DNA fragments undergoing the electrophoresis, a DNA ladder with fragments of known sizes (commercially obtained) is usually run alongside the DNA fragments of interest to serve as a reference. The addition of ethidium bromide, a fluorescent dye that intercalates between DNA bases, allows the visualisation of the DNA using an ultraviolet (UV) transilluminator.

Depending on the expected size of the DNA fragment to be separated, agarose gels of between 1-3% (w/v) were prepared, in general, larger fragments were analysed on lower percentage gels, and vice versa. To prepare a 1% (w/v) agarose gel, for instance, 1.5g of agarose (Geneflow, UK) was dissolved in 150mL 1X tris/acetate/ETDA (TAE) buffer in a conical flask and microwaved until the agarose was completely dissolved and solution was transparent. The solution was allowed to cool to a temperature below 60°C before adding Ethidium bromide (Sigma-Aldrich, UK) to the agarose-TAE solution to a final concentration of 0.5µg/ml. The solution was mixed by swirling the flask gently, poured into a gel tray fitted with the desired well comb and allowed to solidify in a fume hood. A mixture of PCR product to be separated and loading dye (in a 5:1 ratio) was loaded into individual wells on the agarose gel submerged in gel tanks containing 1X TAE buffer and electrophoresed at 100-120V for approximately 45 minutes. PCR products were run alongside 10µl 1Kb Plus DNA Ladder (Invitrogen, UK) at 0.5µg/µl concentration to serve as size reference for separated DNA fragments. After electrophoresis, gels were visualised and imaged using an UV transilluminator (U:Genius, Syngene, UK).

2.3.2.8 Agarose Gel Extraction of DNA

PCR amplicons, digested inserts (Section 2.3.2.10) and linearized plasmid backbones were purified from agarose gels using the QIAquick Gel Extraction kit (Qiagen, UK) as per the manufacturer's

instructions. Agarose gels with products to be purified were electrophoresed until the bands were sufficiently separated for easy isolation. Using a UV transilluminator, the bands of interest were visualised and excised from the gel with a sterile scalpel blade. Each slice of gel containing a band of interest was then placed in a 1.5mL microcentrifuge tube. The weight of the gel slice was then calculated by subtracting the weight of the empty microcentrifuge tube from the total weight of the gel slice plus microcentrifuge tube. Three volumes of Buffer QG were added for each volume of gel (100mg of gel ~100µl), then incubated for 10mins at 50°C in a water bath. The tube was swirled intermittently to facilitate the dissolving of the gel slice. One volume of isopropanol (*w/v*) was then added to the solubilised gel, mixed and transferred to a QIAquick spin column and centrifuged at 13,000 rpm for 1 minute for DNA to bind to the column's membrane. The flow-through was discarded and any residual traces removed by washing columns with 500µl of Buffer QG. The flow-through was discarded and 750µl of Buffer PE (diluted in 100% ethanol as per the manufacturer's recommendation) added to the column, left at room temperature for 5 minutes, and then centrifuged at 13,000 rpm for 1 minute. The flow-through was discarded and column spun again at high speed to remove residual ethanol from the column. The column was then transferred to a new sterile 1.5mL microcentrifuge tube, 30µl of molecular grade water was applied directly to the membrane of each column and left for 1 minute at room temperature. The column was then centrifuged at 13,000 rpm for 1 minute to elute the DNA. Purified DNA samples were stored at -20°C until required.

2.3.2.9 PCR product Purification

PCR amplicons of desired sizes were purified for downstream applications using QIAquick PCR purification kit (Qiagen, UK) as per the manufacturer's instructions. The columns in the kit contain a silica membrane that can bind up to 10µg DNA (100bp to 10kb), allowing removal of other components of the PCR reaction, such as primers, nucleotides, and products of <40mers. Five volumes of Buffer PB was added to each volume of PCR product and mixed gently by pipetting up and down. The sample was then applied to the QIAquick spin column and centrifuged at 13,000 rpm for 1 minute. The flow-through was discarded, and 750µl of wash Buffer PE (diluted in 100% ethanol as per manufacturer's

recommendation) was added to column and centrifuged at 13,000 rpm for 1 minute. Flow-through was discarded and the column spun for a further 1 minute at 13000rpm to remove residual ethanol. The column was then transferred to a new sterile 1.5mL microcentrifuge tube and 30µl of molecular grade water was applied directly to the membrane of the column and allowed to incubate at room temperature for 1 minute. The column was then spun at 13,000 rpm for 1 minute to elute the DNA. Purified products were stored at -20°C until required.

2.3.2.10 Restriction Endonuclease Digestion

Restriction endonucleases are bacterial enzymes which digest double-stranded DNA at specific recognition sites (typically 4-8bp long). The digested fragments can then be separated using agarose gel electrophoresis (Section 2.3.2.7) and gel-purified (Section 2.3.2.8) for subsequent downstream applications. Depending on the sequence of the DNA to be digested and the choice of enzymes, digestion reactions can be performed with a single enzyme (single digest reaction) or with two enzymes simultaneously (double digest reaction). Appropriate restriction enzymes were used to digest PCR amplicons, inserts and plasmid backbones in CutSmart Buffer following manufacturer's instructions (New England Biolabs, UK). Unless otherwise stated, reactions comprised 1µl of restriction enzyme(s), 1µg DNA, 5µl of 10X CutSmart buffer and molecular grade water to a final volume of 50µl. Digestion reactions were incubated at 37°C in a water bath for 1 hour (unless otherwise stated). Where required, restriction enzymes were heat inactivated by placing the reaction on a heat block at temperatures recommended by the manufacturer. 10µl 6X gel loading dye (New England Biolabs) was added to the inactivated samples before analysis by agarose gel electrophoresis (Section 2.3.2.7). The resulting products were gel-purified (Section 2.3.2.8) for subsequent use. Digested samples were used immediately for ligation reactions or stored at -20°C until required.

2.3.2.11 Ligation of DNA fragments

2.3.2.11.1 TA cloning of PCR products

Purified PCR amplicons, where necessary, were used for ligation reactions using the pGEMT-Easy vector II systems (Promega, UK) according to manufacturer's instructions. The pGEM-T Easy vectors are linearized vectors with a single 3´-terminal thymidine at both ends (known as sticky ends) for ligation of PCR products with terminal adenine (A) overhangs at both ends usually produced by amplification with certain *Taq* polymerases. The vector contains the T7 and SP6 RNA polymerase promoters flanking a multiple cloning site with the α-peptide coding region of the enzyme β-galactosidase. Insertional activation of the α-peptide allows recombinant clones to be directly identified by colour screening on indicator plates (LB agar supplemented with X-gal, IPTG and ampicillin). pGEM-T Easy also contains an ampicillin resistance gene for vector positive clone selection. Generally, an insert:vector molar ratio from 3:1 to 1:1 was used, depending on the concentration of inserts, in a reaction comprising 5µl of 2X Rapid ligation buffer, 50ng PGEMT-Easy vector, 1µl T4 DNA ligase and ddH_20 to a final volume of 10µl. Reaction was mixed by gently pipetting up and down and left to incubate for 1 hour on the bench at room temperature.

2.3.2.11.2 Sticky End Cloning

For cloning of DNA fragments into expression vectors to be subsequently used for gene transfection experiments (Section 2.3.4.3), inserts were either cloned to pGEM-T Easy vectors (Section 2.3.2.11.1) before subcloning into expression vectors or directly cloned into expression vectors using T4 DNA ligase (Invitrogen, UK). In general a 3:1 insert:vector molar ratio was used. Ligation reactions comprised 1µl of T4 DNA ligase, 4µl of 5X T4 ligase buffer (Invitrogen), 3-6µl of digested insert, 1uL of linearized vector (from digested plasmid backbones (Section 2.3.2.10)) and ddH_20 in a total reaction volume of 20µl. Reactions were mixed by gently pipetting up and down and incubated at room temperature for 1 hour at room temperature or overnight at 4°C. Expression vectors and inserts of interest were digested and gel-purified (Sections 2.3.2.10 and 2.3.2.8) before ligation reactions. Specific expression

vectors used and conditions are contained in the methods sections of the relevant experimental chapters. In all cases, appropriate controls were also set up following manufacturer's instructions.

2.3.2.12 Transformations

Transformation is a method by which bacterial cells take up foreign genetic material from their environment. The technique is used in molecular biology to produce multiple copies of recombinant genetic material. For ligations performed with pGEMT-Easy vector system II, 50µl of JM109 high efficiency competent cells (supplied as part of the kit) in a microcentrifuge tube were transformed by the addition of 2-5µl plasmid DNA which was then incubated on ice for 30 minutes. The mixture was then heat shocked in a 42°C water bath for 45 seconds and was placed on ice for 5 minutes. SOC media (950µl; Life Technologies, UK) was added to the transformation reaction and incubated in a 37°C shaker set at 250rpm for 1.5 hours, after which 100µl of the transformed culture was spread onto pre-warmed Luria's Broth (LB) agar plate containing ampicillin (100µg/mL), ITPG (25µg/mL) and X-gal (25µg/mL). Plates were incubated inverted at 37°C overnight.

For DNA fragments cloned into expression vectors, 2-5µl of ligation reaction was used to transform 50µl subcloning efficiency DH5α competent cells (Invitrogen, UK) in microcentrifuge tubes. The tubes were kept on ice for 30 minutes, then heat shocked at 42°C for 20 seconds and finally placed on ice for 2 minutes. 950µl of SOC media was added to the transformation reaction and incubated in a 37°C shaker for 1 hour at 250rpm. 100µl of the transformed culture was spread on pre-warmed LB agar plates containing appropriate antibiotics and incubated inverted at 37°C overnight.

2.3.2.13 Colony screening

Colonies from overnight incubation of cells transformed with pGEM-T Easy vector were identified based on their ampicillin resistance and β-galactosidase activity. Growing cells on LB agar containing ampicillin (Sigma, UK) ensured that only colonies with ampicillin resistance conferred by the pGEM-T Easy vector thrived on the plates. Upon successful cloning of insert into multiple cloning sites of the pGEM-T Easy vector, the activity of the β-galactosidase gene present at the multiple cloning site is

interrupted. The presence of the ITPG and *X-gal* in the LB agar plates enables a blue and white selection method, where white colonies represents cells containing inserts. In cases where the colour of colonies was not obvious after overnight incubation, plates were kept in the fridge at 4°C for a few hours to improve contrast between blue and white colonies. Colonies from expression vectors were selected based on their respective antibiotic resistance.

To confirm whether a selected (white) colony had the correct insert, restriction enzyme digestion of purified plasmids (Section 2.3.2.10) and/or colony PCR (Section 2.3.2.14) were used. Restriction enzyme digestion was also used, in some cases, to verify the orientation of inserts in a plasmid.

2.3.2.14 Colony PCR

As a quick screen to ensure colonies had the desired insert, a sterile pipette tip was used to carefully pick a colony. The pipette tip was used to streak a LB agar plate containing the appropriate selection antibody and then the same tip was used to inoculate a PCR reaction mix. The PCR reaction and conditions used were the same as described in Section 2.3.2.6, except that ddH_20 was used in place of the template. The primers used for the colony PCR reactions were the same as previously used in amplifying the desired fragment. These PCR products were analysed by agarose gel electrophoresis and the presence of a band corresponding to the size of the expected insert was an indication that a recombinant had been made successfully and could be used for downstream applications such as minipreps.

2.3.2.15 Site-Directed Mutagenesis

Site-directed mutagenesis is a technique used to introduce desired mutations (insertions, deletions and substitutions) into recombinant clones using custom-made mutagenic primers. Generally, site-directed mutagenesis involves two main steps. First, a mutant-strand synthesis step in which a non-methylated mutant strand containing the desired mutation is amplified from the template strand in a PCR reaction involving the mutagenic primers, plasmid DNA and a high-fidelity polymerase enzyme. It is then followed by a second step in which the methylated template strand is degraded, the mutant

strand is phosphorylated and circularised using appropriate enzymes before being used to transform competent cells.

Throughout this thesis, the Q5 Site-directed mutagenesis kit (New England Biolabs, UK) which utilizes the Q5 Hot Start High-Fidelity DNA Polymerase, was used to introduce desired mutations to gene constructs for subsequent gene transfection experiments. All reactions were assembled in accordance with manufacturer's instructions. Mutagenesis primers and their corresponding annealing temperatures were designed and determined, respectively, using the NEBaseChanger online tool (https://nebasechanger.neb.com/) and were ordered from Sigma Aldrich (UK). Mutagenesis primers and their conditions can be found in section 5.3.2. First, mutant strands of gene constructs were generated using the following PCR amplification reaction and conditions;

Q5 Hot Start High-Fidelity 2X Master Mix	12.5 µl
Forward Primer (10 µM)	1.25 µl
Reverse Primer (10 µM)	1.25 µl
Plasmid template (1-25 ng)	1 µl
ddH2O	4 µl
Total	**25 µl**

Cycles	Step	Temperature (°C)	Duration
1	Initial denaturation	98	30 s
25	Denaturation	98	10 s
	Annealing	Variable	10-30 s
	Extension	72	20-30 s/Kb
1	Final extension	72	2 m

Mutant strand synthesis was followed by a KLD (kinase, ligase, *Dpn1*) reaction in which methylated template strands were digested with *Dpn1*, kinase and ligase phosphorylated and circularised synthesised mutant strands, respectively, in a single reaction. The reaction comprised 5µl 2X KLD Reaction Buffer, 1µl 10X KLD enzyme mix, 1µl PCR product and 3µl ddH_20 to a 10µl final volume, was incubated at room temperature for 5 minutes and 5µl of the reaction used to transform 50µl DH5α competent cells (Transformation, Section 2.3.2.12). Plasmid DNA was purified from colonies (Minipreps, Section 2.3.2.2) and screened for targeted mutations using Sanger sequencing (Source Bioscience, UK).

2.3.2.16 Sequencing

2.3.2.16.1 Sanger Sequencing

Sanger sequencing is a method of sequencing that utilises chain termination PCR. In this chain termination method, a DNA template of interest is replicated by a polymerase enzyme in the presence of a custom primer and a mix of deoxyribonucleotides (dNTPs) and fluorescently-labelled dideoxynucleotides (ddNTPs). In the ddNTP bases, the hydroxyl group (OH) attached to the 3' carbon is replaced with hydrogen (H) which prevents polymerase from forming another phosphodiester bond once a ddNTP is randomly incorporated into the growing dNTP strand. This results in the formation of several oligonucleotide copies of the DNA of interest consisting of different lengths. The random incorporation of ddNTPs continues until all bases in the template DNA have been read. Eventually, all the chain termination oligonucleotides are ordered from the shortest to the longest using capillary gel electrophoresis. The fluorescence of each terminal ddNTP is used to determine the identity of each base and ordered to determine the 5' to 3' sequence of the template DNA. The output is called an electropherogram, showing the fluorescent peak of each nucleotide along the entire length of the template.

Sanger sequencing was performed by Source Biosciences. For each sequencing reaction, 5µl of template DNA (at 10ng/µl for PCR products and 100ng/µl for Plasmid DNA) and 5µl of sequencing primer (3.2µM) were provided as recommended by the company. In most instances, custom-designed primers were used to sequence PCR products in both directions. In other instances, Source Bioscience stock primers were used for sequencing plasmid DNA from specific sites in the plasmid backbone. The specific primers used for sequencing reactions are detailed in the methods section of relevant experimental chapters. The chromatograph from each sequencing reaction was visualised using Chromas Lite software (http://technelysium.com.au/wp/chromas/) and ApE software (https://jorgensen.biology.utah.edu/wayned/ape/)http://jorgensen.biology.utah.edu/wayned/ape/ was used to align sequence data to reference sequences.

2.3.2.16.2 Whole Exome Sequencing

Whole Exome sequencing (WES) of all participants involved in the study was performed by the Next Generation Sequencing facility of the University of Leeds, UK. Sequencing and data analysis protocols were in common with protocols used in the UKIRDC (Arno et al., 2016a, Fiorentino et al., 2018). Genomic DNA from each participant (200ng) was processed according to the Agilent SureSelect XT Library Prep protocol (Agilent Technologies, Santa Clara, CA). Exons were captured using a SureSelect Exome V5 Capture library. After hybridization and indexing, 100bp paired end sequencing was performed (Illumina HiSeq 2500 sequencer, Illumina Inc., San Diego, CA) at a mean coverage of 100 times. Reads were aligned to the hg19 human genome reference sequence (build GRCh37) using Novoalign v.2.08 (Novocraft, Selangor, Malaysia). Duplicate reads were marked with Picard tools MarkDuplicates. Variant calling was performed using GATK (GenomeAnalysisToolkit) (Broad Institute, USA), creating gVCF formatted files for each sample. The final variant calling for individual gVCF files was performed using the GATK Genotype gVCFs module. Variant joint calling (joint genotyping) was carried out using the HaplotypeCaller in GVCF mode. Variant quality scores recalibration (VQSR) was done on the joint-called VCF files separately for single nucleotide variants (SNVs) and indels (insertions or deletions).

Resulting variants were annotated using ANNOVAR software based on Ensembl gene and transcript definitions. Candidate variants were filtered based on function (non-synonymous, presumed loss-of-function, or splicing) and a minor allele frequency (MAF) of ≤0.001 using several data sets, including an exome-sequencing control data set of approximately 4,000 individuals from the University College London (UCL) Exomes consortium (UCLEx), NHLBI GO Exome Sequencing Project (ESP; evs.gs.washington.edu/EVS/), and 1000 Genomes phase 1 data set. Variants were further manually interrogated for variant call quality, predicted pathogenicity, and biologic plausibility using predictive tools such as Polymorphism Phenotyping v2 (PolyPhen-2; http://genetics.bwh.harvard.edu/pph2/), Sorting Intolerant From Tolerant (SIFT; https://sift.bii.a-star.edu.sg/) and Combined Annotation Dependent Depletion (CADD; https://cadd.gs.washington.edu/). Candidate variants were then ranked,

considering the likely mode of inheritance for each family, prioritizing rare variants with a MAF of ≤0.001 in the Genome Aggregation Database (gnomAD; release 170228/ gnomad.broadinstitute.org). Candidate variants were then prioritized based on previous association of the gene with a compatible phenotype and biologic plausibility using Phenopolis (phenopolis.org), a platform for studying the pleiotropy of genes. Copy number variations (CNVs) in the genomic regions were assessed in the WES data using the Exome Depth calling algorithm.

2.3.3 RNA

2.3.3.1 RNA Extraction

RNA extraction from cell lines was performed using an RNeasy Mini Kit (Qiagen, UK). All work surfaces were cleaned using ddH_2O and 96-100% ethanol prior to the beginning of RNA extraction. Cell pellets were resuspended and lysed with an appropriate volume of buffer RLT supplemented with 10µl β-mercaptoethanol per every 1mL of RLT buffer. The cell lysate was homogenised by centrifuging at full speed in a QIAshredder spin column for 2 minutes. RNA isolation was performed following manufacturer's instructions. RNA was eluted in 30µl RNase-free water, RNA yields were determined by Nanodrop spectrometry (Section 2.3.2.4) and stored at -80°C until required.

For RNA extraction from neural retina tissue (and other animal tissue samples used), animals were sacrificed, eyes enucleated and neural retina was quickly dissected in sterile PBS. Dissected tissue was placed on dry ice for immediate RNA extraction or stored at -80°C for future use. Frozen tissue was thawed on ice before use. Tissue samples were disrupted using a handheld plastic pestle homogenizer in 0.75-1mL of TRIzol™ (Invitrogen, UK) in a new 1.5mL microcentrifuge tube**.** The homogenate was either processed immediately or frozen on dry ice and stored at -80°C until required. To isolate RNA, the homogenate (in TRIzol) was incubated for 5 minutes at room temperature to ensure complete dissociation of the nucleoproteins complex. Chloroform (200µl) was added to the samples, vortexed vigorously and incubated for 7 minutes at room temperature before being centrifuged (12,000 x *g*) for 15 minutes at 4°C to separate the sample into three phases: an organic phase containing protein, an

interphase containing DNA and an upper aqueous phase containing RNA. The colourless upper aqueous phase (containing the RNA) was carefully transferred to a new tube containing 10µg RNase-free glycogen (Invitrogen). Isopropanol (500µl) was then added and incubated for 10 minutes at room temperature, then centrifuged (12,000 x *g*) for 10 minutes at 4°C to precipitate total RNA as a gel-like pellet at the bottom of the tube. The supernatant was discarded, and the RNA pellet was washed with 1mL of 75% ethanol. RNA was re-pelleted by centrifuging (7,500 x *g*) for 5 minutes at 4°C. The supernatant was removed and RNA pellet was air-dried for 5-10 minutes. The dried pellet was then resuspended in 20µl molecular grade RNase-free water, incubated at 56°C in a water bath for 15 minutes to ensure it had completely dissolved. The sample was quantified using Nanodrop spectrometry (Section 2.3.2.4) and stored at -80°C until required.

2.3.3.2 cDNA synthesis

To study the expression of genes of interest in human and mouse tissues, cDNA was made from human RNA (Clontech, USA) or mouse RNA templates. cDNA synthesis was performed using qScript cDNA synthesis kit (Quantabio, USA) following manufacturer's instructions. Reactions comprised up to 1µg of RNA, 4µl of qScript 5x Reaction Mix, 1µl of qScript Reverse Transcriptase (RT) enzyme and RNase-free water to a final volume of 20µl. Conditions used were 5mins at 25°C, 30mins at 42°C, 5mins at 85°C and samples held at 4°C on a thermocycler. Gene expression was examined using 1:10 dilution of the synthesised cDNA as starting template and specific forward and reverse expression primer pairs designed from coding exons of genes of interest using end-point PCR conditions (Section 2.3.2.6).

2.3.4 Cell Culture

2.3.4.1 Cell Lines

Human Embryonic Kidney 293 (HEK293T) cells were obtained from the Oxford Autoimmune Neurology Group, University of Oxford, UK. Madin-Darby Canine Kidney II (MDCK II) cells used in this thesis were a kind gift from Prof. Karl Matter of the Institute of Ophthalmology, University College London (UCL),

UK. Both HEK293T and MDCKII cells were cultured in Dulbecco's Modified Eagle Medium – High glucose (DMEM HG, Sigma UK) supplemented with 10% Fetal Bovine Serum (FBS) (*v*/v), 1% Penicillin/Streptomycin (*v*/v), 1% L-glutamine (*v*/v) and 1% Non-essential amino acids (NEAA) (*v*/v). hTERT RPE-1 cells (referred to as RPE1) were cultured in DMEM F12 50:50 medium (Corning, UK) supplemented with 10% Fetal Bovine Serum (FBS) (*v*/v), 1% Penicillin/Streptomycin (*v*/v), 1% L-glutamine (*v*/v) and 1% Non-essential amino acids (NEAA) (*v*/v). Unless otherwise stated, cells were maintained within T75 culture flasks (Corning, UK) and all cell cultures were maintained in humidified tissue culture incubator at 37°C with 5% CO_2. Cells were fed with fresh media every 2-3 days and were passaged when they reached 70-90% confluence.

2.3.4.2 Cell Passaging and seeding

In routine cell culture, cells increase in number, release toxic metabolites as well as use up nutrients as they stay in culture for some days. As such, cells are usually split into smaller densities and grown in fresh medium to prolong their life span in a process called passaging. To passage cells, old culture media was removed from flasks and cells were washed once with 3-5mL of pre-warmed sterile PBS. To detach cells from the base of the flasks, 3mL of TrypLE™ Express solution (Gibco, UK) was added to the cell monolayer and the flask was incubated at 37°C for 5-10 minutes. Cells were observed under the microscope to ensure complete detachment. Pre-warmed culture media (7mL) was added and gently pipetted up and down to ensure cells were resuspended. To subculture, 1-2mL of the cell suspension was added to pre-warmed culture media in a new T75 flask and maintained in a humidified incubator at 37°C with 5% CO_2. The remaining cell suspension was either discarded or used for subsequent transfection experiments. If cells were to be used for transfection, the remaining cell suspension from the T75 flask was transferred into a sterile 15mL tube and centrifuged at 300 x *g* for 5 minutes at 20°C. The supernatant was discarded and cells resuspended in 10mL of fresh pre-warmed media.

To quantify cells, 20µl of cell suspension was mixed with 20µl of neat trypan blue (1:1 ratio) in a 1.5mL microcentrifuge tube and 10µl of this suspension loaded into designated wells on TC10 cell counter sample slides. Sample slides were then inserted into the TC20 Automated Cell Counter (Bio-Rad, UK)

for automated estimation of total and viable cells, following manufacturer's instructions. In all cases, cell count per flask was performed in duplicate and average numbers used to estimate the cell density of the original suspension. Cells were seeded at the following densities; 300,000 cells per well in 6-well plates, 150,000 cells per well in 12-well plates or 50,000 cells per well in 24-well plates. Cells were initially seeded at a range of densities in order to determine optimal plating densities. Cells to be subsequently used for immunocytochemistry were seeded onto poly-L-lysine (PLL) treated glass cover slips placed in wells or onto *Trans*well polycarbonate membrane inserts (Corning, UK) following manufacturer's instructions. In all cases, cell culture was carried out in standard positive pressure ventilation hoods in a designated tissue culture laboratory, following aseptic techniques.

2.3.4.3 Cell Transfection

To evaluate the function of genes and proteins of interest, cell transfection, a technique that enables the introduction of foreign nucleic acids (DNA and RNA) into eukaryotic cells to produce genetically modified cells, is often used. Depending on the purpose and method used, the transfected gene or gene product in the host cell could exist stably (continue to be present after cell replication) or transiently (expressed for a limited time).

To transfect cells, seeded plates were incubated overnight at 37°C with 5% CO_2 before transfection. Transient transfection of cells was achieved using Lipofectamine 3000 (Invitrogen, UK) by adding lipid-DNA complex to each well. Transfection media was constituted according to manufacturer's instructions and amounts of reagents were scaled appropriately to the well size. For instance, to transfect cells in a 6-well plate, transfection media per well was made as follows; First, a DNA dilution was made comprising 2.5µg of plasmid DNA and 5µl of P3000 reagent in 150µl of Opti-MEM™ serum-free culture media (Thermo Fisher Scientific, UK). Secondly, a Lipofectamine 3000 reagent dilution was made by adding 7.5µl of Lipofectamine 3000 reagent to 150µl of Opti-MEM™ serum-free culture media and vortexing briefly. Solutions from both dilutions were then added together in a 1.5mL microcentrifuge tube to constitute a transfection media of ~300µl in volume. This transfection media was mixed by pipetting up and down before being allowed to incubate at room temperature for 15

minutes to enable Lipofectamine-DNA complexes to form. Generally, 3µl of transfection reagent per 1µg of DNA (3:1 reagent to DNA ratio) was used. Cells were then transfected by adding the transfection media directly to the complete DMEM culture media in each well in a drop-wise fashion while gently rocking the plate to ensure an even distribution of complexes. Transfected cells were then returned to the 37°C incubator for 24 - 48 hours before cells were analysed.

2.3.4.4 Immunocytochemistry

Immunocytochemistry (ICC) is a technique used to identify and localise specific proteins in cells using antibodies designed to bind to a part of the protein of interest, known as the antigen. The principle of ICC are similar to that of IHC (Section 2.3.7.3) except that ICC applies to cultured cells whereas IHC looks at a mix of different cells within a tissue section.

Immunocytochemistry for transfected cells was carried out 24 to 48 hours post-transfection. Wells were emptied of media and cells washed once with PBS to remove traces of media. Cells were fixed for 20 minutes using 4% paraformaldehyde (PFA) (*v*/v) in PBS. Cells were then permeabilized with 0.3% triton (*v*/v) in PBS for 10 minutes and blocked with appropriate serum (10%) (*v*/v) made in 0.1% triton (*v*/v) in PBS. Cells were incubated with primary antibody diluted in appropriate serum (2%) (*v*/v) made in 0.1% triton (*v*/v) in PBS for 1 hour at room temperature or overnight at 4°C. A list of all antibodies used can be found in Appendix E and F. Cells used as controls were treated with the antibody dilution medium (serum (2%) in 0.1% triton in PBS (*v*/v)). Cells were washed 3 times for 5 minutes each with 0.1% triton in PBS before being stained with appropriate fluorophore-conjugated secondary antibodies for 1 hour at room temperature. Secondary antibodies were raised against the host species of the primary antibody and dilutions were made in appropriate serum (2%) made in 0.1% triton in PBS. After secondary antibody incubation, cells were washed 3 times for 5 minutes each with 0.1% triton (*v*/v) in PBS before being stained with the nuclear stain 4',6-diamidino-2-phenylindole (DAPI; Sigma-Aldrich, UK) at 1:2000 dilution in PBS. Cover slips or membranes with cells were mounted unto polylysine coated slides using ProLong Diamond Antifade mounting medium (Invitrogen) and allowed to dry overnight in a dark room at room temperature. Slides were stored at 4°C prior to imaging.

2.3.5 Protein

2.3.5.1 Protein extraction

Protein extraction from cell pellets and neural retina were performed by lysis in ice-cold radioimmunoprecipitation (RIPA) buffer (Sigma Aldrich, UK) supplemented with cOmplete™ mini EDTA-free protease inhibitor (PI, Roche, UK) as per manufacturer's instruction (1 tablet to 10mL RIPA buffer). Cell pellets were initially resuspended in 100µl volume of RIPA/PI buffer, intermittently agitated on vortex while on ice for 30 minutes and then sonicated with a Qsonica Sonicator Q500 (Fisher Scientific, USA) at 20% power for 10 seconds. Retina tissue samples (and other animal tissue samples used) were disrupted using handheld plastic pestle homogenizer in ice-cold 80-100µl RIPA/PI, then sonicated for 10 seconds. Samples were constantly agitated using a tube rotator at 4°C for 1 hour before being centrifuged at 12,000rpm at 4°C for 20 minutes in a microcentrifuge. The supernatant (protein lysate) was gently transferred into a new microcentrifuge tube and placed on ice. Aliquots of protein lysate (10-20µl) were taken for protein quantification (Section 2.3.5.2) while the remaining amount was stored at -80°C for subsequent use.

2.3.5.2 Bicinchoninic acid (BCA) Assay

Bicinchoninic acid (BCA) assay is a method used to measure the concentration of total protein in a sample using colourimetric assessment. This technique is essential to ensure that equal amounts of protein (extracted from tissue or cells) are used in downstream applications, such as western immunoblotting (WB). Using the Pierce BCA Protein Assay Kit (Thermo Fisher Scientific, USA) and following manufacturer's instructions, 25µl each of Bovine Serum Albumin (BSA) standards (0, 25, 50, 100, 250, 500, 750, 1000, 2000 µg/mL) and protein lysates were pipetted into a clear flat-bottomed 96-well plate in triplicate. To each well containing protein samples to be measured and standard, 200µl of BCA reagent, prepared according to manufacturer's instruction, was added. The plate was then incubated for 30 minutes at 37°C after which colourimetric absorbance readings were taken at 562nm

using the iMark™ microplate reader (Bio-Rad, UK). A sample absorbance curve was plotted against a standard curve of BSA to determine the protein concentration of each sample.

2.3.5.3 Western Blotting

Western blot (WB) is a technique that enables the detection of specific proteins from cell and tissue lysates. Lysate samples from cell lines and mouse retina used for WB in this thesis were prepared as described in Section 2.3.5.1 above and kept at -80°C. Samples were initially allowed to thaw slowly on ice. First, 10-30µg of total protein samples, diluted with RIPA/PI buffer to achieve desired concentrations, were solubilised in 2X Laemmli buffer (Sigma Aldrich, UK) and denatured at 95-100°C on a heat block for 5 minutes. Laemmli buffer contains β-mercaptoethanol and sodium dodecyl sulphate (SDS) which denatures proteins and neutralises their positive charges to ensure that they are sorted by size instead of shape or charge during electrophoresis. Denatured samples were then loaded into wells of a pre-cast 10% Criterion™ Tris-Glycine extended (TGX™) gel (Bio-Rad, UK) for sodium dodecyl sulphate polyacrylamide gel electrophoresis (SDS-PAGE). In all cases, 5-10µl of BLUeye prestained protein ladder (Geneflow, UK) was loaded alongside samples. SDS-PAGE of denatured protein samples was achieved by subjecting the loaded gel to electrophoresis at 100V in a gel tank (Bio-Rad, UK) with Tris/Glycine/SDS running buffer (National Diagnostics, USA) for approximately 1 hour and 45 minutes. The protein from the gel was blotted onto polyvinylidene difluoride (PVDF) membranes using the Trans-Blot Turbo transfer system (Bio-Rad, UK) following manufacturer's instructions. Membranes were washed twice for 5 minutes each with 0.1% Tween-20 in TBS (TBST) (*v*/v) at room temperature on a plate shaker before being blocked with 3% BSA in PBST for 1 hour. Membranes were then stained with appropriate primary antibody diluted in blocking buffer and allowed to incubate overnight at 4°C on a plate shaker. Subsequently, membranes were washed three times for 7 minutes each time with 0.1% Tween-20 in TBS (*v*/v) on a shaker at room temperature, and then incubated with HRP-conjugated secondary antibodies diluted in blocking buffer for 30 minutes on a shaker at room temperature. Membranes were washed three times for 7 minutes each with 0.1% Tween-20 in TBS (*v*/v) before being developed with Clarity Western ECL Substrate (Bio-Rad) for

imaging. In all WB experiments, detection of β-actin or GAPDH was used as loadig controls. Where subsequent re-probing of membranes was necessary, membranes were stripped with ReBlot Plus Strong Antibody Stripping Solution (Sigma, UK) following manufacturer's instructions. Stripped membranes were then re-blocked and re-probed as indicated above. A list of antibodies and concentrations used in WB experiments can be found in Appendix E.

2.3.5.4 Imaging

The processed PVDF membranes were imaged using the Odyssey Fc imaging system (LI-COR Inc., USA), using the chemiluminescence filter. Image acquisition parameters were optimised for each image to reduce background and maximise band detection. Images were then analysed using the Image Studio Lite software (version 5.2.5, LI-COR Inc., USA). Where detected protein was to be quantified, expression level relative to β-actin was calculated from acquired images using in-built densitometry tools.

2.3.6 Mouse Lines and Animal Husbandry

Unless otherwise stated, all C57BL/6J mice used in this study were purchased from Charles River Laboratories, UK. All procedures were in accordance with local and UK Home Office guidelines concerning the use of animals in scientific research as well as adhering to the Association for Research in Vision and Ophthalmology Statement for use of animals in ophthalmic and vision research. Generally, mice used in this study were of either sex and were adults aged 21 days and over. Mice were sacrificed using Schedule 1 procedures.

2.3.7 Histology

2.3.7.1 Tissue Preparation

Eyes were enucleated, punctured once through the cornea with a fine needle, washed once in PBS and then fixed in 4% paraformaldehyde (PFA) (*v*/v) in PBS for 1 hour at room temperature or overnight at 4°C. Eyes were then cryoprotected in 30% sucrose (*w*/v) made in PBS overnight at 4°C. Using microsurgical instruments, cryoprotected eyes were dissected to remove cornea, iris and lens in PBS under a dissection microscope. Dissected eyecups were then placed again into 30% sucrose made in PBS in an Eppendorf tube until the eyecup sunk to the bottom of the tube.

2.3.7.2 Embedding and Cryostat Sectioning

Eyecups were decanted from the Eppendorf tubes. Using a pair of tweezers, eyecups were briefly washed in PBS and dried briefly before being immersed at the desired orientation in optimal cutting temperature (OCT) compound (VWR, USA) contained in aluminium moulds. The specimens were then snap frozen by placing mould containing OCT and eyecup in a slurry of isopentane and dry ice, then stored at -80°C prior to cryosectioning. Frozen tissue blocks were cryosectioned at -20°C on a Cryostat (Leica Biosystems, UK) at 12-micron thickness and collected on Polylysine coated glass slides (Thermo Fisher, USA), left to dry on the bench overnight and stored at -80°C until required.

2.3.7.3 Immunohistochemistry

Immunohistochemistry (IHC) was used to identify and localise proteins of interest in retina tissue sections using antibodies. Generally, IHC is achieved by using immunoglobulins antibodies raised in animal species to target the antigen of interest in tissue samples. Fluorescently conjugated secondary antibody that binds to the primary antibody is then used to allow the antigen to be visualised.

In this thesis, IHC experiments were carried out as follows: Slides with tissue sections were removed from -80°C freezer and allowed to thaw to room temperature. A perimeter around tissue sections on

slides were carefully created using hydrophobic barrier pen (Thermo Fisher, USA) to serve as barriers for solutions to be used subsequently. Before being stained with appropriate primary antibodies, sections were permeabilized with 0.3% triton (*v*/v) in PBS for 10 minutes and blocked with appropriate serum (10%) (*v*/v) made in 0.1% triton in PBS (*v*/v) for 1 hour at room temperature. Primary antibodies in appropriate serum (2%) made in 0.1% triton in PBS were added and slides were incubated overnight at 4°C. Sections used as controls were treated with antibody dilution solution only. Sections were washed 5 times 5 minutes with 0.1% triton (*v*/v) in PBS before being stained with appropriate fluorescent conjugated secondary antibodies (serum (2%) made in 0.1% triton in PBS) for 1 hour at room temperature. Details of specific antibodies used can be found in methods sections of relevant experimental chapters. Sections were washed 3x5minutes with 0.1% triton (*v*/v) in PBS before being stained with a nuclear stain DAPI (1:2000; Sigma-Aldrich, UK) in PBS. Sections were dried and then mounted with a coverslip using ProLong Diamond antifade mounting medium (Invitrogen, UK) and allowed to dry overnight in dark room conditions at room temperature and stored at 4°C prior to imaging.

2.3.8 Microscopy

2.3.8.1 Evos LED microscopy

To acquire fluorescence micrographs of processed cells (such as post-transfected cells) in culture, the EVOS FL Auto 2 Cell Imaging System (Thermo Fisher Scientific, USA) was used. For each image, the focus for transmission and fluorescent channels was individually determined. The gain level for each channel was adjusted to a level which avoided signal saturation. Settings were kept the same within experiments to allow comparison of wells.

2.3.8.2 Confocal laser microscopy

Fluorescent images of fixed cells and retinal sections were acquired using the LSM-710 inverted laser confocal microscope system (Zeiss, Germany). GFP-positive cells and areas of interest were first

located using epifluorescence illumination before taking a series of XY optical sections of varying thickness depending on the experiment. The fluorescence of DAPI, GFP, Alexa-568, 647 were excited using laser of appropriate wavelength. In the 568nm channel, the pinhole size was set to 1 Airy Disc unit (AU) and standardised across all other channels. The gain and offset were adjusted to avoid pixel intensity saturation in any part of the image. Identical settings were used between slides and were re-loaded for future imaging sessions to allow reliable comparison of images. Image processing such as brightness adjustment and contrast enhancement was made using Image J software (Version 1.8.0, NIH, USA)

2.3.9 Bioinformatic Methods

2.3.9.1 Protein Sequence Analysis

To evaluate the conservation of variant protein across different species, amino acid sequence of MTSS1 for different species were retrieved from NCBI Protein database (https://www.ncbi.nlm.nih.gov/protein) and aligned using Clustal Omega (https://www.ebi.ac.uk/Tools/msa/clustalo/).

2.3.10 Web Resources (URLs)

https://www.ncbi.nlm.nih.gov/

https://www.ensembl.org/index.html

https://genome.ucsc.edu/

http://technelysium.com.au/wp/chromas/

https://jorgensen.biology.utah.edu/wayned/ape/

https://www.ncbi.nlm.nih.gov/protein

https://www.ebi.ac.uk/Tools/msa/clustalo/

https://imagej.nih.gov/ij/download.html

https://evs.gs.washington.edu/EVS/

https://nebasechanger.neb.com/

http://genetics.bwh.harvard.edu/pph2/

https://sift.bii.a-star.edu.sg/

https://cadd.gs.washington.edu/

https://gnomad.broadinstitute.org/

https://phenopolis.org/

3 Identification of candidate genes

3.1 Introduction

In the past, clinicians have categorised various inherited retinal dystrophy (IRD) cases based on their clinical presentations, ages of onset and known inheritance patterns, leading to phenotypic categories of IRDs such as RP, Stargardt disease, Choroideremia and others (Henderson, 2020). Although phenotypic categories still have a useful place in clinical practice today, cases within one category could present with broad clinical variability as well as overlapping with other categories as discussed in section 1.2. As such, the process of identifying the genetic variant underlying a particular phenotype (commonly called molecular diagnosis) has become an essential component of diagnosing and managing IRDs (Pontikos et al., 2020). Among other benefits, knowing the genetic basis of an IRD affords clinicians the ability to make prognostic predictions of a case and to determine which individuals would benefit most from specific treatments as various novel therapies make their way into the clinic (www.clinicaltrials.gov). Also, due to the broad phenotypic overlap that exist between certain IRD subgroups, there are instances in which identifying the genetic basis of cases help in classifying them into the appropriate phenotypic categories (Motta et al., 2019, Arno et al., 2016b).

This has led to the development of diagnostic genetic tests which are used to screen genes known to be responsible for a specific phenotype for pathogenic variants in newly diagnosed patients (Farrar et al., 2017). This can involve (i) selectively screening specific genes known to be commonly associated with a particular phenotype using Sanger sequencing (Ramkumar et al., 2017) or (ii) targeted capture and sequencing of all exons of genes known to be related to a specific phenotype using next generation sequencing (NGS) (Huang et al., 2018). While diagnostic genetic testing is increasingly becoming accessible and relevant in diagnosing IRDs at the molecular level, there are still many cases and families in which no pathogenic variants are found in the known IRD genes. Various factors could account for this observation, which include: the level of accuracy of variant detection by these genetic testing panels; the possibility of disease-causing variants lying in intronic, regulatory or poorly covered regions

of the screened genes; and the possibility that these unsolved IRD cases could be caused by novel genes. Also, in contrast with genes such as *RHO* and *ABCA4* which have been reported to be responsible for IRDs in large cohorts (Pontikos et al., 2020), trends observed in recently identified IRD genes such as *AHR* (Zhou et al., 2018) and *POC5* (Weisz Hubshman et al., 2018) suggest that most of the yet-to-be-identified IRD genes could be genes with variants that are limited to individual families or relatively smaller cohorts.

Therefore, this study aimed to identify novel candidate genes/variants causing the retinal phenotypes observed in four families recruited through the Oxford Eye Hospital that are genetically unsolved after standard genetic testing. In addition to identifying the novel genes underlying the IRD in these patients, this process will also allow further insight into new genes that are essential for photoreceptor cell/RPE function, increasing our understanding of these cells. Whole exome sequencing (WES) was carried out on probands and selected members of each family and taking advantage of genetic databases and bioinformatic tools, the sequencing data from each family were analysed and putative variants prioritised for segregation. Genes with variants that were identified to co-segregate with the IRD case in each family were further investigated by searching available literature and genetic databases to identify expression patterns and putative function. Furthermore, gene expression using end-point PCR and cDNA from human tissues was assessed to confirm expression of these segregating genes in the mammalian retina. Based on their identified retinal expression and potential role in the mammalian retina, some of these segregating genes, now referred to as candidate genes, were selected for further molecular and functional analysis in subsequent chapters of this thesis.

3.2 Aims

The overall aim of experiments outlined in this chapter was to identify and select candidate genes for IRDs. The specific objectives were:

1. To analyse whole-exome sequencing (WES) data from selected individuals from four families with IRDs of unknown genetic cause and prioritise potentially pathogenic variants
2. To perform segregation analysis for prioritised variants in each family
3. To conduct preliminary analysis on genes with variants segregating in each family as plausible candidate genes for IRDs

3.3 Methods

All methods used in this chapter, unless described below, have been described in the general methods section in Chapter 2.

3.3.1 Participant recruitment

Families attending the Oxford Eye Hospital who had previously been screened on the RP11 gene panel by the Oxford Genetics Laboratory and no genetic diagnosis obtained for them were recruited into the study. The list of genes on the RP111 gene panel can be found in Appendix A. Pedigrees of at least three generations were drawn for each family to ascertain the inheritance pattern and to enable the identification of more family members. Three families with adRP (3004, 3013 and 3027) and one family with autosomal dominant macular dystrophy (adMD) (3032) were recruited. Families in this study were considered to have conditions with dominant modes of inheritance due to the disease phenotype being present in at least two successive generations and the absence of known consanguinity. Where possible, more than one affected individual in each family was selected for whole exome sequencing (WES). This was done in order to reduce the anticipated large number of sequence variants as comparison of WES data from individuals within the same family should eliminate benign variants and prioritise only shared variants for segregation analysis. Where possible, individuals recruited into the study underwent clinical assessment at the Oxford Eye Hospital to ascertain their disease state. Where a visit to the clinic was not possible, for reasons such as the participant not living within reasonable commuting distance or immobility due to ageing/illnesses, records from the individual's Optician were requested and examined extensively before inclusion in the study.

3.3.2 Whole-exome sequencing

Whole-exome sequencing (WES) was performed as described previously (see 2.3.2.16.2). The initial filtering and annotation of all variants generated by WES was performed by Dr Jing Yu, a Bioinformatician in our research group, as described in section 2.3.2.16.2**.** In brief, variants were

prioritised and assessed for pathogenicity by association of the genes with previously identified phenotypes using Phenopolis (phenopolis.org), an online web server that provides an intuitive interface between genetic and phenotypic databases**.** Variants were further annotated using gnomAD (release 170228/ gnomad.broadinstitute.org) and CADD (cadd.gs.washington.edu) databases before segregation analysis.

3.3.3 Variant analysis

Following the initial filtering and annotation, all rare variants with minor allele frequency of less than 0.001 (MAF<0.001) (see 2.3.2.16.2) were further analysed. These variants were prioritised, and variants meeting the defined criteria were analysed for segregation with disease in each family.

3.3.3.1 Variant prioritization

Putative variants identified from WES for each individual were first sorted based on their inheritance pattern, whether dominant, recessive or X-linked. Where more than one affected individual had undergone WES in a family, variants were filtered in order to obtain shared variants. Shared variants were then prioritised based on their gnomAD frequencies. As all 4 families recruited into the study exhibited dominant inheritance patterns, shared heterozygous variants with a gnomAD frequency of 0.00 (i.e. not present in the general population) were prioritised for segregation analysis. Where no plausible candidate(s) was found to co-segregate with the condition among variants with 0.00 gnomAD frequency, additional variants with gnomAD frequencies of up to $4.3E^{-5}$ were subsequently prioritised. The $4.3E^{-5}$ cut-off used in this study is a commonly used cut-off in the UKIRDC as an agreed cut-off for dominant IRDs. Finally, the CADD scores of variants, a prediction of their level of deleteriousness, were considered. Although variants with CADD scores of less than 7.00 are generally considered to be less damaging (Itan et al., 2016, van der Velde et al., 2017), in this study we considered all variants within the $4.3E^{-5}$ gnomAD frequency cut-off for segregation analysis irrespective of their CADD scores.

3.3.3.2 *Variant validation*

The variants prioritised from the WES data were validated in the proband and any other individuals who had undergone WES using Sanger sequencing (described in section 2.3.2.16.1). PCR was performed as described in section 2.3.2.6 and the products analysed by gel electrophoresis (see 2.3.2.7). PCR products were purified (see 2.3.2.9) and sent for Sanger sequencing. All primer sequences are listed in Appendix B**.** Variants that were not found to be present in WES subjects upon direct Sanger sequencing were considered false positives and were excluded from subsequent segregation analysis.

3.3.3.3 *Segregation analysis*

Variants that were validated were then used for segregation analysis in other available family members (affected and unaffected) that had been recruited into the study. The primers and PCR conditions used for validation were used to amplify the genomic region of interest (see 2.3.2.6), purified (see 2.3.2.9) and sent for Sanger sequencing (see 2.3.2.16.1). The presence or absence of each variant was examined by direct visualisation of the sequencing chromatographs using Chromas Lite software (http://technelysium.com.au/wp/chromas/) and aligning sequencing reads with reference sequences using ApE software (https://jorgensen.biology.utah.edu/wayned/ape/). For all prioritised variants, segregation analysis was carried out in a stepwise manner: variants that were not found to be present in either an affected individual or were present in an unaffected individual were not pursued.

3.3.4 Preliminary analysis of genes with segregating variants

Following segregation analysis, candidate variants, defined as variant(s) that co-segregate with the condition in the respective family, were subjected to further analysis with the aim of identifying evidence to support their potential to cause retinal disease.

3.3.4.1 *Literature and database search*

Publicly available databases such as Gene and Unigene available through the NCBI website (www.ncbi.nlm.nih.gov/), the human retina single cell RNA sequencing (scRNA-seq) dataset (Lukowski et al., 2019), and other online gene and protein expression databases were utilised to determine

expression profiles. For information on gene function and association with other disease phenotypes, PubMed (pubmed.ncbi.nlm.nih.gov/) and Online Mendelian Inheritance in Man (OMIM) (www.omim.org/) databases were examined.

3.3.4.2 Examining gene expression in mammalian retina

The expression pattern of each gene of interest was examined using primers designed in coding regions of the gene of interest and spanning at least 2 exons (described in section 2.3.2.5) and endpoint PCR on a panel of human tissue cDNAs. The PCR was carried out as described in section 2.3.2.6. Primer sequences can be found in Appendix C. Primers to the ubiquitously expressed Beta-actin (*ACTB*) gene were used as an internal positive control, while a no template reaction was used as negative control per each expression reaction. Candidate genes that did not demonstrate retinal expression were excluded from further analysis.

3.3.4.3 Protein conservation across various species

To examine protein conservation across species, the amino acid sequences (and DNA sequences in case of splice variants) of the proteins coded by these genes were obtained from the NCBI Protein database and Ensembl. The sequences were aligned using Clustal Omega (https://www.ebi.ac.uk/Tools/msa/clustalo/).

3.4 Results

3.4.1 Family 3004

Family 3004, of British origin, has 5 members diagnosed with dominant retinitis pigmentosa (adRP) spanning 4 generations (Figure 3.1). The adRP in this family has variable severity with reports of night blindness and decreased dark adaptation commencing in the third decade of life. A summary of symptoms and associated features of the adRP phenotype in this family are shown in Table 3.1**.** Fundus images from the proband (IV-1) depicting the RP phenotype in this family, characterised by bilateral peripheral bone spicule pigmentation, can be found in Figure 3.2. Genomic DNA samples were obtained from 4 of the 5 affected members (II-2, II-3, III-2 and IV-1). DNA was not available for affected individual I-1. DNA samples were also obtained from two unaffected members (III-4 and III-5).

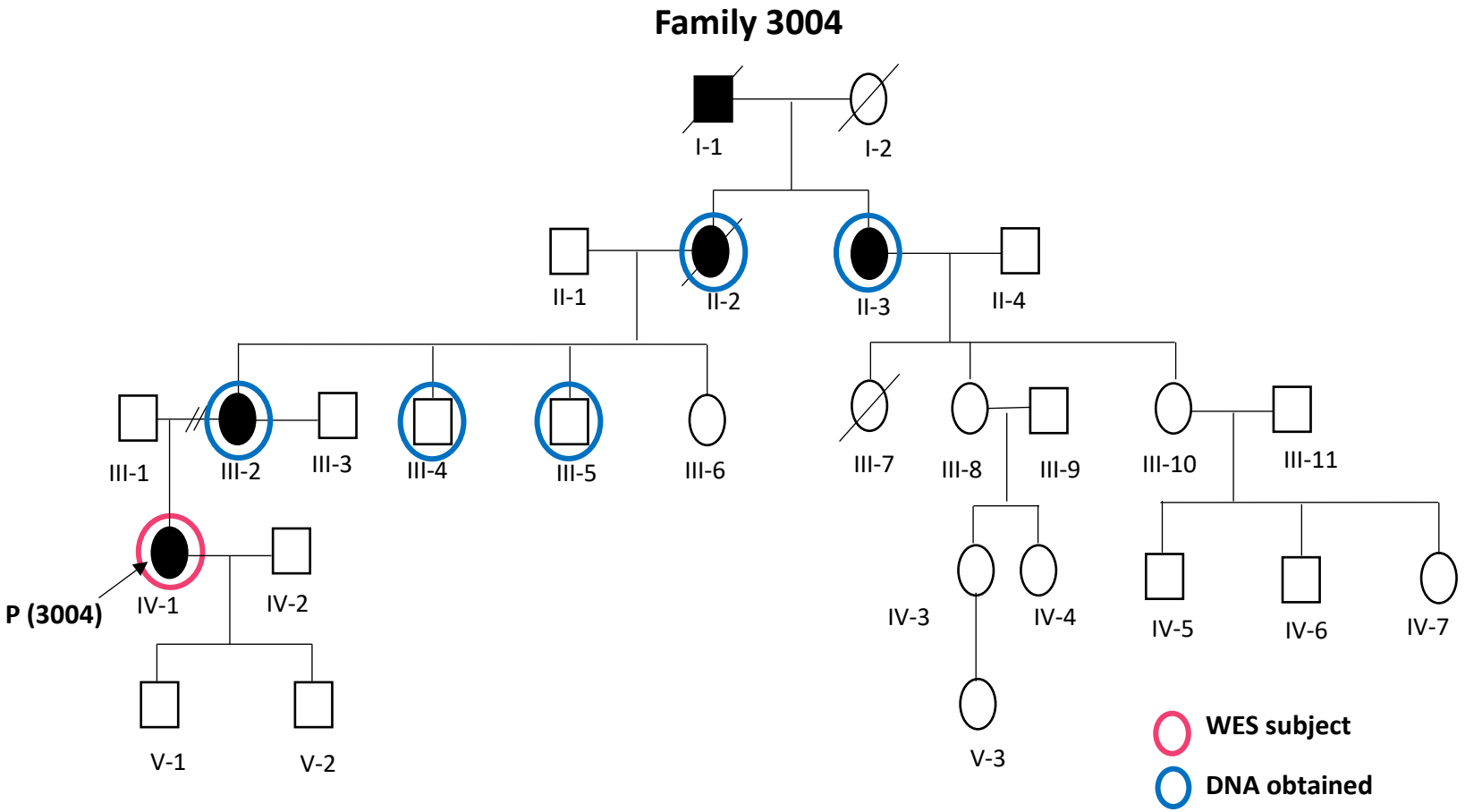
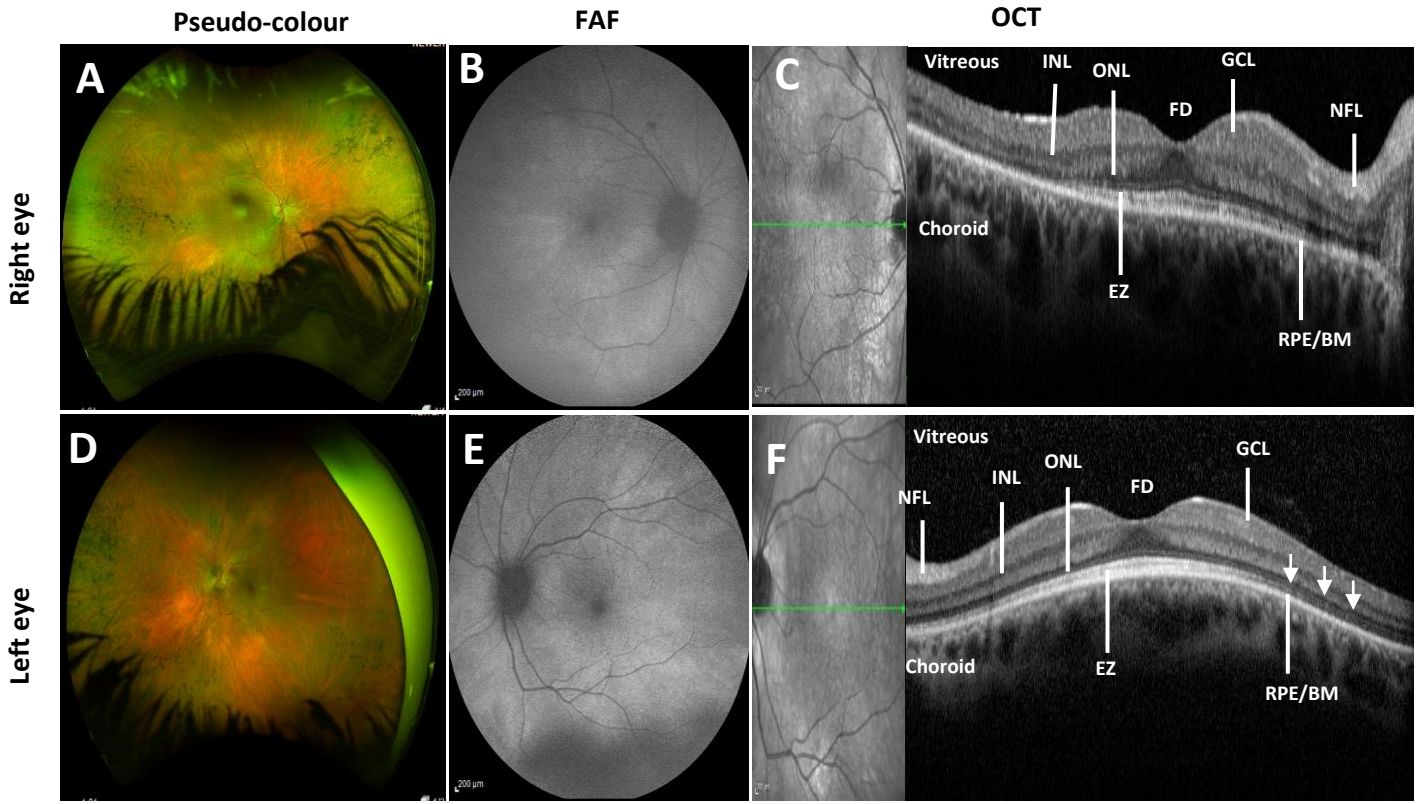


Figure 3.1. Pedigree of family 3004 diagnosed with adRP. Four affected individuals (II-2, II-3, III-2 and IV-1) and two unaffected individuals (III-4 and III-5) were recruited into this study. Circles=women; squares=men; filled symbols=affected; open symbols=unaffected. Symbol with a bar across=deceased; P=Proband.

Table 3.1. Summary of clinical findings in Family 3004 with adRP

Patient	Age of onset	Symptoms	Visual acuity	Fundus	Visual fields/OCT	ERG
III-2	40s	Night blindness, contrast problems, central scotoma	RE: HM LE: HM	Bone spicule pigmentation, No cystoid macular oedema	No visual fields left (Islands), OCT – N/A	N/A
IV-1	29	Night blindness, decreased dark, photosensitivity, photopsia.	RE: 6/5 LE: 6/7.5	Mild atrophic changes at posterior pole and mid-periphery	Constriction (LE>RE),Superior nasal scotoma, enlarged blind spot, normal OCT	Diminished cone and rod responses (rod>cone)

OCT - Optical coherence tomography; ERG – Electroretinography; RE – Right eye; LE – Left eye; HM – Hand motion; N/A – Not available.



Patient: 3004

Figure 3.2. Retina imaging of proband in family 3004 with adRP. (A, D) Widefield fundus pseudo-colour images showing bone spicule pigmentation in the mid-peripheral retina. (B, E) Fundus autofluorescence (FAF) images showing areas of reduced autofluorescence due to RP. (C, F) Spectral domain optical coherence tomography (OCT) images. White arrow heads in F indicate areas of disrupted ellipsoid zone (EZ) due to loss of photoreceptor outer segment in the left retina. FD= Foveal depression; NFL= nerve fibre layer; GCL= ganglion cell layer; INL= inner nuclear layer; ONL= outer nuclear layer; EZ: ellipsoid zone; RPE= retinal pigment epithelium; BM= Bruch's membrane.

3.4.1.1 Segregation analysis in Family 3004

WES was conducted only on the proband (IV-1) of family 3004. Bioinformatic analysis revealed 210 heterozygous variants of which 36 of these had a gnomAD frequency of zero (Table 3.2). Sanger sequencing was used to validate these 36 variants in the proband. Primer sequences are given in Appendix B. Segregation analysis was carried out in a stepwise manner as described in section 3.3.3.3. Segregation analysis of the 34 validated variants was performed using DNA samples from three affected (III-2, II-2, II-3) and two unaffected individuals (III4 and III-5) (Table 3.2). The putative variants in *PCDHB14* and *ANKRD30BL* were not present in the proband and three other affected family members tested. To date it has not been possible to validate the putative *C2orf16* variant as multiple primers and optimizations have not been able to amplify this region in the proband and other affected family members. Also, the sequence in an unaffected family member (II-5) for *CCDC103* was unexpected (homozygous for the variant) and was ruled out from further analysis.

Two variants, one in PARP1 binding protein (*PARPBP)* and the other in karyopherin subunit alpha 7 (*KPNA7)*, were found to segregate with the adRP in this family**.** The chromatograms from the segregation analysis of *PARPBP* and *KPNA7* variants are shown in Figure 3.3**.** The variant reported in *KPNA7* is a heterozygous missense substitution in which adenine at nucleotide position 211 (numbered according to NM_001145715.3) is replaced with guanine resulting in an amino acid change from threonine to alanine (c.211A>G, p.(Thr70Ala), GRCh37 Chr7: 98793780A>G). The variant reported in *PARPBP* is also a heterozygous missense substitution in which adenine at nucleotide position 1258 (NM_017915.5) is replaced with cytosine resulting in amino acid change from isoleucine to leucine (c.1258A>C, p.(Ile420Leu), GRCh37 Chr12:102576400A>C).

Table 3.2 Family 3004: Segregation analysis for variants with a gnomAD frequency of zero.

GENE SYMBOL	Protein change	Nucleotide change	IV-1 (proband)	II-2 (Aff.)	II-3 (Aff.)	III-2 (Aff.)	III-5 (UnAff.)	III-4 (UnAff.)
ACSL1	p.V198I	c.G592A	GA	GG	GG			
ADAM33	p.P90A	c.C268G	CG	CG	CC	CG		
ADARB1	p.L596F	c.C1786T	CT	CC				
ANKRD30BL	p.S19N	c.G56A	GG	GG	GG	GG		
ARPP21	p.I90T	c.T269C	TC	TT				
BFSP2	p.H390R	c.A1169G	AG	AA	AA	AA		
BPHL	p.R231L	c.G692T	GT	GG	GG	GT		
C2orf16	p.1641_1642del	c.4923_4924del	N/A	N/A	N/A	N/A	N/A	
C4BPA	p.T69A	c.A205G	AG	AA	AA	AG		
CCDC103	p.A87T	c.G259A	GA	GA	GA	GA	AA	
DOK1	p.399_399del	c.1195_1196del	Del	Del	No del	Del		
FOXP2	p.R478Q	c.G1433A	GA	GG				
FPR1		19-52250256-C-T	GA	GA	GG	GA		
GTDC1	p.M242I	c.G726A	GA	GG	GG	GG		
HCLS1	p.P331fs	c.993_994insTGAGCCTGAGC	Ins	No ins	Ins	Ins	Ins	
HRC	p.257_261del	c.770_781del	Del	N/A	No del	No del		
KIF16B	p.H1109fs	c.3326delA	A del	A del	A del	A del	A del	
KPNA7	p.T71A	c.A211G	AG	AG	AG	AG	AA	AA
LARGE1	p.R213W	c.C637T	CT	CC	CC	C>T		
M1AP	p.P370A	c.C1108G	CG	CG	CC			
NACC1	p.R333H	c.G998A	G>A	GG	GG	GG		

NDUFAF5	p.G182X	c.G544T	GT	GT	GT	GT	GT	
OSTC	p.Y146C	c.A437G	AG	AA	AA	AA		
PARPBP	p.I266L	c.A796C	AC	AC	AC	AC	AA	AA
PCDHB10	p.A408E	c.C1223A	CA	CC				
PCDHB14	p.G594S	c.G1780A	GG	GG	GG	GG		
SAXO2	p.P39A	c.C115G	CG	CC				
SCAF11	p.C662F	c.G1985T	GT	GG				
SEC23IP	p.C548S	c.G1643C	GC	GG				
SKIV2L2	p.T788A	c.A2362G	AG	AA				
SLC22A13	p.A193G	c.C578G	CG	CC	CC	CC		
SPRR2A	p.S65A	c.T193G	TG	TT	TT	TT		
TMEM82		c.757+1G>A	GA	GA	GG	GA		
TUBGCP6	p.A1281V	c.C3842T	CT	CC	CC	N/A	CT	
USF3	p.Q1467fs	c.4401delG	Del	Del	Ins	Del	Del	
VENTX	p.P48T	c.C142A	CC	CC				

N/A – Not available: sequencing data require further optimization; Aff. – Affected; UnAff. – Unaffected

Variants highlighted in yellow indicate genes with variants that segregate with the disease in the family

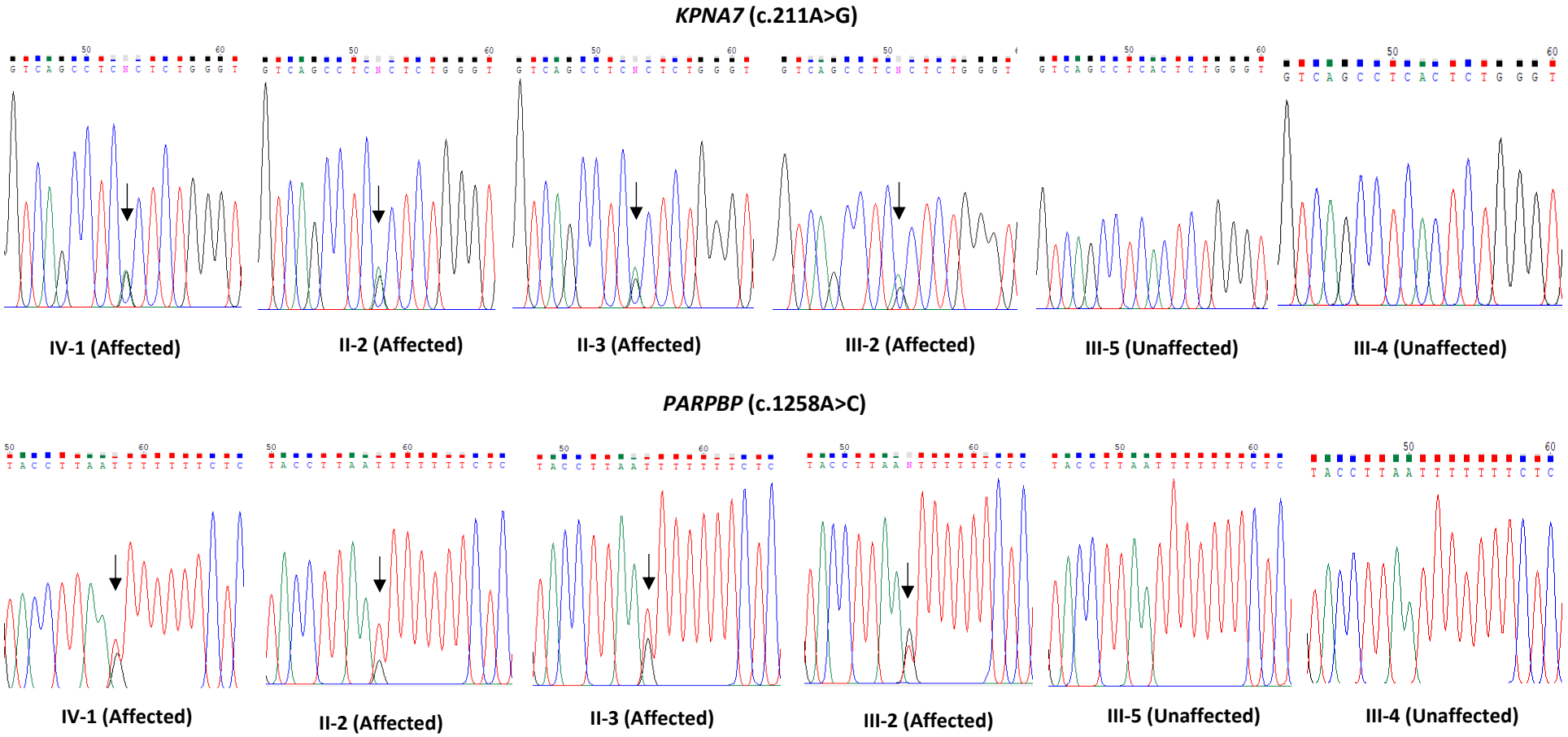


Figure 3.3. Segregation analyses in 3004 family. DNA sequence chromatograms of the T>G heterozygous mutation in *PARPBP* and A>G heterozygous mutation in *KPNA7* identified in all four affected members (IV-1, II-2, II-3 & III-2) which is not present in two unaffected members (III-5 & III-4). The arrow on each chromatogram indicates the position of the identified mutation

3.4.1.2 Preliminary analysis of KPNA7 and PARPBP

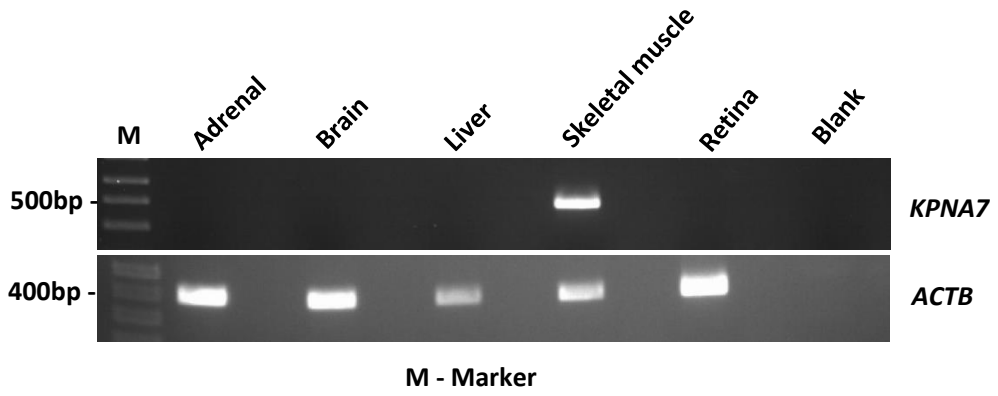
Variants in *KPNA7* and *PARPBP* both segregate with the adRP in family 3004. To determine the plausibility of these genes as candidate genes, further investigations were carried out: (i) PubMed and various databases were searched for information on the known function and expression pattern of these genes, (ii) experimentally determining the expression of these genes in the mammalian retina, and (iii) determining how conserved the amino acids reported to be mutated in these genes are across various species. At the time of this study, neither *KPNA7* nor *PARPBP* had been reported to be expressed in the mammalian retina.

KPNA7 is involved in nuclear protein import (Kelley et al., 2010), and is reported to have an expression pattern that is largely limited to oocyte and early embryonic development (Hu et al., 2010). Expression of *KPNA7* is reported to dip significantly after embryonic development (Oostdyk et al., 2019), limiting its expression in adult tissues to the gall bladder and stomach (NCBI [www.ncbi.nlm.nih.gov/gene/402569]). Mutations in *KPNA7* have been linked to neurodevelopmental anomalies such as infantile spasms and cerebellar malformations (Paciorkowski et al., 2014). A primer pair specific for *KPNA7* (Exon 1_5) and endpoint PCR was used on a panel of human cDNAs, including retina, to determine the expression profile. The expected 585bp fragment was detected only in skeletal muscle (Figure 3.4A) confirming the limited expression previously reported. *KPNA7* expression in gall bladder and stomach is reported in the NCBI panel presented above but these tissues were not on our panel. Also, the NCBI panel described above did not report *KPNA7* expression in skeletal muscle because the tissue was not included on their panel. To confirm that *KPNA7* was indeed not expressed in the mammalian retina, two more expression primer pairs were designed spanning different exons of the gene (Exon 2_6 and Exon 8_10) but expression was only identified in skeletal muscle (primer sequences are listed in Appendix C). This lack of evidence of retinal expression for *KPNA7* has been corroborated by the recently published human retina scRNA-seq dataset (Lukowski et al., 2019) in which *KPNA7* expression was not identified in any of the retinal cell sub-populations.

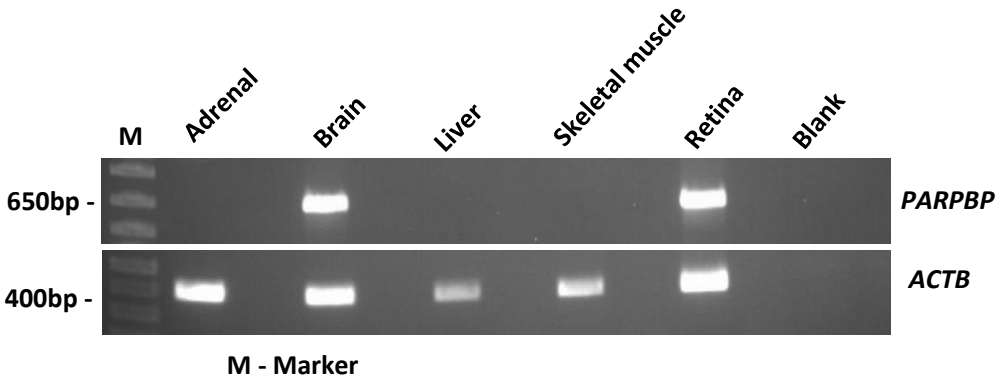
PARPBP has been reported to be involved in regulating DNA repair processes (Piao et al., 2011), and its up/downregulation reported to be linked with prognosis of some cancers (Chen et al., 2020). It is reported to be widely expressed across various tissues in mammals (www.ncbi.nlm.nih.gov/gene/55010). A primer pair specific for *PARPBP* (Exon 2_6) and endpoint PCR was used on a panel of human cDNAs, including retina, to determine the expression profile of *PARPBP*. The expected 688bp fragment was detected in both brain and retina (Figure 3.4B). The expression profile of *PARPBP* reported in the recently published human retina scRNA-seq dataset (Lukowski et al., 2019) was also analysed and it confirmed *PARPBP* expression in the human retina as identified in our experimental data, with the highest expression in rod photoreceptors, followed by RGCs, bipolar cells and the least expression in cones (Appendix D).

Due to the lack of evidence for retinal expression of *KPNA7,* both from the literature (Menon et al., 2019, Lukowski et al., 2019) and the results from the tissue panel, the gene was ruled out as a potential candidate in this family. Therefore, *PARPBP* seemed the more compelling candidate in family 3004 for further characterization (see 3.4.1.3). However, alignment of PARPBP protein sequence from different species showed that the isoleucine amino acid (p.Ile420) altered by the c.1258A>C change in family 3004 is conserved in some but not in all species compared; it is an isoleucine in human, chimpanzee, wolf and chicken, but an asparagine in mouse and rat, a serine in zebrafish, and a proline in frog (Figure 3.4C), suggesting that the amino acid might not be important to the overall protein structure and function.

A.



B.



C.

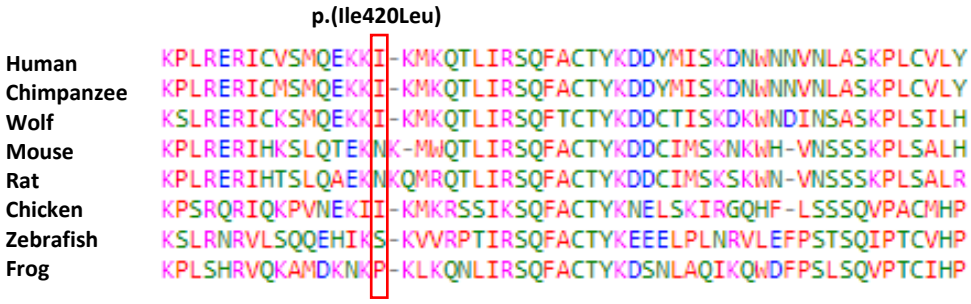


Figure 3.4. Expression of *KPNA7* and *PARPBP*. The expression of genes with variants segregating in family 3004 (*KPNA7* and *PARPB)* was examined using human tissue cDNA. (A)*KPNA7* expression (585bp) was only detected in skeletal muscle. (B) *PARPBP* expression (688bp) was detected in human brain and retina. Beta-actin (*ACTB)* expression was used as positive control. (C) Alignment of PARPBP amino acid sequences from various species. The amino acid (p.(Ile420)) altered by the variant identified in Family 3004 is conserved across some species.

3.4.1.3 Preliminary characterization of PARPBP expression in mammalian retina

Having identified *PARPBP* as a candidate gene for family 3004, we performed preliminary analysis on the gene and protein's expression in the mammalian retina by examining the potential transcripts of *PARPBP* present in the human retina and brain. We also examined the expression of the PARPBP protein in the mouse retina using an antibody specific to human PARPBP to determine in which cells or layers of the retina the protein was expressed.

3.4.1.3.1 Determining the full length of PARPBP transcripts in human retina

From the available literature and gene databases, the *PARPBP* gene has been reported to consist of 11 exons of which exon 1 is non-coding and the remaining 10 exons (1740bp) code for a 579 amino acid protein (Figure 3.5A). The gene is also reported to have several splice variants in various tissues (Borsu et al., 2000a). Since there was no information on *PARPBP* expression in the retina, we examined the potential transcripts present in the retina by amplifying full-length *PARPBP* from human retina cDNA. A primer pair was designed (see 2.3.2.5) starting at the transcription start site in exon 2 with a reverse primer located at the stop site in exon 11 of the *PARPBP* gene. Sequences of all primers used can be found in Appendix C. This primer pair was used to amplify products from human brain and retina cDNA by endpoint PCR (see 2.3.2.6) which were then analysed on agarose gels. From human brain cDNA, a 1375bp product (B1) was amplified which was not identified in the retina (Figure 3.5B). This product was cloned (see 2.3.2.11.1) and sequenced (see 2.3.2.16.1) and was found to contain exons 2 to 11 excluding exons 7 and 8 (Figure 3.5B). Using the same primer pair in human retina cDNA, two products of 1206bp (R1) and 1604bp (R2) were amplified which were not obtained from the brain (Figure 3.5B). R1 was cloned and sequenced and contains exons 2 to 11 excluding exons 5, 7 and 8 (Figure 3.5B). R2 consisted of exons 1 to 11 excluding exon 10 (Figure 3.5B).

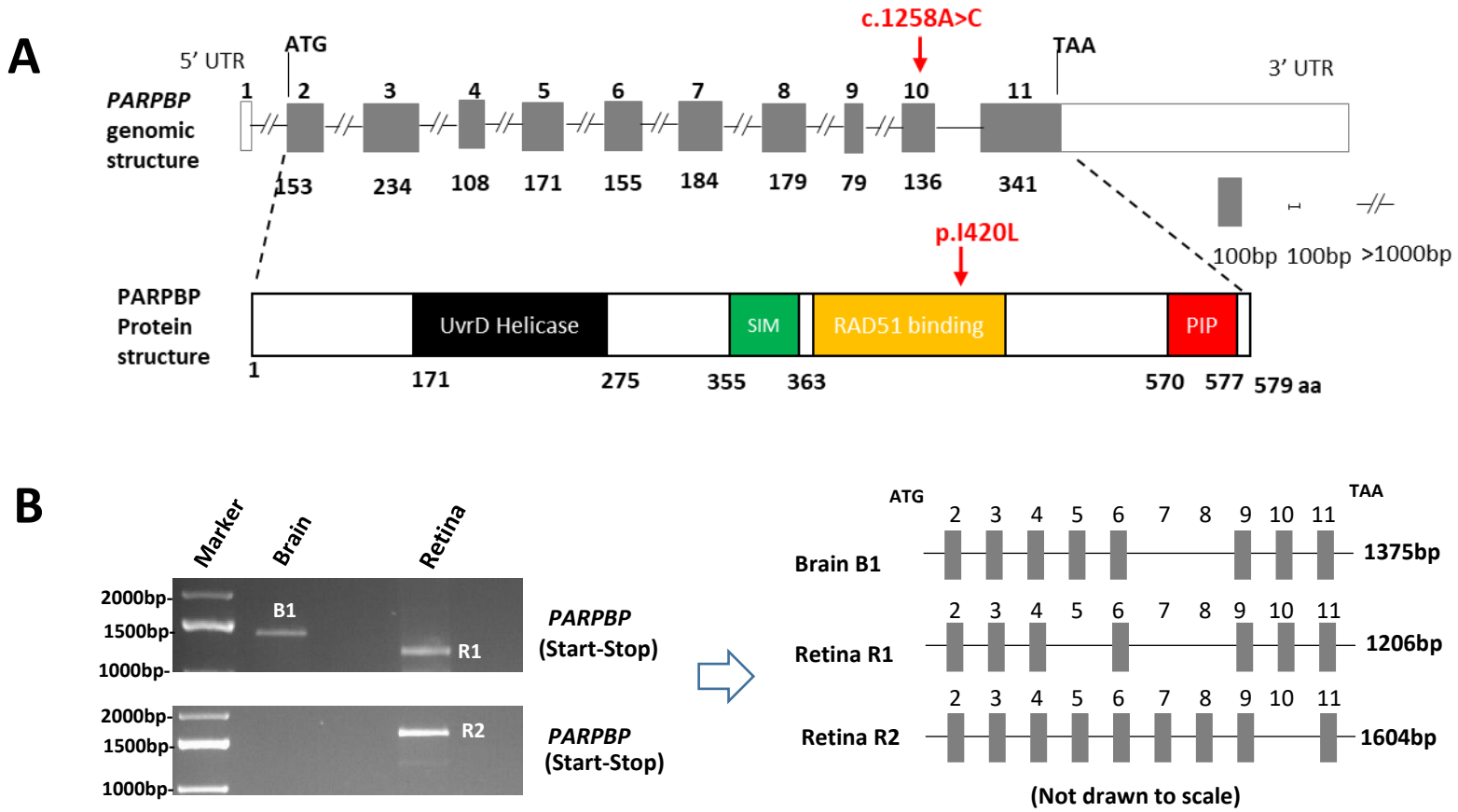


Figure 3.5. Preliminary analysis of *PARPBP* transcripts in the human retina. (A) Schematic diagram of genomic structure of *PARPBP* and the corresponding protein domains. Exons are indicated as boxes and introns as lines. Shaded boxes = coding exons; UTR = Untranslated region; SIM = SUMO-interacting motif; PIP = PCNA-interacting motif. (B)) Full length of *PARPBP* transcripts amplified from human brain and retina using expression primers designed to amplify from start to stop of the full-length coding sequence. A 1375bp product (B1) amplified from brain but not in retina was identified to contain exons 2 to 11 excluding exons 7 and 8. Two products of 1206bp (R1) and 1604bp (R2) were amplified from the retina. R1 contained exons 2 to 11 excluding exons 5, 7 and 8, whiles R2 contained exons 2 to 11 excluding exon 10.

3.4.1.3.2 PARPBP protein expression and localisation in mouse retina

Having detected PARPBP expression in cDNA from human retina, we investigated the Parpbp protein expression in the mouse retina using western immunoblotting (see 2.3.5.3) and immunohistochemistry (see 2.3.7.3) using a commercially available rabbit polyclonal antibody designed to the N-terminal amino acids 115-191 of human PARPBP (#NBP1-93969, Novus Biologicals, UK). The amino acid sequence of this human N-terminal antibody had 57.14% similarity with the mouse Parpbp protein. The antibody was used to probe lysates from wild-type mouse brain and retina through western immunoblotting (see 2.3.5.3) but no bands of the expected size of the Parpbp protein (64kDa) (Borsu et al., 2000b) was detected after several optimisation steps, including varying antibody concentrations and varying amounts of protein (data not shown).

The antibody was used to immunohistochemically stain adult wild-type mouse retinal cryosections. Using this human N-terminal PARPBP antibody at an optimised concentration of 1:200, PARPBP-positive labelling was detected in the cells of the inner nuclear layer and in the ganglion cells of the adult mouse retina (Figure 3.6). No PARPBP-positive staining was identified in the photoreceptor layer of the adult retina. For a gene to be responsible for a photoreceptor-associated phenotype such as RP, the gene or its product must be expressed in the photoreceptors. Therefore, we went on to stain sections from developing wild-type mouse retina to investigate if Parpbp expression may be detected in the photoreceptors during early stage(s) of development. Retinal sections from P0, P4, P8, P12, P16 and Adult mice were immunohistochemically stained with the N-terminal PARPBP antibody. PARPBP-positive staining was detected at all the developmental time points examined (Figure 3.6).

At P0 and P4 when the retina consists of only two main layers, the GCL and neuroblastic layer (NBL), Parpbp-positive staining is strongly present in the GCL and cells in the lower half of the NBL, although some positive staining is also seen in a few cells at the upper half of the NBL cells at P4 (Figure 3.6B). From P8, where photoreceptor cells have fully differentiated from the NBL to form the ONL, PARPBP-positive staining continues to be prominent in the INL and the GCL into adulthood. Additionally, some cells in the photoreceptor layer appear to demonstrate some weak Parpbp-positive staining from P8

to P16, becoming more evident at P16 (Figure 3.6E). Surprisingly, this Parpbp-positive staining in the photoreceptor layer is not seen in the adult retina. An antibody specific to Brn3a (POU class 4 homeobox 1), a ganglion cell marker, was used to localise Parpbp staining in the GCL. Both Brn3a and Parpbp staining in the GCL were detected from P0. As expected, Protein Kinase C alpha (PKCα) staining, used as a marker of bipolar cells and their processes, is absent at P0 but present at P4 and becomes well-defined as the retina matures into adulthood.

3.4.2 Family 3013

Family 3013, of British origin, has 3 members diagnosed with adRP spanning 2 generations (Figure 3.8). The adRP in this family is of variable onset and severity with some cases being asymptomatic. A summary of the adRP phenotype and associated features in this family are shown in Table 3.3. Fundus images from the proband (II-4) depicting the RP phenotype in this family, characterised by bilateral peripheral bone spicule pigmentation, can be found in Figure 3.9. A total of 6 individuals in this family were recruited, including 3 affected (II-4, II-5, and III-5), 2 unaffected (III-3 and III-4), and an individual with an indeterminate disease status (II-2). Genomic DNA was obtained from all 6 individuals.

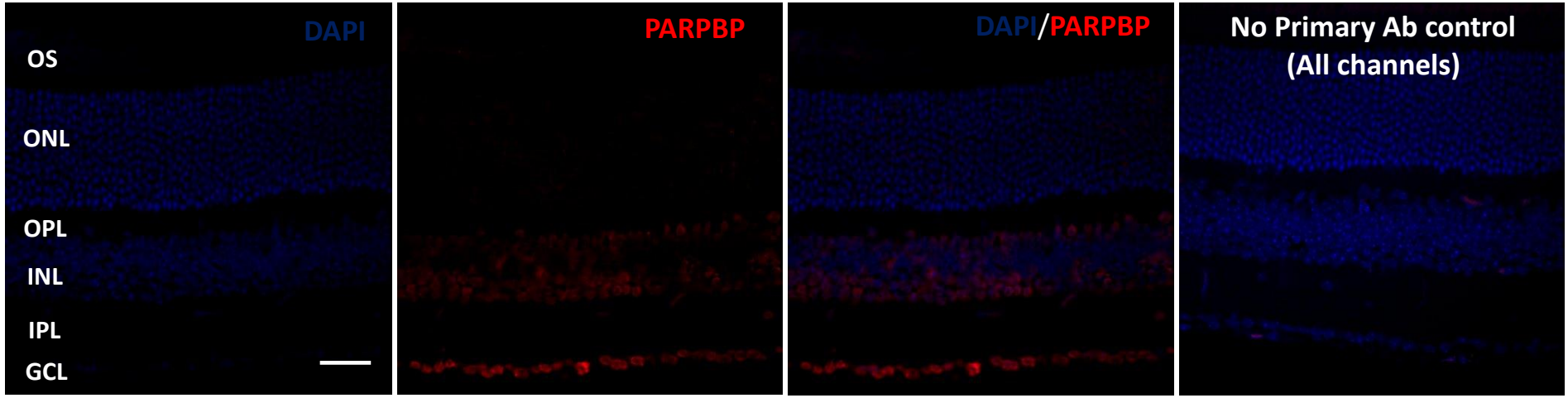


Figure 3.6. Immunohistochemical staining of wild type mouse retina with PARPBP antibody. Human N-terminal PARPBP antibody (115-191aa) was used to stain cryosections from adult wild-type mouse retina. PARPBP-positive staining (red) was identified to be present in cells of the INL and GCL. Sections stained with secondary antibodies only were used as controls. DAPI (blue) was used to stain the nuclei. OS = Outer segment; ONL = Outer nuclear layer; OPL = Outer plexiform layer; INL = Inner nuclear layer; IPL = Inner plexiform layer; aa = amino acid; Ab = Antibody. Scale bar = 20µm.

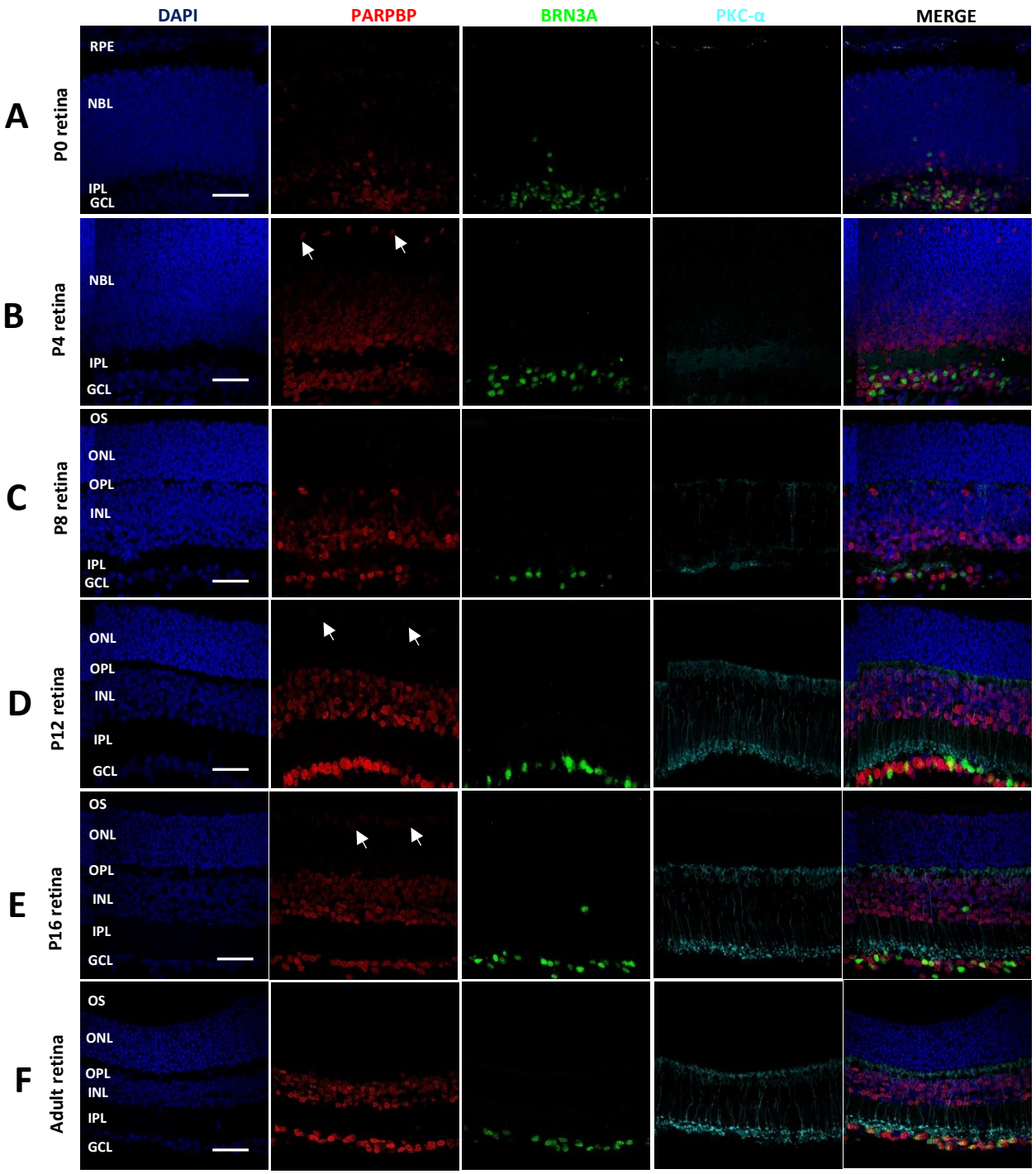


Figure 3.7. Parpbp protein expression in developing mouse retina. Immunohistochemical staining was conducted on frozen sections from wild-type mouse retina sections at various developmental stages. Parpbp-positive staining (red) was detected predominantly in the INL and GCL at all the time points examined, while weak staining was detected in the photoreceptor layer from P4 to P16 (white arrows). BRN3A (green) was used to label ganglion cells. DAPI (blue) was used to stain the nuclei. PKC-alpha (cyan) which stains bipolar cells was used as retinal marker. RPE = Retinal pigment epithelium; OS = Outer segment; ONL = Outer nuclear layer; OPL = Outer plexiform layer; INL = Inner nuclear layer; IPL = Inner plexiform layer; GCL = Ganglion cell layer; NBL = Neuroblastic layer. Scale bar = 20µm

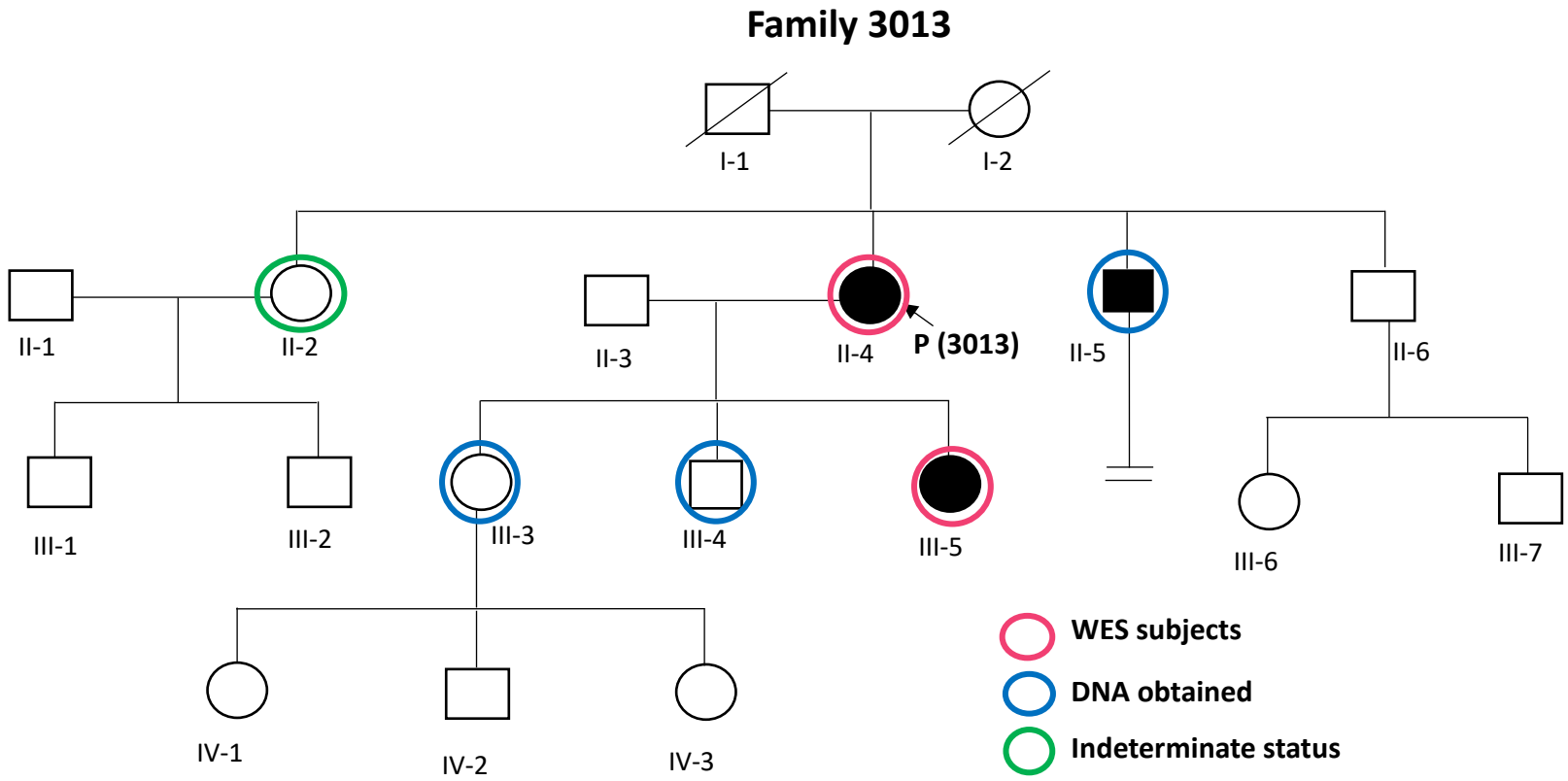
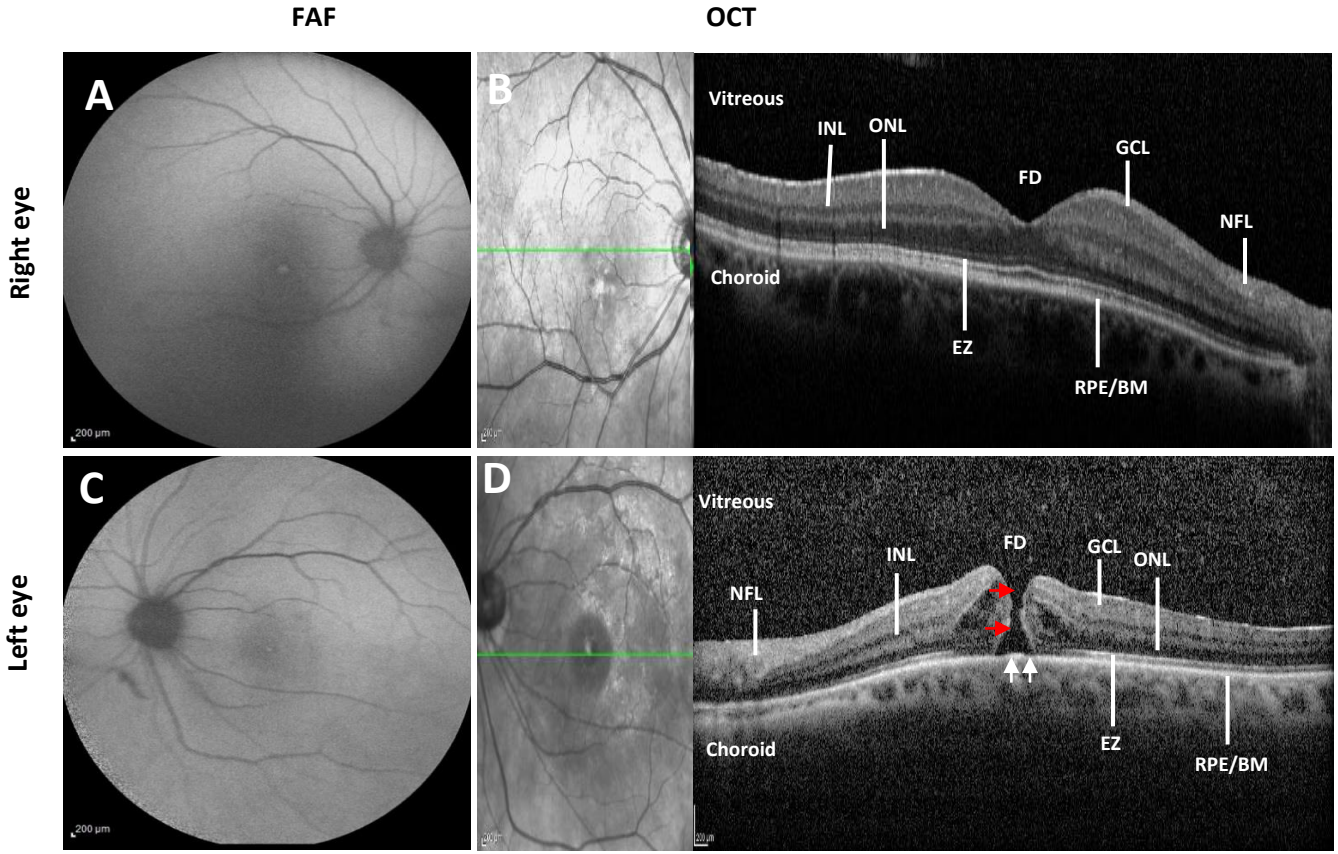


Figure 3.8: Pedigree of family 3013 diagnosed with adRP. Three affected individuals (II-4, II-5, and III-5) and two unaffected individuals (III-3 and III-4) were recruited into this study. Circles=women; squares=men; filled symbols=affected; open symbols=unaffected. Symbol with a bar across=deceased; P=Proband.

Table 3.3. Summary of clinical findings in Family 3013 with adRP

Patient	Age of onset	Symptoms	Visual acuity	Fundus	Visual fields/ OCT	ERG
II-4	59	Photosensitivity, photopsia, scotoma (LE), decreased visual acuity	RE: 6/7.5 LE: 6/48	Peripheral bone spicule pigmentation (BE)	Peripheral restrictions, No scotoma; OCT within normal limits	RE: Normal cone responses, abnormal rod and RPE responses; LE: Abnormal cone, rod and RPE responses
II-5	N/A	Asymptomatic	RE: 6/7.5 LE: 6/5	Peripheral bone spicule pigmentation (BE)	Full visual field; OCT within normal limits	Broadly normal responses with borderline rod response (BE)
III-5	N/A	Asymptomatic	RE: 6/7.5 LE: 6/5	Bone spicule pigmentation in far periphery, 300^{o} (BE)	Full visual field with mild peripheral changes; OCT within normal limits	Normal rod, cone and RPE function, reduced macular responses

OCT - Optical coherence tomography; ERG – Electroretinography; BE – both eyes; RE – Right eye; LE – Left eye; HM – Hand motion; N/A – Not available.



Patient: 3013

Figure 3.9. Retina imaging of proband in family 3013 with adRP. (A, C) Fundus autofluorescence (FAF) images showing reduced autofluorescence in the inferior retina of right eye and in the central retina of the left eye. (B, D) Spectral domain optical coherence tomography (OCT) images showing relatively normal retinal layers in right eye and foveal hole (red arrowheads) indicative of scotoma in left eye and an absent ellipsoid zone (EZ) in the macular region (white arrowheads). Widefield fundus pseudo-colour images for this patient were not available. FD= Foveal depression; NFL= nerve fibre layer; GCL= ganglion cell layer; INL= inner nuclear layer; ONL= outer nuclear layer; EZ: ellipsoid zone; RPE= retinal pigment epithelium; BM= Bruch's membrane.

3.4.2.1 Segregation analysis in Family 3013

The proband (II-4) and her affected daughter (III-5) from family 3013 underwent WES. Bioinformatic analysis revealed II-4 and III-5 shared 99 heterozygous variants of which 15 had gnomAD frequency of zero (Table 3.4)**.** Sanger sequencing was used to investigate these variants and 14 of these 15 were validated in the proband and III-5, primer sequences are given in Appendix B. Segregation analysis was carried out in a stepwise manner as described in section 3.3.3.3. Segregation analysis for the 14 validated variants in this family was performed using DNA samples from an affected brother (II-5), unaffected of daughter (III-3) and unaffected son (III-4) of the proband (Table 3.4). A DNA sample was obtained from the proband's sister (II-2) who was initially recruited as an unaffected. However, visual changes were noted in her on a subsequent visit to the clinic and we are waiting for further clinical evaluation to confirm her status. As her status is currently undetermined, she was not used in the segregation analysis. To date it has not been possible to validate the putative *SET* variant as multiple primer pairs and optimizations have not been able to amplify this region in any of the family members.

Two variants, one in myosin VB (*MYO5B*) and the other in piezo type mechanosensitive ion channel component 1 (*PIEZO1*), were found to segregate with the adRP in this family. The chromatograms from the segregation analysis of *MYO5B* and *PIEOZ1* variants are shown in Figure 3.10. The variant reported in *MYO5B* is a heterozygous substitution from guanine to adenine at c.5314-1G>A (GRCh37 Chr18: 47361795G>A, NM_001080467.3) and is predicted to alter splicing (MutationTaster, [https://www.mutationtaster.org/]). The variant reported in *PIEZO1* is a heterozygous missense variant in which cytosine at nucleotide position 6280 (NM_001142864.4) is replaced by guanine leading to an amino acid change from leucine to valine (c.6280C>G, p.(Leu2094Val), GRCh37 Chr16: 88786253C>G).

Table 3.4. Family 3013: Segregation analysis for variants with gnomAD frequency of zero.

GENE SYMBOL	Protein change	Nucleotide change	II-4 (proband)	III-5 (Aff.)	II-5 (Aff.)	III-3 (UnAff.)	III-4 (UnAff.)	II-2 (IND.)*
BBS9	p.E838K	c.G2512A	GA	GA	GA			
CIT	p.N661fs	c.1983delT	T del	T del	TT			
CRYAB	p.F51S	c.T152C	TC	TC	TT			
FAT4	p.L287P	c.T860C	TC	TC	TT			
KIN	splicing	c.558+1G>T	GT	GT	GT			
MYO5B	splicing	c.283-1G>A	GA	GA	GA	GG	GG	GA
MYO9A	p.V1836F	c.G5506T	GT	GT	GG			
PABPC4L	p.Q134K	c.C400A	CA	CA	CC			
PIEZO1	p.L16V	c.C46G	CG	CG	CG	CC	CC	CC
REG1B	p.D76fs	c.227_228ins GG	Del	Insert	Insert			
SEC24D	p.P261L	c.C782T	CT	CT	CC			
SET	p.S4C	c.C11G	N/A	N/A	N/A			
SLC22A13	p.L177V	c.C529G	CG	CG	CC			
TRPM4	splicing	c.3461+1G>T	GT	GT	GG			
URAD	p.Q145X	c.C433T	CT	CT	CC			

N/A – Not available: sequencing data require further optimization; Aff. – Affected; UnAff. – Unaffected; IND. – Indeterminate.

*Status to be reassessed due to recently reported visual changes

Variants highlighted in yellow indicate genes with variants that segregate with the disease in the family

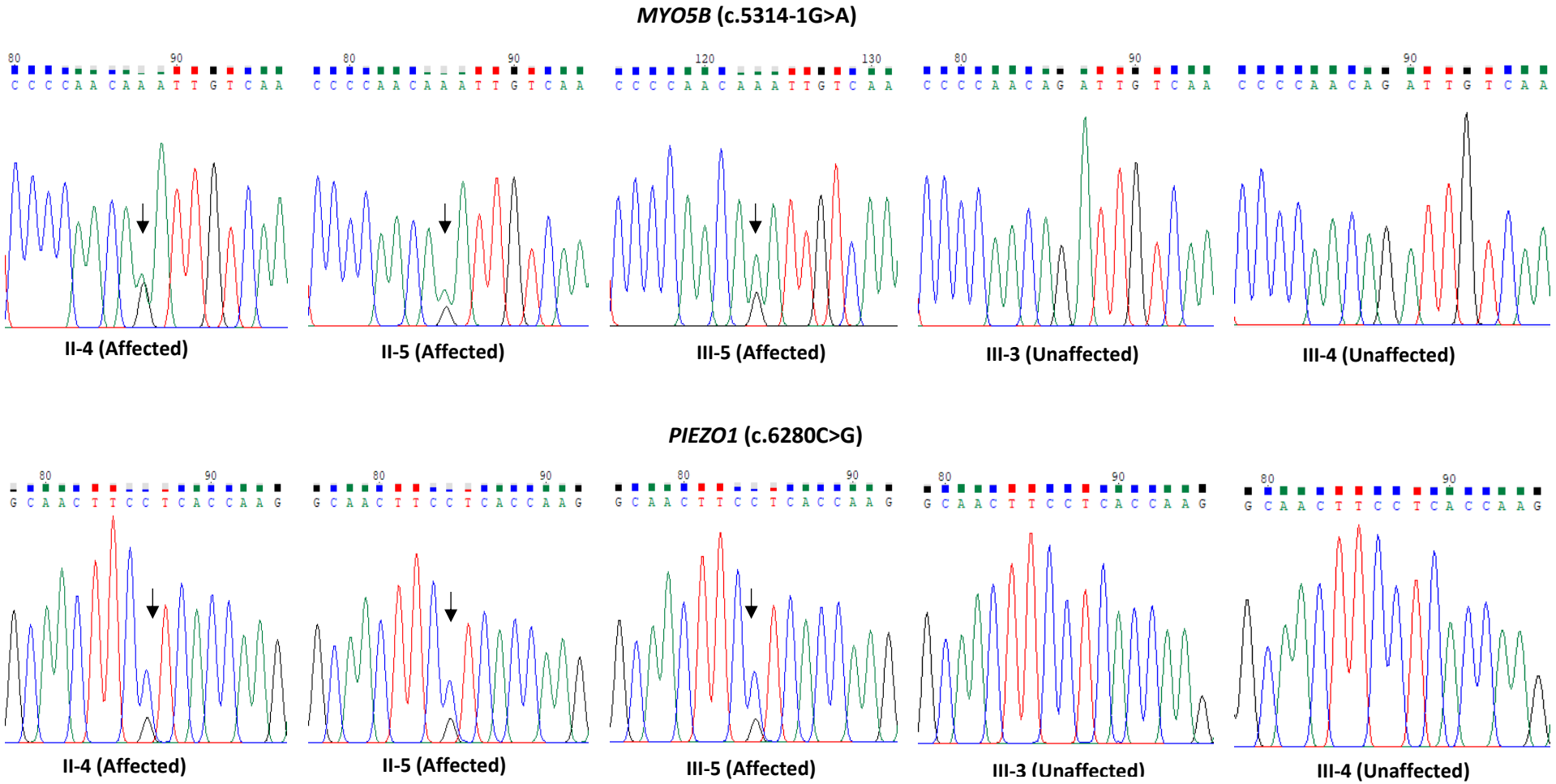


Figure 3.10. Segregation analyses in 3013 family. DNA sequence chromatograms of the G>A heterozygous variant in *MYO5B* and C>G heterozygous variant in *PIEZO1* identified in all three affected members (II-3, II-5, & III-5) which is not present in two unaffected members (III-3 & III-4). The arrow on each chromatogram indicates the position of the identified mutation.

3.4.2.2 Preliminary analysis of MYO5B and PIEZO1 genes

Variants in *MYO5B* and *PIEZO1* both segregate with the adRP in family 3013. At the time of this study, neither *MYO5B* nor *PIEZO1* had been reported to be expressed or have a functional role in the mammalian retina. As such, further investigation was carried out on these two genes to determine the plausibility of these variants as disease causing.

A search in the available literature and gene databases revealed *MY05B* to be a gene that is broadly expressed in mammalian tissues (www.ncbi.nlm.nih.gov/gene/4645), involved in plasma membrane recycling, and mutations in the gene have been associated with microvillus inclusion disease (Müller et al., 2008). Using a primer pair specific for *MYO5B* (Exon37_39) and endpoint PCR on a panel of human cDNAs, including retina, we examined the expression profile of *MYO5B* in human tissues. The expected 730bp product was detected in both human brain and retina (Figure 3.11A). The expression profile of *MYO5B* as reported by the human retina scRNA-seq dataset (Lukowski et al., 2019) was also analysed and it revealed that *MYO5B* expression was reported in several retinal cell subpopulations: rod photoreceptors showed the highest level of expression, followed by bipolar cells, cones and the least expression in RGCs. The scRNA-seq data also showed MYO5B has relatively higher levels of expression in all retinal cells compared to PIEZO1 expression (Appendix D). Alignment of DNA sequences from multiple orthologues of *MYO5B* revealed that the splice acceptor site and the mutated nucleotide identified in family 3013 are conserved across species (Figure 3.11B), an indication that the mutated sequence could be important in the proper splicing of the gene.

PIEZO1 is reported to be ubiquitously expressed (www.ncbi.nlm.nih.gov/gene/9780) and encodes a protein that acts as a mechanically-activated ion channel that links mechanical stimuli to biological signals (Coste et al., 2010). Mutations in *PIEZO1* have been linked to dehydrated hereditary stomatocytosis (Albuisson et al., 2013) and upregulation of the gene has been reported as a prognostic biomarker for malignant gliomas (Zhou et al., 2020). Using a primer pair specific for *PIEZO1* (Exon40_45) and endpoint PCR on a panel of human cDNAs, including retina, we determined the expression profile of *PIEZO1* in human tissues. The expected 874bp product was detected in both

human brain and retina (Figure 3.11B). The expression profile of *PIEZO1* as reported by the human retina scRNA-seq dataset (Lukowski et al., 2019) was also analysed and it revealed that *PIEZO1* expression was reported in several retinal cell sub-populations, with the highest expression found in rod photoreceptors, followed by cones, RGCs and bipolar cells with the least expression (Appendix D). Alignment of PIEZO1 protein sequence from different species showed that the leucine amino acid (p.Leu2094) altered by the *PIEZO1* variant identified in family 3013 is highly conserved across species (Figure 3.11C), and is suggestive of the potential importance of the mutated amino acid to the protein structure and function.

As both *MYO5B* and *PIEZO1* are expressed in human retina, from the current data, further investigation is required to determine the more compelling candidate for this family. Obtaining DNA samples from other affected and unaffected family members may help in excluding one these. Also, identifying the where these proteins localise in the mammalian retina could also be useful in identifying the more compelling candidate. However, these further steps have not been explored due to time limitations.

3.4.3 Family 3027

Family 3027, of British origin, has 2 members diagnosed with adRP spanning two generations (Figure 3.12). The adRP in this family has its onset in the early 40s marked by night blindness. A summary of symptoms and associated features of the adRP phenotype in this family is shown in Table 3.5. Fundus images from the proband (II-5) depicting bilateral bone spicule pigmentation with a macular sparing RP phenotype are shown in Figure 3.13. A total of 4 individuals were recruited from this family, including two affected individuals (II-5 and III-6) and two unaffected individuals (II-3 and III-7). Genomic DNA was obtained from all 4 individuals.

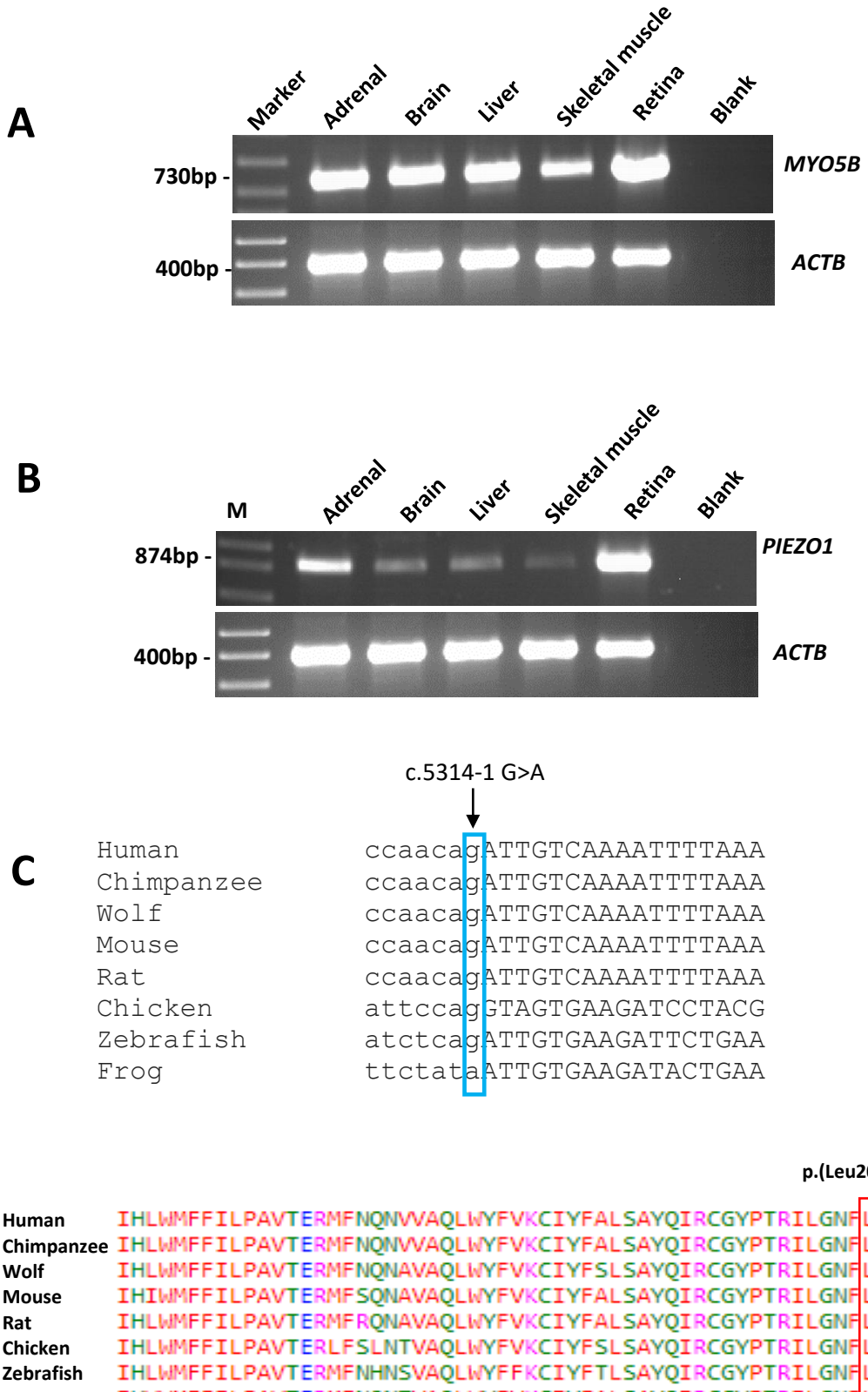


Figure 3.11. *MYO5B* and *PIEZO1* expression and conservation across species. (A) *MYO5B* expression in a panel of human tissue cDNAs including retina. (B) *PIEZO1* expression in a panel of human tissue cDNAs including retina (C) Alignment of multiple *MYO5B* DNA sequences from different species shows that the acceptor splice site sequence containing the variant identified in family 3013 (c.5314-1) is conserved. (C) Alignment of PIEZO1 sequences from various species shows p.(Leu2094) is highly conserved.

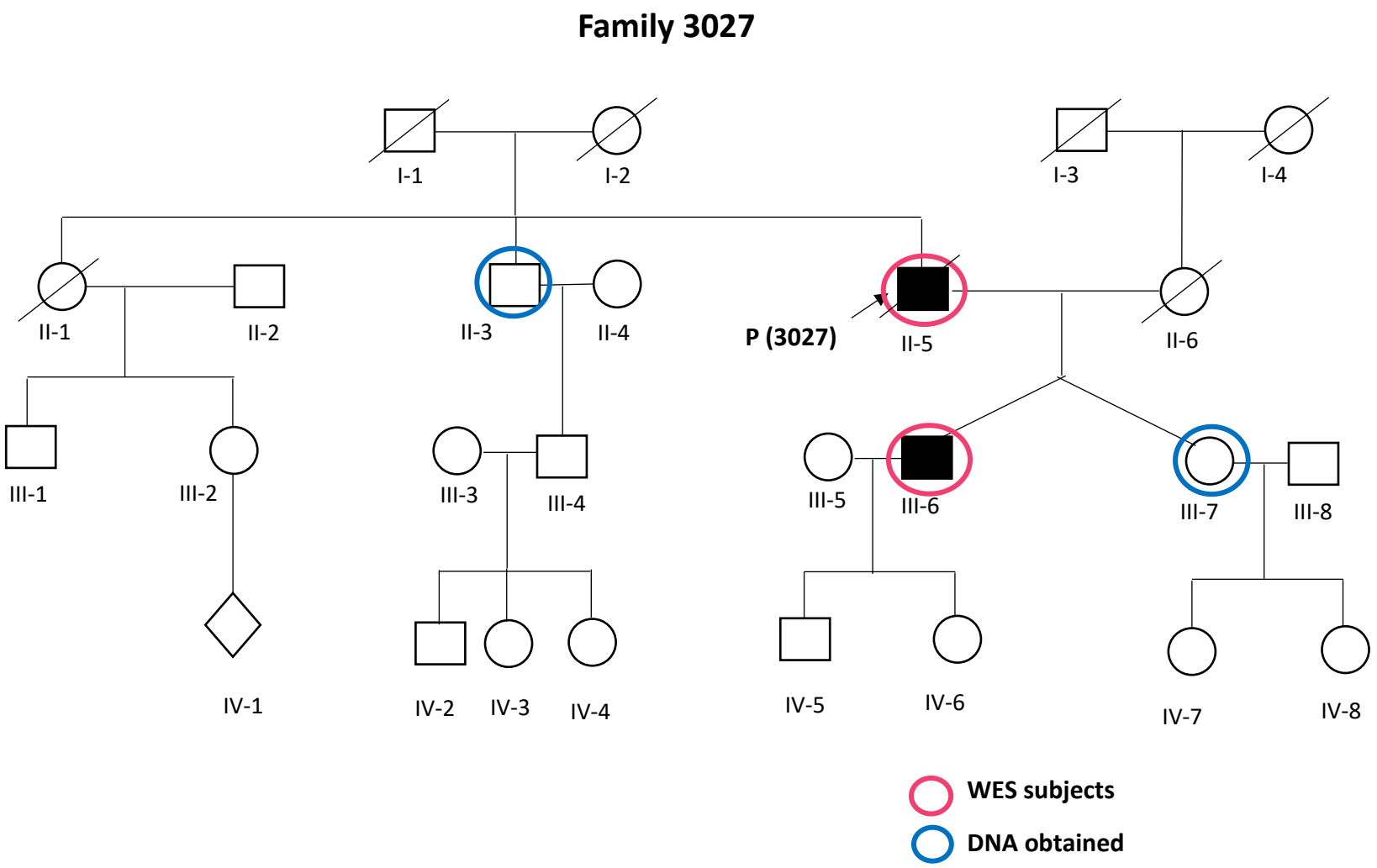
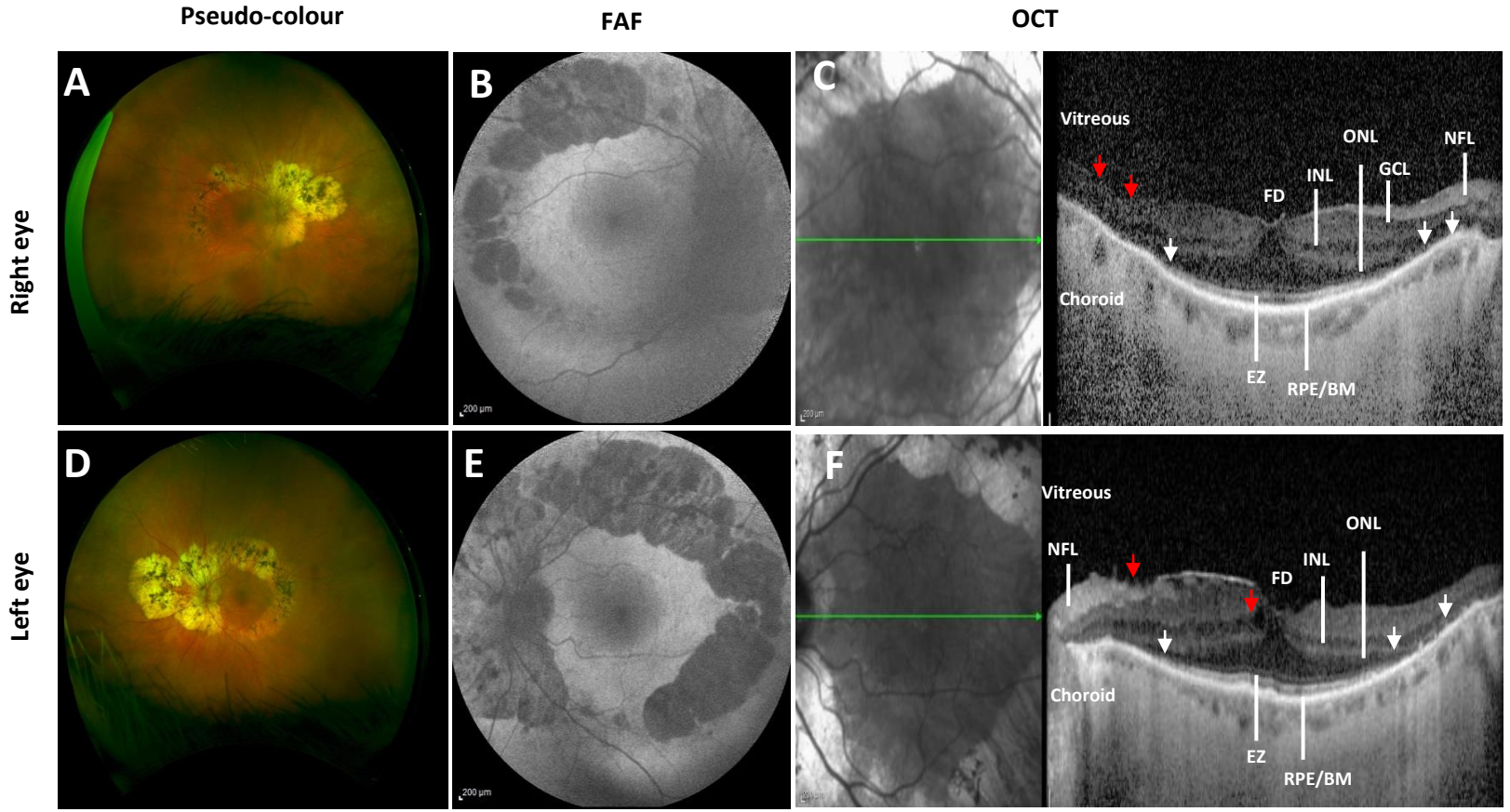


Figure 3.12. Pedigree of family 3027 diagnosed with adRP. Two affected individuals (II-5 and III-6) and two unaffected individuals (II-3 and III-7) were recruited into this study. Circles=women; squares=men; filled symbols=affected; open symbols=unaffected. Symbol with a bar across=deceased; P=Proband.

Table 3.5. Summary of clinical findings in Family 3027 with adRP

Patient	Age of onset	Symptoms	Visual acuity	Fundus	Visual fields/OCT	ERG
II-5	43	Misty vision, glare sensitivity, denies night blindness	RE: 6/30 LE: 6/20	Bone spicule pigmentation, chorioretinal atrophy with macular sparing (BE)	Visual fields: ring of field loss (BE) OCT: centrally preserved retina	N/A
III-6	46	Night blindness, decreased dark adaptation	RE: 6/10 LE: 6/6	Mild pigmentary retina pathology (BE), macular atrophy above arcades	Visual fields: concentric mid-peripheral scotoma with central 10^{o} sparing (BE); OCT: centrally preserved retina	Reduced rod responses, normal cone responses (BE)

OCT - Optical coherence tomography; ERG – Electroretinography; BE – both eyes; RE – Right eye; LE – Left eye; HM – Hand motion; N/A – Not available.



Patient: 3027

Figure 3.13. Retina imaging of proband in family 3027 with adRP. (A, D) Widefield fundus pseudo-colour images showing bone spicule pigmentation and chorioretinal atrophy with macular sparing in both eyes. (B, E) Fundus autofluorescence (FAF) images showing large areas of hypoautofluorescence in the mid-periphery surrounding the macular of both eyes. (C, F) Spectral domain optical coherence tomography (OCT) images showing generalised loss of photoreceptor integrity layers (white arrowheads) and retinal layers (red arrowheads) except in the fovea. FD= Foveal depression; NFL= nerve fibre layer; GCL= ganglion cell layer; INL= inner nuclear layer; ONL= outer nuclear layer; EZ: ellipsoid zone; RPE= retinal pigment epithelium; BM= Bruch's membrane.

3.4.3.1 Segregation analysis in Family 3027

WES was conducted on the proband (II-5) and his affected twin son (III-6) in family 3027. Bioinformatic analysis revealed 94 heterozygous variants shared between II-5 and III-6 and 22 of these had a gnomAD frequency of zero. Sanger sequencing was used to analyse these variants and all 22 were validated, primer sequences are given in Appendix B. Segregation analysis was conducted on these 22 validated variants using DNA samples from two unaffected relatives (III-7 and II-3) (Table 3.6) and only the variant in metastasis suppressor 1 (*MTSS1*) was found to segregate with the adRP in this family. DNA sequencing chromatograms from segregation analysis of the *MTSS1* variant is shown in Figure 3.14. The *MTSS1* variant identified in this family is a heterozygous 3-base pair non-frameshift deletion of GAA (c.637_639del) resulting in the deletion of a glutamic acid at amino acid position 213 of the MTSS1 protein (c.637_639del, p.(Glu213del), Chr8: 125579410GAAA-A, NM_001282971.2).

Table 3.6. Family 3027: Segregation analysis for variants with gnomAD frequency of zero

GENE SYMBOL	Protein change	Nucleotide change	II-5 (proband)	III-6 (Affected)	III-7 (Unaffected)	II-3 (Unaffected)
CACNA1E	p.K412N	c.G1236C	GC	GC	GC	GC
CCDC80	p.L179M	c.C535A	CA	CA	CA	CC
DNTTIP2	p.H339Y	c.C1015T	CT	CT	CC	CT
DOPEY1	p.Q1184H	c.G3552C	GC	GC	GC	GC
FAT1	p.E3846K	c.G11536A	GA	GA	GA	GA
GALNT5	p.V612A	c.T1835C	TC	TC	TT	TC
GATA6	p.A176T	c.G526A	GA	GA	GG	GA
HSP90AB1	p.642_644del	c.1924_1932del	Del present	Del present	No Deletion	Del present
HSPA9	p.Q400X	c.C1198T	CT	CT	CT	CT
KHDC1	p.Q72E	c.C214G	CG	CG	CG	CG
KIF5B		c.2368-4C>T	CT	CT	CT	CT
LPA	p.G1178A	c.G3533C	GC	GC	GC	GG
MED16	p.L333Q	c.T998A	TA	TA	TA	TT
MTSS1	p.99_99del	c.295_297del	Deletion present	Deletion present	No deletion	No deletion
PIGZ	p.Q2X	c.C4T	CT	CT	CC	CT
POLH	p.T129A	c.A385G	AG	AG	AA	AG
PRKCDBP	p.R180G	c.C538G	CG	CG	CG	CC
RP11-80H18.3 (HTD2)	p.R41G	c.C121G	CG	CG	CC	CG
SENP1	p.V516E	c.T1547A	TA	TA	TT	TA
TRAF3IP1	p.E202D	c.G606T	GT	GT	GT	GT
TRMT1	p.E38G	c.A113G	AG	AG	AG	AA
ZNF451	p.K666E	c.A1996G	AG	AG	AA	AG

Highlighted in yellow is a gene whose variant segregates with the disease in the family

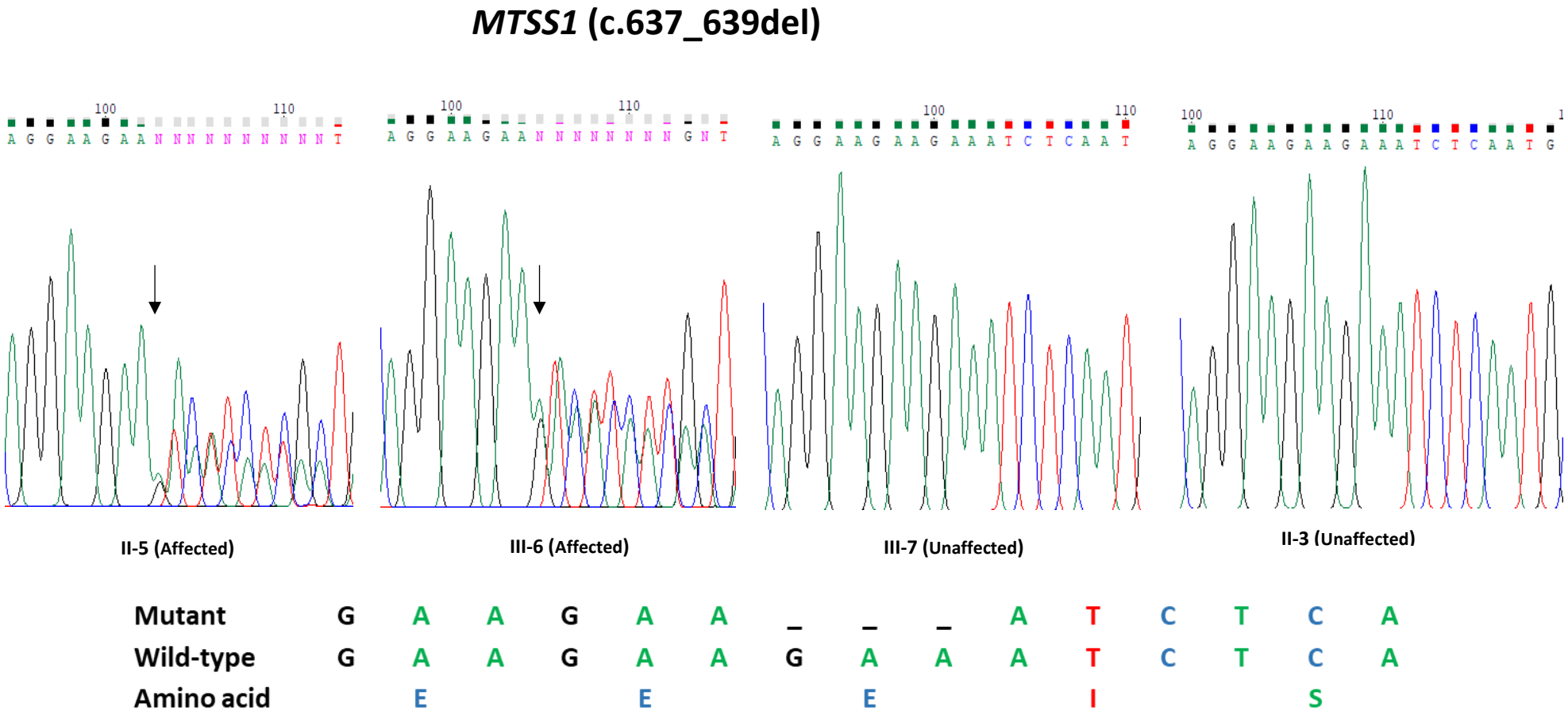


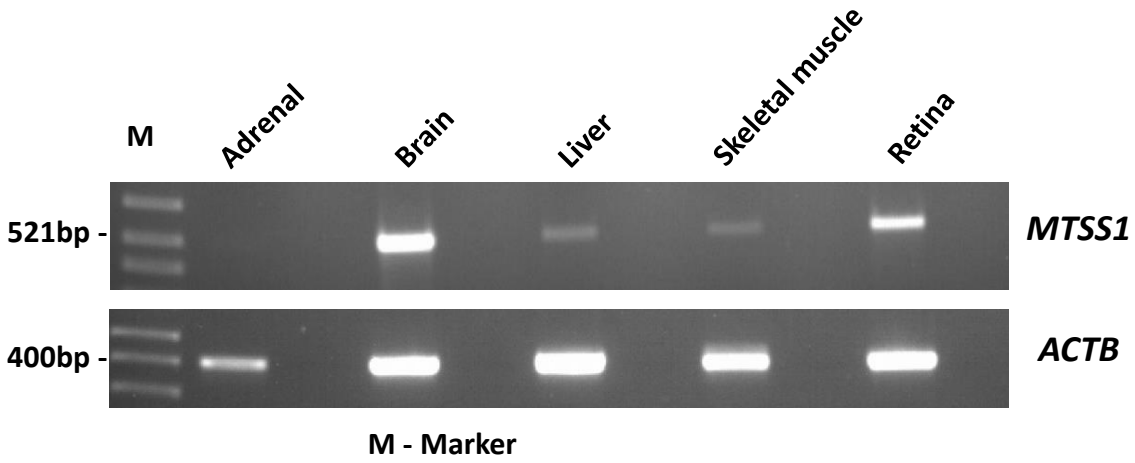
Figure 3.14. MTSS1 variant segregates with adRP in family 3027. DNA sequence chromatograms of heterozygous non-frameshift deletion in *MTSS1* (c.637_639del) observed in 2 affected members (II-5 and III-6) but not in 2 unaffected relatives (III-7 and II-3). Arrow on each DNA chromatogram indicate position of identified mutation. The wild-type and mutant sequences with corresponding amino acids are shown below the chromatograph.

3.4.3.2 Preliminary analysis of the MTSS1 gene

The variant in *MTSS1* was found to segregate with the adRP in family 3027. At the time of this study, there was no information on the expression or functional role of *MTSS1* in the mammalian retina in available literature and gene databases. To determine the plausibility of the *MTSS1* variant, the expression profile and function of MTSS1 was investigated in available literature, by examining its expression in retina experimentally and also examining how conserved the deleted amino acid is across species.

MTSS1 is a known to be a ubiquitously expressed protein (www.ncbi.nlm.nih.gov/gene/9788) whose role in F-actin binding/bundling, cell membrane dynamics and cancer metastasis has been well studied in other mammalian tissues (Saarikangas et al., 2011, Yu et al., 2016) except in the retina. Using a primer pair specific for *MTSS1* (Exon2_8) and endpoint PCR on a panel of human cDNAs, we detected an expected 521bp product in human brain, liver, skeletal muscle, retina (Figure 3.15A), confirming its reported ubiquitous expression. The expression profile of *MTSS1* as reported in the recently published human retina scRNA-seq dataset (Lukowski et al., 2019) was analysed and it revealed that *MTSS1* expression had been identified in multiple retinal cell populations in the adult human retina, confirming our experimental expression data. The highest expression of MTSS1 in the human retina was in the rod photoreceptor cells, followed by RGCs, bipolar cells and the cones respectively (Appendix D). Alignment of MTSS1 protein sequence from different species showed that the glutamic acid (p.Glu213) reported to be deleted in family 3027 patients is conserved in across all the species compared (Figure 3.15B), suggesting it could be important in the normal function of the MTSS1 protein. Characterisation of *MTSS1* as a candidate for IRDs can be found in Chapter 4**.**

A



B

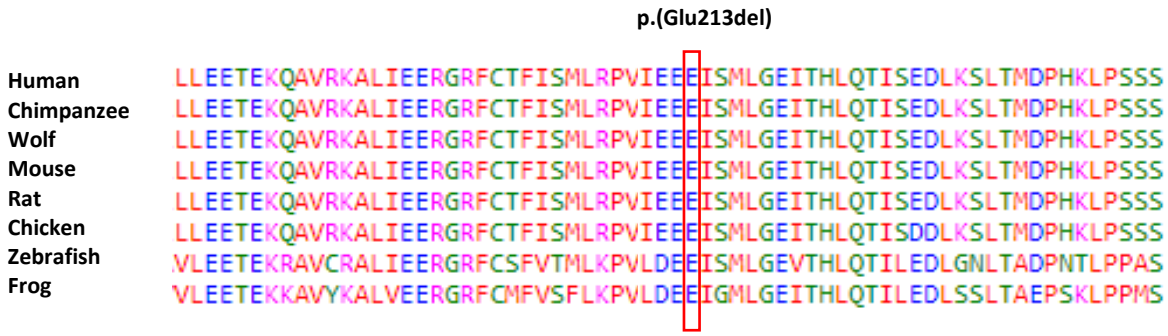


Figure 3.15. *MTSS1* gene expression and protein conservation. **(A)** *MTSS1* expression panel from human tissue cDNA. *MTSS1* expression was detected in human brain, liver, skeletal muscle and retina. *ACTB* expression was used as positive control. **(B)** The amino acid (p.Glu213) that is deleted in MTSS1 in affected individuals in 3027 family is highly conserved across species.

3.3.4 Family 3032

Family 3032, of British origin, has 6 members diagnosed with dominant macular dystrophy spanning 4 generations (Figure 3.16). The macular dystrophy phenotype in this family has variable reported ages of onset ranging from 30s to 60s. Table 3.7 contains a summary of the symptoms and features of the macular dystrophy phenotype reported in this family. Fundus images from the proband (V-2) depicting the macular dystrophy phenotype diagnosed in this family are shown in Figure 3.17. Genomic DNA was obtained from a total of 5 individuals in this family including 4 affected (III-1, IV-2, V-2 and V-3), an unaffected (IV-9). Samples could not be obtained from two affected individuals (II-1 and II-2) as they are deceased.

3.4.3.3 Segregation analysis in Family 3032

WES was conducted on the proband (V-2), his affected mother (IV-2) and his affected maternal grandfather (III-1) in family 3032. Bioinformatic analysis revealed that the three subjects shared 48 heterozygous variants of which only 4 had a gnomAD frequency of 0 so expanding the analysis to include variants with a frequency of up to 4.3E-5 identified 13 more variants (Table 3.8). Sanger sequencing was used to analyse them and 16 of these 17 variants were shown to be present in the three affected family members that underwent WES. Primer sequences are given in Appendix B**.** Segregation analysis for the 16 validated variants was performed using DNA samples from an affected (V-3) and an unaffected (IV-9) individual. This enabled us to exclude 10 variants as they did not segregate (Table 3.8). One variant could not be validated as it was reported in a non-coding gene (*AC112721.1*) whose sequence is not yet characterised and made it difficult to design primers. Therefore, variants in 6 genes (*CD4, TLL2, DNMBP, SERPINA10, PLCE1 and EPB41L3*) have been identified for further segregation analysis in this family once more family members have been recruited.

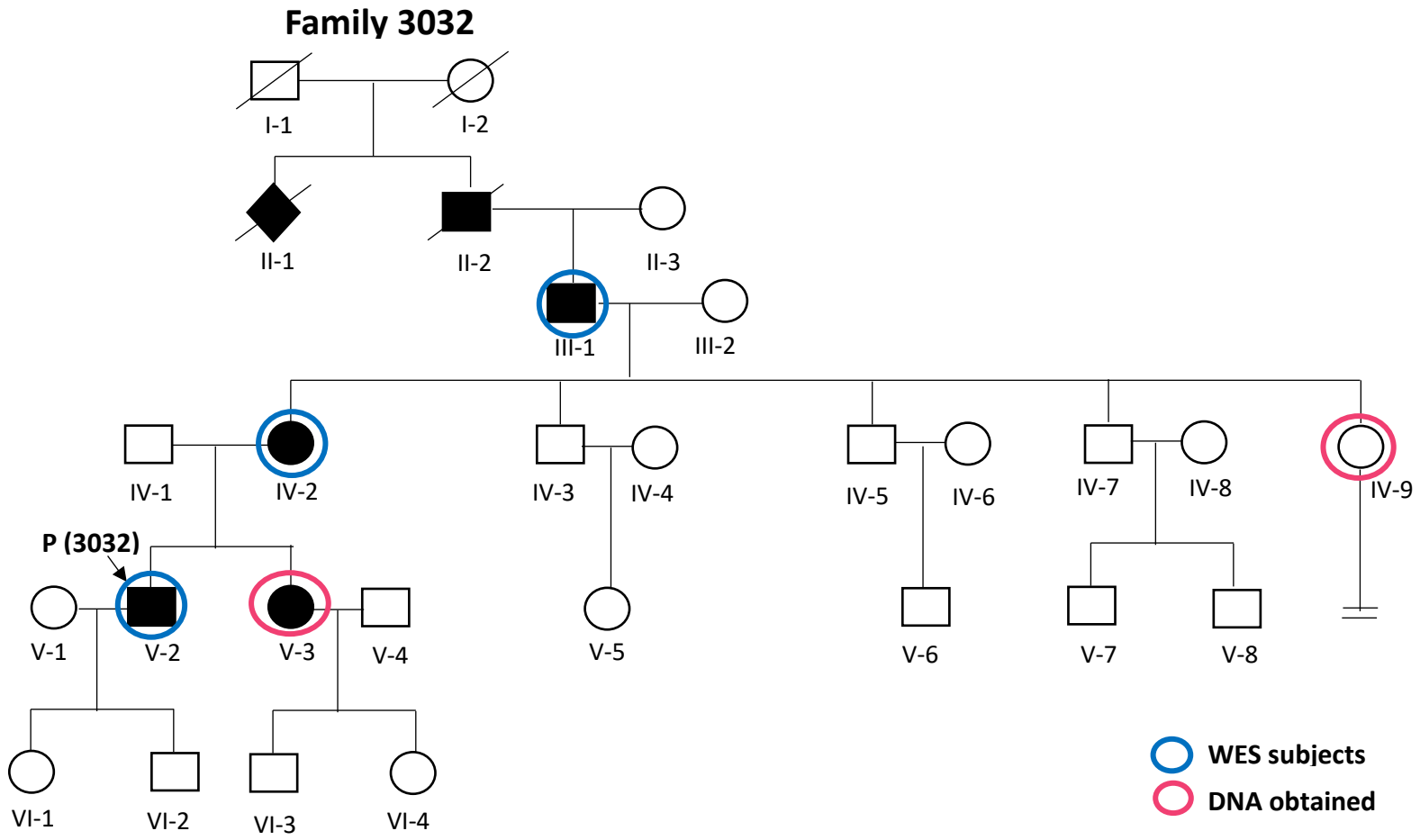
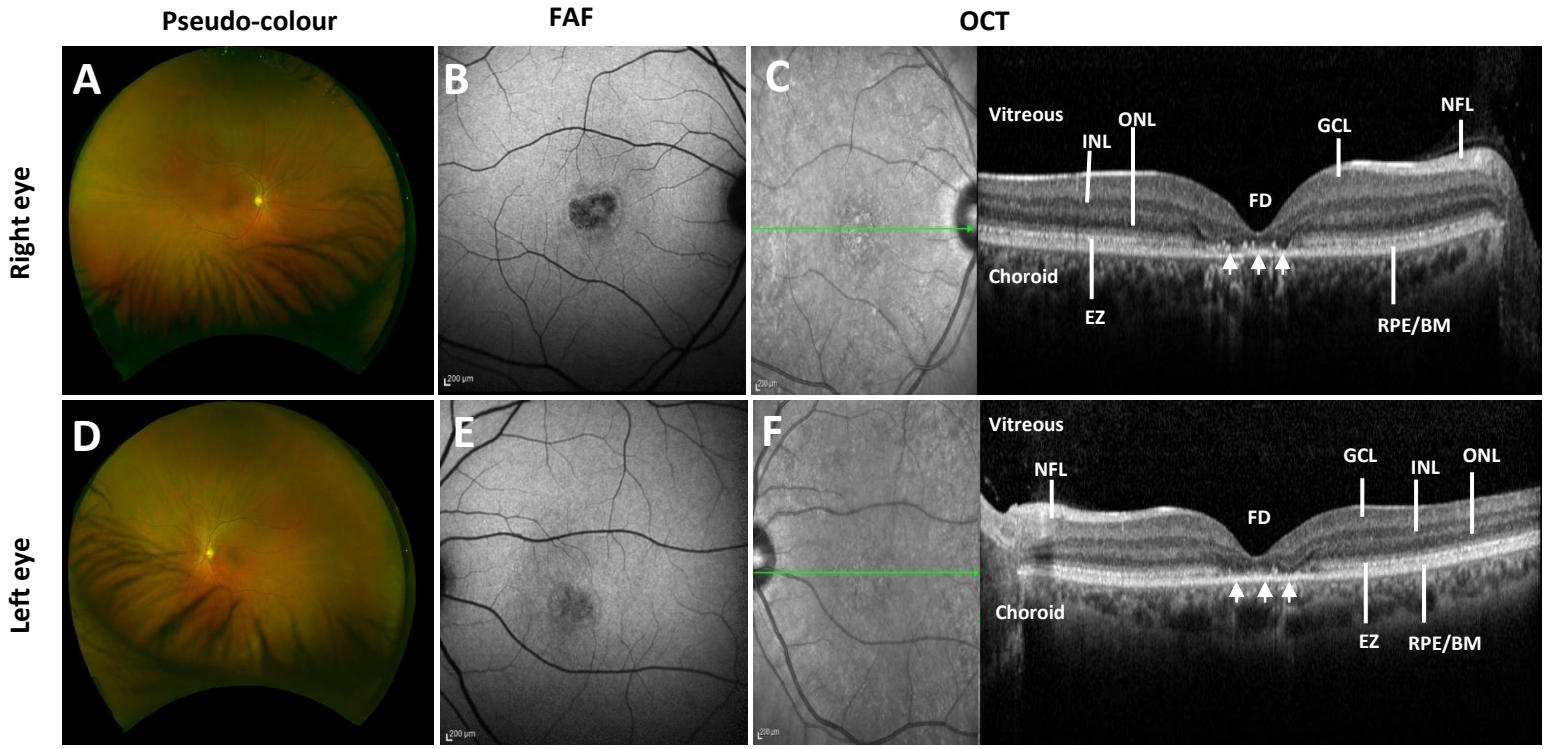


Figure 3.16. Pedigree of family 3032 diagnosed with dominant macular dystrophy. Four affected individuals (III-1, IV-2, V-2 and V-3) and one unaffected individual (IV-9) were recruited into this study. Circles=women; squares=men; filled symbols=affected; open symbols=unaffected. Symbol with a bar across=deceased; P=Proband.

Table 3.7. Summary of clinical findings in Family 3032 with dominant macular dystrophy

Patient	Age of onset	Symptoms	Visual acuity	Fundus	Visual fields/OCT	ERG
III-1	63	Blurred central vision	RE: 6/240 LE: 6/240	Widespread chorioretinal atrophy involving posterior pole and mid-peripheral retina	VF: Central scotoma OCT: extensive retinal atrophy	N/A
IV-2	62	Blurred central vision	RE: 6/30 LE: 6/38	Decreased foveal autofluorescence; Drusenoid change (RE>LE); Degenerating RPE	Central scotoma, full peripheral visual fields	N/A
V-2	42	Blurred central vision	RE: 6/30 LE: 6/30	Decreased foveal autofluorescence	Small central scotoma, full peripheral visual fields	Normal cone and rod responses; changes in multifocal and pattern responses
V-3	N/A	Asymptomatic	RE: 6/38 LE: 6/38	Decreased foveal autofluorescence	N/A	N/A

OCT - Optical coherence tomography; ERG – Electroretinography; BE – both eyes; RE – Right eye; LE – Left eye; HM – Hand motion; N/A – Not available.



Patient: 3032

Figure 3.17. Retina imaging of proband in family 3032 with dominant macular dystrophy. (A, D) Widefield fundus pseudo-colour images. (B, E) Fundus autofluorescence (FAF) images showing a central area of diminished autofluorescence (RE>LE). (C, F) Spectral domain optical coherence tomography (OCT) images showing disrupted ellipsoid zone (EZ) in the fovea (white arrowheads) in both eyes. RPE and retinal layers in the parafoveal region remain well organised and intact. FD= Foveal depression; NFL= nerve fibre layer; GCL= ganglion cell layer; INL= inner nuclear layer; ONL= outer nuclear layer; EZ: ellipsoid zone; RPE= retinal pigment epithelium; BM= Bruch's membrane.

Table 3.8. Family 3032: Segregation analysis for variants with gnomAD frequency of 0 – 4.3E^{-5}

GENE SYMBOL	gnomAD frequency	Protein change	Nucleotide change	V-2 (Aff.)	IV-2 (Aff.)	III-1 (Aff.)	V-3 (Aff.)	IV-9 (UnAff.)
CD4	0	p.S341G	c.A1021G	AG	AG	AG	AG	AA
MYH11	0	p.P1933fs	c.5799_5800insC	G Ins	G Ins	G Ins	No G ins	No G ins
PABPN1	0	p.A11P	c.G31C	GC	GC	GC	N/A	GC
TMEM245	0	p.V202M	c.G604A	GA	GA	GA	N/A	GA
CCAR1	2.16E-05	p.E1030K	c.G3088A	GA	GA	GA	GG	GG
DNMBP	2.03E-05	p.F31S	c.T92C	TC	TC	TC	TC	TT
ENAM	3.25E-05	p.N315S	c.A944G	AG	AG	AG	AA	AG
EPB41L3	1.22E-05	p.R98Q	c.G293A	GA	GA	GA	GA	GG
FOXK1	8.45E-06	p.L426V	c.C1276G	CG	CG	CG	CG	CG
FRMD3	2.44E-05	p.A149V	c.C446T	CT	CT	CT	CC	CT
GALNT9	3.13E-05	p.Q72H	c.G216T	GT	GT	GT	GT	GT
OR1E2	2.44E-05	p.I92V	c.A274G	AA	AA	AG	AA	AA
PLCE1	3.25E-05	p.Y1563C	c.A4688G	AG	AG	AG	AG	AA
SERPINA10	3.97E-05	p.M269I	c.G807A	GA	GA	GA	GA	GG
SPON2	3.25E-05	p.321_322del	c.963_965del	_del	_del	_del	_del	_del
TLL2	3.23E-05	p.G473C	c.G1417T	GT	GT	GT	GT	GG

N/A – Not available: sequencing data require further optimization; Aff. – Affected; UnAff. – Unaffected.

Genes highlighted in yellow indicate genes with variants found to segregate with the disease in the family so far.

3.4.3.4 *Preliminary analysis of the six genes segregating in family 3032*

Six genes (*CD4, TLL2, DNMBP, SERPINA10, PLCE1 and EPB41L3*), out of the 16 examined, were found to contain variants that segregate with the macular dystrophy in family 3032 (see Table 3.8). To narrow down the more probable candidate(s) from these six genes, the expression profile of these genes was investigated in two recently published datasets (Lukowski et al., 2019, Menon et al., 2019) that used single cell RNA sequencing (scRNA-seq) to analyse the expression profile of various genes in the different cell types present in the adult human neural retina. These datasets shows that *DNMBP*, *EPB41L3* and *PLCE1* are all expressed in retinal cells including the rod and cone photoreceptors, bipolar and RGCs (levels of expression of each gene per retinal cell can be found in Appendix D). *CD4* expression was reported to be limited to Muller glia and retinal microglia, while no expression was reported for *TLL2* and *SERPINA10*. Based on these datasets, we could potentially rule out *TLL2* and *SERPINA10* as being less likely to be responsible for the macular dystrophy phenotype observed in this family as we would expect the candidate genes to show expression in the retina, particularly in the photoreceptors. As such, prioritised candidates for further segregation or investigation are *CD4*, *DNMBP*, *EPB41L3* and *PLCE1*.

3.5 Discussion

Using next generation sequencing (NGS) technology, we have sequenced the exomes of individuals with inherited retinal dystrophy in four different families who are yet to have a genetic diagnosis. Affected members in these families initially underwent standard NHS genetic testing on the appropriate disease panel (Appendix A) and no genetic diagnosis was found, hence the need for whole-exome sequencing (WES). We have also taken advantage of currently available comparative genetic databases such as gnomAD and 1000 genomes as well as predictive bioinformatics tools like CADD, PolyPhen, and SIFT to prioritize candidate variants from thousands of variants derived from WES (see 3.3.2). As discussed in section 1.3.5, the advent of NGS and its application in IRDs has enabled the identification of genes with significant roles in retinal function and disease, such as *TSPAN12*, which would have otherwise not been considered relevant (Nikopoulos et al., 2010). As such, the use of the NGS technology in this study offered the potential of identifying new genes that have not been previously associated with retinal function or disease.

For four families with dominant forms of retinal dystrophies (3004, 3013, 3027 and 3032), segregation analyses using DNA from other affected and unaffected family members have allowed us to identify a single candidate gene for each of two families (3004 and 3027) while two potential candidate genes have been identified for family 3013. For family 3032, a list of six genes were found to have variants that segregate with the condition so far. Of these, 2 genes were excluded when their expression profiles from the human retina scRNA-seq data (Lukowski et al., 2019, Menon et al., 2019) were examined. Four remaining genes (*CD4*, *DNMBP*, *EPB41L3* and *PLCE1)* have been prioritised for further investigation and obtaining DNA samples from other unaffected family members for segregation analysis could help to narrow down this list. While CD4 expression is reportedly limited to the retinal Muller glia and retinal microglia, and may be considered unlikely to cause the disease in this family especially due to its lack of expression in the photoreceptors, it is important to note that Menon *et al.* (2019) in their scRNA-seq data reported that genes enriched in retinal glia, vascular and cone photoreceptor cells are more likely to cause macular degeneration (Menon et al., 2019). This explains

why CD4 was not excluded from the list of potential candidates put forward for further analysis in family 3032. At the time of writing this thesis, efforts are still underway to recruit more participants from families 3013 and 3032 in which a single candidate gene has not been identified. However, the recruitment process has been stalled since the Covid-19 pandemic began.

In family 3027, we only found one variant in the *MTSS1* gene that segregates with the disease. In family 3004 we found variants in two genes, *PARPBP* and *KPNA7*, segregating with the condition in the family but *KPNA7* was excluded due to the lack of identified expression in the human retina. For family 3013, variants in two genes, *MYO5B* and *PIEZO1,* were found to segregate with adRP. For a gene to cause a retinal disease phenotype, the gene or its product must be expressed in retinal tissues. Since there was no information in the literature on the retinal expression and function of all these candidate genes, we conducted preliminary experiments to examine their expression in the human retina. We have shown for the first time, using commercially available human retina cDNA, expression of *PARPBP, MYO5B, PIEZO1* and *MTSS1* in the human retina. Although identifying retinal expression of these genes does not necessarily mean they are causal in these families, we used this as a step to determine how relevant these genes could be to retinal function and also to enable us to eliminate some candidates in families where variants in more than one gene segregated with disease. Accordingly, the variant in *KPNA7* was determined to be less likely to cause retinal disease segregated in family 3004 due to the failure to detect its expression in the retina using different primer pairs. This was also confirmed by analysing the human retina scRNA-seq dataset (Lukowski et al., 2019). With both *MYO5B* and *PIEZO1* identified as being expressed in the human retina, we were unable to select one as the more plausible candidate gene for family 3013 at this stage. However, rectifying the clinical status of family member II-2 is crucial in prioritising one over the other. This is because, considering the genotype of II-2 for *MYO5B* and *PIEZO1* from the segregation analysis (Table 3.4), the variant in *MYO5B* would be the only one segregating in family 3013 as the candidate gene if II-2 is determined to be affected whereas the variant in *PIEZO1* will be the only one segregating should II-2 be determined to be unaffected upon further clinical assessment.

As a preliminary step to understanding how important the variants identified in these genes are to the normal function of the genes and their proteins, we examined how conserved the variants are by aligning DNA and protein sequences from different species. The finding that the amino acids altered in MTSS1, PARPBP and PIEZO1 proteins, and the altered splice site in the *MYO5B* gene, are located in well conserved areas of these proteins suggests that they could be playing an important role in the structure and function of these proteins, and that being altered could be detrimental.

Preliminary analysis of PARPBP protein expression in the mouse retina using a commercially available antibody detected PARPBP-positive staining predominantly in the INL and GCL in the adult mouse retina. Examining Parpbp staining in the developing retina, however, revealed some positive staining in some cells in the developing photoreceptor layer, especially at P16, indicating that Parpbp expression in the photoreceptors of the mammalian retina could be developmentally regulated. If PAPRPBP expression in the photoreceptors is limited to early retinal development, it could still be relevant to the adRP phenotype identified in family 3004 since the disease is of early onset (see Table 3.1). Meanwhile, data from the scRNA-seq by Menon *et al*. (2019) (Menon et al., 2019), suggest that *PARPBP* is expressed in the rod photoreceptors of the adult human retina. Although the PARPBP antibody used here did not detect Parpbp staining in the photoreceptors of adult mouse retina, this might be due to the antibody's inability to detect some isoforms of the protein in the retina. Our preliminary *PARPBP* transcript data presented in this chapter indicate that different transcripts of the gene are present in the retina (see Figure 3.5B). At the same time, there is evidence from previous studies that the different retinal cell types could express cell type-specific transcripts of the same gene (see discussion in section 4.5). As such, it will be important to examine Parpbp localisation in the developing and adult retina using other PARPBP antibodies as well as further characterising the transcripts that are expressed.

Taken together, experiments in this chapter enabled us to identify rare variants that segregate with disease in the participating families. Although these variants are in genes not previously linked to retinal disease, we have confirmed their expression in human retina, making them interesting

candidates worth investigating further. As such, one of the candidate genes identified in this chapter, *MTSS1*, was characterised further in the subsequent chapters in an attempt to elucidate which parts of the retina it localises, its potential role in the retina and how the variant identified in the gene might influence the function of the MTSS1 protein.

4 Characterisation of *MTSS1* expression in mammalian retina.

4.1 Introduction

Analysis of the rare variants identified by NGS in Family 3027 revealed only 1 variant, c.637-639del in *MTSS1,* which segregated with the adRP in the family (see 3.4.3.1). The *MTSS1* gene was first identified in 2002 as part of a study analysing differences in gene expression in metastatic versus non-metastatic cell lines (Lee et al., 2002). It was found to be expressed in cell lines derived from benign tumours such as bladder papilloma (RT4), bladder superficial transitional cell cancer (5637) and bladder invasive transitional cell cancer (HT1376 and T24) cell lines but absent (or down-regulated) in cell lines derived from metastatic tumours such as metastatic bladder transitional cell cancer (TCCSup) and metastatic breast cancer (SkBr30), and hence was originally called missing in metastasis (*MIM*) with a predicted role in metastasis suppression (Lee et al., 2002). The 316bp fragment obtained by Lee *et al*. (Lee et al., 2002), was cloned and used to probe a normal multiple tissue Northern blot and detected a transcript of approximately 5.3kb in spleen, thymus, prostate, testis, uterus, colon and peripheral blood. The fragment was also sequenced and showed 100% homology to the human KIAA0429 partial gene transcript (GenBank accession no.: AB007889) which mapped to chromosome 8q24.1 (Ishikawa et al., 1997). *MTSS1* expression in the heart, kidney, liver, brain and neuronal cell lines has also been reported (Mattila et al., 2003, Yu et al., 2016).

Subsequent studies identified a human homologue, *MIM-B*, (GenBank accession no.: AK027015) that consists of 15 exons (Woodings et al., 2003) and one of 14 exons (Genbank accession no.: AF086645) (Loberg et al., 2005) which is missing the 12bp exon 7 found in *MIM-B* (Figure 4.1A and B). The clone described by Lee *et al*. (Lee et al., 2002) corresponds to the sequence from the end of exon 12 and exons 13-15 in AK027015 (Figure **4.1**C). The mouse orthologue, *Mtss1*, was first identified by Mattila *et al*. in 2003 as part of a study trying to identify proteins containing a WH2 domain (WASP homology domain-2) which interacts with monomeric actin. They identified a gene that showed strong sequence

homology to the human *MIM* (Mattila et al., 2003). A subsequent report from the same group reported a variant of *Mtss1* (AK030533) that had a start site in exon 4 (Figure **4.1**D). Several splice variants of *MTSS1*/*Mtss1* have since been described (Glassmann et al., 2007, Nixdorf et al., 2004) including one that contains exon 12a instead of 12 (Figure **4.1**E). The Ensembl gene database documents 18 human and 12 mouse confirmed and potential transcripts of *MTSS1/Mtss1* (https://www.ensembl.org), demonstrating that the *MTSS1/Mtss1* genes undergo alternate splicing.

The human and mouse transcripts that consist of 15 exons (AK027015 and AY214918 respectively) are predicted to encode a protein of 759 amino acids with a predicted molecular weight of 82.6 kDa (Woodings et al., 2003). An alignment of the predicted human and mouse protein sequences shows that they are 96.6% identical (Figure 4.2). The longest transcript of *MTSS1* (AK027015; Figure **4.1**A) is predicted to encode a protein that is 759aa long and contains multiple functional motifs: (i) an N-terminal IRSp53/MIM homology domain (IMD) made up of amino acids 1 to 250; (ii) a C-terminal Wiskott-Aldrich syndrome protein (WASP) homology 2 (WH2) domain consisting of the last 35 amino acids of the protein; and (iii) a regulatory region sandwiched between the IMD and WH2 domains comprising amino acids from positions 251 to 724 (Xie et al., 2011) (Figure 4.3). The IMD domain, coded by exons 1 to 9, has been shown to be involved in both F-actin binding and F-actin bundling by two groups (Yamagishi et al., 2004, Gonzalez-Quevedo et al., 2005), although its F-actin bundling role has been contested (Lee et al., 2007). The IRSp53/MIM homology domain (IMD) has also been shown to possess membrane-binding affinities, courtesy its I-BAR (Inverse Bin/amphiphysin/Rvs) domain properties (see section 5.1), enabling interaction and deformation of membranes rich in phosphatidylinositol 4,5 bisphosphate ($PI(4,5)P_2$) (Saarikangas et al., 2015). The WH2 domain, encoded by the last exon of *MTSS1*, has been shown to be involved in binding to actin monomers and is involved in the organisation of actin cytoskeleton by facilitating the assembly of actin monomers to newly forming actin filament ends, a process known as actin nucleation (Welch and Mullins, 2002, Yarar et al., 2002). The central regulatory region of MTSS1 comprises multiple domains, including a coiled-coil domain, a lysine-rich domain, a proline-rich domain, and a serine-rich domain, which have been shown to provide interactive binding sites for cortactin (a protein involved in actin nucleation and

stabilization) (Lin et al., 2005), receptor-type protein tyrosine phosphatase δ (RPTPδ) (Gonzalez-Quevedo et al., 2005, Woodings et al., 2003), Sufu (a metastasis suppressor protein), Gli (a transcription factor) (Callahan et al., 2004), and other partners (Xie et al., 2011).

Although *MTSS1/Mtss1* has been studied in several mammalian tissues and cell lines, its expression and role in the mammalian retina had not been previously described. The identification of *MTSS1* as a candidate gene for the adRP in family 3027 prompted us to undertake an in-depth investigation of its expression in the mammalian retina. This chapter describes how we investigated the expression of MTSS1 gene and protein in the mammalian retina. Using gene expression techniques and cDNAs, we examined *MTSS1/Mtss1* expression across various human and mouse tissues including the retina. In the retina, we determined which transcripts of *MTSS1* are present, and examined the 5' untranslated region (5' UTR) of the gene using the 5' Rapid Amplification of cDNA Ends (5' RACE) technique. We also assessed MTSS1 protein expression in the retina using commercially available MTSS1 antibodies to determine in which cells or layers the protein is expressed.

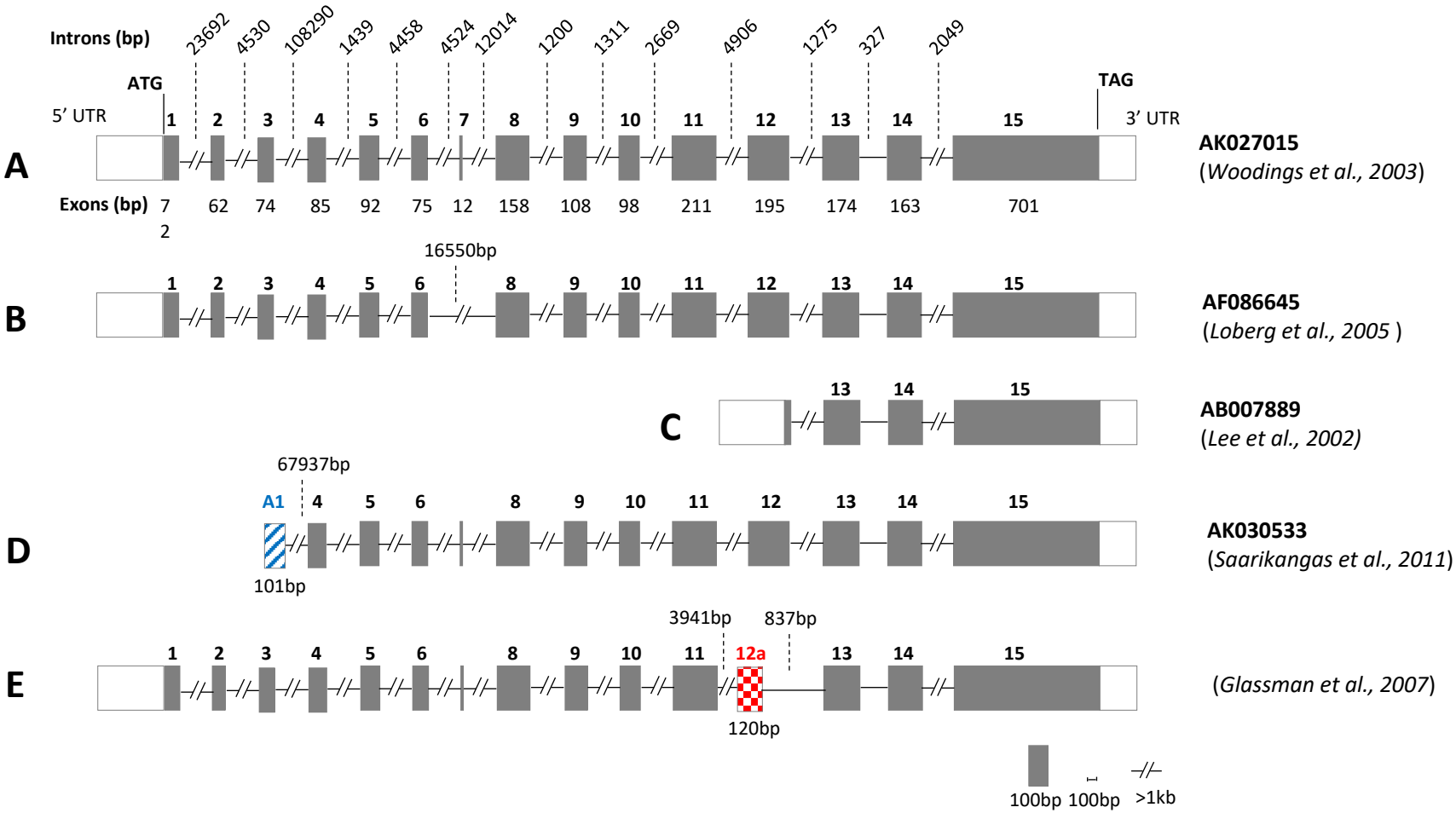

Introns (bp)
23692
4530
108290
1439
4458
4524
12014
1200
1311
2669
4906
1275
327
2049
ATG
TAG
5' UTR
3' UTR
A
Exons (bp)
7
2
62
74
85
92
75
12
158
108
98
211
195
174
163
701
AK027015
(Woodings et al., 2003)
16550bp
B
AF086645
(Loberg et al., 2005)
C
AB007889
(Lee et al., 2002)
67937bp
A1
D
101bp
AK030533
(Saarikangas et al., 2011)
3941bp
837bp
12a
E
120bp
(Glassman et al., 2007)
100bp
100bp
>1kb

Figure 4.1. Genomic structures of *MTSS1* transcripts. **(A)** Schematic diagram of exons and introns of the AK027015 transcript of *MTSS1* which encodes a 759 amino acid protein, the longest reported transcript of MTSS1. Intron and exon sizes are indicated above and below, respectively. **(B)** A schematic of the AF086645 transcript of *MTSS1* missing the 12bp exon (exon 7) which encodes a 755 amino acid protein. **(C)** Schematic of the transcript of MTSS1 first to be identified with only 3 coding exons encoding a 356 amino acid protein. **(D)** Alternative transcript of *MTSS1* (AK030533) with a non-coding exon/promoter located in intron 3 (highlighted in blue) and an alternate transcription start site in exon 4. **(E)** A transcript of MTSS1 in which the canonical exon 12 is replaced with a 120bp alternate exon (12a). All exon and intron sizes are the same as stated in (A) unless otherwise indicated. UTR = Untranslated region, represented by clear boxes. Grey-shaded boxes represent coding exons.

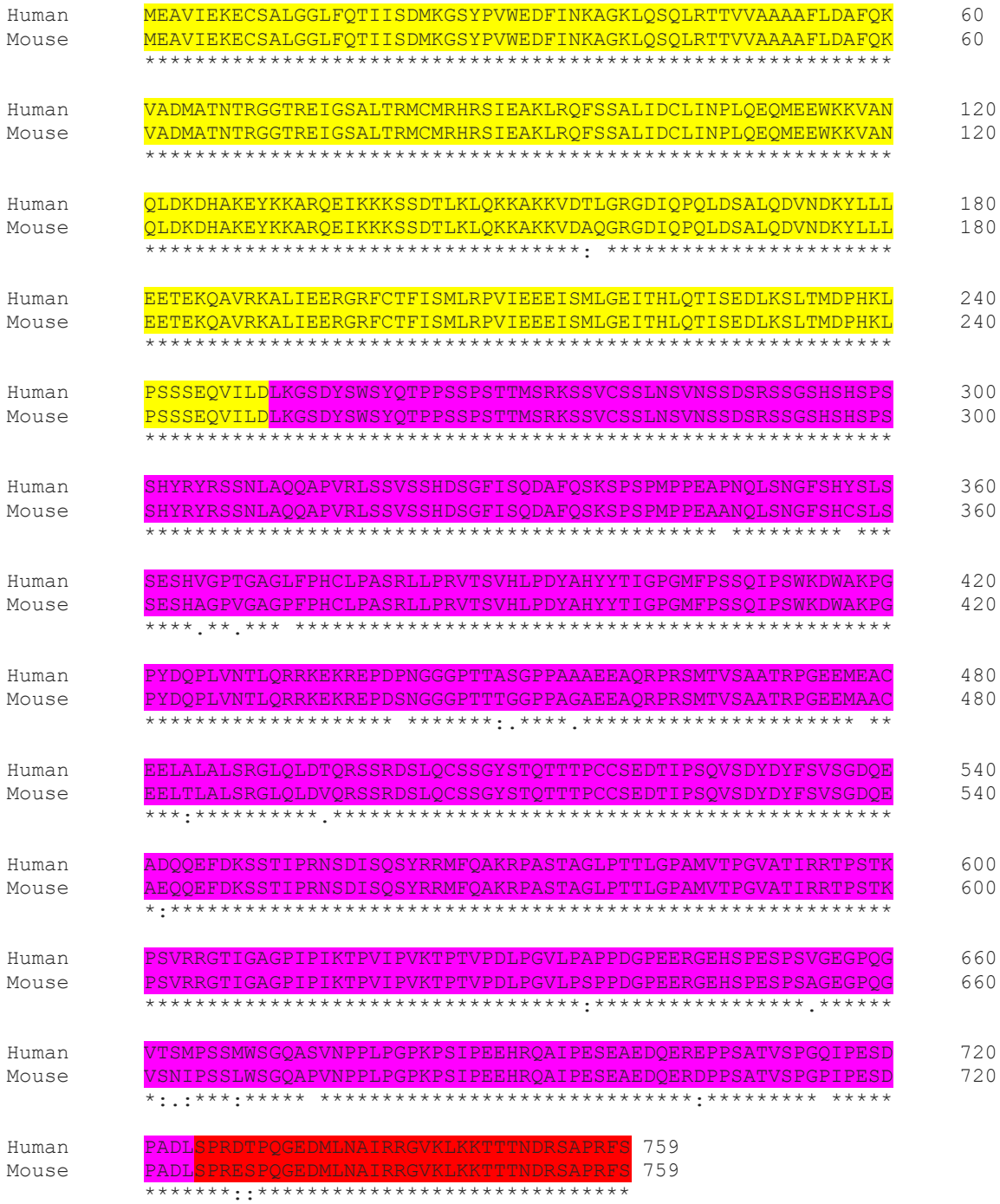


Figure 4.2. Comparison of human and mouse *MTSS1/Mtss1* protein sequence. (A) Alignment of protein sequences from human MTSS1 and mouse Mtss1 shows 96.6% identity. IMD (IRSp53/MIM homology domain) involved in F-actin binding (yellow, 1-250 aa); a central region containing scaffolding and regulatory domains (purple, 251-724 aa); WH2 (Wiskott – Aldrich syndrome protein homology 2) domain known to bind actin monomers (red, 725-759 aa).

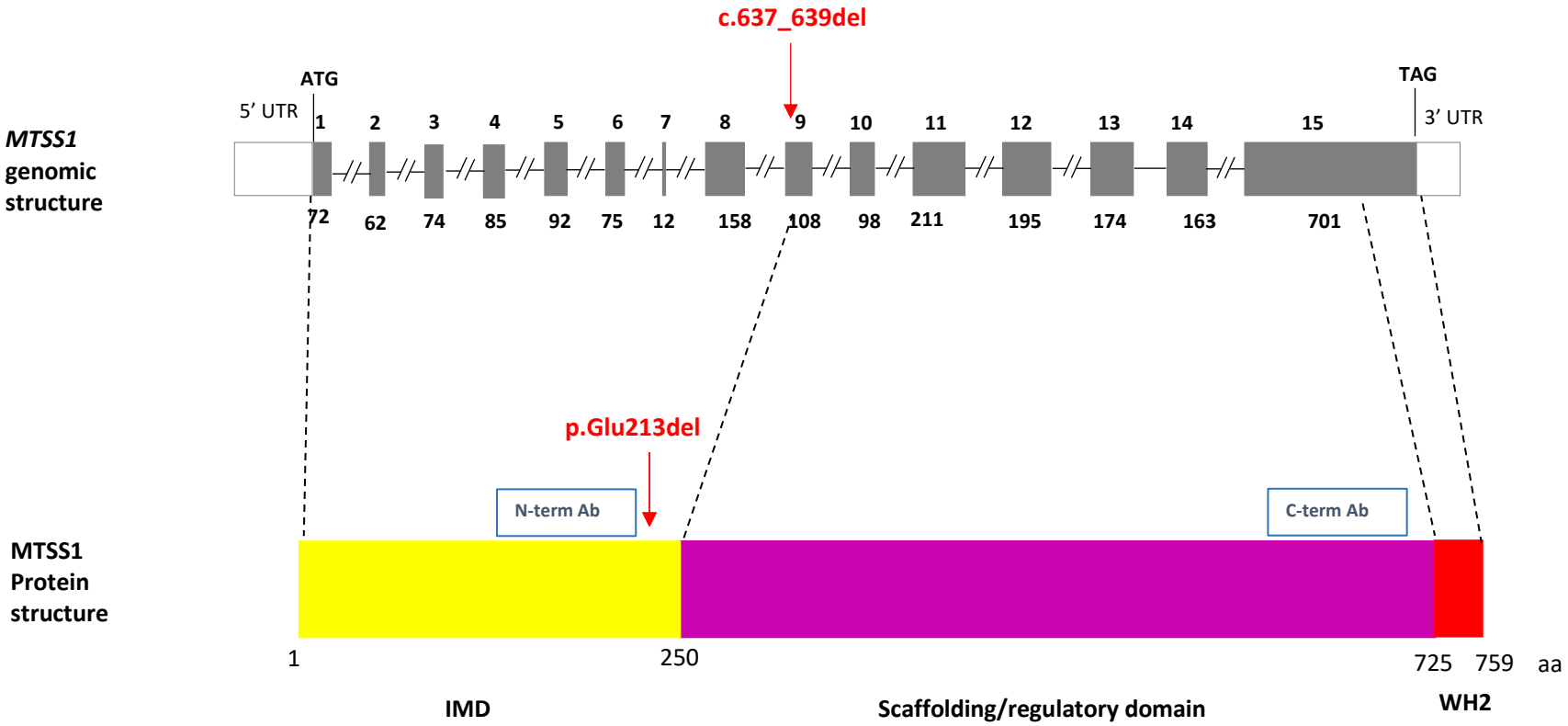


Figure 4.3. Schematic diagram of genomic structure of MTSS1 and corresponding protein domains. The location of the MTSS1 variant (c.637_639del/p.Glu213del) identified in family 3027 is indicated in exon 9 and in the IMD domain of the protein. Positions of the two antibodies (N-terminal (150-200 aa) and C-terminal (670-720 aa) used in immunostaining experiments are also indicated. Exons are indicated as boxes and introns as lines. Shaded boxes = coding exons; UTR = Untranslated region; IMD = IRSp53/MIM homology domain; WH2 = Wiskott – Aldrich syndrome protein homology 2 domain; aa = amino acid; Ab = Antibody.

4.2 Aims

The overall aim of experiments in this chapter was to evaluate the retinal expression of *MTSS1*. The following objectives were pursued to achieve this aim:

1. To determine *MTSS1* gene expression in the retina from RNA isolated from human and mouse retina and related cell lines
2. To evaluate expression and localization of Mtss1 protein in mouse retina

4.3 Methods

All methods used in this chapter, unless described below, have been described in the general methods section in Chapter 2.

4.3.1 5' Rapid Amplification of cDNA Ends (5' RACE)

5' Rapid Amplification of cDNA Ends (5' RACE) is a technique used to characterise the transcription start site and 5' untranslated regions (UTR) of gene transcripts using mRNA as a template. It uses the SMART (Switching Mechanism At 5' end of RNA Transcript) cDNA synthesis technology to isolate the complete 5' sequence of targeted transcripts when only part of the sequence is known (Scotto-Lavino et al., 2006). The technique also offers the ability to generate full-length cDNAs using reverse transcription reactions (Zhu et al., 2001). The SMARTer RACE 5'/3' kit (#634858, Takara Bio Inc., USA) was used to perform 5' RACE according to manufacturer's instructions. In brief, 5' RACE-ready cDNA is made from total mRNA template using a reverse transcriptase that adds several residues of known sequence to the end of an mRNA template during cDNA synthesis, forming a universal primer (forward) at the 5' end of the sequence. Gene-specific primers (GSPs) of 23 to 28 base pairs in length, designed to a region of known sequence in the transcript of interest, can be used as reverse primers in conjunction with the universal 'forward' primer to amplify a target transcript from RACE-ready cDNAs. The GSPs are designed to contain a 15bp sequence overlap that permits rapid In-Fusion cloning of the

amplified product into a linearized pRACE vector (Takara Bio Inc., USA) to enable the products to be sequenced by Sanger sequencing.

4.3.1.1 Primary touchdown 5' RACE PCR

5' RACE-ready cDNA was made from 1µg each of total RNA from mouse brain and retina according to manufacturer's instructions. Total RNA from mouse heart (provided in kit) was used as a positive control. Each 5' RACE-ready cDNA made was diluted with 90µl of Tricine-EDTA Buffer as recommended by manufacturer before being used for RACE reactions. Primary 5' RACE PCR amplification was performed according to the following reaction and touchdown PCR conditions:

1 µl	RACE-ready cDNA template
5 µl	10X Universal primer mix (UPM)
1 µl	Gene-specific Primer (10 µM)
1.5 µl	dH_2O
41.5 µl	Master mix (15.5 µl dH_2O + 25 µl 2X SeqAmp Buffer + 1 µl SeqAmp DNA Polymerase)
50 µl	**Total**

Step	**Temperature (°C)**	**Duration**	**Cycles**
Step 1	94	30 s	5
	72	3 m	
Step 2	94	30 s	5
	70	30 s	
	72	3 m	
Step 3	94	30 s	25
	68	30 s	
	72	3 m	

4.3.1.2 Nested PCR reaction

The primary RACE touchdown PCR was then followed by a nested PCR comprising the following reaction and conditions:

5 µl	Touchdown RACE PCR product (diluted 1:50 with Tricine-EDTA Buffer)
1 µl	UPM Short
1 µl	Nested Gene-Specific Primer (10 µM)
43 µl	Master mix (17µl dH_2O + 25µl 2X SeqAmp Buffer + 1µl SeqAmp DNA Polymerase)
50 µl	**Total**

Temperature (°C)	**Duration**	**Cycles**
94	30 s	20
65	30 s	
72	1 m	

4.3.1.3 5' RACE product cloning and sequencing

5' RACE products (10µl) were analysed on 1.2% (w/v) agarose gels through electrophoresis (section 2.3.2.7) and bands were carefully excised under UV transilluminator and gel-purified using NucleoSpin Gel and PCR Clean-Up Kit according manufacturer's instructions (Takara Bio In. USA). Purified products were eluted in 20µl of dH_20 after which 7µl of the eluted product was used for In-Fusion cloning into pRACE vector. Briefly, a cloning reaction of 10µl total volume comprised: 7µl of eluted RACE product, 1µl of linearized pRACE vector, and 2µl of In-Fusion HD Master Mix. The reaction was incubated at 50^{o}C for 15 minutes and then placed on ice, ready for transformation. For transformation, 2.5µl of the clone reaction was transformed into 50µl of Stellar Competent Cells in a microcentrifuge tube by incubating the reaction on ice for 30 minutes, followed by heat-shocking for 45 seconds at 42^{o}C and incubating on ice for 2 minutes, all according to manufacturer's instructions (Takara Bio In. USA). SOC

medium (950µl) was added to transformed cells and 100µl of the culture plated on ampicillin-resistant plates as described previously (see 2.3.2.12). For each sample, 10 independent colonies were collected and plasmid DNA isolated using QIAprep Spin Miniprep kit following the manufacturer's instructions (Qiagen, UK) (see 2.3.2.13). The presence of inserts was analysed by digesting isolated plasmid DNA with *EcoRI* and *HindIII* restriction enzymes (see 2.3.2.10). Sequencing of clones were done using M13F and M13R sequencing primers through Sanger Sequencing (see 2.3.2.16.1).

4.4 Results

4.4.1 *MTSS1* gene expression

4.4.1.1 Expression in mammalian tissues

To determine the expression profile of *MTSS1* in mammalian tissues, a panel of human and mouse tissue cDNAs and endpoint PCR (see 2.3.2.6) was used. *MTSS1* expression was detected in 4 of 5 human tissues tested including retina (see Figure 3.15). To investigate *Mtss1* expression in mouse tissues, endpoint PCR with forward and reverse primers in exons 8 and 11 respectively, was performed on a panel of cDNAs from adult mouse tissues. *Mtss1* expression (an expected 432bp band) was identified in all 11 tissues examined including adrenal, brain, heart, kidney, liver, lung, skeletal muscle, pancreas, retina, spleen and testis (Figure **4.4**A), indicating the ubiquitous nature of the *Mtss1* gene reported previously (Loberg et al., 2005). Sequences of all primers used can be found in Appendix B.

4.4.1.2 Expression in developing retina

Using mouse retina cDNA isolated from different developmental time-points, we investigated the expression pattern of *Mtss1* from birth into adulthood. Using forward and reverse primers in exons 2 and 6 respectively, *Mtss1* expression (an expected 380bp band) was identified in mouse retina at all developmental time points examined, including postnatal day 0 (P0), P4, P8, P12, P16 and adult mice (**Figure 4.4**B). This result was corroborated by the expression profile of *Mtss1* reported in the retina of *Nrl*-knockout (*Nrl*-KO) and WT mice from the flow-sorted RNA-seq dataset (source: retseq.nei.nih.gov) (Kim et al., 2016). In this dataset, *Mtss1* was expressed early in development (at P2) and was maintained in the adult mouse, although at a relatively lower level compared to the level of expression at P2 in WT mice (Figure **4.4**C). In the *Nrl*-KO mice, retinal expression of *Mtss1* was also detected at P2 and was found to increase over time (Figure **4.4**C).

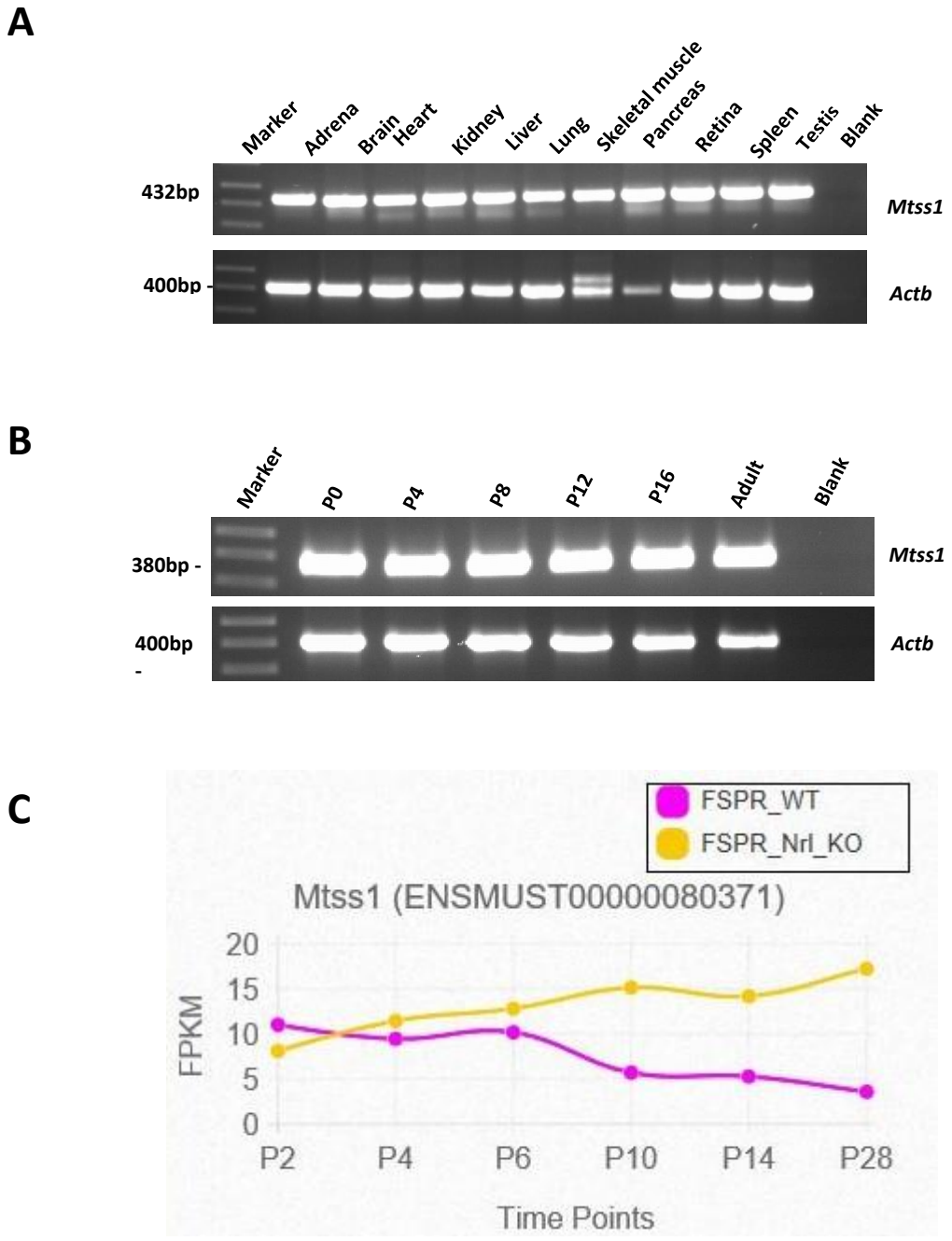


Figure 4.4. *Mtss1* expression in mouse retina. **(A)** *Mtss1* expression panel of mouse tissue cDNA. *Mtss1* expression was detected in all tissues considered including adrenal, brain, heart, kidney, liver, lung, skeletal muscle, pancreas, retina, spleen and testis. β-actin (*Actb*) expression was used as positive control. **(B)** *Mtss1* expression in mouse retina at different developmental stages. *Mtss1* expression was detected from birth into adulthood. **(C)** Flow-sorted RNA-seq data showing expression patterns of *Mtss1* at various developmental stages in WT and *Nrl*-knockout mice (source: retseq.nei.nih.gov). *Mtss1* expression (fragments per kilobase of exon per million reads mapped; FPKM) in retina is present in both WT and *Nrl*-KO mice during development and adulthood.

4.4.1.3 Expression in rodless, coneless and rodless/coneless transgenic mice retina

Having demonstrated that *Mtss1* is expressed in the retina, we sought to determine whether the gene is expressed in a particular cell type or in multiple cell types. Initially, cDNA from the retina of transgenic mice lacking rod photoreceptors (rodless), mice lacking cone photoreceptors (coneless) and mice lacking both rods and cones (rodless/coneless) was used as template. *Mtss1* expression (an expected 432bp band) was identified in all three transgenic mice examined (Figure 4.5A), indicating that the *Mtss1* is expressed in multiple cell types in the retina.

4.4.1.4 Expression in human retina-derived cell lines

The expression of *MTSS1* was also examined in human retina-derived cell lines. Using cDNA from the human retinal pigment epithelium-derived ARPE-19 cell line and retinoblastoma-derived WERI-Rb-1 and Y79 cell lines, *MTSS1* expression (an expected 521bp band with primers in exon 2 and 8) was identified to be present in all 3 cell lines examined (Figure 4.5B). Both WERI-Rb-1 and Y79 cells, established cell lines derived from human retinoblastoma tumours previously (Reid et al., 1974, McFall et al., 1977), have been reported to have photoreceptor-like properties (Oshikawa et al., 2011, Herman et al., 1989).

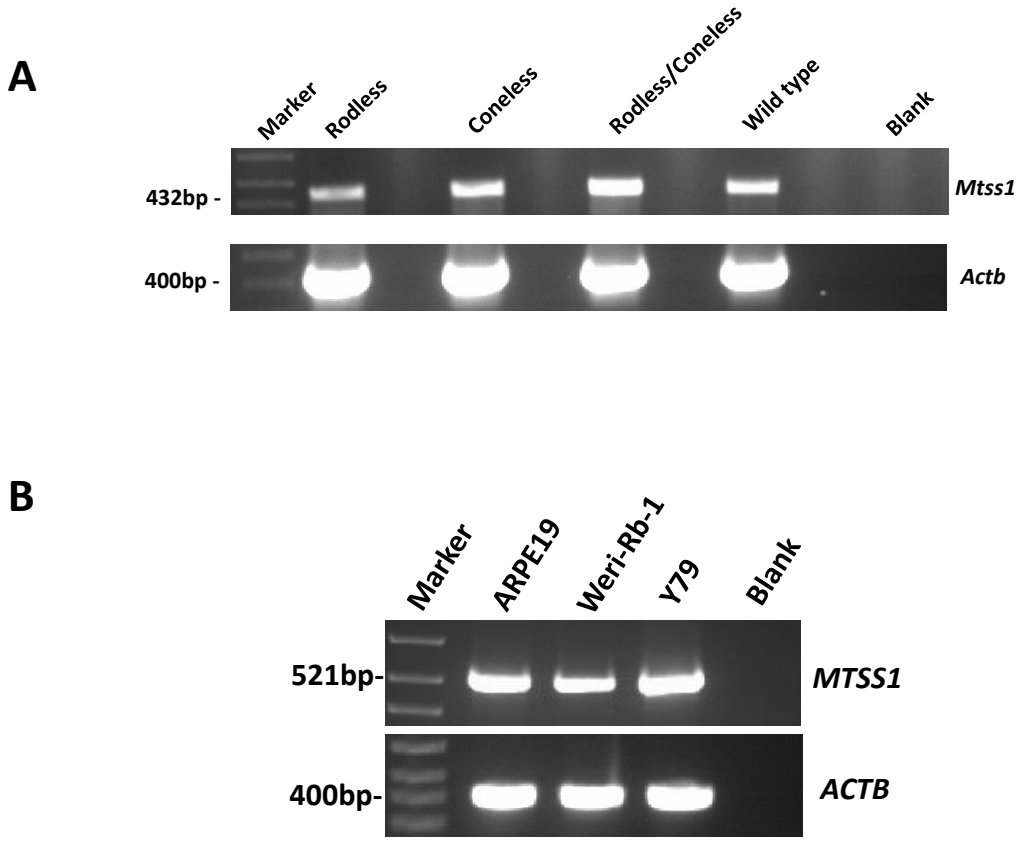


Figure 4.5. *Mtss1/MTSS1* expression in transgenic mice and human retina-derived cell lines. (A) *Mtss1* expression was examined using a panel of cDNA from rodless, coneless and rodless/coneless mice. *Mtss1* expression was detected to be present in the retina of all three transgenic mice. β-actin (*Actb*) expression was used as a loading control. (B) *MTSS1* expression was examined in cDNAs from human retina-derived cell lines. *MTSS1* expression was identified in all cell lines examined including ARPE19, Y79 and Weri-Rb-1 cells.

4.4.1.5 Determining the full length of MTSS1 transcripts in the retina

Previous studies have reported *MTSS1* to have multiple alternately spliced variants expressed in different tissues (Loberg et al., 2005, Sistig et al., 2017). Having established that *MTSS1 is* expressed in the human retina, we decided to investigate the transcript profile. This was to enable us to determine the potential splice variants that are expressed in the retina and compare with those expressed in the brain.

Primer pairs were designed (see 2.3.2.5) comprising a forward primer located at the transcription start site in exon 1 and a reverse primer located at the stop site in exon 15 of the *MTSS1* gene (Figure **4.1**A). Sequences of all primers used can be found in Appendix C. These primers were used to amplify products from human brain and retina cDNA using endpoint PCR (see 2.3.2.6). From human brain cDNA, a 2268bp product was amplified (Figure 4.6A). This product was cloned (see 2.3.2.11.1) and sequenced (see 2.3.2.16.1) and contained exons 1 to 15 excluding exon 7 (Figure 4.6A), a transcript which corresponds to the 755 amino acid transcript previously described (Loberg et al., 2005) (Figure **4.1**B). The same primer pair was used to amplify *MTSS1* from human retina cDNA but failed to amplify the expected product 2268bp, despite optimising the PCR protocol by varying annealing temperatures, extension times, number of cycles and the amount starting cDNA template. However, a product of 1550bp length was obtained from the human retina cDNA (Figure 4.6A). This 1550bp product was also amplified from human brain cDNA on a different occasion. Cloning and sequencing these 1550bp products from both brain and retina revealed they contain exons 1 to 11 (excluding exon 7) and the remaining sequence corresponds to the first 416 bases of intron 11 and the last 99 bases of exon 15 including the stop codon (Figure 4.6A).

To confirm that the transcript with retained intron 11 was not an artefact, a primer pair with a forward primer in exon 11 and a reverse primer within the first 416bp of intron 11 was designed and used to amplify a 386bp product from human retina (Figure 4.6B). This 386bp product was gel-purified and sequenced, and was found to align with the genomic reference sequence of that region of the *MTSS1* gene, indicating that human brain and retina has a transcript of *MTSS1* with retained intron 11. It is

uncertain, however, if this potential transcript with retained intron 11 is translated into a protein as there was no record of this transcript in the Ensembl database and the amplified sequence did not maintain an open reading frame (ORF).

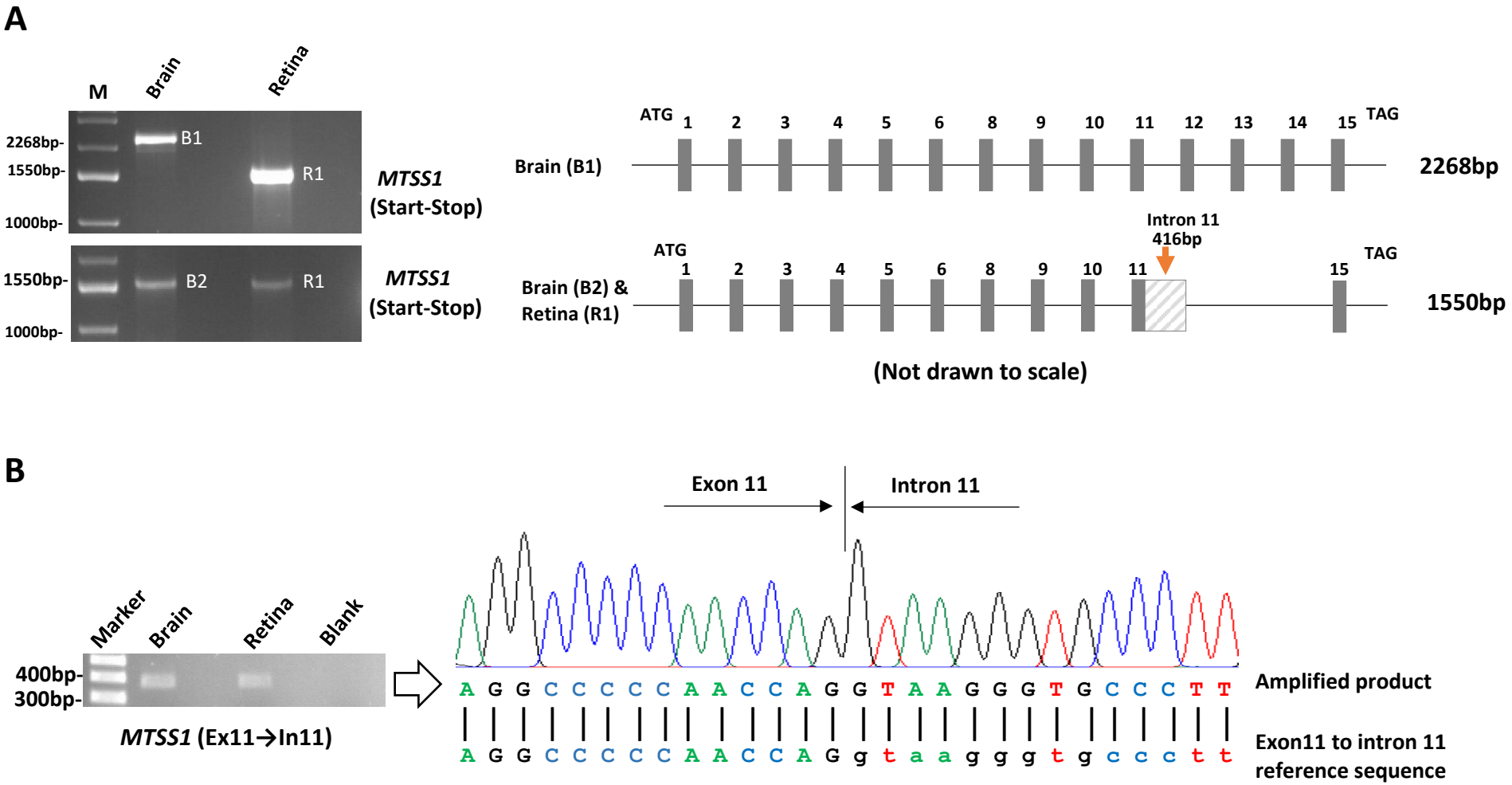


Figure 4.6. Amplification of full length *MTSS1* sequence from human retina. (A) Full length of *MTSS1* transcripts amplified from both human brain and retina using expression primers designed to amplify from start to stop of the full-length coding sequence. A 2268bp product amplified from brain but not in retina was identified to be the canonical transcript of *MTSS1* coding for the 755aa protein. A transcript with a retained intron 11 and missing exons 12, 13, and 14 was identified in both brain and retina. **(B)** The transcript with retained intron 11 was confirmed to be a real transcript expressed in human brain and retina using primers designed to amplify from exon 11 to intron 11. The amplified product when sequenced, aligned with the reference sequence.

4.4.1.5.1 Alternate splicing of *MTSS1* in human retina between exons 11 and 13

As depicted in (Figure **4.1**B and E), *MTSS1* is reported to express some transcripts that either have exon 12 or 12a in tissues such as the cerebellum (Glassmann et al., 2007). It was unclear whether the retina has either or both of these transcripts. As such, we designed primers spanning where these two exons are located to elucidate if these exons (or transcripts these exons) existed in the human retina. Using pair of primers with the forward primer in exon 11 and the reverse primer in exon 13, several products of varying sizes were amplified from both human brain and retina cDNA (Figure 4.7). The products were carefully excised, gel-purified (see 2.3.2.8) and Sanger sequenced (see 2.3.2.16.1).

A 597bp product (B1) containing exons 11, 12a, 12 and 13 was amplified from the brain (Figure 4.7B) but not in the retina. However, four other products similar in the brain and the retina were obtained. These included: a 477bp product (B2 and R1) containing exons 11, 12 and 13 (Figure 4.7B); a 402bp product (B3 and R2) containing exons 11, 12a and 13 (without exon 12) (Figure 4.7B); a 282bp product (B4 and R3) containing only exons 11 and 13 (without exons 12 or 12a) (Figure 4.7B); and a 231bp product (B5 and R4) containing exons 11 and 13 but missing the first 51bp of exon 13 (Figure 4.7B). Although the full-length CDS of MTSS1 amplified from human retina (Figure 4.6A) did not contain exon 12, 12a and 13, the products identified using primers in exon 11 and 13 (Figure 4.7B) suggest the presence of *MTSS1* transcripts that have these exons in the retina. A product of ~350bp amplified from the retina, located between bands R2 and R3 in Figure 4.7, was unable to be purified and sequenced.

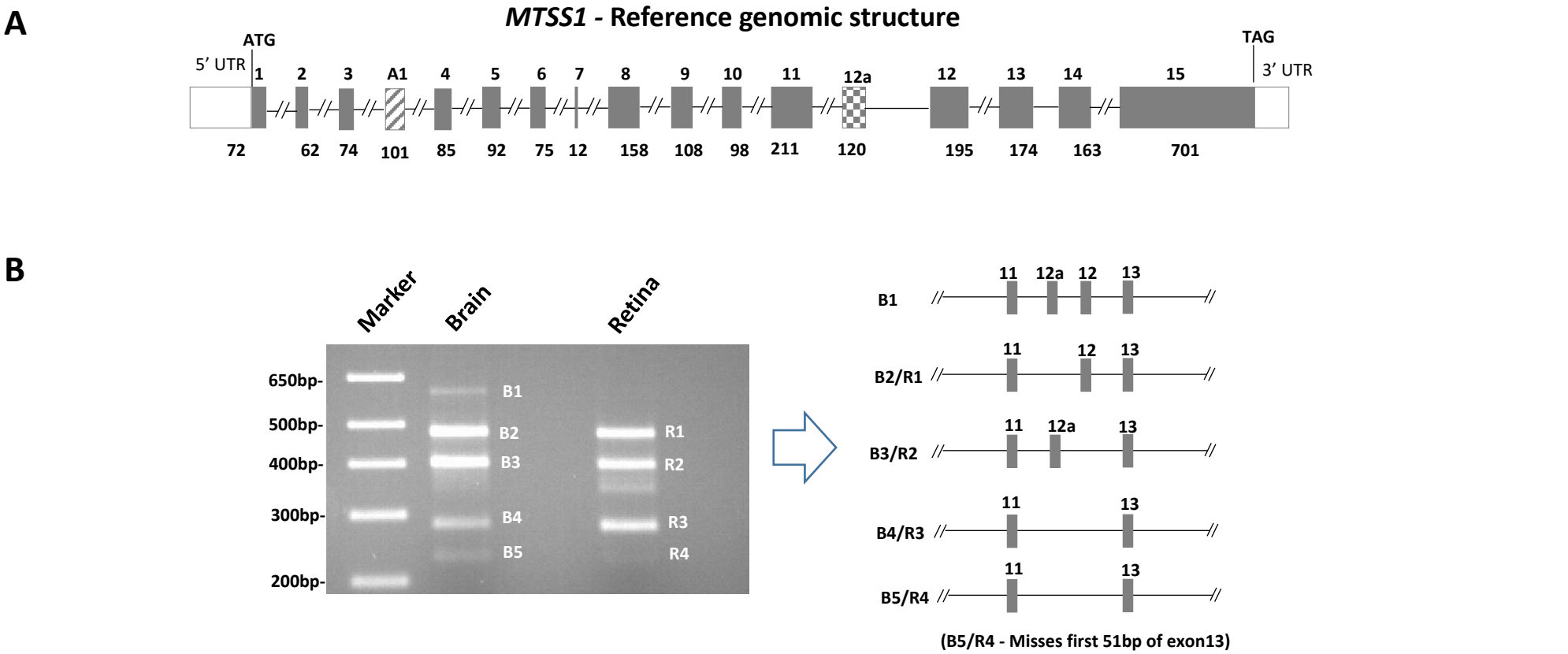


Figure 4.7. Alternate splicing of MTSS1 in human retina between exons 11 and 13. (A) Genomic structure of longest transcript of *MTSS1* modified to include alternate exons A1 and 12a. **(B)** Expression PCR with MTSS1 primers amplifying exon 11 to exon 13 from human brain and retina cDNA. This was to determine whether the retina expressed transcripts containing exon 12a, a previously reported transcript with a unique function in brain. Products of varying sizes were amplified between the brain and retina. Products were gel-purified, cloned and Sanger sequenced to determine analyse the sequence differences. A transcript containing both exons 12 and 12a was detected in brain but not in retina. Four other transcripts were found to be common between brain and retina, including transcripts containing exon 12a (B3/R2), lacking exon 12a (B2/R1) and transcripts lacking both exons 12 and 12a.

4.4.1.5.2 No transcript with the 12bp exon 7 was identified in brain and retina

The longest transcript of *MTSS1* is 2280bp long and encodes a 759 amino acid protein (Figure **4.1**A). It consists of 15 exons of which exon 7 is only 12bp in length (Figure **4.1**A) (Woodings et al., 2003, Loberg et al., 2005). Although this exon has been previously reported to be present in some tissues and cell lines (Woodings et al., 2003, Ota et al., 2004), none of the transcripts or products amplified from brain and retina in this study were found to contain this exon. To investigate this further, specific primer pairs with the forward located in exon 6 and a reverse primer located in exon 8 were used to amplify cDNA from human brain and retina but this failed to obtain a product that contained this exon Figure 4.8A. This suggests that it is less likely that this 12bp exon is expressed in the human brain and retina.

4.4.1.5.3 *Mtss1* transcript with transcription start site in exon 4 expressed in retina

Mtss1 has been reported to have multiple promoters within the gene (Brown et al., 2018). As such, there are reports transcripts resulting from 3 alternate transcription start sites in downstream exons other than the main transcription start site found in exon 1 (Brown et al., 2018, Saarikangas et al., 2011, Lee et al., 2002). One such transcript (AK030533) is reported to have a start site in exon 4, with a non-coding exon/promoter region located in intron 3 (Saarikangas et al., 2011). Retinal expression of this alternate transcript had not been examined previously. Therefore, we designed a forward primer in the predicted non-coding exon in intron 3 sequence (hereafter referred to as exon A1) and a reverse primer in exon 4. The expected product of 183bp was detected in mouse retina cDNA but not in the brain cDNA (Figure 4.8B).

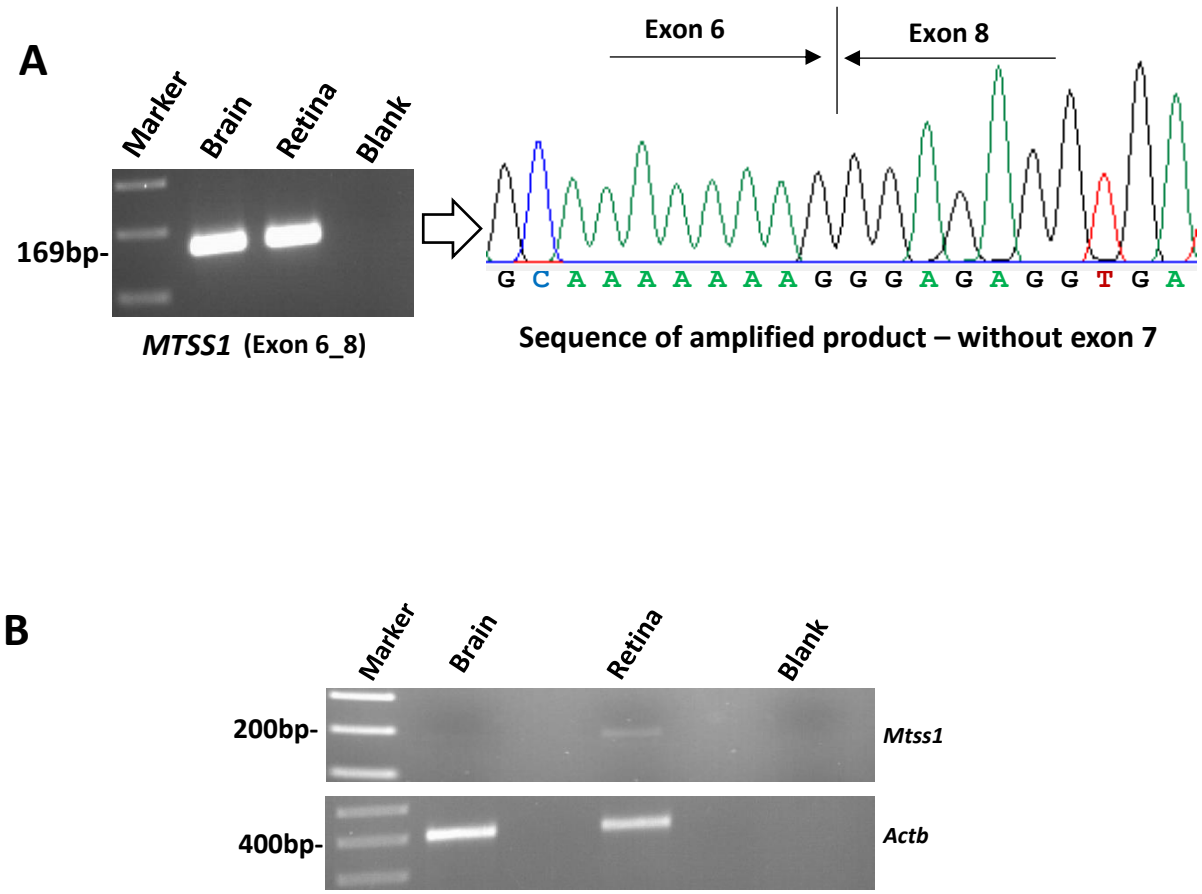


Figure 4.8. Alternate exons and transcripts of *MTSS1*/*Mtss1* in retina. (A) The absence of 12bp exon 7 in human brain and retina. The presence of the putative 12bp exon 7 was examined in all PCR products amplified with primers bordering around this exon, including primers in exon 6 and 8, but the exon was not detected to be present. **(B)** *Mtss1* transcript AK030533 with a non-coding exon/promoter in intron 3 and an alternate transcription start site in exon 4 was detected to be expressed in mouse retina but not in brain. β-actin (*Actb*) expression was used as positive control**.**

4.4.1.6 Analysis of 5' UTR of Mtss1 in mouse brain and retina

The mammalian retina is reported to express some tissue-specific transcripts of some genes through alternative splicing events (Aísa-Marín et al., 2021). An example of this is shown in Figure 4.8B, where the alternate transcript AK030533 of *Mtss1* is found to be expressed in the mouse retina but not in brain. From our present expression data (Figure **4.4**A) and previous expression data (Lee et al., 2002), *Mtss1* is ubiquitously expressed in mammalian tissues. This made us interested in investigating whether *Mtss1* might have different promoters and transcription start sites in different tissues. As such, we considered it important to examine the 5' untranslated region (UTR) of *Mtss1* in mouse retina and brain using 5' RACE (see 4.3.1).

4.4.1.6.1 The *Mtss1* has the same canonical transcription start site in brain and retina

To analyse the beginning of the transcripts of *Mtss1* in the brain and retina, a primary 5' RACE was performed (see 4.3.1) with a gene-specific primer (GSP) in exon 2 (Figure 4.9A). Sequences of all primers used in 5' RACE experiments can be found in Appendix C. In both brain and retina, a ~700bp product was amplified (Figure 4.9B). Both products were gel-purified and cloned into the pRACE vector. Four independent clones each from both brain and retina were sequenced with M13F and M13R primers (primer sequences can be found in Appendix C). Analysis of the sequencing data showed the 5' RACE products amplified from brain and retina to contain exons 1 and 2 of *Mtss1* (including the non-coding region of exon 1) with a common transcription start site in exon 1 (Figure 4.9C). Notably, the sequence of the non-coding region of exon 1 of the brain was found to be 163bp longer (going up further into the 5' UTR) compared to sequence from retina.

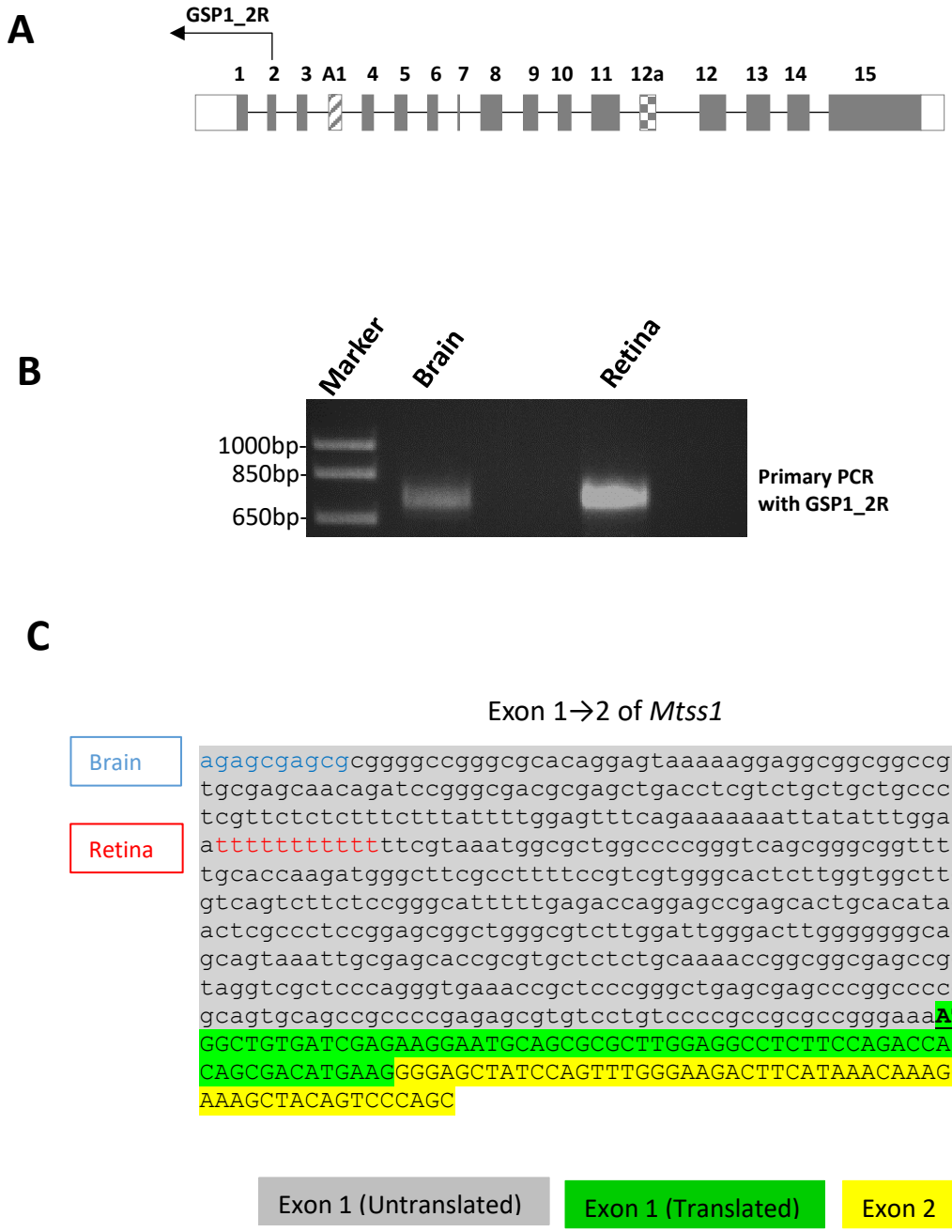
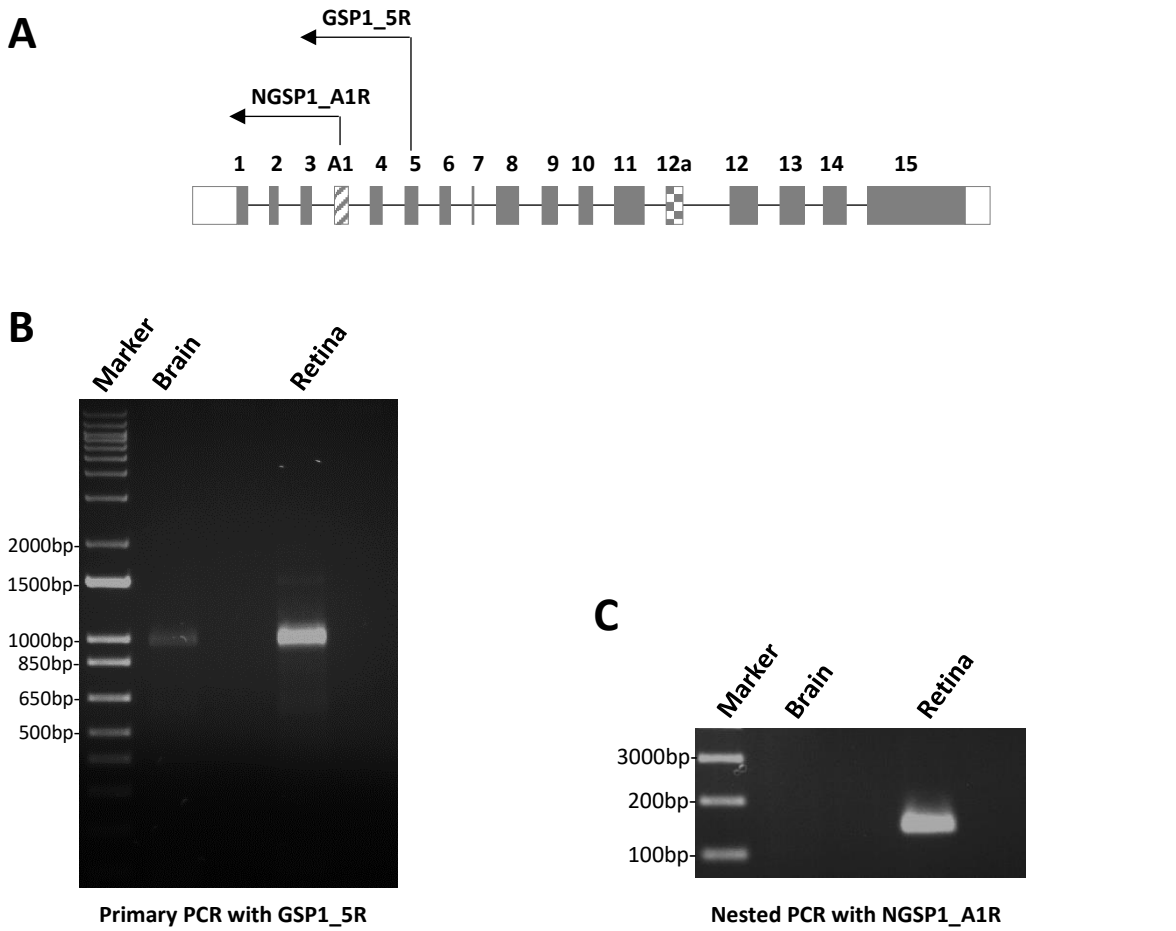


Figure 4.9. Analysis of 5' UTR of Mtss1 in mouse brain and retina. **(A)** Genomic structure of *Mtss1* gene indicating location of 5' RACE primers. **(B)** A primary 5' RACE was performed using a gene-specific primer (GSP) located in exon 2 on 5' RACE-ready cDNA from mouse brain and retina. 5' RACE products from mouse brain and retina visualised on a 1.2% agarose gel. Both bands were excised, gel-purified and cloned into pRACE vector to be sequenced. **(C)** 5' UTR sequence of *Mtss1* analysed from RACE products from brain and retina. Both products contained exon 2 and exon 1 with a common translation start site in exon 1 for brain and retina. Untranslated part of exon 1 in brain was found to be 163bp longer (indicated in blue) compared to the untranslated part of exon 1 of the retina (indicated in red). UTR = untranslated region; RACE = Rapid amplification of cDNA Ends.

4.4.1.6.2 AK030533 transcript of *Mtss1* in retina confirmed by 5' RACE

Having identified the expression of the AK030533 transcript in the retina but not in brain (Figure 4.8), we were also curious to analyse the 5' UTR of this transcript which has its start site in exon 4 and an untranslated exon in intron 3. We performed an initial 5' RACE amplification with a gene-specific primer in exon 5 followed by a nested PCR with GSP in exon A1 (Figure 4.10A and B) using brain and retina 5' RACE-ready cDNA (see 4.3.1). As identified in our previous expression PCR data (Figure 4.8), expression of the AK030533 transcript was not identified in the brain. Instead, a band of ~150bp was identified only in retina in the nested 5'RACE with the gene specific primer in exon A1 (Figure 4.10C). This product from the retina was gel-purified and cloned into a pRACE vector. Eight independent clones were sequenced with M13F and M13R primers (primer sequences located in Appendix C) and we identified a sequence that aligned with exon A1 genomic reference sequence (Figure 4.10D), indicating the presence of this exon and its putative transcript in the retina.



D Exon A1 → Exon 4 of *Mtss1* from retina

ggatgatacggtgtaaacccaagtgcaacacttgttccttgtcctggaactggagggagtgatgggct
gtgtaaacataacccttgacctcccagggacggtggctctcctggactctggatccag**GTGGTACCCG**
GGAGATCGGCTCAGCTCTCACCAGAATGTGCATGCGGCACCGGAGCATCGAGGCCAAGCTGAGGCAGT
TCTCCAG

Exon A1 (Untranslated) | Exon 4 (Untranslated) | Exon 4 (Translated)

Figure 4.10. 5' RACE confirms retina-specific transcript of *Mtss1*. (A) Genomic structure of *Mtss1* gene indicating location of 5' RACE primers. **(B)** A primary 5' RACE was performed using a gene-specific primer (GSP) located in exon 5 on 5' RACE-ready cDNA from mouse brain and retina followed by a nested PCR with a GSP in exon A1. Products from primary 5' RACE performed with GSP in exon 5 were analysed on a 1.2% agarose gel. Prominent bands are seen at ~1000bp in both brain and retina, together with some faint bands. **(C)** Nested PCR with nested gene-specific primer (NGSP) in exon A1 on initial primary 5' RACE products was performed. Expression of exon A1 was detected in the retina but not in brain. The band in retina was gel-purified and cloned into pRACE vector to be sequenced. **(D)** Sequence of nested 5' RACE product from retina.

4.4.2 MTSS1 protein expression and localisation

4.4.2.1 Protein expression in mouse retina using western immunoblotting

Having detected *MTSS1* gene expression in cDNA from both human and mouse retinas, we sought to assess Mtss1 protein expression in the mouse retina through western immunoblotting (see 2.3.5.3). Two commercially available rabbit polyclonal antibodies were used: one designed to the N-terminal amino acids 150-200 of human MTSS1 (#NBP2-24717**,** Novus Biologicals, UK) and the other raised to the C-terminal amino acids 670-720 of the human MTSS1 protein (#NBP2-24716**,** Novus Biologicals, UK) (Figure 4.3). The amino acid sequence of these human N-terminal and C-terminal antibodies had 96.1% and 94.1% similarity with the mouse Mtss1 protein respectively. The antibody concentration was optimised using 1:400, 1:800, 1:1000 and 1:1200 dilutions to determine the best concentration to be used. For the N-terminal antibody, a 1:1200 was identified to be optimal and was used to probe 20µg of lysate from mouse brain and retina (see 2.3.5.1). A band corresponding to the molecular weight of the full length of the Mtss1 protein (~100kDa) was detected in both brain and retina (Figure 4.11A). Additional bands of lower molecular weight (~60 and ~85kDa) were detected to be present in the retina, and these could possibly represent the other MTSS1 transcripts as described in section 4.4.1.5.

The C-terminal antibody detected faint bands of the expected size (~100kDa) when it was used to probe 10µg lysate from mouse brain and retina 1:400 dilution (Figure 4.11B). These bands were not detected at 1:800 dilution (Figure 4.11C). Strong clear bands of ~70kDa and ~65kDa were detected in retina lysate, while a band of ~70kDa was identified in brain lysate, at both 1:400 and 1:800 dilution of the C terminal antibody (Figure 4.11B & C). These bands did not match the molecular weights of the additional bands detected with the N-terminal antibody.

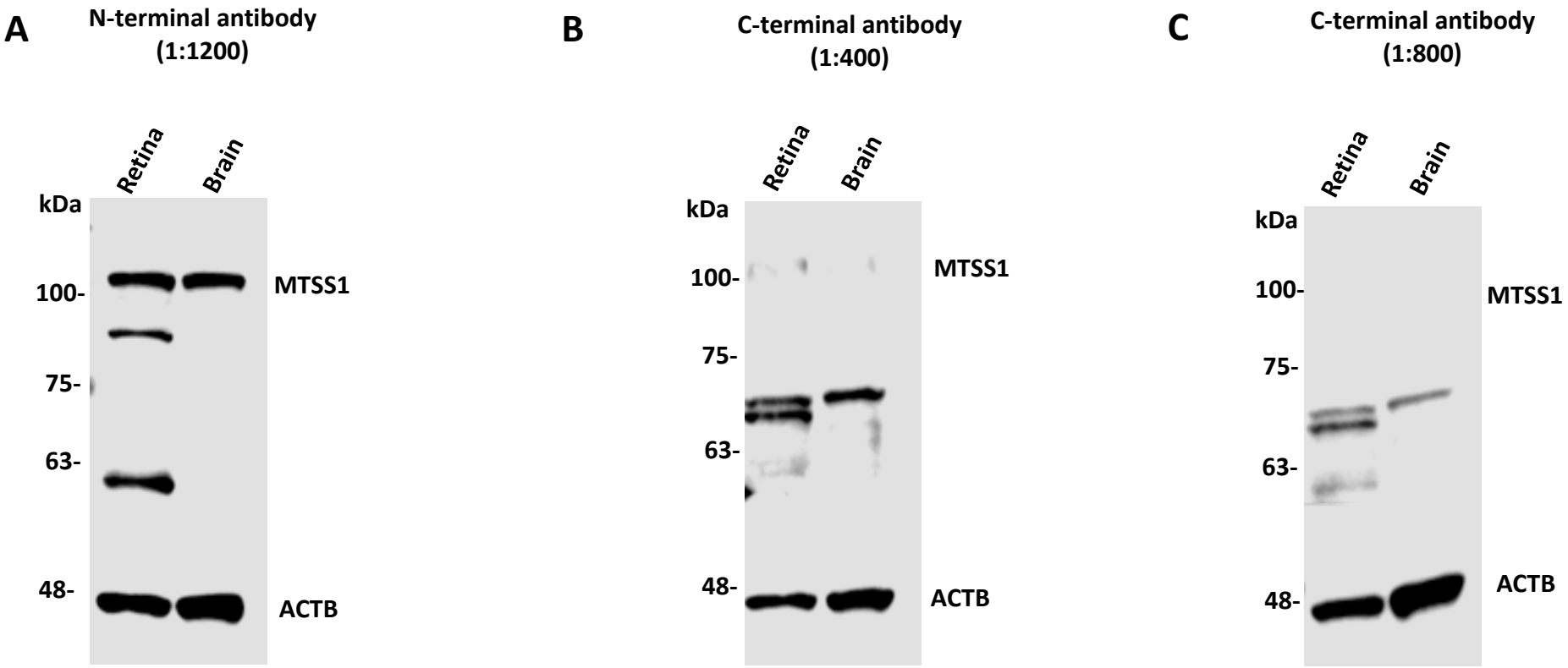


Figure 4.11. MTSS1 protein expression in retina and brain assessed by western immunoblotting. (A) N-terminal human MTSS1 antibody (#NBP2-24717, Novus Biologicals, UK) raised to amino acids 150-200 was used to probe 20µg of protein lysates from wild-type mouse retina and brain. Bands corresponding to the expected molecular weight of Mtss1 (~100kDa) were detected in both brain and retina. Additional bands of ~ 60kDa and ~85kDa were seen in retina. **(B & C)** C-terminal human MTSS1 antibody (#NBP2-24716, Novus Biologicals, UK) raised to amino acids 670-720 was used to probe 10µg of protein lysates from wild-type mouse retina and brain. Expected bands of full length MTSS1 (~100kDa) was detected faintly at 1:400 and additional bands of lower molecular weight (~65kDa and 70kDa) were detected in both brain and retina. β-actin (ACTB) was used as a loading control.

4.4.2.2 Mtss1 is expressed in rod photoreceptors of the retina

Immunohistochemical staining of adult wild-type mouse retinal sections was performed using the N-terminal and C-terminal commercial rabbit polyclonal MTSS1 primary antibodies (see 4.4.2.1 for details). A list of all antibodies used for immunohistochemistry can be found in Appendix E and F. Using the N-terminal antibody (1:100), MTSS1 antibody labelling was detected in the outer retina, an area corresponding to the outer and inner segments (OS and IS) of the photoreceptors, as well as the outer and inner plexiform layers (OPL and IPL) of the inner retina (Figure 4.12A). The C-terminal MTSS1 antibody (1:100) also detected MTSS1-positive staining in the outer retina in areas corresponding to the OS and IS of the photoreceptors, and the OPL, bipolar cells and IPL of the inner retina (Figure 4.12B), similar to the staining pattern obtained with the N-terminal antibody. However, the staining intensity of the C-terminal antibody, especially in the photoreceptor layer, was weaker compared to that obtained with the N-terminal antibody. Together with the results obtained from the western immunoblotting (see 4.4.2.1), the N-terminal antibody was chosen as the preferred antibody to be used in subsequent applications (unless otherwise stated).

Since the photoreceptor layer contains both rods and cones, it was important to determine whether the MTSS1 staining pattern detected was in rods, cones or in both. To do this, we co-stained wild-type mouse retina sections with N-terminal MTSS1 antibody and peanut agglutinin (PNA) which labels cone photoreceptors. We found no co-localisation of PNA and MTSS1 staining, suggesting that MTSS1 staining/expression in the photoreceptor layer was restricted to rod photoreceptors (Figure **4.13**A). To confirm that the N-terminal MTSS1 antibody indeed localised to rod photoreceptors, we stained retina sections from *Nrl*-EGFP transgenic mice in which rod photoreceptors are endogenously labelled with GFP (Akimoto et al., 2006). By staining retina sections from these *Nrl*-EGFP mice with the N-terminal MTSS1 antibody, we found MTSS1 staining in the photoreceptors co-localising with the GFP in the rod photoreceptors (Figure **4.13**B).

To confirm whether MTSS1 staining in the rod photoreceptors is in both outer and inner segments or is limited to only the inner segment, we stained wild-type mouse retina sections with the MTSS1 N-

terminal antibody and an antibody for rhodopsin (1D4; #MA1-722, Thermo Fisher Scientific, USA) which labels the outer segments of rod photoreceptors. We identified colocalization of MTSS1 with 1D4 at the proximal part (base) of the rod outer segments (Figure 4.13C), suggesting that MTSS1 is expressed in both the outer and inner segments of rod photoreceptors.

4.4.2.3 Co-localising MTSS1 staining in outer plexiform layer (OPL), inner plexiform layer (IPL) and ganglion cell layer (GCL)

The MTSS1-positive staining was also detected in areas of the inner retina corresponding to the OPL, IPL and GCL. To confirm the MTSS1-positive staining in these areas, commercially available antibodies known to be specific markers of these areas were used. Using an antibody that labels synaptic processes (Synaptophysin; Novus Biologicals, UK), colocalization of MTSS1 and synaptophysin was identified in the OPL and IPL, indicating Mtss1 expression in the synaptic processes of the retina (Figure 4.14A). A GCL marker, Brn3a (Santa Cruz Biotech, USA), was also used to co-localise MTSS1 staining in the GCL (Figure 4.14B).

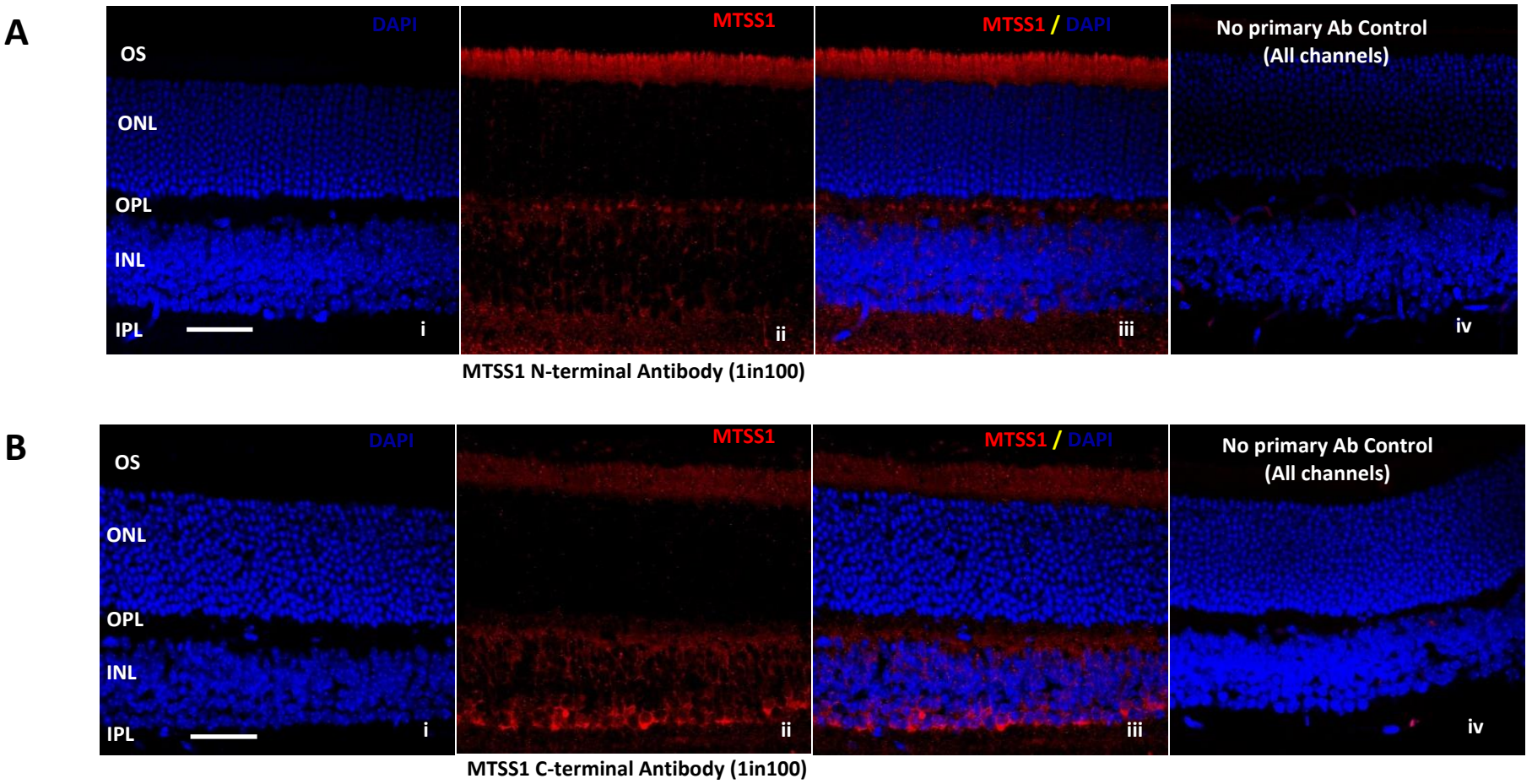
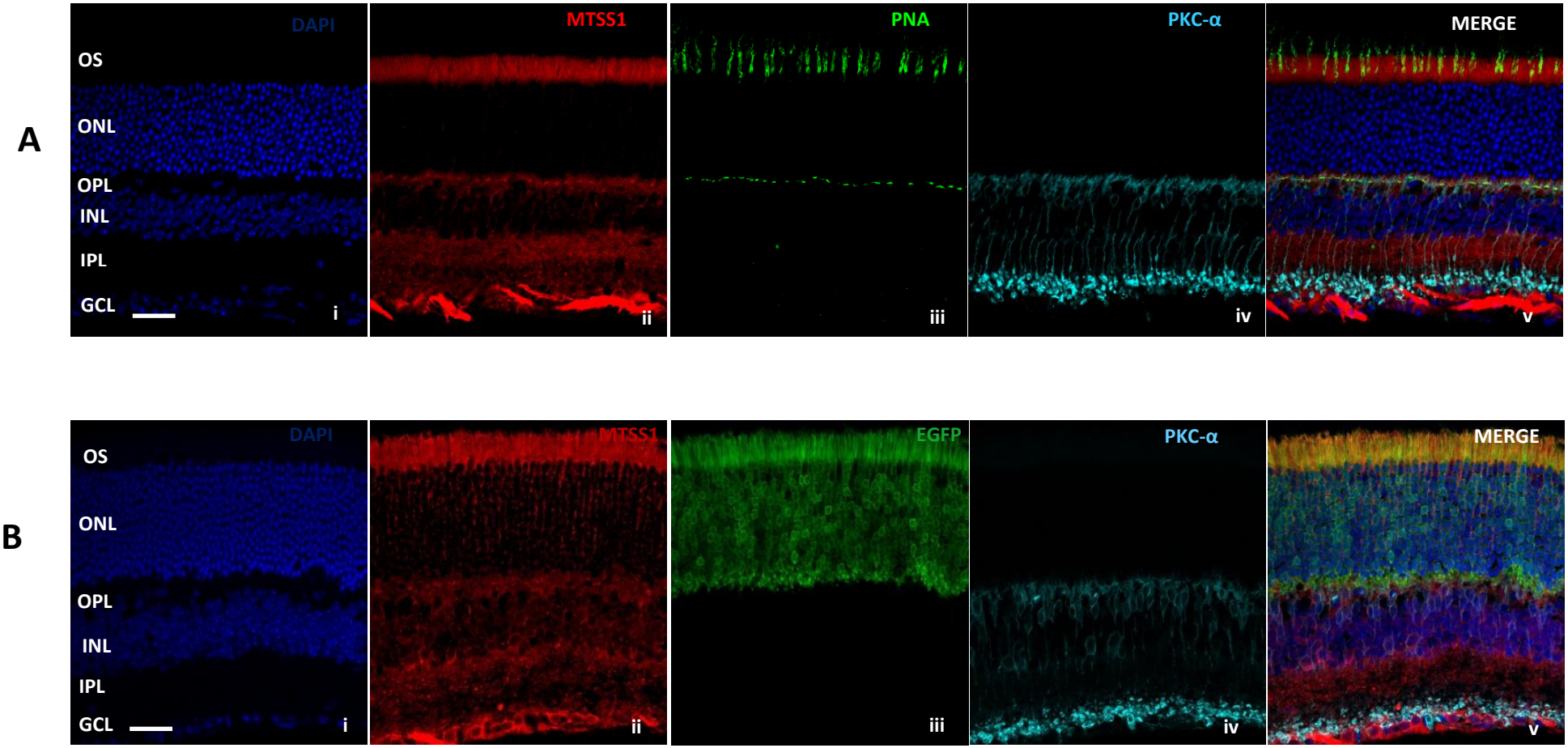


Figure 4.12. Immunohistochemical staining of wild type mouse retina with MTSS1 antibodies. (A) N-terminal MTSS1 antibody staining (red) on frozen retina sections from wild type mouse. (B) C-terminal MTSS1 antibody staining (red) on frozen retina sections from wild type mouse. MTSS1 (red) localizes to multiple areas of the retina including photoreceptors in the outer retina and parts of the inner retina. (A-iv & B-iv) Sections stained with secondary antibodies only were used as controls. DAPI (blue) was used to stain the nuclei. OS = Outer segment; ONL = Outer nuclear layer; OPL = Outer plexiform layer; INL = Inner nuclear layer; IPL = Inner plexiform layer. Scale bar = 20µm


A
DAPI
MTSS1
PNA
PKC-α
MERGE
OS
ONL
OPL
INL
IPL
GCL
i
ii
iii
iv
v
B
DAPI
MTSS1
EGFP
PKC-α
MERGE
OS
ONL
OPL
INL
IPL
GCL
i
ii
iii
iv
v

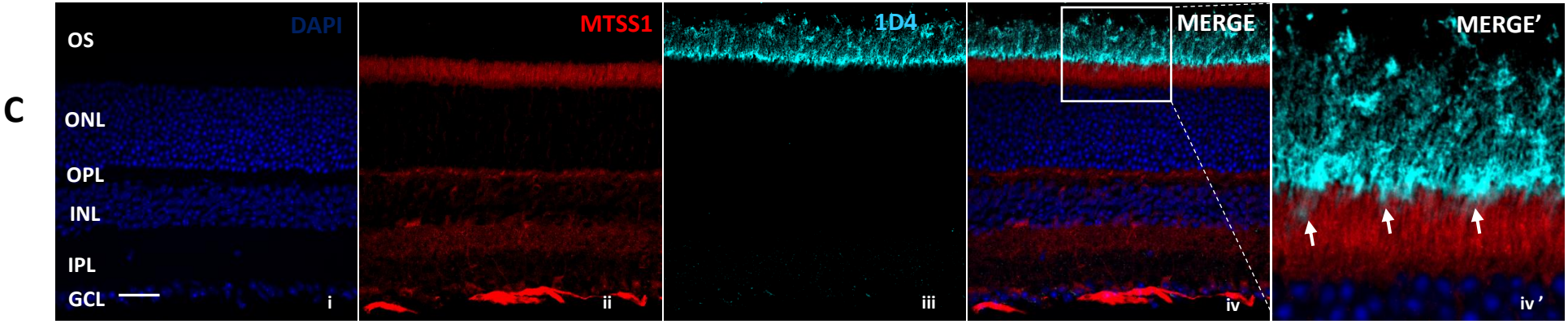


Figure 4.13. Mtss1 protein is expressed in rod photoreceptor cells of the mouse retina. (A) MTSS1 antibody (red) was used to stain frozen wild type mouse retina sections along with PNA (green) which labels cone photoreceptors. Note how MTSS1 staining in the photoreceptor layer can be distinguished from PNA-labelled cone photoreceptors. **(B)** MTSS1 (red) was used to label retina sections from *Nrl*-EGFP mice in which rod photoreceptors are endogenously labelled with GFP (green). MTSS1 staining (red) was found to overlap with GFP (green) in rod photoreceptors. **(C)** MTSS1 antibody (red) was used to stain retina sections along with a rhodopsin antibody (1D4) that labels rod photoreceptor OS. MTSS1 labelling is seen prominently in the IS and continues into the base of the OS. Boxed area in C-iv is expanded as C-iv' showing colocalization of MTSS1 and 1D4 at the base of the rod OS (arrows). DAPI (blue) was used to stain the nuclei. PKC-alpha (cyan) which stains bipolar cells was used as retinal marker. OS = Outer segment; ONL = Outer nuclear layer; OPL = Outer plexiform layer; INL = Inner nuclear layer; IPL = Inner plexiform layer; GCL = Ganglion cell layer. Scale bar = 20µm.

4.4.2.4 Mtss1 protein is expressed in retina throughout development

To determine the expression pattern and potential relevance of Mtss1 during the development of the retina, we examined Mtss1 expression in developing wild-type mouse retina. Retinal sections from P0, P4, P8, P12, P16 and Adult mice were immunohistochemically stained with N-terminal MTSS1 antibody. Consistent with findings from our gene expression studies in which *Mtss1* gene expression was identified in a panel of cDNA from developing mice retina at P0, P4, P8, P12, P16 and adult (Figure **4.4**B), Mtss1-positive staining was detected at all the developmental time points examined (Figure 4.15).

At P0 and P4 when photoreceptor cells are yet to differentiate from the neuroblastic layer (NBL), Mtss1-positive staining is strongly present in the GCL and IPL, although some staining is seen at the top of the NBL, possibly representing differentiating photoreceptor cells (Figure 4.15A and B). Mtss1 staining in the OPL and photoreceptor layer begin to become apparent from P8 into adulthood with staining in the photoreceptor inner and outer segments becoming more prominent in the adult retina (Figure 4.15C-D). PNA-staining of cone photoreceptor cells is absent from P0 to P8, consistent with the lack of well differentiated photoreceptors at these stages. From P12 onwards when PNA staining is detected, no colocalization is observed between PNA-positive cells (cones) and Mtss1-positive cells, further signifying that Mtss1 expression in the photoreceptor layer is limited to rods. Protein Kinase C alpha (PKCα) positive staining, used as a marker of bipolar cells and their process, is absent at P0 but is present at P4 and becomes well-defined as the retina matures into adulthood.

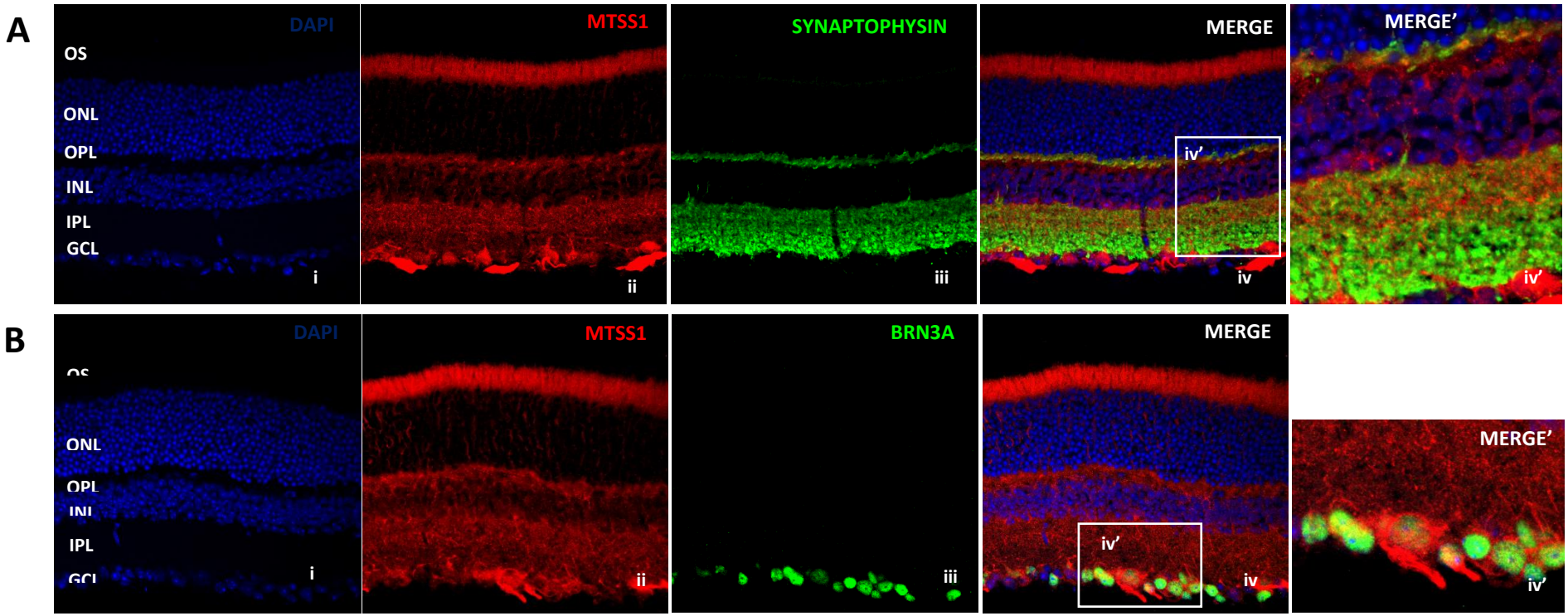


Figure 4.14. Mtss1 expression in synaptic layers and ganglion cell layer. (A) MTSS1 N-terminal antibody (red) was used to stain frozen wild type mouse retina sections along with synaptophysin (green) which labels the synapses that make up the OPL and IPL. (B) Brn3a (green), a marker of ganglion cells was used to localise MTSS1 staining (red) in ganglion cells of the GCL. DAPI (blue) was used to stain the nuclei. OS = Outer segment; ONL = Outer nuclear layer; OPL = Outer plexiform layer; INL = Inner nuclear layer; IPL = Inner plexiform layer; GCL = Ganglion cell layer. Scale bar = 20µm

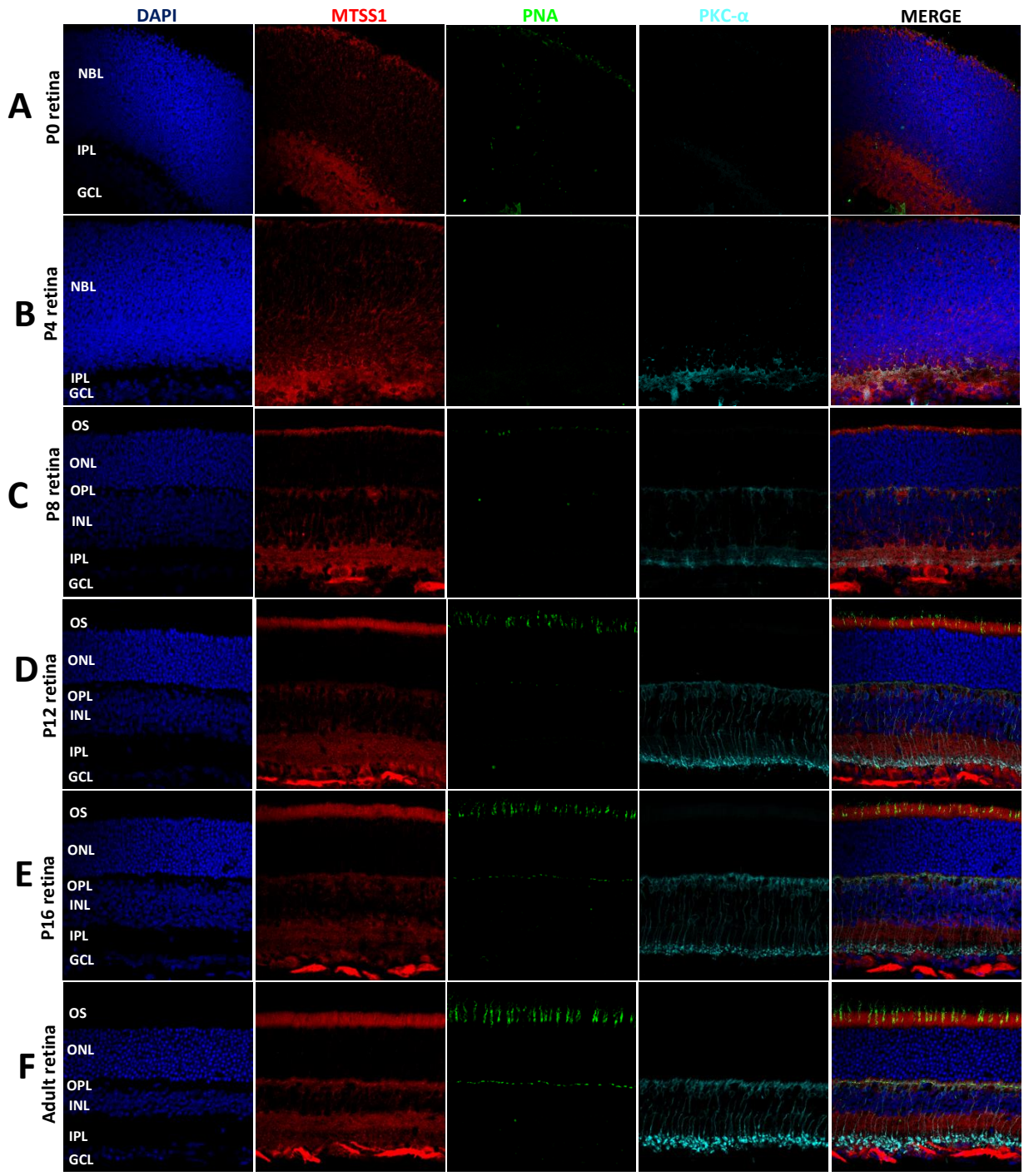


Figure 4.15. Mtss1 protein expression in developing mouse retina. Immunohistochemical staining of MTSS1 (red) was conducted on frozen sections from wild-type mouse retina sections at various developmental stages. PNA (green) was used to label cone photoreceptors. DAPI (blue) was used to stain the nuclei. PKC-alpha (cyan) which stains bipolar cells was used as retinal marker. OS = Outer segment; ONL = Outer nuclear layer; OPL = Outer plexiform layer; INL = Inner nuclear layer; IPL = Inner plexiform layer; GCL = Ganglion cell layer; NBL = Neuroblastic layer. Scale bar = 20µm

4.5 Discussion

We hypothesised that for *MTSS1* to be able to cause an RP phenotype, the gene and its product, like other genes implicated in RP, must first of all be expressed in the retina, and particularly in the photoreceptors. In this chapter, we have confirmed that *MTSS1* is expressed in the mammalian retina at both the gene and protein levels. We have demonstrated, using end-point PCR and cDNA from human and mouse retina, that the *MTSS1* gene is expressed in the mammalian retina, and also detected multiple transcripts of the gene that are expressed in the retina. Using immunohistochemistry, we have also demonstrated that the Mtss1 protein is expressed in the rod photoreceptors (and not cones), and other areas of the retina including the synaptic layers, bipolar cells and ganglion cell layer. Most importantly, we have shown that in rod photoreceptors, Mtss1 localises to the inner and outer segments, and suggest that it could have a potential role in rod photoreceptor physiological function. Indeed, most RP conditions are associated with mutations in proteins expressed in these regions of the rod photoreceptors (Blackshaw et al., 2001).

Although our findings in this chapter confirm the expression of *MTSS1* in the mammalian retina as expected of a gene likely to cause an IRD phenotype, our findings also agree with previous studies that *MTSS1* is a widely expressed gene (Loberg et al., 2005). It then raises the question as to why a mutation in a gene/protein that is widely expressed in other tissues will only cause a retinal phenotype. However, it is not uncommon to find genes that are widely expressed in mammalian tissues being implicated in non-syndromic RP, with *ADIPOR1* (Zhang et al., 2016), *ARL3* (Strom et al., 2016) and *IMPDH1* (Bowne et al., 2006) being examples. Reasons for this remain unclear, although some speculations could be made, including: (i) the extremely high metabolic demands placed on retinal cell machinery, an example being the photoreceptor OS turnover rate (Pan et al., 2021), and (ii) alteration in function of retina-specific isoforms of these genes (Bowne et al., 2006, Popova et al., 2017). The idea of the mammalian retina possessing retina-specific transcripts of genes widely expressed in other tissues is not alien. As such, previous studies have found the retina to express unique transcripts of genes including *FRMPD1* (Campla et al., 2019), *CERKL* (Garanto et al., 2011), *IMPDH1* (Bowne et al.,

2006) and *CRB1* (Ray et al., 2020). Generally, it is estimated that only about 1.2% of the entire human genome are coding exons, making approximately 25,000 - 30,000 genes in the human genome (Consortium, 2012). However, the human genome is able to achieve the complexity and diversity of the proteome necessary for normal development and function by producing multiple isoforms of mRNA from genes through alternative splicing and gene regulation events (Liu et al., 2017). In fact, it has been established that over 95% of all multiexon genes in the human genome undergo various alternate splicing events to produce the multiple transcripts in a tissue-, cell- and time-specific manner (Pan et al., 2008, Wang et al., 2008). The retina, which is an extension of the central nervous system (CNS), is known to be a perfect example of how tissue-specific gene transcript expression contributes to normal tissue function and disease (Aísa-Marín et al., 2021). In the case of *MTSS1*, it is therefore not surprising that it appears to have several transcripts in the retina detected by both gene expression PCR and western blot, as well as having a transcript (AK030533) that was not detected in the brain, also identified by two independent techniques: expression PCR and 5' RACE. Although this AK030533 transcript could be expressed in other tissues aside the retina (Saarikangas et al., 2011), the fact that it is expressed in the retina and not in the brain is suggestive that there could be transcripts of *Mtss1* with varying functional roles between the retina and the brain.

Attempts to amplify and clone the full-length coding sequence of *MTSS1* from human retina failed to amplify the two known longest transcripts (AK027015 and AF086645; Figure **4.1**A and B), despite the AF086645 transcript being amplified from the brain using the same technique. The inability to amplify the full-length coding sequence of these longest transcripts from the retina is notable. Possible explanations could be that these transcripts are either less abundant or are not expressed in the retina. The former is particularly possible since the end-point PCR technique, the main techniques used to determine gene expression from cDNA in this thesis, is known to be biased towards amplifying the most abundant transcripts. To address the latter possibility of the absence of these transcripts in the retina, gene expression PCRs with primers targeting specific exons 11 and 13 of these transcripts (Figure 4.7B) gave an indication that this full-length transcript is present in the retina. Although

determined to be present, it could be suggested that the longest known transcripts of *MTSS1* may not be the most abundant of MTSS1 transcripts in the human retina.

Interestingly, our results from expression PCR with primers spanning exons 11 and 13 also revealed the presence of *MTSS1* transcripts with alternately spliced exons in the retina (Figure 4.7B). Aside the transcript containing the traditional exon 12, a transcript containing the alternate exon 12a (without exon 12), and another transcript with neither exon 12 nor 12a were detected in the retina. The transcript with exon 12a (Figure **4.1**E) was previously reported to be exclusively expressed in the cerebellum and that the expression of transcripts with exon 12 or 12a in the CNS was developmentally regulated (Glassmann et al., 2007). This involved the down-regulation of the exon 12 transcript and the upregulation of the exon 12a transcript which occurred at the point of neuronal maturation of cerebellar Purkinje cells and resulted in extensive dendritic arborisation (Sistig et al., 2017, Glassmann et al., 2007). Relating exons 12 and 12a to the protein sequence and structure of MTSS1, the two exons encode 65 and 40 amino acids, respectively, which correspond to the central regulatory domains of the MTSS1 protein (Figure 4.3).

Glassman *et al*. (2007) studied the functional implications of having exon 12 or 12a isoforms expressed and predicted alteration of the binding sites for Fyn and Src, two tyrosine kinases involved in the regulation of cerebellar cell migration and histogenesis, encoded by exon 12 (Glassmann et al., 2007). Indeed, the switch from exon 12 to 12a splice variants has been reported to occur at the end of cell migration and commencement of neuritogenesis in cerebellar granule and Purkinje cells, suggesting that these two splice variants have tissue, cell-type and time-specific expression and functional attributes (Sistig et al., 2017). Identifying that these transcripts of *MTSS1* are also expressed in the adult human retina does not only highlight the similarity between the retina and the brain, but also an indication that the expression pattern of *MTSS1* splice variants and their corresponding functional roles in the retina may also be cell-type specific and developmentally regulated. It will, therefore, be interesting to know if these two splice variants have different levels of expression and/or areas of

localisation in the developing and adult retina. A single schematic representation summarising all the splice variants of *MTSS1* identified in both brain and retina is presented in Figure 4.16.

Given that the clinical diagnosis of the disease phenotype in the 3027 family is RP, it is expected that the causal gene for this family would be expressed in the human retina, especially in the retinal photoreceptors, since most known RP genes are expressed in the photoreceptors (Ali et al., 2017). Also, RP is a rod-dominant condition in which rod dysfunction and degeneration precedes that of cone photoreceptors (Narayan et al., 2016). Accordingly, most of the genes implicated in RP are rod-enriched genes (Blackshaw et al., 2001). Results from MTSS1 immunolocalization studies using MTSS1 N- and C-terminal antibodies revealed that MTSS1 expression identified in the photoreceptor layer is restricted to the rods: MTSS1-positive staining did not colocalize with PNA-positive cone photoreceptors whiles MTSS1-positive staining colocalized with GFP-labelled rod photoreceptor outer and inner segments from Nrl-EGFP mice, consistent with what is expected of the RP phenotype.

In addition to MTSS1 expression in rod photoreceptors, its expression was identified in other layers of the retina such as the OPL, bipolar cells, IPL and GLC. These results are in agreement with two datasets which suggested MTSS1 is expressed by multiple retinal cell types: (i) our gene expression data in the transgenic mice retina (Figure 4.5A) which detected *Mtss1* expression in rodless, coneless, and rodless/coneless mice retinas, and (ii) a recently published scRNA-seq dataset that detected *MTSS1* expression in multiple retinal cell populations including photoreceptors, RGCs and bipolar cells of the adult human retina (Lukowski et al., 2019). Again, it is not uncommon to find genes implicated in rod-dominant IRD phenotypes being expressed in cells of the inner retina. Previously implicated genes such as *CERKL* (Garanto et al., 2011) and *IMPDH1* (Bowne et al., 2006) are expressed by multiple cells types in the retina and cause rod-dominant phenotypes. In the developing retina, Mtss1-positive staining was detected in the GCL and synaptic layers at P0 and expression in these is maintained into adulthood (Figure 4.15). Similar to the brain, the formation and development of synapses and synaptic processes is a crucial part of normal retinal development and function (Huang et al., 2020). At the same time, several studies have implicated Mtss1 to play a role in the development and maturation of synaptic

processes and synapses in brain tissue and neuronal cultures (Yu et al., 2016, Sistig et al., 2017, Brown et al., 2018). It is, therefore, possible that might contribute to the development of the extensive synaptic processes and connections necessary for normal retina function, hence its strong expression in the synaptic layers of the inner retina in early development.

It is important to note that, while the N-terminal antibody did not stain the retinal bipolar cell bodies, MTSS1-positive staining in the bipolar cells was detected upon staining with the C-terminal antibody. This raises the question of whether these two MTSS1 antibodies could be detecting different isoforms of the MTSS1 protein which may be differentially expressed in the retinal cell types. The N-terminal antibody detects amino acids 150-200 whiles the C-terminal antibody detects amino acids 670-720 of the MTSS1 protein. Considering that results from this study suggest the presence of MTSS1 splice variants with varying exon combinations in the retina, the possibility of these two antibodies detecting different isoforms of the protein in the retina cannot be ruled out. Also, the idea that different MTSS1 isoforms could be differentially expressed in the various retinal cell types is likely, owing to reports from previous studies that showed differential and cell-specific expression of Mtss1 isoforms between peripheral tissues, granule and Purkinje cells of the cerebellum (Sistig et al., 2017, Glassmann et al., 2007). On the issue of antibodies detecting other isoforms of Mtss1 in the retina, both the N-terminal and C-terminal antibodies detected additional bands of lower molecular weights aside the full length Mtss1 in the western blot experiments (Figure 4.11). Although these bands may represent other isoforms of Mtss1 expressed in the retina, this is inconclusive as the bands did not exactly match the molecular weights of the known Mtss1 isoforms predicted based on their amino acid sequences. This observation is, however, not uncommon as it is well known that observed molecular weights of proteins detected during SDS-PAGE are mostly larger than the predicted size, a phenomenon that is often attributable to chemical modification and post-translational modifications of many proteins (Guan et al., 2015). A typical example of this is the full length MTSS1 protein (AK027015) which is

predicted to be 82.6kDa based on its amino acid sequence (Woodings et al., 2003) but has consistently been detected at ~100kDa (Saarikangas et al., 2011, Sistig et al., 2017).

In conclusion, results presented in this chapter provides substantial novel evidence that *MTSS1/Mtss1* is expressed in the mammalian retina and is expressed in rod photoreceptors as predicted of a gene that may cause RP phenotype. MTSS1 may have a role in development and maintenance of normal retinal function from early stages of development through to adulthood, consistent with its detected expression at various developmental stages. Also, MTSS1 has several isoforms in the retina which may be expressed in cell-specific and developmentally-regulated manner. These results highlight the need for an extensive investigation to unravel and understand the full complement of *MTSS1* transcripts in the retina and their potential roles. With multiple lines of evidence from this study pointing to the expression of MTSS1 gene and protein in the mammalian retina, there is also the need to examine the potential function of the MTSS1 protein in the retina, potential binding partners and the effect of the variant identified in family 3027 could have on the protein structure and function.

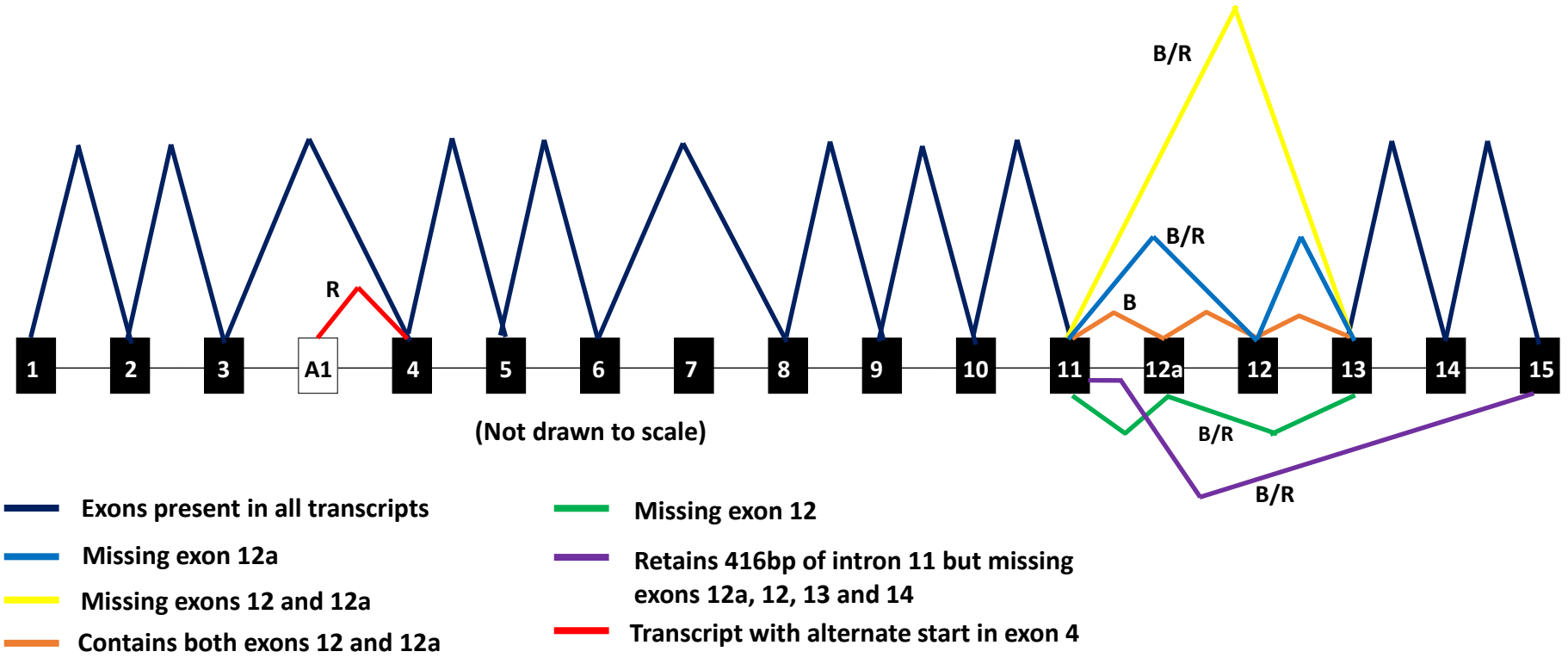


Figure 4.16. Schematic representation summarising the alternate splice variants of *MTSS1* identified in brain and retina. With the exception of transcript AK030533 with a non-coding exon in intron 3 and an alternate translation start site in exon 4 identified only in retina, all other MTSS1 transcripts identified started from exon 1. None of the transcripts identified contained exon 7 (a 12bp exon). Between exon 11 and exon 13, splice variants with various exon combinations were identified. Each splice variant is colour coded (colour atlas shown above). Exons are represented by rectangles and introns by lines. B = Transcripts identified in brain only; R = Transcript identified in retina only; B/R = Transcripts identified in both brain and retina.

5 Functional characterisation of MTSS1 in mammalian retina and cells

5.1 Introduction

The role of MTSS1 in tumourigenesis and metastasis suppression was proposed when the gene was first identified by Lee *et al.* in 2002 (Lee et al., 2002). Although the exact mechanisms by which it suppresses tumour metastasis remain unclear, it has been postulated to be associated with its role in regulating actin cytoskeleton network in cells (Woodings et al., 2003). As such, its role in regulating actin cytoskeleton through its two spatially separated actin-binding domains, an N-terminal IRSp53/MIM homology domain (IMD) and a C-terminal Wiskott-Aldrich syndrome protein (WASP) Homology 2 (WH2) domain (Figure 4.3), has been well studied (Xie et al., 2011). This has provided insights into how the protein regulates various cellular processes including cell morphogenesis and cell motility (Xie et al., 2011).

The C-terminal WH2 domain has been shown to be involved in actin monomer binding (Lee et al., 2002). Proteins containing WH2 homology domains have an affinity for actin monomers and are involved in regulating cell polarity, cell motility and actin organisation (Paunola et al., 2002). Specifically, the WH2 domain of MTSS1 has been reported to have high affinity for ATP-bound G-actin, an active form of G-actin needed for actin polymerization (Mattila et al., 2003). Actin assembly in cells and plasma membrane processes, such as filopodia and lamellipodia, are assembled through two main actin nucleating pathways: the Arp2/3 protein complex and formins (Blanchoin et al., 2014). The Arp2/3 protein complex induces the nucleation of new actin filaments off the sides of existing ones to form branched networks such as those found in lamellipodia, while the formin family of proteins organise actin into parallel networks, such as those found in filopodia (Blanchoin et al., 2014, Higgs and Pollard, 2001). The WH2 domain of MTSS1 has been reported to be involved in regulating the formation of new actin filaments through direct interaction with the Arp2/3 complex (Woodings et al., 2003). Interaction between MTSS1 and cortactin, an Arp2/3 complex activator, has also been reported

previously, confirming the involvement of MTSS1 in the formation of new branched actin filaments (Lin et al., 2005). MTSS1 has also been shown to bind to DAAM1 (dishevelled associated activator of morphogenesis 1), a member of the formin family, and to regulate the formation of parallel actin networks during filopodia formation to determine final neural morphology (Kawabata Galbraith et al., 2018).

Whereas the WH2 domain binds to actin monomers, the N-terminal IMD domain of MTSS1 has been shown to be involved in binding to actin filaments (F-actin) (Yamagishi et al., 2004). Found in both MTSS1 and insulin receptor substrate p53 (IRSp53), the IMD domain has been reported to be involved in several cellular processes including actin cytoskeleton regulation and plasma membrane dynamics (Yamagishi et al., 2004). The IMD in both MTSS1 and IRSp53 has high affinity for phospholipid-rich membranes and has been reported to be involved in plasma membrane curvature sensing and bending necessary for cellular processes such as endocytosis, cell morphogenesis and cell motility (Saarikangas et al., 2015, Yu et al., 2011). This membrane-bending property is attributable to the similarity of the IMD structure with the BAR (Bin-Amphiphysin-Rvs) domain, a crescent-shaped anti-parallel helical dimer that binds preferentially to highly curved negatively charged membranes (Peter et al., 2004). Despite similarity in structure with other BAR proteins, the IMD of MTSS1 and IRSp53 are reported to have an opposite curvature which determines the type of membrane curvature they sense and induce: BAR proteins induces positive membrane curvature causing membrane invaginations as seen in endocytosis whereas the IMD senses and induces negative membrane curvatures to produce plasma membrane protrusions such as filopodia and lamellipodia (Zhao et al., 2011). This opposite membrane sensing property of MTSS1 to other BAR domain containing proteins has earned MTSS1 the name inverse-BAR (I-BAR) domain containing protein (Zhao et al., 2011). Consequently, cells overexpressing MTSS1 have been reported to form actin-rich plasma membrane protrusions, microspikes, lamellipodia and membrane ruffles (Woodings et al., 2003, Mattila et al., 2003). While the membrane-bending abilities of MTSS1 have long been attributed to the F-actin binding affinity of its IMD, it has been reported that the F-actin binding sites, located on either ends of the IMD domain, coincide with

the binding sites for phosphatidylinositol-4,5-bisphosphate ($PI(4,5)P_2$), and that the latter might explain its membrane deforming abilities owing to the fact that the $PI(4,5)P_2$ is a component of the plasma membranes (Mattila et al., 2007).

Studies on MTSS1 have largely focused on unravelling its role in metastasis. Hence, most of what is known about the gene and its protein are from studies from tumour and tumour-related cell lines. However, being a multifunctional multidomain protein that is widely expressed across mammalian tissues, there is increasing interest in pinpointing its potential role in other mammalian tissues. In mouse kidney, for example, it has been reported to be required for maintaining the integrity of intercellular junctions and enhancing the actin assembly at intercellular junctions in MDCK cells through interaction with E-cadherin (CDH1), a junctional protein in epithelial cells that links actin cytoskeleton to adherens junctions (Saarikangas et al., 2011). In support of its role in intercellular junctions, interaction between the IMD and Rac1, a Rho-family GTPase involved in regulating actin dynamics in cell-cell contacts, was previously reported in COS-7 cells (Suetsugu et al., 2006). Dawson *et al.* (2012) also reported that MTSS1 was required for rapid cell-cell adherens junction formation and maintenance through activation of Rac1 (Dawson et al., 2012). MTSS1 has also been found to play a role in neuronal cell function. In the cerebellar Purkinje cells, MTSS1 is reported to be involved in the formation and maturation of dendrites and synaptic contacts (Sistig et al., 2017, Saarikangas et al., 2015, Glassmann et al., 2007).

Thus, functional studies on MTSS1 have confirmed it to be a cytoskeletal scaffolding protein involved in the regulation of the actin cytoskeleton and plasma membrane dynamics through interaction with actin, actin-related proteins and phospholipid-rich plasma membranes in multiple cell lines and mammalian tissues (Lin et al., 2005, Yu et al., 2011, Dawson et al., 2012). However, the function of MTSS1 in the retina has not been previously described. As such, to investigate the potential function of Mtss1 in the mammalian retina, we adopted 3 approaches. First, we conducted co-immunohistochemical staining of wild-type mouse retina with Mtss1 antibodies and antibodies specific for some of the previously reported binding partners of Mtss1. Secondly, we investigated the

effect of the MTSS1 variant c.637_639del, p.(Glu213del) identified in family 3027 on the predicted protein structure, subcellular localisation and co-localisation with actin using *in silico* predictive programmes as well as transfecting wild-type and mutant constructs of MTSS1 into cell lines. Finally, we examined the potential effect of the loss of *Mtss1* expression in the mouse retina using a knockout model.

5.2 Aims

The overall aim of experiments outlined in this chapter was to investigate the role of MTSS1 in the mammalian retina and to determine how mutations may affect this role. The specific objectives were:

1. To assess colocalization of MTSS1 and previously reported binding partners in the mammalian retina
2. To determine the effect of the c.637_639del, p.(Glu213del) variant identified in family 3027 on the structure and subcellular localisation of MTSS1 protein using predictive *in silico* tools and *in vitro* approaches
3. To determine the retinal phenotype of a mouse model lacking *Mtss1*

5.3 Methods

The general methods used in this section are described in Chapter 2 and referenced as appropriate. Those specific to this chapter are described below.

5.3.1 *In vitro* expression of *MTSS1*

A 2268bp full-length human *MTSS1* clone in pGEM-T vector (purchased from Sino Biological Inc., China) encoding the 755aa transcript of MTSS1 (AF086645; Figure 4.1) was digested with *Sal I* and *Sac II* restriction enzymes (New England Biolabs, UK) using the double digest protocol described previously (see 2.3.2.10). The digested insert was purified (see 2.3.2.8) and ligated (see 2.3.2.11) into the plasmid backbone of the pEGFPC1 mammalian expression vector which had also been cut with *Sal I* and *Sac II* restriction enzymes (see 2.3.2.10). The ligation reactions were used to transform DH5α competent

cells (Invitrogen, UK) (see 2.3.2.12) and grown on kanamycin-resistant LB agar plates. Recombinant plasmid DNA was purified from colonies (see 2.3.2.2) and screened by sequencing using the primers: EGFP_C_F and MTSS1_Stop20 (see Appendix C for primer sequences**)**. One verified clone named pEGFPC1_MTSS1_WT was further cultured and purified by midiprep (see 2.3.2.3) for gene transfection experiments (see 2.3.4.3). The pEGFPC1_MTSS1_WT construct was then used as template to make a mutant MTSS1 construct of the full-length transcript (pEGFPC1_MTSS1_Mut) with the c.637_639del mutation using site-directed mutagenesis (see 5.3.2).

To make an expression construct for the MTSS1 alternate transcript AK030533, its coding region was amplified from the pGEM-T_MTSS1 clone with primers made to the alternate start site in exon 4 (MTSS1_Ex4_start) and the stop site in exon 15 (MTSS1_Stop) as described (see 2.3.2.5). Primer sequences can be found in Appendix C. The amplified AK030533 coding sequence was then cloned into pGEM-T easy and the protocol described above was used to generate full-length WT and mutant constructs. For ease of identification, the WT expression construct of this AK030533 transcript was labelled as WT_MTSS1_4start and its corresponding mutant construct labelled as Mut_MTSS1_4start.

5.3.2 Site directed mutagenesis

Site directed mutagenesis was performed as described in section 2.3.2.15. Primers used to generate the c.637_639del mutation were 5'-ATCTCAATGCTAGGGGAAATAAC–3' (forward) and 5'–TTCTTCAATCACTGGCCG – 3' (reverse), used at an annealing temperature of 63^{o}C.

5.3.3 Mtss1 knockout mouse retina analysis

5.3.3.1 Eye and retinal tissue preparation

Eye tissue from *Mtss1* knockout (KO) transgenic mice (Saarikangas et al., 2011) were obtained from the laboratory of Dr Pieta Mattila based in the University of Turku, Turku, Finland. For histological and immunohistochemistry studies, eyes from the *Mtss1* KO mice and their age-matched wild-type (WT) littermates were enucleated, fixed and cryopreserved in 30% sucrose by a collaborator (Alexey Vladimirovich Sarapulov) based in the Mattila lab, by following protocols described in section 2.3.7.1.

The tissues were shipped in 30% sucrose at 4^{o}C to Oxford where the retinas were dissected, embedded and cryosectioned following protocols described in section 2.3.7.2. For studies in which RNA and protein were to be extracted, retinas were dissected in PBS followings enucleation and immediately snap-frozen in liquid nitrogen by Mr Sarapulov in Turku prior to being shipped on dry ice to Oxford for RNA and protein extraction.

5.3.3.2 RNA and protein extraction from Mtss1 KO mice retina

Protein and RNA were extracted simultaneously from snap-frozen retinas received from Turku using the RNeasy Mini kit (Qiagen, UK) by following manufacturer's instructions.

5.3.3.2.1 RNA extraction

Samples were allowed to thaw on ice and then 350µl of buffer RLT with 1% β-mercaptoethanol was added to each sample. Each sample was homogenised for 20 seconds using a hand-held homogeniser and RNase-free pestle. The samples were centrifuged at full speed (17,000 x *g*) on a microcentrifuge for 3 minutes to pellet the cell debris. The supernatant was removed and the cell pellet was discarded. An equal volume (350µl) of 70% ethanol was added to each sample. The samples were mixed by pipetting and the solution was transferred into RNeasy spin columns and spun at 10,000 x *g* for 30 seconds. The flow through was transferred to a microcentrifuge tube and kept on ice for protein extraction (see 5.3.3.2.2).

Buffer RWI (700µl) was added to the column and centrifuged at 10,000 x *g* for 30 seconds, and the flow through discarded. On-column DNase treatment was carried out by adding DNase solution (10µl of DNase I +70 µl of buffer RDD) to the column which was left to incubate at room temperature for 15 minutes. Buffer RWI (35µl) was added to the column, centrifuged at 10,000 x *g* for 30 seconds and the flow through was discarded. Buffer RPE (500µl) was added to the column and centrifuged at 10,000 x *g* for 30 seconds and the flow through was discarded. A further 500µl of buffer RPE was then added to the column, centrifuged at 10,000 x *g* for 2 minutes and the flow through again discarded. The column

was placed into a new microcentrifuge tube and centrifuged at 17,000 x *g* for 1 minute to remove excess buffer. The column was placed into a new labelled microcentrifuge tube and 30µl of RNase-free water was added to the column and left to incubate at room temperature for 1 minute. The column was centrifuged at 10,000 x *g* for 1 minute to elute RNA. The eluate was pipetted back onto the column and left to incubate at room temperature for 1 minute. The column was centrifuged at 10,000 x *g* for 1 minute and the flow through (RNA) was kept on ice for cDNA synthesis (see 2.3.3.2) or stored at -80°C until needed.

5.3.3.2.2 Protein extraction

This was carried out with the flow through set aside on ice during the RNA extraction step (see 5.3.3.2.1) to enable simultaneous protein extraction from the same retina sample. Four volumes of ice-cold acetone was added to each sample and were incubated on ice for 30 minutes. The samples were centrifuged at 17,000 x *g* for 30 minutes at 4°C to pellet the protein. The supernatant was carefully removed and the pellet washed in 100µl of ice-cold 100% ethanol. The ethanol was removed and the pellets were air-dried on ice for 5 minutes. 50µl of 1% SDS was added to each sample and the pellet was resuspended by repeated pipetting. The samples were incubated at 95°C on a heat block for 3 minutes and were mixed by pipetting. This process was repeated. The samples were then centrifuged at 17,000 x *g* for 3 minutes. The supernatant was transferred to a labelled microcentrifuge tube and stored at -20°C for protein quantification (see 2.3.5.2) and subsequent western immunoblotting experiments (see 2.3.5.3).

5.3.3.3 Haematoxylin and Eosin (H&E) staining

Hematoxylin and eosin (H&E) staining was performed using a H&E Stain kit (Abcam, UK) according to the manufacturer's instructions. Frozen retina sections were allowed to equilibrate to room temperature before use. The solutions used were held in EasyDip slide staining jars (Simport Scientific, Canada). Slides were held in EasyDip slide staining racks (Simport Scientific, Canada) during the staining process. Sections were firstly hydrated in distilled water for 5 minutes and then immersed into a jar

containing Mayer's Hematoxylin (Lillie's modification) and incubated for 5 minutes. Slides were rinsed in two changes of distilled water to remove excess stain and then immersed in a jar containing Bluing Reagent and incubated for 15 seconds. The slides were then rinsed in two changes of distilled water and dipped in absolute alcohol, excess alcohol was blotted off. Slides were immersed in a jar containing Eosin Y Solution (Modified alcoholic) and incubated for 3 minutes. They were then rinsed in absolute alcohol and dehydrated using three changes of absolute alcohol. The slides were cleared of excess alcohol, mounted with coverslips using ProLong Diamond antifade mounting medium (Invitrogen, UK) and allowed to dry overnight in the dark at room temperature prior to imaging using a Leica DFC 700T camera system fitted to a Leica DMF5000 microscope.

5.4 Results

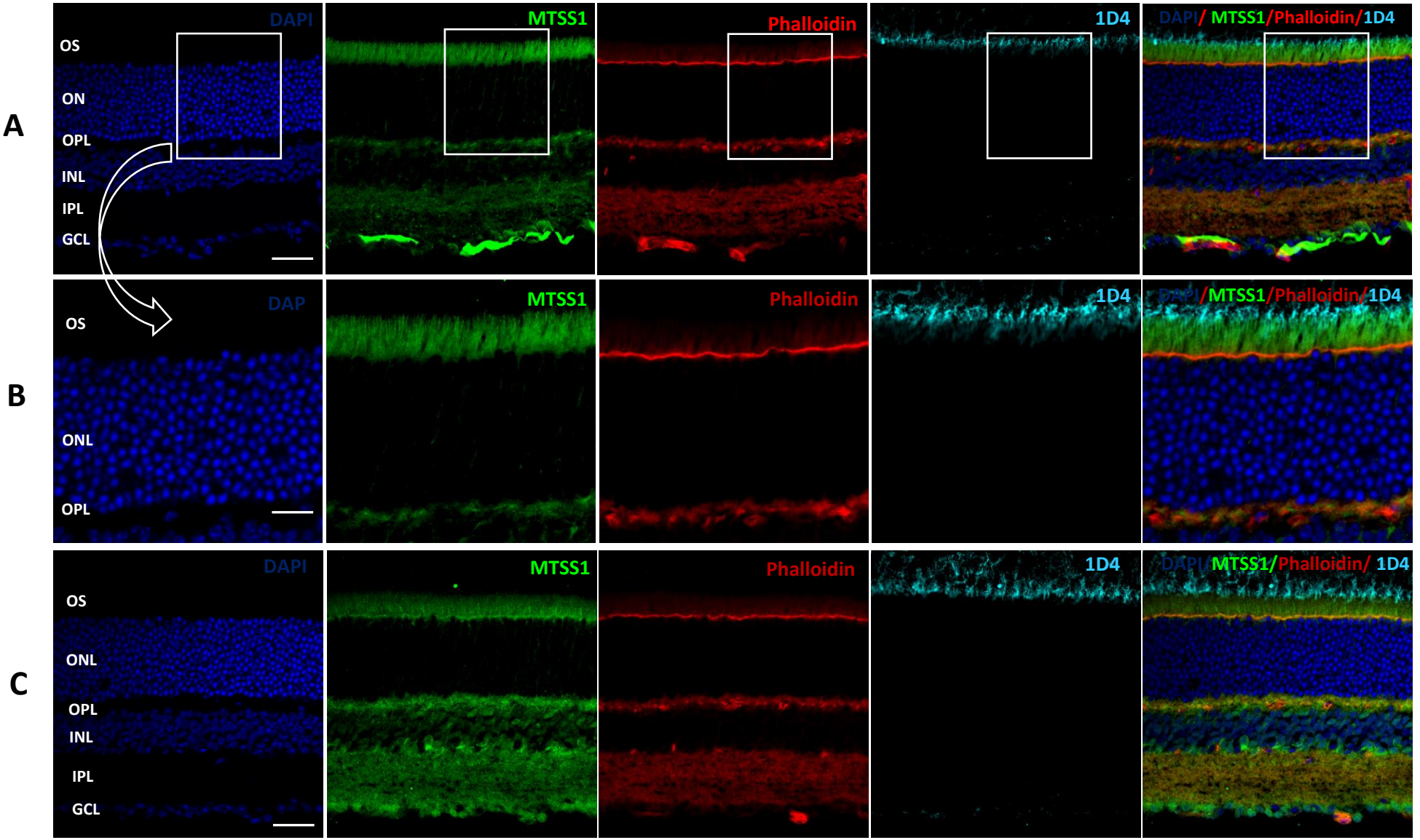
5.4.1 Colocalization of MTSS1 with previously reported binding partners in wild type mouse retina

Previous studies have reported various binding partners of MTSS1 in other tissues, including its interaction with actin filaments (F-actin), cortactin (CTTN), and DAAM1 (dishevelled associated activator of morphogenesis 1) (Kawabata Galbraith et al., 2018, Saarikangas et al., 2011, Lin et al., 2005). We sought to investigate colocalization between MTSS1 and some of these reported binding partners through immunostaining of retina sections.

To determine if MTSS1 colocalises with F-actin in the retina, we performed double immunostaining of adult WT mouse retina cryosections with MTSS1 antibodies (N-terminal and C-terminal) and Phalloidin–Tetramethylrhodamine B isothiocyanate (Phalloidin-TRITC, Sigma UK), a marker for F-actin (Lengsfeld et al., 1974). We previously confirmed that the MTSS1 antibody detects a protein with the same molecular weight as MTSS1 using western blotting (see 2.3.5.3) and that the actin stain (Phalloidin) has been previously extensively validated in tissues including retinal tissue (Xi et al., 2005). Phalloidin staining of (F-actin) was identified at the outer limiting membrane (OLM), photoreceptor inner segments as well as in the two synaptic layers of the retina (Figure 5.1) as reported in previous studies (Xi et al., 2005). The F-actin staining was found to colocalise with MTSS1 staining in the OLM, the inner segments of the photoreceptors and in the two synaptic layers of the mouse retina obtained with both the N- and C-terminal MTSS1 antibodies used (Figure 5.1).

To determine if MTSS1 colocalises with CTTN and DAAM1 in the mouse retina, we obtained mouse monoclonal antibodies for CTTN and DAAM1 (#sc-55579 and #sc-100942; Santa Cruz Biotechnology, USA). These antibodies had not been previously validated in retinal tissue so we first confirmed them with western immunoblotting. The DAAM1 antibody (at 1:400 concentration) was used to probe 20µg of lysate from adult mouse brain and retina and a band corresponding to the full-length size of DAAM1 protein (123kDa) (Yan et al., 2018) was detected, indicating that the protein is expressed in the

mammalian retina (Figure 5.2). The CTTN antibody, however, was unable to detect any protein band in the brain and retina lysates. As such, the CTTN antibody was not taken further for immunohistochemistry staining. The DAMM1 antibody was used to stain adult WT mouse retina cryosections but this failed to give any positive staining despite several optimisation steps including using varied concentrations and varied incubation times (data not shown). Therefore, the lack of appropriate commercially available CTTN and DAAM1 antibodies suitable for double immunostaining with the MTSS1 antibody made it impossible to assess colocalization of MTSS1 with CTTN and DAAM1 in the mouse retina in this thesis.


A
B
C
DAPI
MTSS1
Phalloidin
1D4
DAPI / MTSS1/Phalloidin/1D4
OS
ON
OPL
INL
IPL
GCL
DAP
ONL
MTSS1/Phalloidin/ 1D4

D

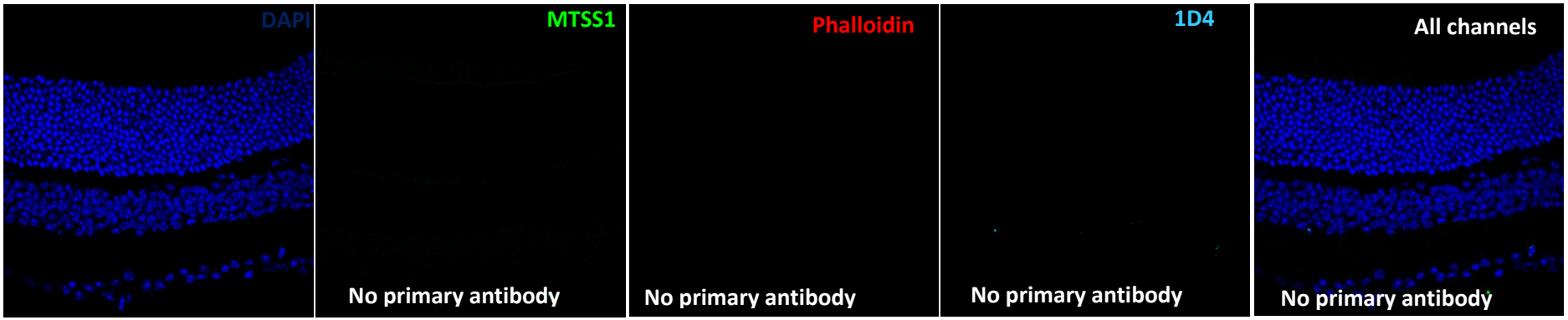


Figure 5.1. MTSS1 staining colocalises with F-actin in the photoreceptors and synaptic layers. (A) MTSS1 N-terminal antibody (green) was used to stain frozen wild type mouse retina sections along with Phalloidin-TRITC (red) which labels F-actin and is a known binding partner of MTSS1. (B) High magnification of an area from A emphasizing the localisation of MTSS1 (green), F-actin (red) and their colocalization. (C) MTSS1 C-terminal antibody (green) was also used to stain frozen sections of retina from wild type mouse. In A-C, MTSS1 staining (green) is seen to overlap with Phalloidin-TRITC (red) staining in the photoreceptor layer and synaptic layers. (D) Sections were stained with only secondary antibodies as controls (showing merged image for all channels). 1D4 (cyan) which labels rhodopsin was used as a marker for rod photoreceptor outer segments. DAPI (blue) was used to stain the nuclei. OS = Outer segment; ONL = Outer nuclear layer; OPL = Outer plexiform layer; INL = Inner nuclear layer; IPL = Inner plexiform layer; GCL = Ganglion cell layer. Scale bar = 20µm (A, C, D); 10µm (B)

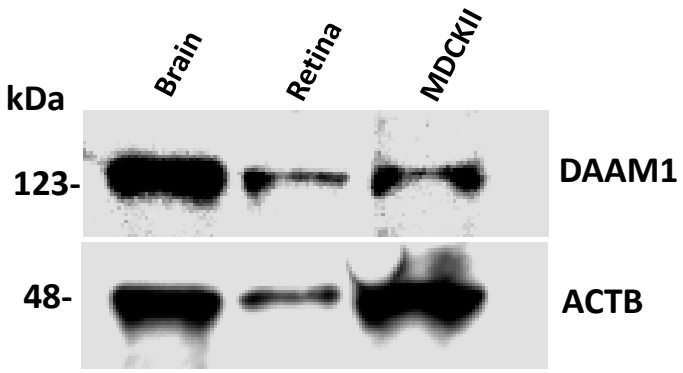


Figure 5.2. DAAM1 protein expression in the mammalian retina. A band corresponding to full-length DAAM1 protein (123kDa) was detected in lysates from mouse brain and retina when probed with DAAM1 mouse monoclonal antibody (#sc-100942, Santa Cruz Biotechnology, USA). Lysate from MDCKII cells was probed alongside the brain and retina samples as a positive control.

5.4.2 Functional characterisation of *MTSS1* p.(Glu213del) variant

In order to investigate if the variant in *MTSS1* (c.637_639del, p.(Glu213del)), shown to segregate with the adRP in family 3027, has an effect on the protein's function and localisation in cells, *in silico* tools were used. Secondly, we transfected several cell lines with WT and mutant MTSS1 expression constructs and investigated differences in expression pattern between WT and mutant transfected cells.

5.4.2.1 *In silico analysis of MTSS1 variant*

To determine the pathogenicity and potential effect of the c.637_639del, p.(Glu213del) variant on the structure and function of the MTSS1 protein, predictive *in silico* programs used included Mutation taster and mCSM. Mutation taster (http://www.mutationtaster.org/) predicted the p.(Glu213del) variant to be disease causing, and also predicted it to cause the loss of the IMD domain of the MTSS1 protein as well as the loss of other domains downstream of p.Glu213 due to potential splice site changes that may arise from the deletion. Also, analysis of the position of the variant (Glu213) using the mCSM program (http://biosig.unimelb.edu.au/mcsm/), which predicts the effect of mutations in proteins using graph-based signatures (Pires et al., 2016), revealed that substituting the glutamic acid residue at position 213 to any other amino acid would result in destabilizing changes to the protein-protein affinity of MTSS1 (Table 5.1). These predictions from mCSM, despite predicting the effect of substitutions, highlight the importance of the amino acid (p.Glu213), found to be deleted in our patients, in maintaining the functional properties of MTSS1.

Table 5.1 Predicted protein-protein affinity Change (ΔΔG) upon mutation of p.(Glu213) of MTSS1.

Index	Chain	Wild Residue	Residue Position	Mutant Residue	RSA (%)	Predicted ΔΔG	Outcome
1	A	E	213	A	12.4	-2.037	Highly Destabilizing
2	A	E	213	V	12.4	-1.733	Destabilizing
3	A	E	213	L	12.4	-1.584	Destabilizing
4	A	E	213	G	12.4	-2.184	Highly Destabilizing
5	A	E	213	S	12.4	-3.049	Highly Destabilizing
6	A	E	213	W	12.4	-2.467	Highly Destabilizing
7	A	E	213	T	12.4	-2.928	Highly Destabilizing
8	A	E	213	Q	12.4	-2.664	Highly Destabilizing
9	A	E	213	C	12.4	-2.002	Highly Destabilizing
10	A	E	213	R	12.4	-1.887	Destabilizing
11	A	E	213	P	12.4	-1.733	Destabilizing
12	A	E	213	D	12.4	-1.875	Destabilizing
13	A	E	213	F	12.4	-2.274	Highly Destabilizing
14	A	E	213	I	12.4	-1.584	Destabilizing
15	A	E	213	H	12.4	-1.01	Destabilizing
16	A	E	213	N	12.4	-3.046	Highly Destabilizing
17	A	E	213	M	12.4	-0.685	Destabilizing
18	A	E	213	Y	12.4	-2.329	Highly Destabilizing
19	A	E	213	K	12.4	-2.086	Highly Destabilizing

RSA = residue relative solvent accessibility

Amino acid codes:

A = alanine; C = cysteine; D = aspartic acid; E = glutamic acid; F = phenylalanine; G = glycine; H = histidine; I = isoleucine; K = lysine; L = leucine; M = methionine; N = asparagine; P = proline; Q = glutamine; R = arginine; S = serine; T = threonine; V = valine; W = tryptophan; Y = tyrosine.

5.4.2.2 Subcellular localisation of Wild-type and mutant MTSS1 in vitro

In silico programmes, although useful in predicting the pathogenicity of variants and their effect on protein structure and function, can only serve as approximate indicators and it is important that these predictions are tested in cell and animal models. We, therefore, decided to investigate the effect of the c.637_639del; p.(Glu213del) variant on MTSS1 by transfecting different cell lines with wild-type and mutant constructs of MTSS1 (see 2.3.4.3) and examining differences in their subcellular localisation, interaction with actin and cell morphology that may be attributable to the mutant constructs.

Both wild-type and mutant MTSS1 constructs were made in the pEGFPC1 expression vector (see 5.3.1) which has a green fluorescence protein (GFP) tag at the N-terminus of the multiple cloning site. This resulted in the expression of a fusion protein (GFP-MTSS1) which can be observed under a fluorescent microscope following transfection. Three cell lines were used: HEK293T (ECACC 85120602; epithelial cells derived from human embryonic kidney) (Lin et al., 2014); MDCKII (ECACC 00062107; epithelial cells derived from the kidney of a normal adult Cocker Spaniel) (Barker and Simmons, 1981) and hTERT RPE-1 (ATCC CRL-4000; commonly called RPE1; derived from human retina pigment epithelial cells) (Rambhatla et al., 2002). All three cell lines were first examined for endogenous expression of MTSS1 using primers (*MTSS1*_Exon2_8R; Appendix C) and end-point PCR (see 2.3.2.6). All three cell lines were found to express *MTSS1* endogenously (Figure 5.3), indicating their suitability for the transfection studies, in that they had the cell machinery necessary to drive the expression of exogenous MTSS1. Transfected cells were examined in two stages: imaging of live cells at 24 hours post-transfection using the EVOS fluorescence microscope (see 2.3.8.1), and by confocal imaging (see 2.3.8.2) following fixation and immunofluorescence staining (see 2.3.4.4). In most cases, live cell images captured with the EVOS fluorescence microscope are presented alongside images from confocal imaging to demonstrate that the fixation and immunofluorescence steps did not alter the subcellular localization or phenotype of the cells.

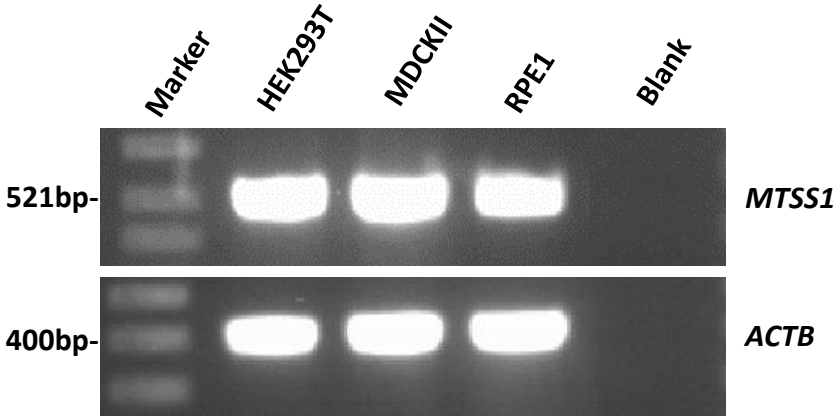


Figure 5.3. *MTSS1* expression in HEK2938, MDCKII and RPE1 cell lines. *MTSS1* expression was examined, using a primer pair (Exon2_8) and endpoint PCR, in all 3 cell lines to be used as *in vitro* models for MTSS1 transfection studies. All 3 cell lines were found to express *MTSS1* endogenously. Beta-actin expression (ACTB) was used as a loading control.

5.4.2.2.1 Wild-type and mutant MTSS1 in HEK293T and MDCKII cells

HEK293T and MDCKII cells were seeded at 70,000 and 50,000 cells per well, respectively, in 24 well plates (as described in section 2.3.4.2) and were transfected with 500ng of DNA after 24 hours in culture (see 2.3.4.3). As transfection constructs produced GFP-MTSS1 fusion proteins, transfection efficiency was estimated by the number of GFP-positive cells observed under a fluorescent microscope. To confirm that the protein being overexpressed in the transfected cells was indeed MTSS1, 10µg of cell lysate from HEK293T cells transfected with WT MTSS1, mutant MTSS1, and untransfected controls were probed with MTSS1 N-terminal antibody (1:1000; Novus Biologicals, UK) and a monoclonal GFP antibody (1:1000; Sigma, UK) using western immunoblotting (see 2.3.5.3). Two bands of ~100kDa and 135kDa molecular weights were observed using the N-terminal MTSS1 antibody: the ~100kDa band corresponding to the expected size of the endogenously expressed MTSS1 protein was detected in all three samples; the ~135kDa corresponding to the expected size of the GFP-MTSS1 fusion protein was detected only in samples from cells transfected with WT and Mutant MTSS1 (Figure 5.4A). When these samples were probed with the anti-GFP antibody, a similar ~135kDa band corresponding to the expected size of the GFP-MTSS1 fusion protein was detected in lysates from cells transfected with WT and mutant MTSS1 constructs but not in the untransfected cells (Figure 5.4B). The results, obtained with these two different antibodies, confirmed: (i) that the protein being expressed by our expression construct upon transfection was MTSS1, and (ii) that the N-terminal MTSS1 antibody, also used in staining MTSS1 in retinal tissue, was specific in detecting the full-length MTSS1 protein.

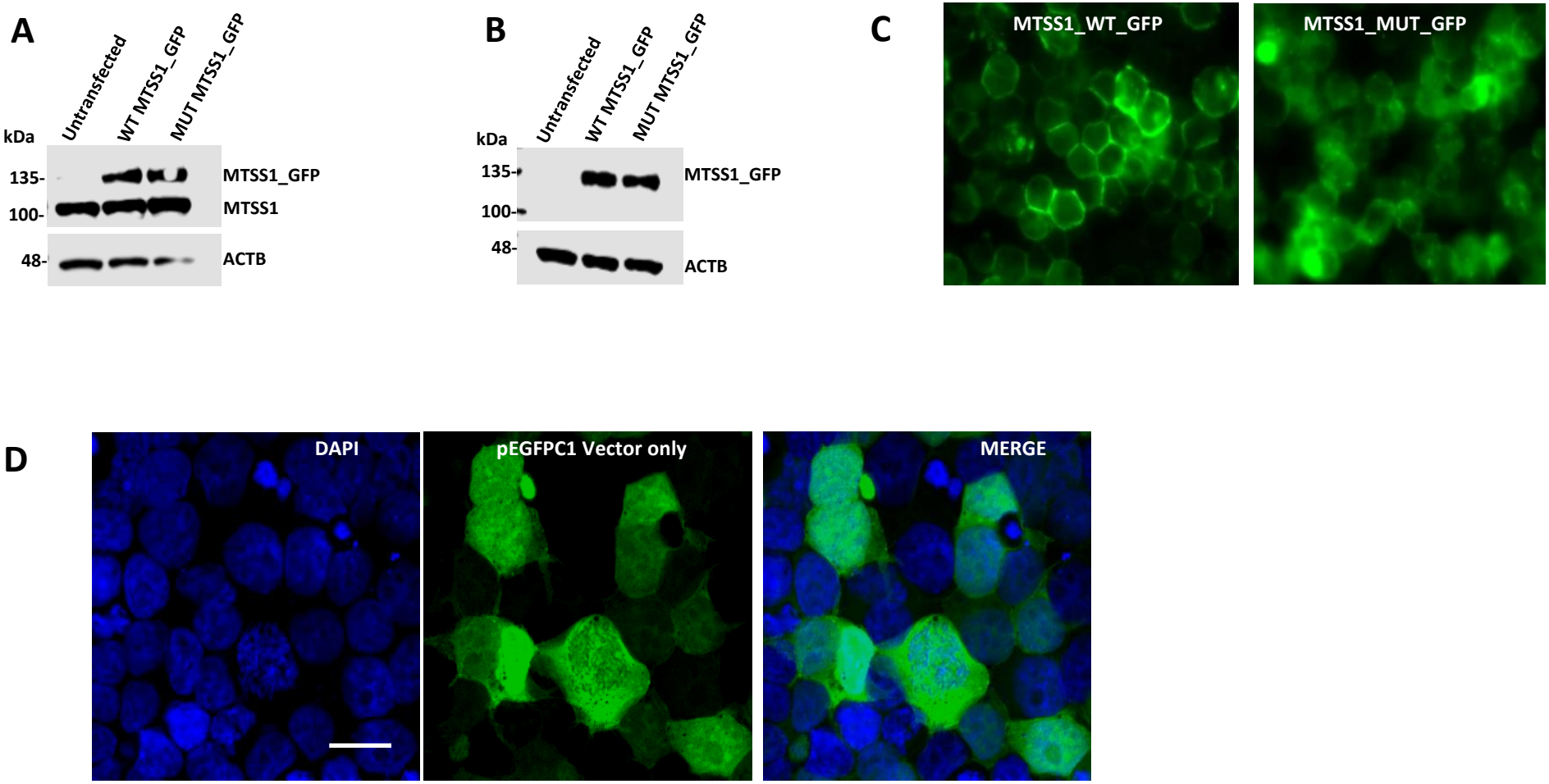
We examined cells transfected with WT MTSS1 and mutant MTSS1 at 24 hours post transfection for any observable differences, using the fluorescence microscope for live cells and the confocal microscope for fixed cells. In HEK293T cells transfected with full-length WT MTSS1, well-defined cell-cell junctional contacts were observed, with the overexpressed WT MTSS1 protein (GFP signal) prominent at the intercellular junctions, observed under the fluorescence microscope (Figure 5.4C). However, HEK293T cells transfected with mutant MTSS1 had less defined cell-cell junctional contacts

and the expression of mutant MTSS1 (GFP signal) was more diffused and cytoplasmic (Figure 5.4C). This difference between WT and mutant-expressing HEK293T cells observed upon live cell imaging was confirmed when cells were fixed, stained and examined under confocal microscopy, indicating that the fixation and immunocytochemistry steps did not affect the localization of the overexpressed proteins. Wild-type MTSS1 localised closely to the cell surface (plasma membrane) (Figure 5.4E). Mutant MTSS1 was found to localise at the cell surface and diffusely within the cytoplasm (Figure 5.4F). In addition to the diffuse staining pattern within the cytoplasm, the GFP_MTSS1 signal was found to aggregate in concentrated spots (Figure 5.4F). Transfected HEK293T cells were labelled with phalloidin-TRITC which labels F-actin, a reported binding partner of MTSS1 (Saarikangas et al., 2011). In cells transfected with WT MTSS1, F-actin staining was found to colocalise with the entire GFP_MTSS1 signal along the plasma membrane (Figure 5.4E). In HEK293T cells overexpressing mutant MTSS1, however, colocalization of F-actin staining with mutant GFP_MTSS1 signal was limited to the area along the plasma membrane but not with the mutant GFP_MTSS1 signal distributed within the cytoplasm (Figure 5.4F).

Similar results were obtained when MDCKII cells were transfected with WT and mutant MTSS1 expression constructs. In live MDCKII cells overexpressing WT MTSS1, observed using the fluorescence microscope, full-length WT MTSS1 localisation was prominent at the intercellular junctions whereas mutant MTSS1 appeared to be diffused across the cytoplasm (Figure 5.5A&B). Confocal imaging of MDCKII cells fixed and stained with Phalloidin-TRITC to label F-actin demonstrated colocalization between F-actin and WT GFP_MTSS1 along the plasma membrane and at intercellular junctions (Figure 5.5D). Mutant GFP-MTSS1 fusion protein localised to the cell surface and cytoplasm with F-actin staining only colocalising with the GFP along the cell surface (Figure 5.5E).

To ascertain that the pattern of subcellular localisation observed with the GFP-MTSS1 construct was due to the localization of the MTSS1 protein and not the GFP, both HEK293T and MDCKII cells were transfected with the pEGFPC1 vector only as controls. The pattern of localization in cells expressing only GFP from the vector was nonspecific and different compared to the patterns observed for the

GFP-MTSS1 fusion proteins (Figure 5.4D and Figure 5.5C). This indicated that the patterns of localisation observed in the GFP-MTSS1 transfected cells were driven by the MTSS1 and not the GFP.


A
Untransfected
WT MTSS1_GFP
MUT MTSS1_GFP
kDa
135-
100-
48-
MTSS1_GFP
MTSS1
ACTB
B
Untransfected
WT MTSS1_GFP
MUT MTSS1_GFP
kDa
135-
100-
48-
MTSS1_GFP
ACTB
C
MTSS1_WT_GFP
MTSS1_MUT_GFP
D
DAPI
pEGFPC1 Vector only
MERGE

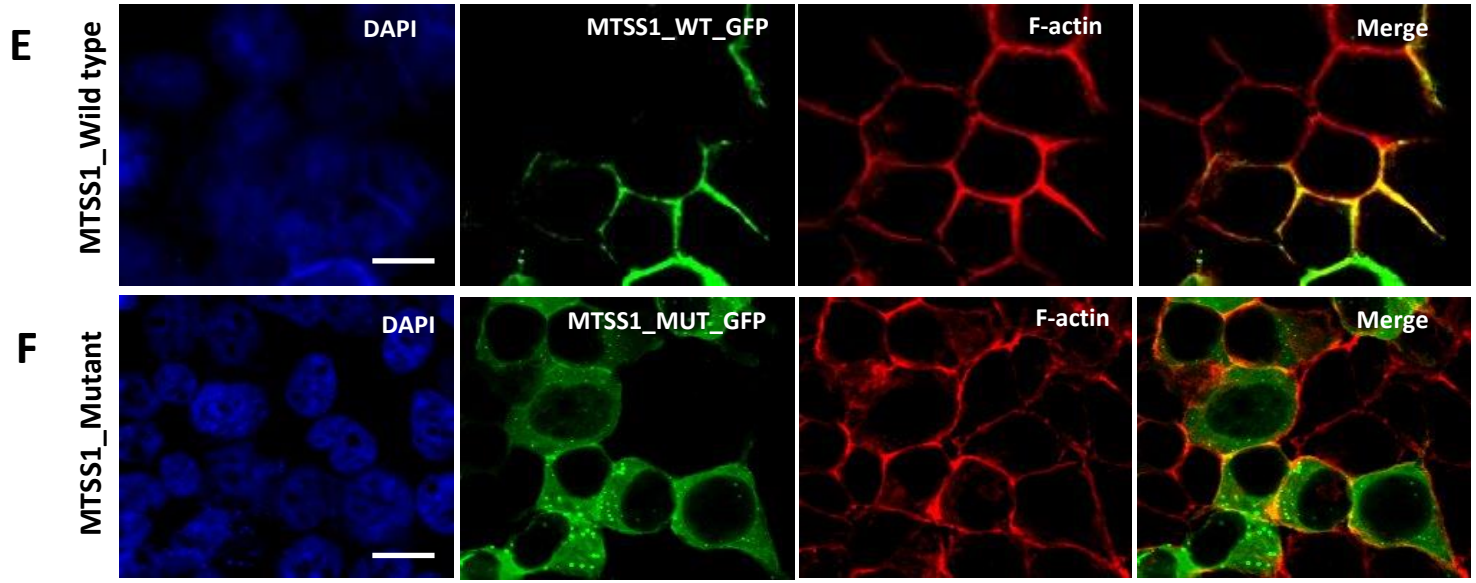
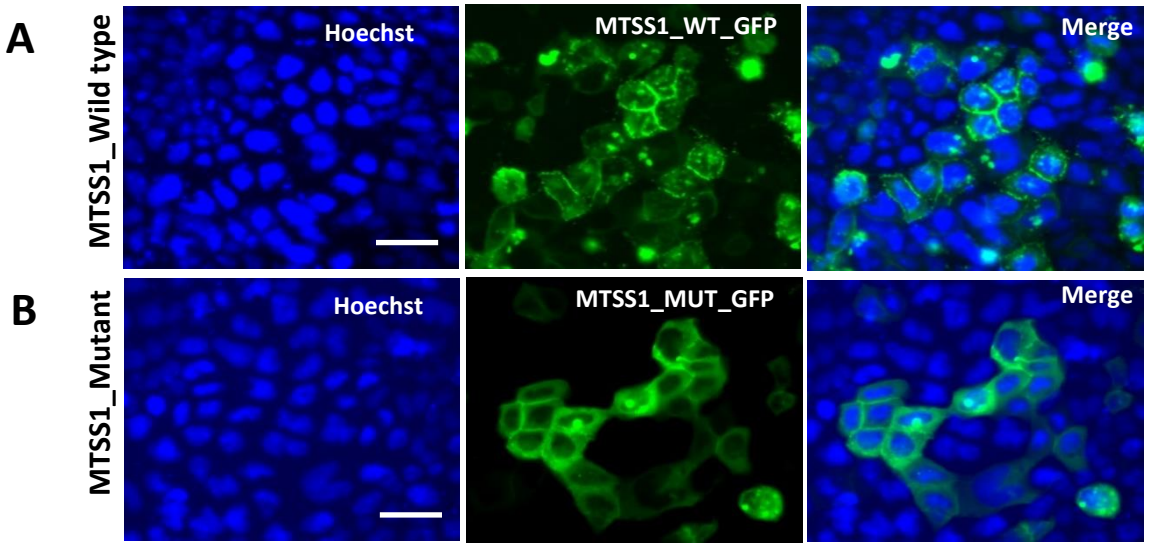
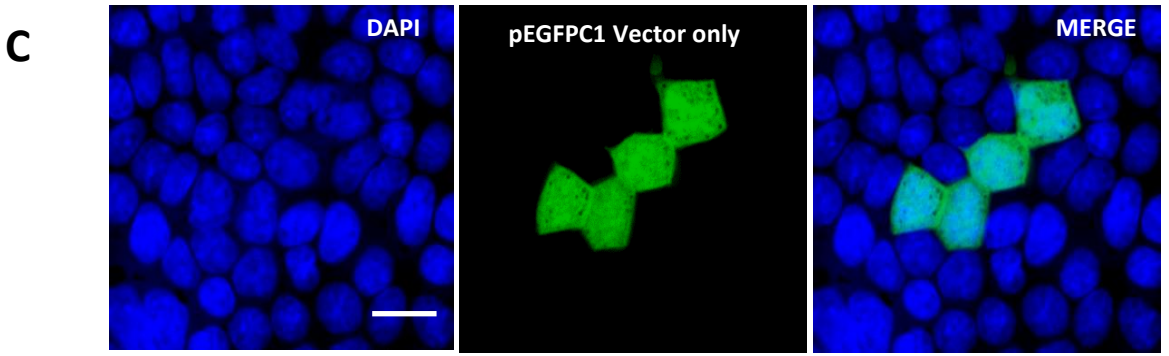


Figure 5.4. Wild-type and mutant MTSS1 overexpression in HEK293T cells. (A) Lysates from cells overexpressing WT and mutant MTSS1 were probed with N-terminal MTSS1 antibody through western immunoblotting. Endogenous MTSS1 with molecular weight of ~100kDa was detected in all three samples whereas MTSS1-GFP fusion protein with molecular weight of ~135kDa was detected only in cells transfected with the MTSS1 expression constructs. (B) Lysates from cells overexpressing WT and mutant GFP-MTSS1 were probed with a GFP antibody (Sigma, UK). MTSS1-GFP fusion protein with molecular weight of ~135kDa was detected in cells transfected with the MTSS1 expression constructs but not detected in untransfected cells. ACTB (β-actin) was used as loading control in both A and B. (C) Live HEK293T cells transfected with WT and mutant MTSS1 24 hours post-transfection imaged with a fluorescence microscope. (D) HEK293T cells transfected with pEGFPC1 vector only as a control. (E) WT GFP-MTSS1 (green) localises closely to the plasma membrane of HEK293T cells and colocalises with F-actin staining (red) at the intercellular junctions. (F) Mutant GFP-MTSS1 (green) localises to the cytoplasm of HEK293T cells. Colocalization of mutant GFP-MTSS1 with F-actin staining (red) is limited to areas close to the plasma membrane but not with the mutant GFP-MTSS1 distributed in the cytoplasm. DAPI was used to label cell nuclei. Scale bar = 40µm (C); 20µm (D, E, F).


A
MTSS1_Wild type
Hoechst
MTSS1_WT_GFP
Merge
B
MTSS1_Mutant
Hoechst
MTSS1_MUT_GFP
Merge


C
DAPI
pEGFPC1 Vector only
MERGE

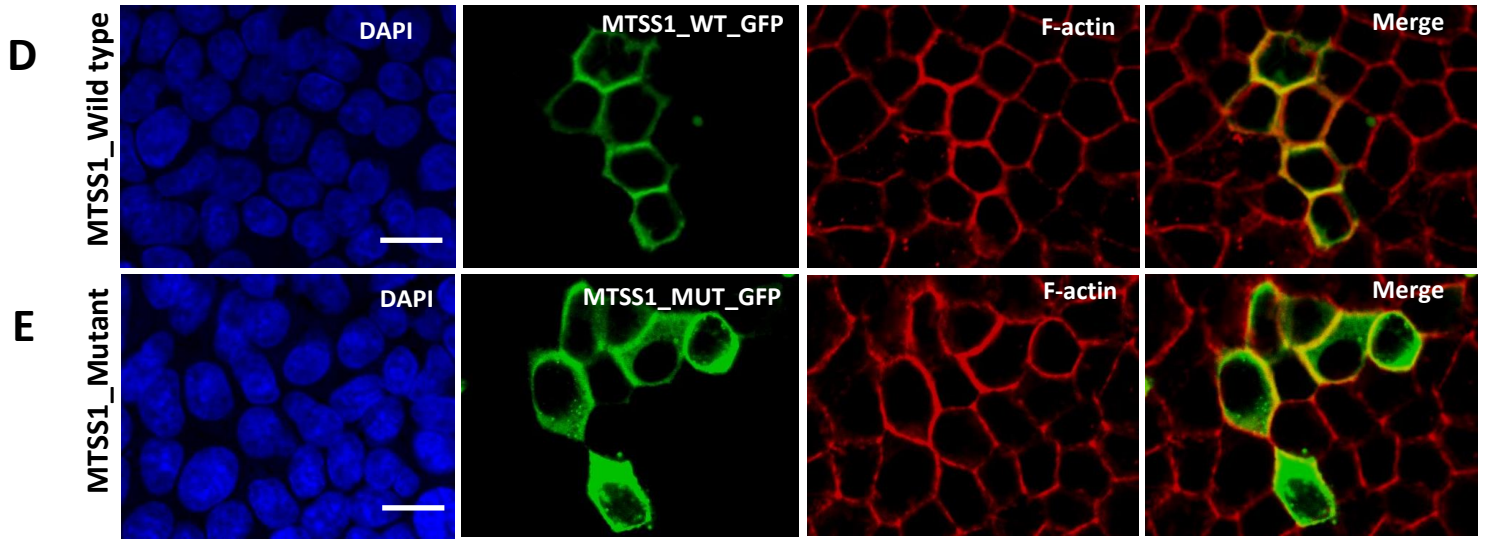


Figure 5.5. Wild-type and mutant MTSS1 transfection in MDCKII cells. (A) Live MDCKII cells overexpressing WT GFP-MTSS1 24 hours post-transfection imaged with a fluorescence microscope (B) Live MDCKII cells overexpressing mutant GFP-MTSS1 24 hours post-transfection imaged with a fluorescence microscope. (C) MDCKII cells transfected with pEGFPC1 vector only as a control. (D) WT GFP-MTSS1 (green) localizes closely to the plasma membrane of MDCK cells and colocalises with F-actin staining (red) at the intercellular junctions. (E) Mutant GFP-MTSS1 (green) localises to the cytoplasm of MDCKII cells. Colocalization of mutant GFP-MTSS1 with F-actin staining (red) is limited to areas along the intercellular junction but not with the mutant GFP-MTSS1 protein distributed in the cytoplasm. DAPI was used to label cell nuclei. Scale bar = 40µm (A, B); 20µm (C, D, E)

5.4.2.2.2 Wild-type and mutant MTSS1 in RPE1 cells

Having explored the effect of the c.637_639del; p.(Glu213del) variant on MTSS1 in HEK293T and MDCKII , both of kidney epithelial cell origin, we then used a human retina pigment epithelium-derived cell line (RPE1). RPE1 cells were seeded (see 2.3.4.2) at 100,000 cells per well in 24 well plates and transfected with 500ng of full-length WT and mutant GFP-MTSS1 constructs after 24 hours in culture (see 2.3.4.3). When live cells were examined 24 hours post-transfection under the fluorescence microscope, cells overexpressing full-length WT GFP-MTSS1 were found to have developed extensive cellular processes containing the GFP signal from WT GFP-MTSS1 fusion protein compared to cells overexpressing mutant MTSS1 (Figure 5.6A). Transfected cells were fixed, stained with phalloidin-TRITC through immunocytochemistry (see 2.3.4.4) and imaged with a fluorescent microscope (Leica DM2500). Cells overexpressing full-length WT MTSS1 were found to have developed extensive MTSS1-enriched (GFP signal) membrane protrusions and processes (Figure 5.6C) while less processes were observed in cells overexpressing mutant MTSS1 (Figure 5.6D). Colocalization between GFP-MTSS1 and F-actin (labelled with phalloidin) was observed in cells overexpressing WT GFP-MTSS1 compared to cells overexpressing mutant GFP-MTSS1 (Figure 5.6C and D).

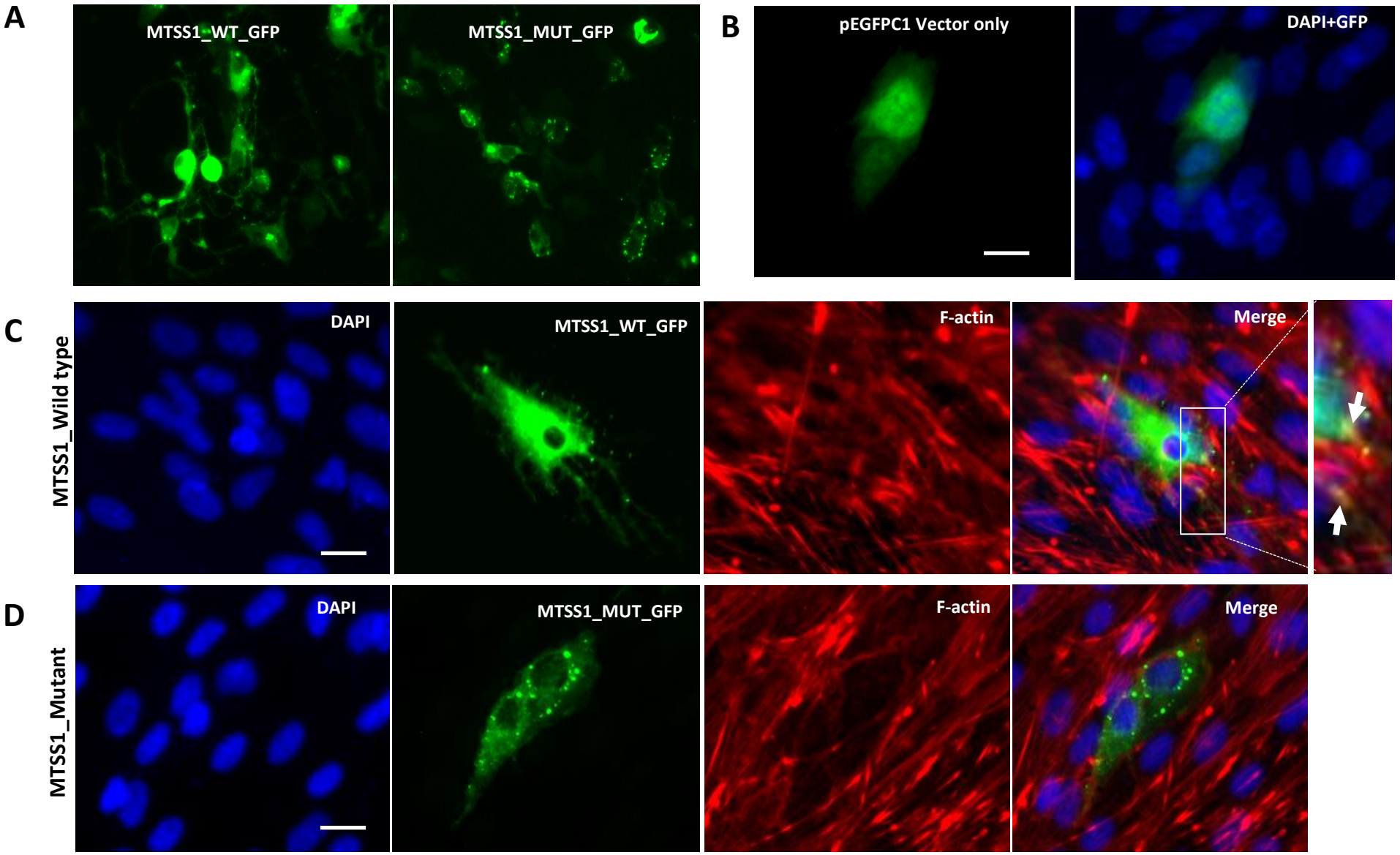

A
MTSS1_WT_GFP
MTSS1_MUT_GFP
B
pEGFPC1 Vector only
DAPI+GFP
C
MTSS1_Wild type
DAPI
MTSS1_WT_GFP
F-actin
Merge
D
MTSS1_Mutant
DAPI
MTSS1_MUT_GFP
F-actin
Merge

Figure 5.6. Wild-type MTSS1 overexpression in RPE1 cells induces formation of extensive cellular processes. (A) Live RPE1 cells overexpressing WT GFP-MTSS1 versus cells overexpressing mutant GFP-MTSS1 imaged with the fluorescence microscope 24 hours post-transfection. (B) RPE1 cells transfected with pEGFPC1 vector only as a control. (C) WT GFP-MTSS1 (green) induces extensive GFP-MTSS1-rich cellular processes which are not present in cells overexpressing mutant GFP-MTSS1 (D). F-actin was stained with phalloidin-TRITC (red). Boxed section of images was expanded to show colocalization of MTSS1 (GFP) with F-actin (arrows), in cells overexpressing WT GFP-MTSS1. DAPI was used to label cell nuclei. Scale bar = 40µm (A); 20µm (B, C, D)

5.4.2.3 MTSS1 alternate transcript AK030533 localises to the cytoplasm

The AK030533 transcript of MTSS1 which has an alternate transcription start site in exon 4 was found to be expressed in mouse retina (section 4.4.1.5.3). However, there was no information in literature on the subcellular localisation of this transcript. As such, we generated an expression construct containing the wild-type coding sequence of this transcript in pEGFPC1 expression vector, which was named WT_MTSS1_4start to differentiate it from the full-length WT construct used previously (see 5.3.1). Unlike the full-length WT MTSS1 which localised to the plasma membrane (Figure 5.4B ad C), the WT_MTSS1_4start construct, when overexpressed in HEK293T cells, localised to the cytoplasm (Figure 5.7). Also, no observable difference was found between the subcellular localisation of the equivalent mutant construct (Mut_MTSS1_4start) and that of WT_MTSS1_4start construct at 24 hours post-transfection (Figure 5.7). Phalloidin staining (F-actin) was found to colocalise with GFP at the cell periphery but not with the GFP-MTSS1 signal distributed across the cytoplasm.

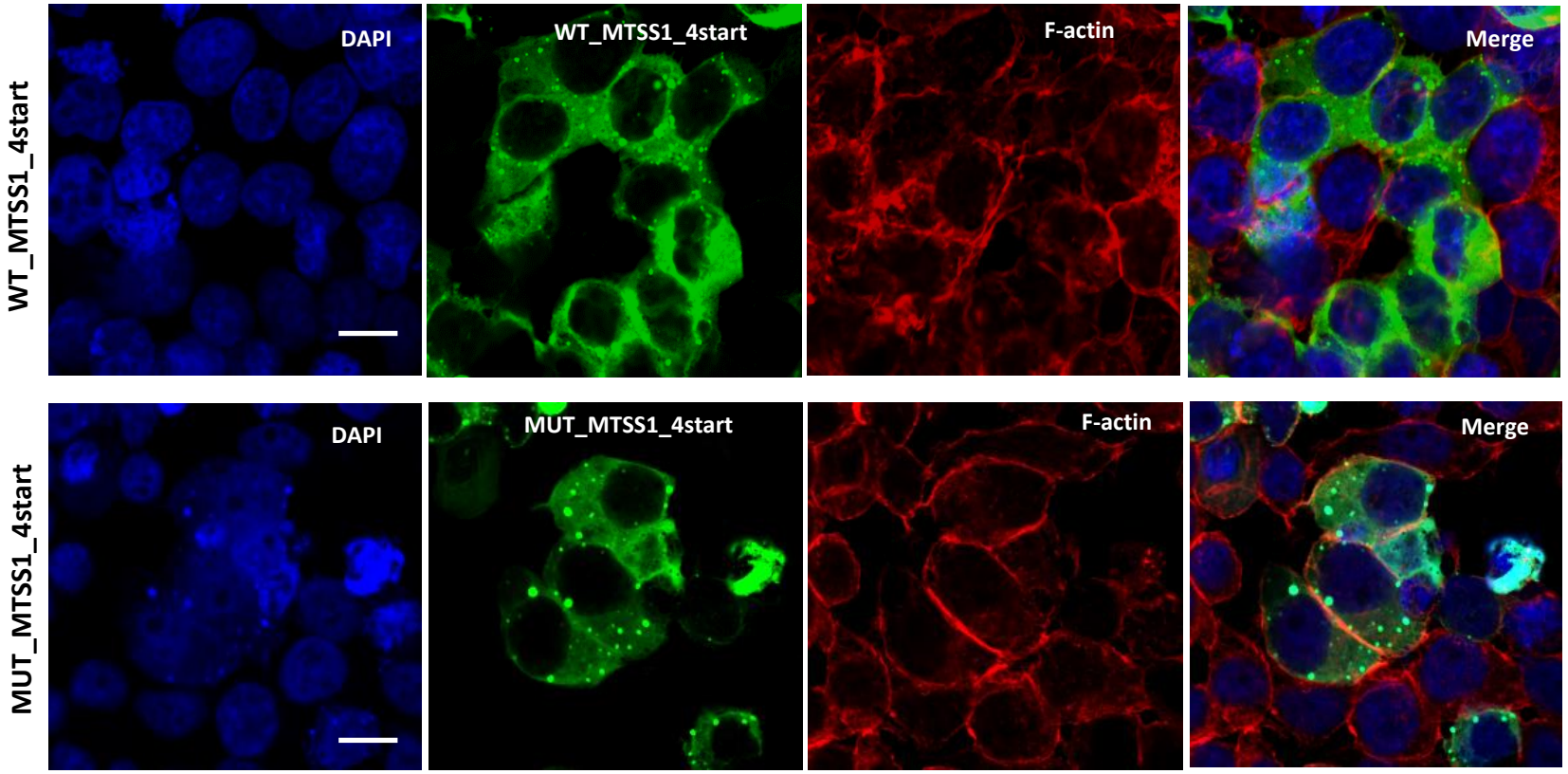


Figure 5.7. Transfection of AK030533 transcript constructs in HEK293T cells. Wild-type and mutant constructs of the AK030533 transcript of MTSS1 with an alternate start site in exon 4 was transfected into HE293T cells to determine their subcellular localisation. (A) WT AK030533 was found to localise to the cytoplasm. (B) Mutant construct of AK030533 bearing the p.(Glu213del) variant identified in our patients also localised to the cytoplasm with no observable difference between the localisation of mutant and the WT. Scale bar = 20µm

5.4.3 Characterisation of *Mtss1* knockout mouse retina

To further understand the role of Mtss1 in the mammalian retina, we examined retina from *Mtss1* knockout (KO) mice (Saarikangas et al., 2011). Eye tissue from *Mtss1* knockout transgenic mice were obtained from the laboratory of Dr Pieta Mattila at the University of Turku, Turku, Finland. This *Mtss1* KO mouse model, also known as *Mim* KO, was developed by Dr Mattila and her colleagues and has been previously validated (Saarikangas et al., 2011). In brief, the *Mtss1* gene was inactivated in the mouse model (C57Bl/6J) by inserting a neomycin (neo) gene cassette containing several stop codons into exon 1 of the *Mtss1* gene (Figure 5.8). The in-frame stop codons in the neomycin targeting cassette inserted into exon1 was proposed to cause destabilization of the Mtss1 transcript through the nonsense-mediated decay (NMD) pathway. Phenotypic and genotypic characterisation of the homozygous mutant mice (*Mtss1*$^{-/-}$) have been published previously (Saarikangas et al., 2011). The *Mtss1* KO mice were reported to grow normally into adulthood with no obvious phenotypic abnormalities compared to age-matched wild-type littermates (Saarikangas et al., 2011), although a recent study has reported some anatomical anomalies in some regions of the brain of aged mutant mice (Minkeviciene et al., 2019).

Cryosections of adult Mtss1 KO mouse retinas were assessed by H&E staining (see 5.3.3.3) and immunohistochemical staining (see 2.3.7.3) with antibodies that label specific layers of the retina. Due to results obtained, we also investigated residual Mtss1 gene and protein expression in the retina of these *Mtss1* KO mice.

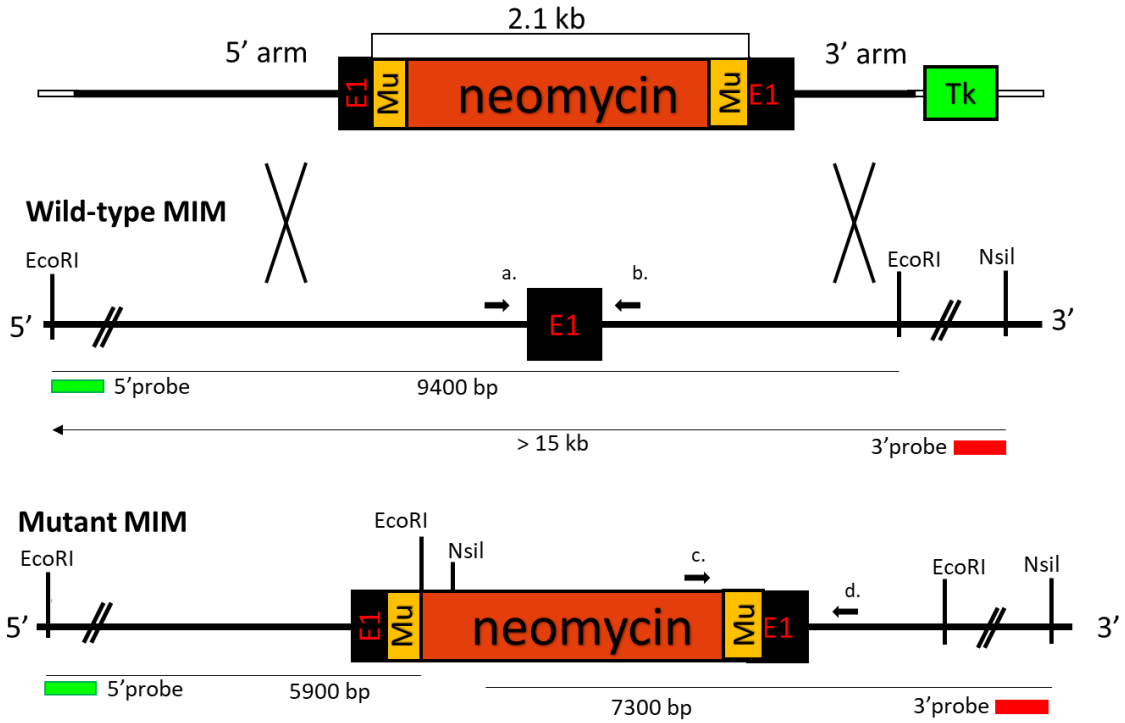


Figure 5.8. Generation of the Mtss1 knockout mice. Figure adapted from (Saarikangas et al., 2011). The *Mtss1* knockout mice was generated by interrupting the mouse *Mtss1* gene by insertion of a neomycin gene cassette into the exon 1 of the gene using Mu transposition. The Neo cassette, with several stop codons should destabilise the rest of the gene though the nonsense-mediated decay pathway.

5.4.3.1 Effect of Mtss1 knockout on retina morphology

Retina cryosections prepared as described in section 5.3.3.1 from Mtss1 KO mice (n=3) and their age-matched WT littermates (n=3) were examined by H&E staining. Of the 3 WT animals that were examined, only one of them was found to have a normal retina (Figure 5.9A) whereas 2 of them were found to have retinas that demonstrated a convoluted structure with extensive folding (Figure 5.9B and C). Similarly, 2 of the 3 KO retinas examined were found to also have a similar phenotype with extensive folding (Figure 5.9E and F) whereas the third had a relatively well organised retina (Figure 5.9D). Despite the WT and KO retinas showing extensive folds of the retinal tissue, a unique feature was seen in two of the KO retinas that was not present in the WT retinas examined. This was enlargement of the ONL and INL in some places and also rosette-like structures characterised by displacement of cells into the INL with a central lumen (Figure 5.9D and E).

Sections from KO animal and corresponding WT retina were also stained immunohistochemically using with the following antibodies: synaptophysin, which labels the synaptic layers; PKCα, which labels bipolar cells; DAPI, which labels the nuclear layers, and the MTSS1 N-terminal antibody used to detect MTSS1 expression (see 4.4.2). Just as seen in the H&E staining, the WT retina was folded extensively, although the integrity of the layers were preserved (Figure **5.10**B and C). Examining the retina of the KO animal by immunohistochemistry also showed the abnormal rosette-like features, characterised by displaced cells forming a circular ring around a central lumen with cells from the outer and inner retina (Figure **5.10**E and F). Although the rosette-like features were limited to only the KO retinas (n=2), the extensive folding of the retinal tissues was found to be present in both WT and KO retinas. It is unclear whether these retinal folds were artefacts resulting from the handling and processing of the retinal tissue or it is a common feature in the background of the mice strain. These folds in the retina, together with the displaced cell layers, made it difficult to quantitatively assess the thickness and cell density of retinal layers between WT and KO.

When retina sections from WT littermates were stained with the N-terminal MTSS1 antibody, the staining pattern observed was similar to what has been described previously in this thesis with expression in the photoreceptors and synaptic layers (Figure **5.10**A and B). Interestingly, when retina sections from the KO mice were stained with the MTSS1 N-terminal antibody, MTSS1-positive staining was identified (Figure **5.10**D, E and F) contrary to what would have been expected of a knockout model. This result could be explained by two possibilities: (i) that the MTSS1 antibody used was non-specific, or (ii) that residual amounts of the Mtss1 protein was still being expressed in the retina of these KO mice, possibly owing to the numerous transcripts that are expressed in the retina. The former was less likely to be the reason since the MTSS1 N-terminal antibody was found to be specific at detecting full-length MTSS1 protein through western blotting from the cell transfection studies (Figure 5.4A and B). Also, the fact that the 2 different MTSS1 antibodies (N- and C-terminal) used in this thesis labelled a protein of the same molecular weight (see Figure 4.11) and identified the same protein in retinal sections (see Figure 4.12) gives an indication of their specificity of the antibody in detecting MTSS1. As such, the latter possibility of there being residual expression of Mtss1 in the KO mouse retina was investigated further in section 5.4.3.2.

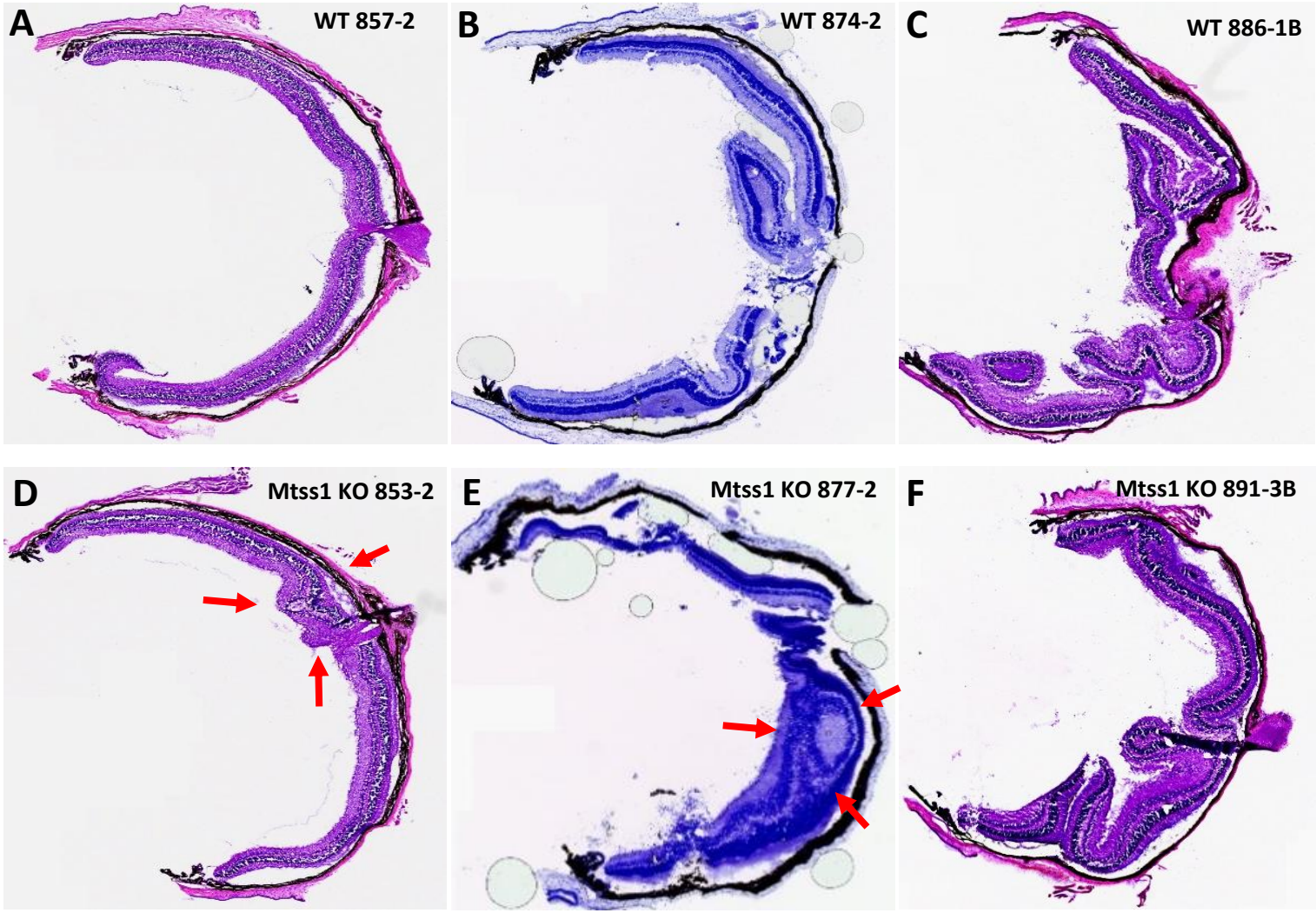
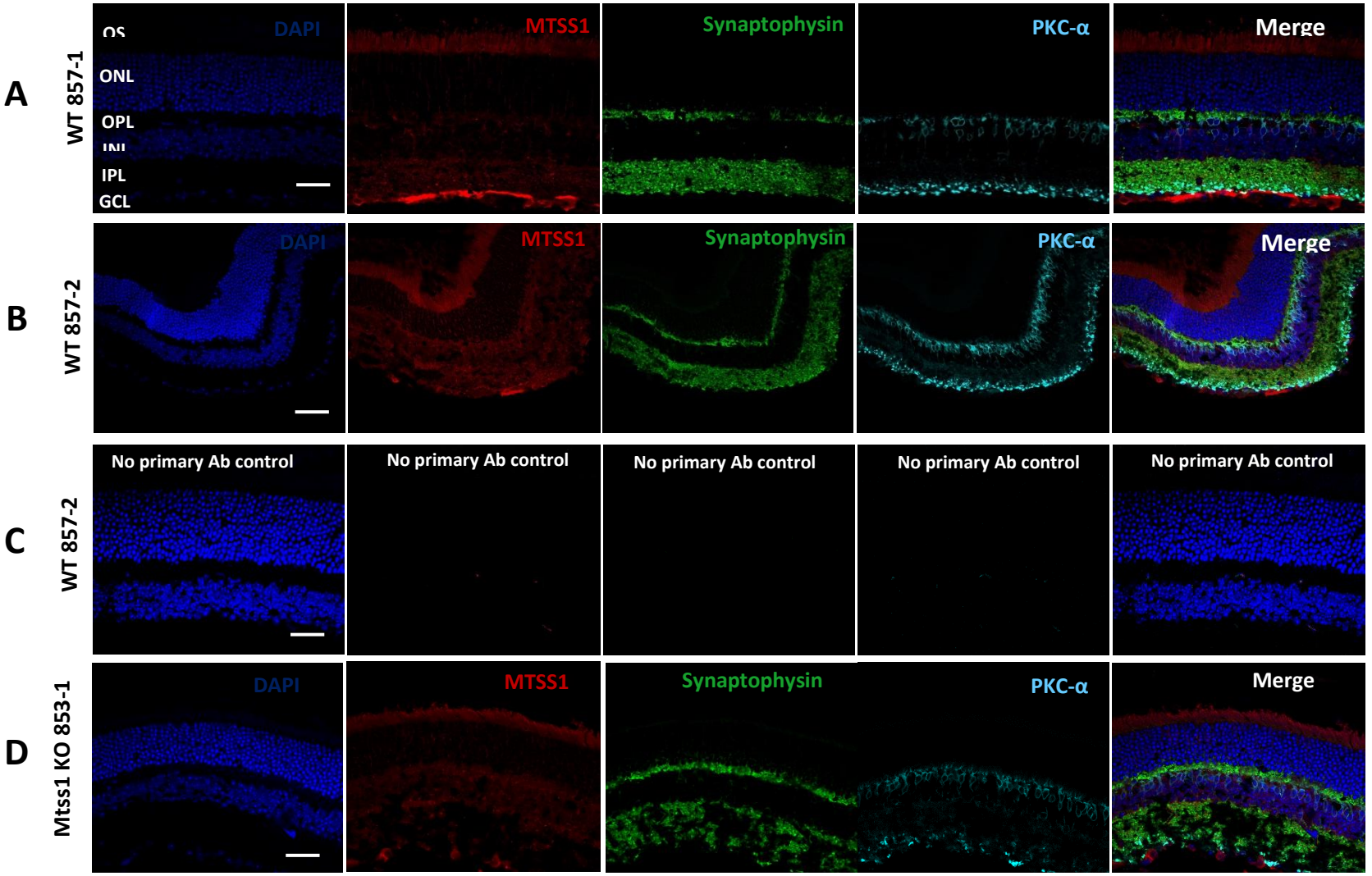

A
WT 857-2
B
WT 874-2
C
WT 886-1B
D
Mtss1 KO 853-2
E
Mtss1 KO 877-2
F
Mtss1 KO 891-3B

Figure 5.9. Haematoxylin and eosin staining of retinas from *Mtss1* knockout mice. Retina sections from 3 adult wild-type (A-C) and 3 age-matched Mtss1 KO littermates (D-F) were analysed through H&E staining. Retinal tissue from both WT and KO animals were found to have folded over generally. The retinas of two KO animals (D&E) were found to have rosette-like features characterised by displacement of cells and thicker than normal ONL and INL with cells organised in a circular pattern around a central lumen (red arrows). KO=knockout, WT=wild-type, ONL=outer nuclear layer, INL=inner nuclear layer.


A
WT 857-1
OS
ONL
OPL
INL
IPL
GCL
DAPI
MTSS1
Synaptophysin
PKC-α
Merge
B
WT 857-2
DAPI
MTSS1
Synaptophysin
PKC-α
Merge
C
WT 857-2
No primary Ab control
No primary Ab control
No primary Ab control
No primary Ab control
No primary Ab control
D
Mtss1 KO 853-1
DAPI
MTSS1
Synaptophysin
PKC-α
Merge

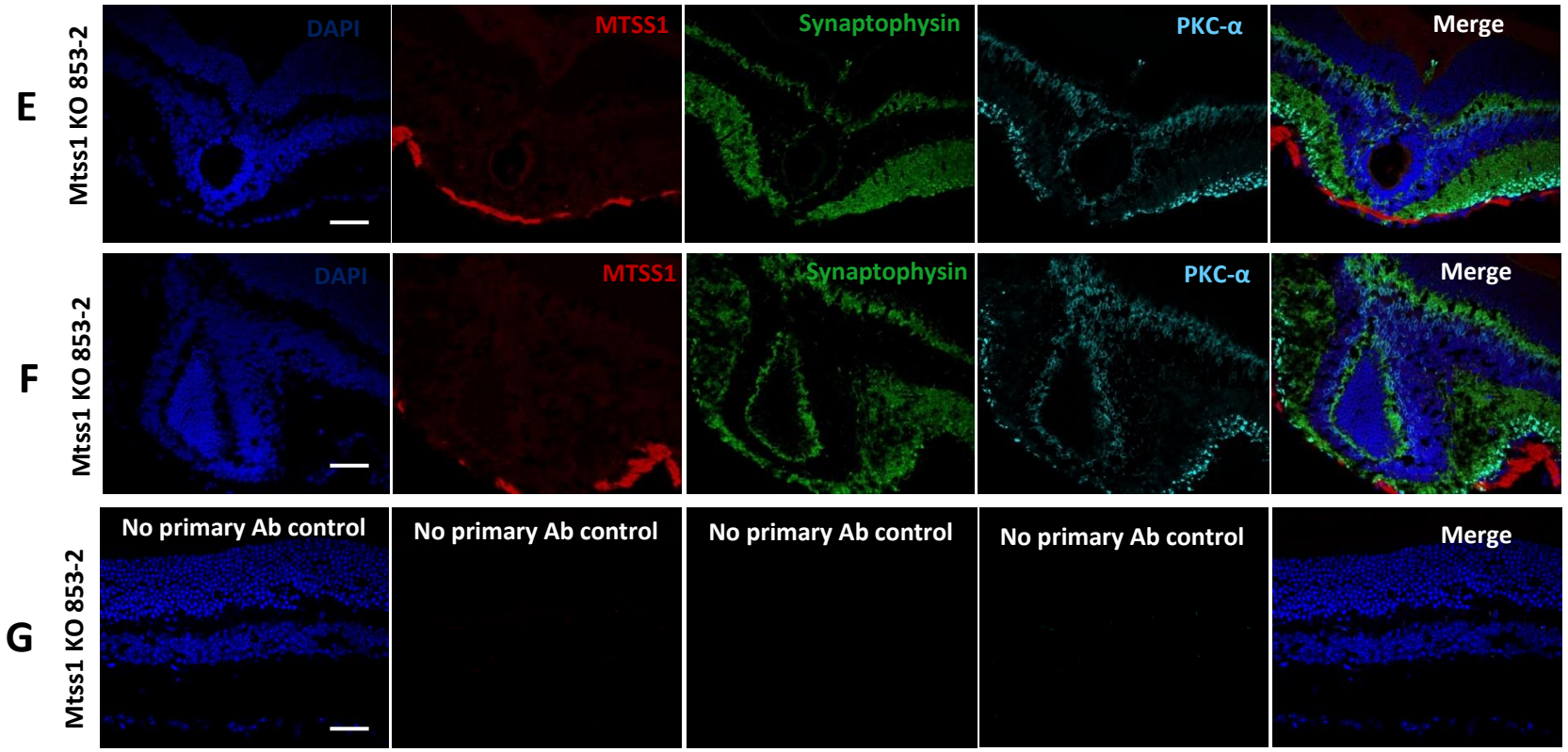


Figure 5.10. Immunohistochemical staining of Mtss1 knockout mouse retina. Selected images of retina sections from adult WT and age-matched Mtss1 KO mouse littermate were labelled with Mtss1 N-terminal antibody (red), Synaptophysin (green), PKCα (cyan) and DAPI (blue), and by H&E staining. (A&B) Sections from wild-type mouse retina. (C&D) Sections from Mtss1 KO mouse retina showing disorganised retina with rosette-like features. (E) Sections of Mtss1 KO mouse retina showing MTSS1-positive staining contrary to what was expected of a knockout. (F&G) Sections stained with secondary antibodies only were used as controls. DAPI (blue) was used to stain the nuclei. OS = Outer segment; ONL = Outer nuclear layer; OPL = Outer plexiform layer; INL = Inner nuclear layer; IPL = Inner plexiform layer. Scale bar = 20µm.

5.4.3.2 Residual Mtss1 expression in the Mtss1 KO retina

To determine whether there was residual expression of Mtss1 in the KO retina, both RNA and protein was extracted from the retinas of *Mtss1* KO animals and their age-matched wild-type littermates (see 5.3.3.2). RNA was used to synthesize cDNA (see 2.3.3.2) and used as template for PCR using several pairs of *Mtss1* primers. Retina lysates were probed with MTSS1 antibodies using western immunoblotting (see 2.3.5.3) for evidence of residual Mtss1 protein expression in the KO retinas.

A primer pair spanning exons 2 to 6 of mouse *Mtss1* was used to amplify the gene from cDNA from the KO mice and WT controls by endpoint PCR. Products of the expected size (380bp) were observed in all samples examined (Figure **5.11**A), suggesting that the KO mice still expressed *Mtss1* in the retina. The *Mtss1* KO mouse model was generated by inserting a neomycin gene cassette into exon 1 (Figure 5.8), so to determine if exon 1 was still expressed in the knockout mice, a primer pair with the forward one targeting the start site in exon 1 and the reverse one in exon 13 was used on cDNA from different KO retinas. While products of the expected size(s) were detected in the 4 WT littermates examined, no products were amplified in any of the 4 KO retinas (Figure **5.11**B). We then investigated the presence of the neomycin cassette in the Mtss1 KO retina using a primer pair with a forward primer targeting a sequence in the neomycin cassette and a reverse primer located in exon 2. The expected product size (~1100bp) was amplified from the KO retina but not in the WT control. These experiments taken together, indicate that the neomycin cassette had been successfully integrated into exon 1 of the Mtss1 gene and no transcripts containing exon 1 are expressed in the KO retinas.

Using western immunoblotting (see 2.3.5.3), 20µg of retina lysates from the KO mice and WT littermates were probed using two MTSS1 antibodies: the N-terminal antibody (#NBP2-24717, Novus Biologicals, UK) and another antibody (#MTSS1-P549, Cell Signalling, USA) obtained from our Finnish collaborators. In both WT retinas probed with these antibodies, protein bands of sizes corresponding to the full-length Mtss1 protein (~100kDa) were detected (Figure 5.11D and E). The same bands were also detected in the KO retinas (Figure 5.11D and E).

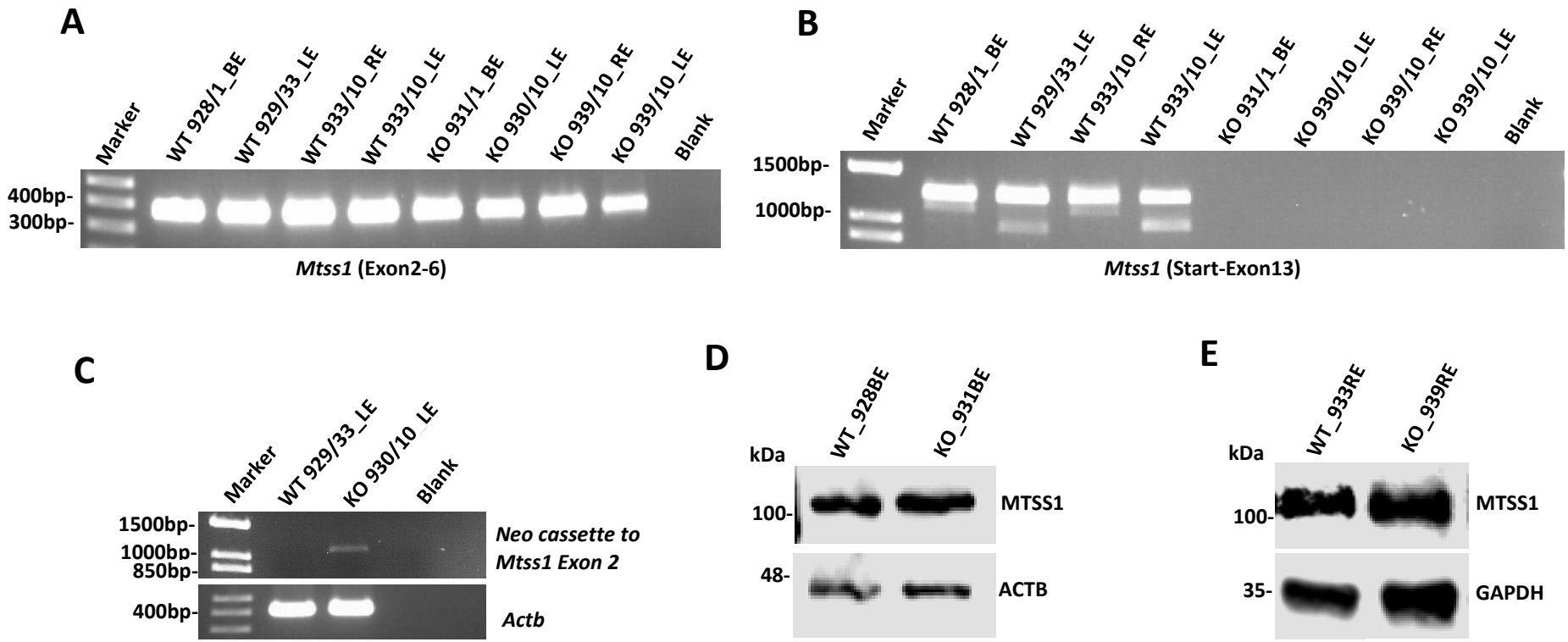


Figure 5.11. Residual expression of Mtss1 gene and protein in retina of *Mtss1* KO mice. Retinal lysate and RNA were extracted from the retinas of Mtss1 KO mice and their WT littermates to be examined for Mtss1 expression. (A) *Mtss1* expression using primers spanning exons 2 and 6. Expected product of size 380bp was amplified from both KO and WT retinas. (B) *Mtss1* expression primers spanning transcription start site in exon 1 and exon 13 detected products in WT retinas but not in any of the KO retinas examined. (C) Expression primers with a forward specific to the neomycin gene cassette and a reverse in Mtss1 exon 2 detected the presence of a neomycin cassette in KO retina but not in WT retina. (D&E) Retina lysates from Mtss1 KO retinas and WT littermates probed with two different MTSS1 antibodies, N-terminal antibody (Novus Biologicals, UK) (D) and MTSS1-P549 antibody (Cell signalling, USA) (D), detected full-length Mtss1 protein in KO the retina.

5.5 Discussion

In this chapter, we set out to determine the function of Mtss1 in the mammalian retina by examining colocalization between Mtss1 staining and previously reported binding partners in the mouse retina, to examine the potential effect of the MTSS1 variant we identified in our patients on the structure and subcellular localisation of the protein using *in silico* programs and *in vitro* models, and to examine the potential effect of the lack of Mtss1 expression in the mammalian retina using a knockout mouse model.

Using two different antibodies specific to MTSS1, we have been able to show for the first time that Mtss1 staining colocalises with F-actin in the photoreceptor and synaptic layers of the mouse retina, which is suggestive that Mtss1 may interact with F-actin in the mammalian retina, similar to previous reports of their interaction in other tissues (Saarikangas et al., 2011). We were able to confirm that DAAM1 is expressed in the retina using western immunoblotting. However, immunohistochemical staining of DAAM1 in the retina was not successful with the antibody used. Time permitting, a positive control would have been included to confirm that the antibody worked for immunohistochemical studies. Previous scRNA-seq studies have suggested that this protein is expressed in the mammalian retina including the photoreceptors (Menon et al., 2019, Lukowski et al., 2019), suggesting a possible interaction with MTSS1. This could imply that further optimisation of the antibody staining was required and/or the use of another DAAM1 antibody. We could not confirm CTTN expression in the retina using western blotting or immunohistochemistry. Previous scRNA-seq studies have suggested that CTTN is expressed in cells of the mammalian retina including photoreceptors (Menon et al., 2019, Lukowski et al., 2019). Since the MTSS1's interaction with CTTN and DAAM1 is linked to its actin binding activities, which we have shown could exist in the mammalian retina in this thesis, it could be suggested that these proteins may be interacting with MTSS1 in the retina and should be investigated further.

Future studies should also investigate MTSS1's colocalization with other potential binding partners of MTSS1 including cadherins. Previous studies have identified E-cadherin (CDH1) as a binding partner of

MTSS1 in epithelial cells (Saarikangas et al., 2011). While CDH1 expression in the retina is reported to be at very low levels and limited to the RPE (Menon et al., 2019, Burke et al., 1999, Yang et al., 2018), and might explain why we did not label it in the retina in this thesis, other proteins in the cadherin family such as CDH4, 8, 13, 9 and 22 have been reported to be expressed by cells of the neural retina including photoreceptor, bipolar and ganglion cells (De la Huerta et al., 2014, Etzrodt et al., 2009). Further studies are required assess potential colocalization of MTSS1 with these other cadherins in the mouse retina. It is important to state that immunohistochemical colocalization studies only provide correlative evidence and that co-immunoprecipitation studies may help to further elucidate if these proteins are directly interacting with one another.

Identifying that Mtss1 colocalises with F-actin in the mouse retina, particularly in the photoreceptor inner and outer segments, may suggest some crucial functional implications. The actin cytoskeleton in the photoreceptors is known to be organised in three main places: (i) as parallel F-actin bundles in the inner segments extending to the microvilli-like calycal processes at the base of the outer segments (Vaughan and Fisher, 1987); (ii) at the distal end of the connecting cilium (proximal outer segment) where photoreceptor disc morphogenesis occurs (Chaitin et al., 1984); and (iii) at the photoreceptor synaptic terminals in the inner plexiform layer (Vaughan and Fisher, 1987). In the inner segments, actin bundles, together with other cytoskeletal fibres, serve as a scaffold for the translocation of proteins and other important molecules such across the connecting cilium into the outer segments to ensure their proper function (Nemet et al., 2014). In fact, it has been shown that the appearance of a high density of actin filaments at the site of new disc formation coincides specifically with the formation of photoreceptor outer segment discs in developing mouse and rat retinas (Chaitin et al., 1988, Arikawa and Williams, 1989). As such, disruption of the actin cytoskeleton in the photoreceptors is reported to be associated with impaired photoreceptor development and function, including abnormal disc morphogenesis (Williams et al., 1988, Vaughan and Fisher, 1989, Hale et al., 1996). In line with the crucial role of the actin network in maintaining photoreceptor function, several actin-binding and actin-associated proteins, including fascin 2 (FSCN2) (Wada et al., 2001) and tubby-like protein 1 (TULP1) (Xi et al., 2005), have been implicated in various forms of RP.

Although the exact mechanisms involved in photoreceptor disc morphogenesis remain unclear, the process is reportedly dependent on actin polymerization (Hale et al., 1996). A recent study identified the Arp2/3 protein complex as a key regulator of actin polymerization at the proximal outer segments which, when disrupted, resulted in a halt in the formation of new photoreceptor outer segment discs (Spencer et al., 2019). Again, Spencer *et al.* (2019) also found that the formation of new photoreceptor disc membranes occurred through lamellipodium-like mechanism mediated by the Arp2/3 complex. Interestingly, MTSS1 has been shown to regulate actin polymerization through interaction with the Arp2/3 complex and the formin DAAM1 (Lin et al., 2005), and is also involved in the formation of filopodia and lamellipodium-like structures in epithelial and neuronal cells (Kawabata Galbraith et al., 2018, Woodings et al., 2003). This evidence, together with our identification of MTSS1 colocalization with F-actin in the inner and outer segment of the photoreceptors, could be suggestive that MTSS1 plays an important role in the actin dynamics occurring in the photoreceptors. Equally important to photoreceptor outer segment development and function is transport of proteins and other essential macromolecules from the inner segment to the outer segment across the connecting cilium, a process called intraflagellar transport (IFT; see section 1.1.2.3). This transport is dependent on the highly organised cytoskeleton in the inner segment and across the connecting cilium (Pearring et al., 2013). As MTSS1 has been shown to be involved in binding and bundling of F-actin in other tissues (Yamagishi et al., 2004), it will be interesting to investigate whether MTSS1 contributes to the organisation of the parallel F-actin bundles located in the photoreceptor inner segment. It will also be interesting to investigate whether defect in this F-actin bundling role of MTSS1 might affect the cytoskeletal organisation and related transport of proteins in the photoreceptor inner segment and connecting cilium.

As our second objective, we investigated the effect of the MTSS1 variant identified in our adRP patients in family 3027 on the structure and subcellular localisation of the MTSS1 protein using *in silico* program and *in vitro* models. The c.637_639del variant, which results in the deletion of the glutamic acid located at amino acid position 213 of the MTSS1 protein was predicted by *in silico* tools to be deleterious, with predictions of destabilization of the protein structure, protein-protein interaction and loss of the IMD

domain of the protein. By transfecting various cell lines with mutant and wild-type constructs of full-length MTSS1, we have been able to show that the mutation does indeed alter the localisation and function of the protein at the cellular level. First, we have successfully shown that the mutation alters the subcellular localisation of the MTSS1 protein in two different cell lines (HEK293T and MDCKII) with the wild-type protein localising to the plasma membrane including intercellular junctions whilst the mutant protein localised to cell surface and to the cytoplasm in both cell lines. Secondly, we have also shown, in a human retinal pigment epithelial-derived cell line, that cells overexpressing the full-length wild-type MTSS1 protein developed extensive cellular processes which were not present in cells overexpressing the mutant protein.

As predicted by the *in silico* program, these features observed in cells overexpressing mutant MTSS1 may be attributable to loss of function of the IMD domain of the protein. In a previous study in which constructs containing point mutations that deactivated the IMD domain were overexpressed in MDCKII cells, the investigators observed that the mutant MTSS1 constructs localised to the cytoplasm of MDCKII cells whilst the WT constructs localised to the intercellular junctions (Saarikangas et al., 2011), similar to our observations in MDCKII and HEK393T cells in this thesis. Previous studies have also demonstrated that when cells of neuronal origin were transfected with an MTSS1 construct with an inactive IMD domain, the cells were found to have developed less dendritic cellular processes compared to cells expressing wild-type MTSS1 (Saarikangas et al., 2011), which also correlates with our results from the RPE1 cells. As the IMD of MTSS1 is the domain with binding sites for F-actin and phospholipid-rich plasma membranes (Mattila et al., 2007), the inability of the mutant MTSS1 to localise efficiently to the plasma membrane and intercellular junctions begs the question whether the p.(Glu213del) mutation may have led to deactivation of the IMD domain as predicted by the *in silico* prediction programs. It is important to mention, that the cell lines used as *in vitro* models in this thesis, including RPE1, are all of epithelial origin and that the phenotype seen in these cells when mutant MTSS1 was overexpressed may not be the same when studied in neuronal cell lines. This makes it difficult to make direct extrapolations as to how the mutant protein would behave in the photoreceptor cells which are neuronal. However, the findings from these epithelial cells could still

have some relevance to neuronal cells as previous studies have shown that epithelial cells like HEK293T express some neuronal markers (Shaw et al., 2002, Lin et al., 2014), justifying their use in neuron-related studies.

In a study by Lee *et al.* (2007) that determined the crystal structure of MTSS1 and how it binds to F-actin, the authors reported that the IMD of MTSS1 existed as a dimer with a central cavity that held a number of water molecules. This central cavity was held together by salt bridges formed by specific residues on either side of the two chains, crucial in maintaining the functional dimeric structure of the IMD. Coincidentally, glutamic acid 213 (p.Glu213), the same amino acid found to be deleted in our patients, was identified as one of the important residues that formed one of these salt bridges (Lee et al., 2007). This highlights the importance of the mutated amino acid in maintaining the functional unit of the MTSS1 protein and it is perhaps not surprising that the mutation is predicted to lead to a dysfunctional IMD by *in silico* tools such as MutationTaster. As part of the cell work, we also identified that wild-type constructs of the AK030533 transcript of MTSS1, localised to the cytoplasm (Figure 5.7). This result was as expected since this AK030533 transcript of MTSS1, which misses the first 81 amino acids of the canonical transcript, is predicted to lack a functional IMD domain (Saarikangas et al., 2011). Although this confirms how important a functional IMD domain is to the protein's affinity for the plasma membrane, it also indicates that various transcripts of MTSS1 may localise to different parts of the cell. This might explain how antibodies targeting different isoforms of the protein localised to slightly different areas or cells of the mouse retina (see Figure 4.12).

The last objective of this chapter was to examine the retina of a mouse model supposedly lacking Mtss1 for any abnormalities that could be associated with the loss of Mtss1. Although there were rosette-like features in the retinas of 2 out of the 3 knockout animals which were not present in the wild-type littermates examined, these results were inconsistent and inconclusive. First of all, the extensive folding of the retinas found in some of the wild type and knockout animals made it difficult to quantify these findings. The reason behind the extensive folding in the retina of these mice remain unclear. However, undocumented mishaps such as changes in ambient temperatures that may have occurred

during processing and shipping of eyeballs from our collaborators, or the possibility that the trait is a common feature in the genetic background of these mice cannot be ruled out (Collin et al., 2020a). In support of the latter, it is important to note that previous studies analysing various laboratory mice strains used in genetic manipulation studies have reported the occurrence of unexpected mutations in retinal degeneration genes in the genome of these mice. For instance, a study by Mattapillal and colleagues (2012) identified the presence of the *rd8* mutation in the *crb1* gene which conferred ocular phenotypes to be present in C57BL/6N mice obtained from commercial vendors, developed from embryonic stem cells, as well as those obtained from collaborators (Mattapallil et al., 2012). In fact, other studies also linked the occurrence of ocular abnormalities such as micropthalmia, corneal and lens opacities, retinal flecks and retinal folding to be a frequent occurrence in laboratory mice of the CBL5 origin, owing to underlying genetic mechanisms in these mice (Smith et al., 1994, Simon et al., 2013). The presence of these mutations in the background of these widely used laboratory mice make it difficult to solely attribute observed ocular phenotypes to the gene of interest while also making it difficult to make reliable comparison between mutant mice and wild type controls. This is because littermate controls from these mice have often been found to also exhibit some disease phenotype such as folding and pseudorosettes due to these background mutations (Pritchett-Corning et al., 2012). Therefore, although not examined in this thesis, it may be that the retinal phenotype observed in the *Mtss1* KO mice and their littermate wild type controls used here are due to the presence of some of these confounding mutations, and will be important to investigate in future studies involving these mice.

Also, we identified that the retina of these knockout mice had residual expression of Mtss1, both at the RNA and protein levels: gene expression PCR identified a transcript beginning from exon 2 and western immunoblotting with two different MTSS1 antibodies also detected a protein of size equivalent to that of the full-length Mtss1 protein in the retina of the KO mice, contrary to what was expected for a homozygous knockout model. This, therefore, might explain why MTSS1-positive staining was observed in the Mtss1 KO mice from the immunohistochemistry experiments. Although

the group that generated the knockout mouse reported total loss of the full-length protein, except for the residual expression of the truncated AK030533 transcript in some tissues including the kidney and liver (Saarikangas et al., 2011), our findings here demonstrate that the full-length protein is still expressed in the retina of these mice. This finding, though unexpected, seems to be common in some knockout mouse models of other genes generated for functional study purposes (Hosur et al., 2020). Generally, the occurrence of residual expression of genes in knockout models can be attributed to factors such as the spliceosome system outsmarting gene-targeting strategies through alternate promoter usage, alternate splicing and the expression of multiple transcripts of the targeted gene (Hosur et al., 2020). In the case of Mtss1, results from this thesis and previous studies (Glassmann et al., 2007, Nixdorf et al., 2004) have demonstrated the presence of multiple transcripts, alternate splicing and alternate promoter usage in various tissues, which might explain why the knockout model still expresses the protein. Accordingly, a study which examined another knockout mouse model of Mtss1 also found it to express the full-length of the protein in the spleen and bone marrow (Fahrenkamp et al., 2017), contrary to the total depletion of Mtss1 initially reported (Yu et al., 2011). Since the full-length protein is being expressed in the retina of the knockout mice used in this thesis, it suggests that the model used here is not suitable to be used in investigating any visual and retinal phenotype that may be associated with loss of Mtss1.

In conclusion, findings in this chapter have for the first time confirmed Mtss1 as a protein that colocalises with F-actin in the mammalian retina. Findings from *in vitro* studies of the variant identified in our adRP patients of family 3027 suggest that the variant alters the expression and localisation of the protein at the cellular level. Although the potential effect of the loss of Mtss1 on retina morphology and function could not be fully investigated due to the lack of an appropriate *in vivo* model, the results presented in this chapter provide compelling evidence to support Mtss1 as an important protein in the retina and a likely candidate for IRDs worth investigating further.

6 General discussion

The broad aim of this thesis was to identify new candidate genes responsible for inherited retinal dystrophy (IRD) in families with IRDs where the genetic cause was unknown. Genetically unsolved cases of IRDs remain common despite the impressive progress in the field resulting from the advent of high throughput genetic sequencing and advanced molecular biology techniques. The approach used in this thesis involved analysing whole exome sequencing (WES) data from selected individuals in each of the families involved, prioritising rare variants and analysing them for segregation in the respective families. Genes with variants that segregated with the condition in each family were examined for retinal expression and assessed for their suitability as candidate genes for the condition. For one of the families (3027) in which a single candidate gene was identified, retinal expression, localisation and potential functional consequence of the variant was examined using *in vitro* and *in vivo* models.

6.1 Summary of key findings

In Chapter 3, we analysed WES data from four families of which three had been diagnosed with dominant retinitis pigmentosa (adRP) and one with dominant macular dystrophy. Using protocols described in chapters 2 and 3, a single candidate gene each was identified for two families: 3004 and 3027. In family 3004, one variant (c.1258A>C, p.(Ile420Leu)) in *PARPBP* was found to segregate with the adRP in the family out of 34 rare variants examined. Similarly, one variant (c.637_639del, p.(Glu213del)) in *MTSS1* was found to segregate with the adRP in family 3027 out of 22 rare variants analysed. Variants in two other genes, *MYO5B* and *PIEZO1*, were found to segregate with the adRP in family 3013 out of 14 rare variants. All four candidates (Table 6.1) were analysed to determine if they are expressed in the human retina, as this had not been previously described. Retinal expression was demonstrated for all four, making them interesting candidates for further investigation.

In Chapter 4, *MTSS1* expression in the mammalian retina was further characterised by examining which of the various *MTSS1* transcripts were present in the retina. This was further investigated using mouse

retinal sections to determine which cells/layers of the retina the protein localised to using antibodies specific for the Mtss1. We identified that *MTSS1* had multiple transcripts in the retina, made possible through alternate splicing and the use of alternate promoters in the retina which had been previously reported in other tissues (Glassmann et al., 2007, Nixdorf et al., 2004). While most of the transcripts of *MTSS1* identified in the retina were also found to be present in the brain, the retina was found to express a transcript (AK030533) that was not identified in the brain. Using two different antibodies specific to Mtss1, the protein was found to localise to the inner and outer segments of rod photoreceptors, the synapses in the OPL and IPL, the bipolar cells and in the ganglion cells. The discovery of Mtss1 expression in the photoreceptor layer and that it is limited to the rods is an important discovery. This discovery is in agreement with the common hypothesis that for a gene to cause a rod-dominant IRD phenotype like RP, the gene should be expressed in the rod photoreceptors, similar to most of the genes previously implicated in rod-dominant phenotypes (Ali et al., 2017).

In Chapter 5, we explored the putative function of Mtss1 in the mammalian retina by investigating colocalization of Mtss1 staining in the mouse retina with its previously reported binding partners through immunolocalization studies. By double staining mouse retina sections with Mtss1 antibodies and an antibody for F-actin, a previously reported binding partner of Mtss1 (Saarikangas et al., 2011), we detected colocalization between Mtss1 staining and F-actin staining in the photoreceptors and the two synaptic layers of the retina. Using two *in vitro* cell models (HEK293T and MDCKII), we identified that GFP-tagged MTSS1 proteins containing the p.(Glu213del) mutation identified in family 3027 localised to the cytoplasm whilst the wild-type protein localised to the plasma membrane. In RPE1 cells, overexpression of wild-type MTSS1 led to the development of extensive cellular processes which were less prominent when mutant MTSS1 was overexpressed. Together with predictions from *in silico* tools, we report that the *MTSS1* mutation identified in family 3027 led to changes in the subcellular localisation of the MTSS1 protein.

As the variant in family 3027 is in the IMD domain of the protein, we postulate that perhaps the change in subcellular localisation results from loss of or altered affinity of the domain for the phospholipid-

rich plasma membrane and F-actin. As discussed in section 1.1.2, the plasma membrane of the photoreceptor outer segments rely on membrane-bending mechanisms to develop the extensive functional curvatures required for normal function. MTSS1 has been reported to mediate plasma membrane bending through functional binding sites for F-actin and PI(4,5)P_2-rich membranes located in its IMD domain (Mattila et al., 2007). Since both F-actin assembly and membrane-bending mechanisms in the photoreceptor inner and outer segments are important for the proper development and function of these aspects of the photoreceptor (Nemet et al., 2014, Hale et al., 1996), we also postulate, that the potential loss of or altered affinity of the IMD for F-actin and phospholipids may serve as the mechanism by which the MTSS1 p.(Glu213del) mutation would cause photoreceptor dysfunction and subsequent retinal disease. Consequently, we examined the retina of a transgenic mouse line reported to be lacking *Mtss1*. Findings from analysing retina sections from this knockout mouse model were inconclusive due to excessive folding of the retinas and most importantly, the discovery that the retina of this knockout mouse showed residual expression of Mtss1. However, an uncommon rosette-like feature was identified in some knockout retinas examined and requires further investigation in a larger number of knockout retinas.

6.2 Potential disease mechanism of the MTSS1 p.Glu213del variant

Dominant disease phenotypes resulting from heterozygous gene mutations can cause disease at the cellular level through one of three main mechanisms: haploinsufficiency, dominant negative effect and dominant gain-of-function mechanisms (Fay and Spencer, 2006). Haploinsufficiency, normally occurring from loss of function mutations, is the situation in which a mutation affecting one copy of the gene leads to 50% reduction in the amount of wild type protein required for normal function. In dominant negative effect, the mutation in one copy of the gene leads to a non-functional copy of the protein which either directly interferes with the functional activity of the wild type copy of the protein or interferes indirectly by inhibiting other proteins required for the normal function of the wild type protein. This often effectively results in loss of function of the wild type protein leading to disease. The third mechanism, dominant gain-of-function, describes a mechanism in which the mutation,

depending on its location in the protein, results in an increased/unregulated functional activity of the protein or result in the mutant protein acquiring new biochemical activities due to conformational changes caused by the mutation (Veitia et al., 2018, Levine, 2017).

In the case of the p.Glu213del variant identified in MTSS1, it can be hypothesised that the variant which leads to the deletion glutamic acid 213, located in the IMD domain of the MTSS1 protein, may cause a disease phenotype through a dominant gain-of-function mechanism. Although *in silico* programs used to analyse the p.Glu213del variant predicted the potential loss of a functional IMD domain due to the variant (see section 5.4.2.1), western blot analysis of the overexpressed mutant protein identified a mutant protein product of the same size as the WT MTSS1 protein (see Figure 5.3A and B). This suggests that the mutation did not cause truncation of the MTSS1 protein. Interestingly, a previous study (Lee et al., 2007) identified glutamic acid 213, deleted in our patients, as a crucial component of salt bridges necessary to maintain the functional dimeric unit of the IMD domain of MTSS1. The deletion of this amino acid in the mutant protein, therefore, may have altered the dimeric structure of the IMD domain, giving the mutant IMD a new structural/functional conformation which can then cause dysregulated biochemical activities or protein misfolding. This could, perhaps, explain the observance of punctate intracellular protein inclusions in all the cell models overexpressing the mutant MTSS1 protein (see Figure 5.4F, Figure 5.5E and Figure 5.6D). These intracellular inclusions may be resulting from protein aggregation or actin remodelling activities facilitated by gain-of-function effects of the mutant MTSS1 protein, similar to previous findings of gain-of-function rhodopsin mutations leading protein aggregation in dominant RP (Surgucheva et al., 2005).

Table 6.1. Summary of key candidate genes identified in families presented in order of the strength of evidence.

Family	Gene symbol	Full name	Variant identified	Effect on protein	Retinal expression	Retinal localisation	Functional experiments
3027	*MTSS1*	Metastasis Suppressor 1	c.637_639del	p.(Glu213del)	Present	Rod photoreceptors, Inner and outer plexiform layer (OPL, IPL), retinal ganglion cells (RGCs); Colocalises with F-actin in rods	Variant alters subcellular localisation of MTSS1 in 3 cell lines examined
3004	*PARPBP*	PARP1 binding protein	c.1258A>C	p.(Ile420Leu)	Present	Inner nuclear layer(INL) and Ganglion cell layer (GCL)	Not examined
3013	*MYO5B*	Myosin VB	c.5314-1G>A	Splicing	Present	Not examined	Not examined
3013	*PIEZO1*	piezo type mechanosensitive ion channel component 1	c.6280C>G	p.(Leu2094Val)	Present	Not examined	Not examined

6.3 Relevance to candidate gene identification for IRDs

Next generation sequencing has been widely used in various studies to identify disease-causing genes and mutations involved in IRDs as described in section 1.3.5. Typically, candidate gene identification studies sequence the genome or exome of patients and then employ predictive tools such as PolyPhen, SIFT and CADD in conjunction with various genomic datasets to predict the pathogenicity of variants detected by NGS (see Table 1.2). These predictions, together with the reported/known functional pathways the genes are involved in, are then used to determine which variants are to be considered likely to be responsible for the conditions involved (de Castro-Miró et al., 2016, Astuti et al., 2018). Although this is a widely used and valuable approach, the challenge with this methodology is the likelihood of eliminating variants that are of unknown significance due to limited knowledge about the function of certain genes and the corresponding proteins they make. This is particularly true for genes whose functions are yet to be fully elucidated. As families involved in this study did not have variants in the known IRD genes after being screened on the IRD gene panel in Oxford, we assumed that the disease-causing variants may be identified in genes that have not been previously known to play a role in the retina. All the variants identified from WES in this thesis were annotated with PolyPhen, SIFT and CADD, but we did not use the predicted pathogenicity from these tools as a criteria to exclude any of the variants as done conventionally (Astuti et al., 2018). Instead, the main determining factor for the inclusion of variants in segregation analysis in this thesis was their gnomAD frequencies, a measure of how common or rare these variants are in the general population. As a principle, very rare variants with gnomAD frequencies of 0.00, regardless of their pathogenicity predictions, were all analysed for segregation in the first instance. The use of very rare variants was particularly important here since the conditions of the patients in this thesis were of dominant inheritance patterns.

The approach used herein to identify and characterise candidate genes in this thesis is relatively time consuming and costly considering that only one candidate out of the four families was able to be characterised to an appreciable level. However, it is still a useful approach, in that it led to the

identification of novel candidate genes which had never been linked to IRDs and may have been considered irrelevant to retinal function, as seen with *MTSS1*. Prior to being identified as a candidate gene in this thesis through segregation analysis, much of what was known and reported in the literature for *MTSS1* was its role in cancer metastasis, as depicted by its name: metastasis suppressor 1 protein. In spite of the fact that a large amount of evidence had been published on its actin-binding and membrane-deforming abilities, most of these were interpreted in the light of its predicted role in metastasis. Perhaps, this bias seen in the literature concerning genes whose identification and preliminary characterisation links them to cancers, may have contributed to similar genes being easily discarded if they came up in the search for candidate genes for conditions such as IRDs. As such, findings from this thesis suggest that future studies to identify novel candidate genes for IRDs should employ a holistic approach that goes beyond predicted pathogenicity and known function of genes being examined to include retinal expression, especially as most of the IRD genes yet to be identified may not have any known or obvious functional roles in the retina. Also, previous reports linking certain genes to non-ocular conditions should not be used as a criteria to exclude their potential involvement in retinal function or disease, especially as some genes that are widely expressed across tissues are also known to have tissue-specific transcripts (Zhu et al., 2016, Hekselman and Yeger-Lotem, 2020, Barshir et al., 2014). Additionally, there are examples of genes previously associated with cancers that have also been implicated in IRDs. These include *MERTK* (MER proto-oncogene, tyrosine kinase) which harbours mutations that cause IRDs such as RP and CRD (Parinot and Nandrot, 2016, Gal et al., 2000, Mackay et al., 2010), and *RAB28*, member of RAS oncogene family, which is reported to harbour mutations that cause CRD in different populations (Iarossi et al., 2021, Roosing et al., 2013). This indicates that our association of *MTSS1,* a cancer related gene, with IRD in this thesis is not without precedent.

Studies reporting novel candidate genes for IRDs, especially dominant forms, often report identifying changes in a particular gene in multiple families. While identifying more patients and families with variant(s) in a common gene provides further proof of the gene's pathogenicity, it is becoming clear that the era of identifying many families with disease-causing mutations in common IRD genes such as

RHO and *ABCA4* (Schulz et al., 2017, Pontikos et al., 2020) are coming to an end. We propose that, going forward, new candidate gene for IRDs may involve private mutations limited to individual families or smaller patient cohorts as evidenced by more recently discovered IRD genes such as *AHR, ENSA* and *MIEF1* (Zhou et al., 2020, Yi et al., 2020, Charif et al., 2021). Therefore, the development of methods that enable the authentication of pathogenic variants in such small patient cohorts or families is crucial. That said, the importance of data sharing with groups with common interests in IRD gene identification and access to IRD databases as an avenue of identifying more patients or families that might be harbouring variants in the candidate genes identified in this thesis cannot be underestimated (see 6.4.3).

The approach used to identify candidate genes in this thesis is, however, not without limitations. The first is with the use of whole exome sequencing: although a large proportion of disease-causing mutations are located in the exome, there is also evidence of disease-causing mutations occurring in intronic regions of genes (García Bohórquez et al., 2021, Jamshidi et al., 2019, Qian et al., 2021). In fact, a study that employed both WES and WGS in a large cohort of IRD patients reported some benefit of WGS over WES as a higher pathogenic variant detection rate and identification of disease-causing variants in non-coding and GC-rich regions not covered by WES was reported (Carss et al., 2017). As such, the use of WES in thesis has the risk of missing deep intronic changes that may be pathogenic. At the time of recruiting these families into the UKIRDC study, WES was the preferred/favoured method of sequencing (Chiang et al., 2015). Reasons included the high probability of identifying disease-causing variants in the exome, how relatively expensive whole genome sequencing (WGS) was at the time, and the massive computing and technical resources that were required to handle data from WGS (Strand_NGS, 2021). Over time, the cost of WGS has dropped drastically, with some sequencing companies running WGS for costs as low as £1000 (Schwarze et al., 2018). The availability of high computing logistics needed to handle and store WGS data has also seen a dramatic increase in the present time (Dockery et al., 2021). As such, it will be more prudent for similar future studies to employ WGS, when sequencing affected individuals.

Also, the current cost of sequencing and the availability of computing logistics offer the opportunity of sequencing more family members at the same time. This has the advantage of drastically reducing the number of variants to be analysed since only variants shared between affected individuals of the same family will be prioritised. Evidence of this can be seen in this thesis for the number of variants prioritised for segregation versus the number of participants underwent WES: in family 3004 in which only one subject was sequenced, 36 variants were analysed; in families 3013 and 3027 in which two subjects were sequenced, 15 and 22 variants were analysed respectively; in family 3032 in which three subjects were quenched, 13 variants were analysed (see Chapter 3). Moreover, when unaffected individuals in the same family are sequenced together with affected individuals, it offers the ability to conduct *in silico* segregation analysis and for likely pathogenic candidate variants to be prioritised more quickly. In this thesis, unaffected participants recruited had the region of interest in their genome amplified by PCR and sequenced using Sanger sequencing instead of undergoing WES. However, many recent and ongoing studies, including the GEL rare disease programme, have employed the recruitment and sequencing of probands together with affected and unaffected family members (commonly called the clinical trio) to facilitate disease gene identification process (Weisz Hubshman et al., 2017).

6.4 Future directions

6.4.1 Further characterisation of MTSS1

6.4.1.1 Profile of Mtss1 transcripts in the mammalian retina

Results from this thesis indicate that different transcripts of *MTSS1* are present in the adult human retina. However, the full profile of *MTSS1* transcripts present in the retina remain to be determined. It is important to determine all transcripts of *MTSS1* present in the mammalian retina using techniques such as RNA sequencing (RNA-seq). Also, it will be important to determine the levels of expression of these transcripts in the retina during development and in the adult retina. This will enable us determine

the transcripts that are most abundant in the retina at different developmental time-points and potentially enable us to relate these patterns of expression to their putative functions. For instance, it will be interesting to investigate the pattern and levels of expression of *MTSS1* transcripts with exon 12 and transcripts with exon 12a in the retina using quantitative real-time PCR (qPCR). This approach could also give an indication as to whether these transcripts are also developmentally regulated in the retina as is reported to occur in the cerebellum (Sistig et al., 2017). Understanding the full *MTSS1* transcriptome in the retina will serve an important guide into choosing the appropriate gene-targeting tools and strategies in developing a more appropriate knockout animal model of *Mtss1* (see 6.4.1.4).

6.4.1.2 Effect of p.(Glu213del) on F-actin and phospholipid-binding affinities of MTSS1

It was postulated in Chapter 5 that the p.(Glu213del) mutation in MTSS1 alters the subcellular localisation of the protein in cell models. This effect can probably be attributable to the loss of the IMD domain or altered affinity of the IMD for F-actin and the phospholipid-rich plasma membrane. However, this remains unclear. It will therefore be important to investigate such affinities *in vitro*, through actin co-sedimentation assays (Xi et al., 2005, Kumar et al., 2004) and phospholipid-binding assay (Saric et al., 2021, Xi et al., 2005), respectively. These assays, have been used previously to investigate the effect of mutations on the binding affinities of proteins like TULP1 (Xi et al., 2005) for F-actin and phospholipids. The assays require the expression and purification of the mutant protein from cells and incubating the purified protein with F-actin or phospholipid strips. These assays would be useful in determining the potential effect of the p.(Glu213del) mutation on the binding affinity of MTSS1 for phospholipids and F-actin *in vitro*.

6.4.1.3 Identification of binding partners of Mtss1 in mammalian retina

Although MTSS1 is widely considered to be an actin-binding and plasma membrane-deforming protein, there are proteins that have been reported to interact with MTSS1 to facilitate its perceived role in regulating the actin cytoskeleton and plasma membrane dynamics in other tissues. In this thesis, we were only able to confirm colocalization between Mtss1 and F-actin in the mammalian retina due to

the lack of appropriate antibodies for the other previously reported binding partners such as CTTN and DAAM1. It will be important to confirm that MTSS1 directly binds to these potential binding partners in the mammalian retina using co-immunoprecipitation and pull-down assays. Once immunoprecipitation experiments are carried out on retina lysates, the protein complexes could also be analysed using mass spectrometry to identify the other binding partners of MTSS1 in the retina. Confirmation of interaction between Mtss1 and the putative binding partners could then be verified via co-immunoprecipitation and colocalization studies in the mammalian retina. Identifying the binding partners of MTSS1 in the mammalian retina will broaden our understanding of the potential role it plays in the retina, be it similar or different to what has been reported in other tissues.

Also, whereas Mtss1 staining in the photoreceptors and synaptic layers colocalised with F-actin staining, Mtss1 expression in the bipolar and ganglion cell bodies did not. This observation is not surprising as F-actin staining has not been reported in the cell bodies of bipolar and ganglion cells (Vaughan and Fisher, 1987). It is unclear whether Mtss1 may have the same function in the bipolar and ganglion cells or may have unique interactors leading to different functions. It will, therefore, be important to investigate whether Mtss1 plays similar or varying roles in these cell types of the retina. Employing techniques such as flow cytometry and immunopanning (Fang et al., 2018, Park et al., 2020, Chintalapudi et al., 2017) to isolate these cell types of the retina and identifying components of Mtss1 protein complexes in these cells will help to elucidate this.

6.4.1.4 Development of an appropriate Mtss1 animal model

Animal models of IRDs, especially mouse models, have been useful in identifying IRD candidate genes, understanding mechanisms of retinal pathology and developing therapies for IRDs such as gene therapy (Collin et al., 2020b, Veleri et al., 2015, Chang, 2013). Unfortunately, the *Mtss1* knockout model used in this thesis to evaluate the potential effect of the loss of Mtss1 on retina morphology was not an ideal model (see 5.4.3.2). Having shown in this thesis that Mtss1 is widely expressed in the mouse retina and seems to be associated with F-actin, an important component of the photoreceptor outer and inner segments, the ability to adequately investigate the effect of the loss of Mtss1 on retinal

structure and function is crucial. The use of techniques such as immunohistochemistry and H&E staining as used in this thesis for morphological assessment of a suitable knockout/mutant Mtss1 retina, as well as functional assessments such as ERGs will be useful in unravelling any defect that may be associated with the loss of Mtss1 in the retina.

However, developing a robust transgenic mouse model of *Mtss1* will require the use of more effective gene targeting technologies such as the CRISPR/Cas9 system to ensure the effective depletion of all transcripts of the gene. This is especially necessary since previous knockout mouse models of *Mtss1*, including the one used this thesis, have been shown to demonstrate residual expression of Mtss1 (Fahrenkamp et al., 2017, Saarikangas et al., 2011). While the generation of a *Mtss1*-null mouse model will be useful in unravelling the role of Mtss1 in the retina, it may not be a perfect representation of the disease phenotype observed in our patients. This is because the mutation, p.(Glu213del), identified in the adRP patients of family 3027 may not lead to a total loss of the entire MTSS1 protein but only the loss of the IMD domain. As such, the development of a model bearing the exact mutation will also be useful in unravelling the exact mechanism(s) by which the mutation leads to retinal disease.

6.4.2 Characterisation of other prioritised candidate genes

Due to time limitation, *PARPBP*, *MYO5B* and *PIEZO1* which were also identified as candidate genes in the other families in this thesis, could not be characterised further. Our preliminary analysis of these genes and the respective variants identified in the associated families (described in Chapter 3) suggest that these genes are interesting and worth investigating further. Considering that their expression and potential functions in the retina have not been previously described, it will be important to investigate the transcripts of these genes that are expressed in the retina, which cells or layers in the retina they are expressed in, and to design constructs bearing the respective mutations to investigate their effects on the subcellular expression the proteins, *in vitro*.

6.4.3 Patient screening

Since the candidate genes identified in this thesis were identified in single families, it will be important to screen other IRD patients and families with unknown genetic causes for the possibility of identifying potential disease-causing variants in the candidate genes identified in this thesis. In this regard, databases from initiatives such as the rare disease programme, run by Genomics England (GEL; https://www.genomicsengland.co.uk), which has clinical and genomic data from various patients with IRDs and their families, would serve as a valuable resource in such screenings. In fact, a preliminary search through the GEL rare disease programme database for patients with mutations in *MTSS1* identified some interesting results: 6 individuals with non-syndromic dominant rod-cone dystrophy, 3 with dominant inherited macular dystrophy and others with a combination of IRDs and other comorbidities (see Appendix G) were identified. At the time of writing this thesis, efforts are underway to contact clinicians who recruited these patients into the GEL rare disease programme for further assessments and potential segregation analysis. Another resource available in the UK that could be useful in identifying more patients or families with variants in the candidate genes identified in this thesis is the National Institute of Health Research (NIHR) BioResource – Rare Diseases project (https://bioresource.nihr.ac.uk/using-our-bioresource/our-cohorts/rare-diseases/). Also, sharing details of the candidate genes identified herein with groups who share a common interest in identifying candidate genes for IRDs such as the UK Eye Genetics Group (UK-EGG), the European Retinal Disease Consortium (ERDC) and through GeneMatcher (https://genematcher.org/) will increase the chances of identifying more patients with variants in the candidate genes identified in this thesis.

6.5 Conclusions

I have, in this thesis, identified a rare variant in *MTSS1* that segregates with adRP in a family and have shown that this variant alters the subcellular expression and localisation of the protein in *in vitro* models. For the first time, we have also described expression of MTSS1 in the mammalian retina including the photoreceptors. Other interesting candidate genes, which have never been linked to

IRDs, have also been identified and require further characterization of their expression and role in retinal function and disease. Collectively, findings presented in this thesis indicate that next generation sequencing as an invaluable technique in identifying novel candidate genes that may be responsible for IRDs.

6.6 Covid-19 pandemic impact statement

The Covid-19 pandemic began when I had just entered into the third year of my DPhil research and it posed a major interruption to the progress and completion of my DPhil research. Firstly, my DPhil project was an entirely lab-based project that required continuous access to laboratory facilities. This was, however, not possible from March 2020 to September 2020 when the labs were shut down completely due to the pandemic. This resulted in the loss of 7 months meant for lab work. At the time the lab closures, I had established cell cultures which were being used as *in vitro* models. Unfortunately, I had to discontinue these cell cultures and cryopreserve them due to the lockdown. Although the labs re-opened in September 2020, they have since been running below full capacity, in accordance with recommended safety guidelines, especially as our labs are based in a hospital facility which require more stringent safety measures. Access to essential laboratory facilities has continued to be challenging due to the shift system put in place to enable all staff equal access while maintaining the safety protocols at the same time. Delays in ordering and receiving crucial laboratory reagents due to interruptions caused by the pandemic also impacted my ability to run and complete essential experiments in a timely manner. This impacted my ability to characterise the other candidate genes as I did for *MTSS1,* and to carry out some of the other experiments which have been listed in the future directions section.

Secondly, due to the pandemic, all studies involving human participants were halted. This also affected the progress of my project as additional members of the families reported in my thesis could not be recruited to enable completion of segregation analysis. This partly explains why in two of the families, 3013 and 3032, a single candidate gene could not be identified.

Thirdly, the travel restrictions that came with the pandemic made it difficult for me to visit the lab of our Finnish collaborators who had the *Mtss1* knockout mice. Before the pandemic, plans had been made for me to travel to Turku (Finland) to morphologically and functionally assess the retina of these mice as part of my project. This was not possible due to the travel restrictions. Although we were able obtain some eye tissue from these mice for morphological assessment, this limited the functional assessment which were intended to be carried out on these mice such as OCT and ERGs.

Finally, the pandemic and its protracted lockdown affected my productivity, both in the lab and in writing up this thesis, and to some extent on the state of my mental health. However, I am very grateful to have been able to overcome these unprecedented challenges through the invaluable support of my supervisors, family and friends.

References

AARTSEN, W. M., ARSANTO, J.-P., CHAUVIN, J.-P., VOS, R. M., VERSTEEG, I., CARDOZO, B. N., BIVIC, A. L. & WIJNHOLDS, J. 2009. PSD95β regulates plasma membrane Ca(2+) pump localization at the photoreceptor synapse. *Molecular and Cellular Neuroscience,* 41**,** 156-165.

AARTSEN, W. M., KANTARDZHIEVA, A., KLOOSTER, J., VAN ROSSUM, A. G., VAN DE PAVERT, S. A., VERSTEEG, I., CARDOZO, B. N., TONAGEL, F., BECK, S. C., TANIMOTO, N., SEELIGER, M. W. & WIJNHOLDS, J. 2006. Mpp4 recruits Psd95 and Veli3 towards the photoreceptor synapse. *Hum Mol Genet,* 15**,** 1291-302.

ACH, T., HUISINGH, C., MCGWIN, G., JR., MESSINGER, J. D., ZHANG, T., BENTLEY, M. J., GUTIERREZ, D. B., ABLONCZY, Z., SMITH, R. T., SLOAN, K. R. & CURCIO, C. A. 2014. Quantitative autofluorescence and cell density maps of the human retinal pigment epithelium. *Invest Ophthalmol Vis Sci,* 55**,** 4832-41.

ACLAND, G. M., AGUIRRE, G. D., RAY, J., ZHANG, Q., ALEMAN, T. S., CIDECIYAN, A. V., PEARCE-KELLING, S. E., ANAND, V., ZENG, Y., MAGUIRE, A. M., JACOBSON, S. G., HAUSWIRTH, W. W. & BENNETT, J. 2001. Gene therapy restores vision in a canine model of childhood blindness. *Nature Genetics,* 28**,** 92-95.

ACUNA-HIDALGO, R., VELTMAN, J. A. & HOISCHEN, A. 2016. New insights into the generation and role of de novo mutations in health and disease. *Genome Biology,* 17**,** 241.

ADZHUBEI, I. A., SCHMIDT, S., PESHKIN, L., RAMENSKY, V. E., GERASIMOVA, A., BORK, P., KONDRASHOV, A. S. & SUNYAEV, S. R. 2010. A method and server for predicting damaging missense mutations. *Nature Methods,* 7**,** 248-249.

AÍSA-MARÍN, I., GARCÍA-ARROYO, R., MIRRA, S. & MARFANY, G. 2021. The Alter Retina: Alternative Splicing of Retinal Genes in Health and Disease. *International journal of molecular sciences,* 22**,** 1855.

AKAHORI, M., TSUNODA, K., MIYAKE, Y., FUKUDA, Y., ISHIURA, H., TSUJI, S., USUI, T., HATASE, T., NAKAMURA, M., OHDE, H., ITABASHI, T., OKAMOTO, H., TAKADA, Y. & IWATA, T. 2010. Dominant mutations in RP1L1 are responsible for occult macular dystrophy. *Am J Hum Genet,* 87**,** 424-9.

AKIMOTO, M., CHENG, H., ZHU, D., BRZEZINSKI, J. A., KHANNA, R., FILIPPOVA, E., OH, E. C. T., JING, Y., LINARES, J.-L., BROOKS, M., ZAREPARSI, S., MEARS, A. J., HERO, A., GLASER, T. & SWAROOP, A. 2006. Targeting of GFP to newborn rods by Nrl promoter and temporal expression profiling of flow-sorted photoreceptors. *Proceedings of the National Academy of Sciences of the United States of America,* 103**,** 3890.

AL-MAGHTHEH, M., INGLEHEARN, C. F., KEEN, T. J., EVANS, K., MOORE, A. T., JAY, M., BIRD, A. C. & BHATTACHARYA, S. S. 1994. Identification of a sixth locus for autosomal dominant retinitis pigmentosa on chromosome 19. *Hum Mol Genet,* 3**,** 351-4.

ALBUISSON, J., MURTHY, S. E., BANDELL, M., COSTE, B., LOUIS-DIT-PICARD, H., MATHUR, J., FÉNÉANT-THIBAULT, M., TERTIAN, G., DE JAUREGUIBERRY, J.-P., SYFUSS, P.-Y., CAHALAN, S., GARÇON, L., TOUTAIN, F., SIMON ROHRLICH, P., DELAUNAY, J., PICARD, V., JEUNEMAITRE, X. & PATAPOUTIAN, A. 2013. Dehydrated hereditary stomatocytosis linked to gain-of-function mutations in mechanically activated PIEZO1 ion channels. *Nature Communications,* 4**,** 1884.

ALI, M. U., RAHMAN, M. S. U., CAO, J. & YUAN, P. X. 2017. Genetic characterization and disease mechanism of retinitis pigmentosa; current scenario. *3 Biotech,* 7**,** 251.

ANDERSON, W. F. 1984. Prospects for human gene therapy. *Science,* 226**,** 401-409.

ARIKAWA, K. & WILLIAMS, D. S. 1989. Organization of actin filaments and immunocolocalization of alpha-actinin in the connecting cilium of rat photoreceptors. *J Comp Neurol,* 288**,** 640-6.

ARNO, G., HOLDER, G. E., CHAKAROVA, C., KOHL, S., PONTIKOS, N., FIORENTINO, A., PLAGNOL, V., CHEETHAM, M. E., HARDCASTLE, A. J., WEBSTER, A. R., MICHAELIDES, M. & CONSORTIUM, F. T. U. I. R. D. 2016a. Recessive Retinopathy Consequent on Mutant G-Protein β Subunit 3 (GNB3). *JAMA Ophthalmology,* 134**,** 924-927.

ARNO, G., HULL, S., CARSS, K., DEV-BORMAN, A., CHAKAROVA, C., BUJAKOWSKA, K., VAN DEN BORN, L. I., ROBSON, A. G., HOLDER, G. E., MICHAELIDES, M., CREMERS, F. P. M., PIERCE, E., RAYMOND, F. L., MOORE, A. T. & WEBSTER, A. R. 2016b. Reevaluation of the Retinal Dystrophy Due to Recessive Alleles of RGR With the Discovery of a Cis-Acting Mutation in CDHR1. *Investigative Ophthalmology & Visual Science,* 57**,** 4806-4813.

ARORA, R., KHAN, K., KASILIAN, M. L., STRAUSS, R. W., HOLDER, G. E., ROBSON, A. G., THOMPSON, D. A., MOORE, A. T. & MICHAELIDES, M. 2016. Unilateral BEST1-Associated Retinopathy. *American Journal of Ophthalmology,* 169**,** 24-32.

ARSHAVSKY, V. Y. & BURNS, M. E. 2012. Photoreceptor signaling: supporting vision across a wide range of light intensities. *The Journal of biological chemistry,* 287**,** 1620-1626.

ARSHAVSKY, V. Y., LAMB, T. D. & EDWARD N. PUGH, J. 2002. G Proteins and Phototransduction. *Annual Review of Physiology,* 64**,** 153-187.

ASTUTI, G. D. N., VAN DEN BORN, L. I., KHAN, M. I., HAMEL, C. P., BOCQUET, B., MANES, G., QUINODOZ, M., ALI, M., TOOMES, C., MCKIBBIN, M., EL-ASRAG, M. E., HAER-WIGMAN, L., INGLEHEARN, C. F., BLACK, G. C. M., HOYNG, C. B., CREMERS, F. P. M. & ROOSING, S. 2018. Identification of Inherited Retinal Disease-Associated Genetic Variants in 11 Candidate Genes. *Genes,* 9**,** 21.

AUTON, A., ABECASIS, G. R., ALTSHULER, D. M., DURBIN, R. M., ABECASIS, G. R., BENTLEY, D. R., CHAKRAVARTI, A., CLARK, A. G., DONNELLY, P., EICHLER, E. E., FLICEK, P., GABRIEL, S. B., GIBBS, R. A., GREEN, E. D., HURLES, M. E., KNOPPERS, B. M., KORBEL, J. O., LANDER, E. S., LEE, C., LEHRACH, H., MARDIS, E. R., MARTH, G. T., MCVEAN, G. A., NICKERSON, D. A., SCHMIDT, J. P., SHERRY, S. T., WANG, J., WILSON, R. K., GIBBS, R. A., BOERWINKLE, E., DODDAPANENI, H., HAN, Y., KORCHINA, V., KOVAR, C., LEE, S., MUZNY, D., REID, J. G., ZHU, Y., WANG, J., CHANG, Y., FENG, Q., FANG, X., GUO, X., JIAN, M., JIANG, H., JIN, X., LAN, T., LI, G., LI, J., LI, Y., LIU, S., LIU, X., LU, Y., MA, X., TANG, M., WANG, B., WANG, G., WU, H., WU, R., XU, X., YIN, Y., ZHANG, D., ZHANG, W., ZHAO, J., ZHAO, M., ZHENG, X., LANDER, E. S., ALTSHULER, D. M., GABRIEL, S. B., GUPTA, N., GHARANI, N., TOJI, L. H., GERRY, N. P., RESCH, A. M., FLICEK, P., BARKER, J., CLARKE, L., GIL, L., HUNT, S. E., KELMAN, G., KULESHA, E., LEINONEN, R., MCLAREN, W. M., RADHAKRISHNAN, R., ROA, A., SMIRNOV, D., SMITH, R. E., STREETER, I., THORMANN, A., TONEVA, I., VAUGHAN, B., ZHENG-BRADLEY, X., BENTLEY, D. R., GROCOCK, R., HUMPHRAY, S., JAMES, T., KINGSBURY, Z., LEHRACH, H., SUDBRAK, R., ALBRECHT, M. W., et al. 2015. A global reference for human genetic variation. *Nature,* 526**,** 68-74.

BAINBRIDGE, J. W. B., SMITH, A. J., BARKER, S. S., ROBBIE, S., HENDERSON, R., BALAGGAN, K., VISWANATHAN, A., HOLDER, G. E., STOCKMAN, A., TYLER, N., PETERSEN-JONES, S., BHATTACHARYA, S. S., THRASHER, A. J., FITZKE, F. W., CARTER, B. J., RUBIN, G. S., MOORE, A.

T. & ALI, R. R. 2008. Effect of Gene Therapy on Visual Function in Leber's Congenital Amaurosis. *New England Journal of Medicine,* 358**,** 2231-2239.

BAKER, S. A. & KEROV, V. 2013. Chapter Seven - Photoreceptor Inner and Outer Segments. *In:* BENNETT, V. (ed.) *Current Topics in Membranes.* Academic Press.

BAKONDI, B., LV, W., LU, B., JONES, M. K., TSAI, Y., KIM, K. J., LEVY, R., AKHTAR, A. A., BREUNIG, J. J., SVENDSEN, C. N. & WANG, S. 2016. In Vivo CRISPR/Cas9 Gene Editing Corrects Retinal Dystrophy in the S334ter-3 Rat Model of Autosomal Dominant Retinitis Pigmentosa. *Molecular Therapy,* 24**,** 556-563.

BANIN, E., BARAK, A., BOYER, D. S., DO, D. V., EHRLICH, R., JAOUNI, T., MCDONALD, R., TEALANDER, D. G., GUREVICH, M., COHEN, O., RAZAG, G., HOGGE, G. S. & REUBINOFF, B. 2019. Phase I/IIa Clinical Trial of Human Embryonic Stem Cell (hESC)-Derived Retinal Pigmented Epithelium (RPE, OpRegen) Transplantation in Advanced Dry Form Age-Related Macular Degeneration (AMD): Interim Results. *Investigative Ophthalmology & Visual Science,* 60**,** 6402-6402.

BAREIL, C., HAMEL, C. P., DELAGUE, V., ARNAUD, B., DEMAILLE, J. & CLAUSTRES, M. 2001. Segregation of a mutation in CNGB1 encoding the beta-subunit of the rod cGMP-gated channel in a family with autosomal recessive retinitis pigmentosa. *Hum Genet,* 108**,** 328-34.

BARKER, G. & SIMMONS, N. L. 1981. Identification of two strains of cultured canine renal epithelial cells (MDCK cells) which display entirely different physiological properties. *Q J Exp Physiol,* 66**,** 61-72.

BARSHIR, R., SHWARTZ, O., SMOLY, I. Y. & YEGER-LOTEM, E. 2014. Comparative Analysis of Human Tissue Interactomes Reveals Factors Leading to Tissue-Specific Manifestation of Hereditary Diseases. *PLOS Computational Biology,* 10**,** e1003632.

BEHJATI, S. & TARPEY, P. S. 2013. What is next generation sequencing? *Archives of disease in childhood. Education and practice edition,* 98**,** 236-238.

BELTRAN, W. A. 2009. The use of canine models of inherited retinal degeneration to test novel therapeutic approaches. *Veterinary Ophthalmology,* 12**,** 192-204.

BENNETT, C. F. & SWAYZE, E. E. 2010. RNA targeting therapeutics: molecular mechanisms of antisense oligonucleotides as a therapeutic platform. *Annu Rev Pharmacol Toxicol,* 50**,** 259-93.

BERGER, W., KLOECKENER-GRUISSEM, B. & NEIDHARDT, J. 2010. The molecular basis of human retinal and vitreoretinal diseases. *Progress in Retinal and Eye Research,* 29**,** 335-375.

BESHARSE, J. C. & WETZEL, M. G. 1995. Immunocytochemical localization of opsin in rod photoreceptors during periods of rapid disc assembly. *Journal of Neurocytology,* 24**,** 371-388.

BHOGARAJU, S., ENGEL, B. D. & LORENTZEN, E. 2013. Intraflagellar transport complex structure and cargo interactions. *Cilia,* 2**,** 10.

BLACHARSKI, P. A. 1988. Fundus flavimaculatus. *Retinal dystrophies and degenerations***,** 135-159.

BLACKSHAW, S., FRAIOLI, R. E., FURUKAWA, T. & CEPKO, C. L. 2001. Comprehensive Analysis of Photoreceptor Gene Expression and the Identification of Candidate Retinal Disease Genes. *Cell,* 107**,** 579-589.

BLANCHOIN, L., BOUJEMAA-PATERSKI, R., SYKES, C. & PLASTINO, J. 2014. Actin dynamics, architecture, and mechanics in cell motility. *Physiol Rev,* 94**,** 235-63.

BLANTON, S. H., HECKENLIVELY, J. R., COTTINGHAM, A. W., FRIEDMAN, J., SADLER, L. A., WAGNER, M., FRIEDMAN, L. H. & DAIGER, S. P. 1991. Linkage mapping of autosomal dominant retinitis pigmentosa (RP1) to the pericentric region of human chromosome 8. *Genomics,* 11**,** 857-869.

BORSU, L., PRESSE, F. & NAHON, J.-L. 2000a. The AROM Gene, Spliced mRNAs Encoding New DNA/RNA-binding Proteins Are Transcribed from the Opposite Strand of the Melanin-concentrating Hormone Gene in Mammals*. *Journal of Biological Chemistry,* 275**,** 40576-40587.

BORSU, L., PRESSE, F. & NAHON, J.-L. 2000b. The AROM Gene, Spliced mRNAs Encoding New DNA/RNA-binding Proteins Are Transcribed from the Opposite Strand of the Melanin-concentrating Hormone Gene in Mammals *. *Journal of Biological Chemistry,* 275**,** 40576-40587.

BOWES, C., LI, T., DANCIGER, M., BAXTER, L. C., APPLEBURY, M. L. & FARBER, D. B. 1990. Retinal degeneration in the rd mouse is caused by a defect in the β subunit of rod cGMP-phosphodiesterase. *Nature,* 347**,** 677-680.

BOWNE, S. J., DAIGER, S. P., HIMS, M. M., SOHOCKI, M. M., MALONE, K. A., MCKIE, A. B., HECKENLIVELY, J. R., BIRCH, D. G., INGLEHEARN, C. F., BHATTACHARYA, S. S., BIRD, A. & SULLIVAN, L. S. 1999. Mutations in the RP1 Gene Causing Autosomal Dominant Retinitis Pigmentosa. *Human Molecular Genetics,* 8**,** 2121-2128.

BOWNE, S. J., HUMPHRIES, M. M., SULLIVAN, L. S., KENNA, P. F., TAM, L. C., KIANG, A. S., CAMPBELL, M., WEINSTOCK, G. M., KOBOLDT, D. C., DING, L., FULTON, R. S., SODERGREN, E. J., ALLMAN, D., MILLINGTON-WARD, S., PALFI, A., MCKEE, A., BLANTON, S. H., SLIFER, S., KONIDARI, I., FARRAR, G. J., DAIGER, S. P. & HUMPHRIES, P. 2011. A dominant mutation in RPE65 identified by whole-exome sequencing causes retinitis pigmentosa with choroidal involvement. *Eur J Hum Genet,* 19**,** 1074-81.

BOWNE, S. J., LIU, Q., SULLIVAN, L. S., ZHU, J., SPELLICY, C. J., RICKMAN, C. B., PIERCE, E. A. & DAIGER, S. P. 2006. Why do mutations in the ubiquitously expressed housekeeping gene IMPDH1 cause retina-specific photoreceptor degeneration? *Invest Ophthalmol Vis Sci,* 47**,** 3754-65.

BOWNE, S. J., SULLIVAN, L. S., BLANTON, S. H., CEPKO, C. L., BLACKSHAW, S., BIRCH, D. G., HUGHBANKS-WHEATON, D., HECKENLIVELY, J. R. & DAIGER, S. P. 2002. Mutations in the inosine monophosphate dehydrogenase 1 gene (IMPDH1) cause the RP10 form of autosomal dominant retinitis pigmentosa. *Human Molecular Genetics,* 11**,** 559-568.

BROADGATE, S., YU, J., DOWNES, S. M. & HALFORD, S. 2017. Unravelling the genetics of inherited retinal dystrophies: Past, present and future. *Progress in retinal and eye research,* 59**,** 53-96.

BROWN, A. S., MEERA, P., ALTINDAG, B., CHOPRA, R., PERKINS, E. M., PAUL, S., SCOLES, D. R., TARAPORE, E., MAGRI, J., HUANG, H., JACKSON, M., SHAKKOTTAI, V. G., OTIS, T. S., PULST, S. M., ATWOOD, S. X. & ORO, A. E. 2018. MTSS1/Src family kinase dysregulation underlies multiple inherited ataxias. *Proc Natl Acad Sci U S A,* 115**,** E12407-e12416.

BUJAKOWSKA, K. M., ZHANG, Q., SIEMIATKOWSKA, A. M., LIU, Q., PLACE, E., FALK, M. J., CONSUGAR, M., LANCELOT, M. E., ANTONIO, A., LONJOU, C., CARPENTIER, W., MOHAND-SAÏD, S., DEN HOLLANDER, A. I., CREMERS, F. P., LEROY, B. P., GAI, X., SAHEL, J. A., VAN DEN BORN, L. I., COLLIN, R. W., ZEITZ, C., AUDO, I. & PIERCE, E. A. 2015. Mutations in IFT172 cause isolated retinal degeneration and Bardet-Biedl syndrome. *Hum Mol Genet,* 24**,** 230-42.

BURGESS, R., MILLAR, I. D., LEROY, B. P., URQUHART, J. E., FEARON, I. M., DE BAERE, E., BROWN, P. D., ROBSON, A. G., WRIGHT, G. A., KESTELYN, P., HOLDER, G. E., WEBSTER, A. R., MANSON, F. D.

C. & BLACK, G. C. M. 2008. Biallelic Mutation of BEST1 Causes a Distinct Retinopathy in Humans. *The American Journal of Human Genetics,* 82**,** 19-31.

BURKE, J. M., CAO, F., IRVING, P. E. & SKUMATZ, C. M. B. 1999. Expression of E-Cadherin by Human Retinal Pigment Epithelium: Delayed Expression In Vitro. *Investigative Ophthalmology & Visual Science,* 40**,** 2963-2970.

BURNS, M. E., MENDEZ, A., CHEN, C. K., ALMUETE, A., QUILLINAN, N., SIMON, M. I., BAYLOR, D. A. & CHEN, J. 2006. Deactivation of phosphorylated and nonphosphorylated rhodopsin by arrestin splice variants. *J Neurosci,* 26**,** 1036-44.

CAI, Y., CHENG, T., YAO, Y., LI, X., MA, Y., LI, L., ZHAO, H., BAO, J., ZHANG, M., QIU, Z. & XUE, T. 2019. In vivo genome editing rescues photoreceptor degeneration via a Cas9/RecA-mediated homology-directed repair pathway. *Science Advances,* 5**,** eaav3335.

CALLAHAN, C. A., OFSTAD, T., HORNG, L., WANG, J. K., ZHEN, H. H., COULOMBE, P. A. & ORO, A. E. 2004. MIM/BEG4, a Sonic hedgehog-responsive gene that potentiates Gli-dependent transcription. *Genes Dev,* 18**,** 2724-9.

CAMPLA, C. K., MAST, H., DONG, L., LEI, J., HALFORD, S., SEKARAN, S. & SWAROOP, A. 2019. Targeted deletion of an NRL- and CRX-regulated alternative promoter specifically silences FERM and PDZ domain containing 1 (Frmpd1) in rod photoreceptors. *Hum Mol Genet,* 28**,** 804-817.

CARSS, K. J., ARNO, G., ERWOOD, M., STEPHENS, J., SANCHIS-JUAN, A., HULL, S., MEGY, K., GROZEVA, D., DEWHURST, E., MALKA, S., PLAGNOL, V., PENKETT, C., STIRRUPS, K., RIZZO, R., WRIGHT, G., JOSIFOVA, D., BITNER-GLINDZICZ, M., SCOTT, R. H., CLEMENT, E., ALLEN, L., ARMSTRONG, R., BRADY, A. F., CARMICHAEL, J., CHITRE, M., HENDERSON, R. H. H., HURST, J., MACLAREN, R. E., MURPHY, E., PATERSON, J., ROSSER, E., THOMPSON, D. A., WAKELING, E., OUWEHAND, W. H., MICHAELIDES, M., MOORE, A. T., WEBSTER, A. R. & RAYMOND, F. L. 2017. Comprehensive Rare Variant Analysis via Whole-Genome Sequencing to Determine the Molecular Pathology of Inherited Retinal Disease. *Am J Hum Genet,* 100**,** 75-90.

CHAITIN, M. H., CARLSEN, R. B. & SAMARA, G. J. 1988. Immunogold localization of actin in developing photoreceptor cilia of normal and rds mutant mice. *Exp Eye Res,* 47**,** 437-46.

CHAITIN, M. H., SCHNEIDER, B. G., HALL, M. O. & PAPERMASTER, D. S. 1984. Actin in the photoreceptor connecting cilium: immunocytochemical localization to the site of outer segment disk formation. *J Cell Biol,* 99**,** 239-47.

CHANG, B. 2013. Mouse models for studies of retinal degeneration and diseases. *Methods in molecular biology (Clifton, N.J.),* 935**,** 27-39.

CHARIF, M., WONG, Y. C., KIM, S., GUICHET, A., VIGNAL, C., ZANLONGHI, X., BENSAID, P., PROCACCIO, V., BONNEAU, D., AMATI-BONNEAU, P., REYNIER, P., KRAINC, D. & LENAERS, G. 2021. Dominant mutations in MIEF1 affect mitochondrial dynamics and cause a singular late onset optic neuropathy. *Mol Neurodegener,* 16**,** 12.

CHEN, B., LAI, J., DAI, D., CHEN, R., LIAO, N., GAO, G. & TANG, H. 2020. PARPBP is a prognostic marker and confers anthracycline resistance to breast cancer. *Ther Adv Med Oncol,* 12**,** 1758835920974212.

CHIANG, J. P.-W., LAMEY, T., MCLAREN, T., THOMPSON, J. A., MONTGOMERY, H. & DE ROACH, J. 2015. Progress and prospects of next-generation sequencing testing for inherited retinal dystrophy. *Expert review of molecular diagnostics,* 15**,** 1269-1275.

CHINTALAPUDI, S. R., PATEL, N. N., GOLDSMITH, Z. K., DJENDEREDJIAN, L., WANG, X. D., MARION, T. N., JABLONSKI, M. M. & MORALES-TIRADO, V. M. 2017. Isolation of Primary Murine Retinal Ganglion Cells (RGCs) by Flow Cytometry. *Journal of visualized experiments : JoVE***,** 55785.

CIDECIYAN, A. V., HAESELEER, F., FARISS, R. N., ALEMAN, T. S., JANG, G. F., VERLINDE, C., MARMOR, M. F., JACOBSON, S. G. & PALCZEWSKI, K. 2000. Rod and cone visual cycle consequences of a null mutation in the 11-cis-retinol dehydrogenase gene in man. *Vis Neurosci,* 17**,** 667-678.

CIDECIYAN, A. V., JACOBSON, S. G., DRACK, A. V., HO, A. C., CHARNG, J., GARAFALO, A. V., ROMAN, A. J., SUMAROKA, A., HAN, I. C., HOCHSTEDLER, M. D., PFEIFER, W. L., SOHN, E. H., TAIEL, M., SCHWARTZ, M. R., BIASUTTO, P., WIT, W., CHEETHAM, M. E., ADAMSON, P., RODMAN, D. M., PLATENBURG, G., TOME, M. D., BALIKOVA, I., NERINCKX, F., ZAEYTIJD, J., VAN CAUWENBERGH, C., LEROY, B. P. & RUSSELL, S. R. 2019. Effect of an intravitreal antisense oligonucleotide on vision in Leber congenital amaurosis due to a photoreceptor cilium defect. *Nat Med,* 25**,** 225-228.

CIDECIYAN, A. V., JACOBSON, S. G., HO, A. C., GARAFALO, A. V., ROMAN, A. J., SUMAROKA, A., KRISHNAN, A. K., SWIDER, M., SCHWARTZ, M. R. & GIRACH, A. 2021. Durable vision improvement after a single treatment with antisense oligonucleotide sepofarsen: a case report. *Nat Med,* 27**,** 785-789.

COLLIN, G. B., GOGNA, N., CHANG, B., DAMKHAM, N., PINKNEY, J., HYDE, L. F., STONE, L., NAGGERT, J. K., NISHINA, P. M. & KREBS, M. P. 2020a. Mouse Models of Inherited Retinal Degeneration with Photoreceptor Cell Loss. *Cells,* 9.

COLLIN, G. B., GOGNA, N., CHANG, B., DAMKHAM, N., PINKNEY, J., HYDE, L. F., STONE, L., NAGGERT, J. K., NISHINA, P. M. & KREBS, M. P. 2020b. Mouse Models of Inherited Retinal Degeneration with Photoreceptor Cell Loss. *Cells,* 9**,** 931.

COLLINS, F. & GALAS, D. 1993. A new five-year plan for the US Human Genome Project. *Science,* 262**,** 43-46.

COLLINS, F. S., PATRINOS, A., JORDAN, E., CHAKRAVARTI, A., GESTELAND, R. & WALTERS, L. 1998. New goals for the US human genome project: 1998-2003. *science,* 282**,** 682-689.

CONNELL, G., BASCOM, R., MOLDAY, L., REID, D., MCINNES, R. R. & MOLDAY, R. S. 1991. Photoreceptor peripherin is the normal product of the gene responsible for retinal degeneration in the rds mouse. *Proc Natl Acad Sci U S A,* 88**,** 723-6.

CONSORTIUM, E. P. 2012. An integrated encyclopedia of DNA elements in the human genome. *Nature,* 489**,** 57-74.

COOPER, D. N., KRAWCZAK, M., POLYCHRONAKOS, C., TYLER-SMITH, C. & KEHRER-SAWATZKI, H. 2013. Where genotype is not predictive of phenotype: towards an understanding of the molecular basis of reduced penetrance in human inherited disease. *Human genetics,* 132**,** 1077-1130.

COSTE, B., MATHUR, J., SCHMIDT, M., EARLEY, T. J., RANADE, S., PETRUS, M. J., DUBIN, A. E. & PATAPOUTIAN, A. 2010. Piezo1 and Piezo2 are essential components of distinct mechanically activated cation channels. *Science,* 330**,** 55-60.

CREMERS, F. P., VAN DE POL, D. J., VAN DRIEL, M., DEN HOLLANDER, A. I., VAN HAREN, F. J., KNOERS, N. V., TIJMES, N., BERGEN, A. A., ROHRSCHNEIDER, K., BLANKENAGEL, A., PINCKERS, A. J., DEUTMAN, A. F. & HOYNG, C. B. 1998a. Autosomal recessive retinitis pigmentosa and cone-rod dystrophy caused by splice site mutations in the Stargardt's disease gene ABCR. *Hum Mol Genet,* 7**,** 355-62.

CREMERS, F. P. M., BRUNSMANN, F., VAN DE POL, T. J. R., PAWLOWITZKI, I. H., PAULSEN, K., WIERINGA, B. & ROPERS, H. H. 1987. Deletion of the DXS165 locus in patients with classical Choroideremia. *Clinical Genetics,* 32**,** 421-423.

CREMERS, F. P. M., VAN DE POL, D. J. R., VAN DRIEL, M., DEN HOLLANDER, A. I., VAN HAREN, F. J. J., KNOERS, N. V. A. M., TIJMES, N., BERGEN, A. A. B., ROHRSCHNEIDER, K., BLANKENAGEL, A., PINCKERS, A. J. L. G., DEUTMAN, A. F. & HOYNG, C. B. 1998b. Autosomal Recessive Retinitis Pigmentosa and Cone-rod Dystrophy Caused by Splice Site Mutations in the Stargardt's Disease Gene ABCR. *Human Molecular Genetics,* 7**,** 355-362.

CREMERS, F. P. M., VAN DE POL, D. J. R., VAN KERKHOFF, L. P. M., WIERINGA, B. & ROPERS, H.-H. 1990. Cloning of a gene that is rearranged in patients with choroideraemia. *Nature,* 347**,** 674-677.

CROOKE, S. T. 2017. Molecular Mechanisms of Antisense Oligonucleotides. *Nucleic Acid Therapeutics,* 27**,** 70-77.

CURCIO, C. A., SLOAN, K. R., KALINA, R. E. & HENDRICKSON, A. E. 1990. Human photoreceptor topography. *Journal of Comparative Neurology,* 292**,** 497-523.

DAWSON, J. C., BRUCHE, S., SPENCE, H. J., BRAGA, V. M. M. & MACHESKY, L. M. 2012. Mtss1 Promotes Cell-Cell Junction Assembly and Stability through the Small GTPase Rac1. *PLOS ONE,* 7**,** e31141.

DE CASTRO-MIRÓ, M., TONDA, R., ESCUDERO-FERRUZ, P., ANDRÉS, R., MAYOR-LORENZO, A., CASTRO, J., CICCIOLI, M., HIDALGO, D. A., RODRÍGUEZ-EZCURRA, J. J., FARRANDO, J., PÉREZ-SANTONJA, J. J., CORMAND, B., MARFANY, G. & GONZÀLEZ-DUARTE, R. 2016. Novel Candidate Genes and a Wide Spectrum of Structural and Point Mutations Responsible for Inherited Retinal Dystrophies Revealed by Exome Sequencing. *PLOS ONE,* 11**,** e0168966.

DE HOZ, R., ROJAS, B., RAMÍREZ, A. I., SALAZAR, J. J., GALLEGO, B. I., TRIVIÑO, A. & RAMÍREZ, J. M. 2016. Retinal Macroglial Responses in Health and Disease. *Biomed Res Int,* 2016**,** 2954721.

DE LA HUERTA, I., DUAN, X., YAMAGATA, M. & SANES, J. R. 2014. Expression and role of classical cadherins in the mammalian retina. *Investigative Ophthalmology & Visual Science,* 55**,** 714-714.

DELORI, F. C., DOREY, C. K., STAURENGHI, G., AREND, O., GOGER, D. G. & WEITER, J. J. 1995. In vivo fluorescence of the ocular fundus exhibits retinal pigment epithelium lipofuscin characteristics. *Invest Ophthalmol Vis Sci,* 36**,** 718-29.

DIAS, M. F., JOO, K., KEMP, J. A., FIALHO, S. L., DA SILVA CUNHA, A., WOO, S. J. & KWON, Y. J. 2018. Molecular genetics and emerging therapies for retinitis pigmentosa: Basic research and clinical perspectives. *Progress in Retinal and Eye Research,* 63**,** 107-131.

DO, M. T. H. & YAU, K.-W. 2010. Intrinsically Photosensitive Retinal Ganglion Cells. *Physiological Reviews,* 90**,** 1547-1581.

DOCKERY, A., WHELAN, L., HUMPHRIES, P. & FARRAR, G. J. 2021. Next-Generation Sequencing Applications for Inherited Retinal Diseases. *International Journal of Molecular Sciences,* 22**,** 5684.

DONDERS, F. C. 1857. Beiträge zur pathologischen Anatomie des Auges. *Archiv für Ophthalmologie,* 3**,** 139-165.

DOXAKIS, E. 2021. Therapeutic antisense oligonucleotides for movement disorders. *Medicinal Research Reviews,* 41**,** 2656-2688.

DRYJA, T. P. 1990. Deficiencies in sight with the candidate gene approach. *Nature,* 347**,** 614-614.

DRYJA, T. P., BERSON, E. L., RAO, V. R. & OPRIAN, D. D. 1993. Heterozygous missense mutation in the rhodopsin gene as a cause of congenital stationary night blindness. *Nature Genetics,* 4**,** 280-283.

DRYJA, T. P., FINN, J. T., PENG, Y. W., MCGEE, T. L., BERSON, E. L. & YAU, K. W. 1995. Mutations in the gene encoding the alpha subunit of the rod cGMP-gated channel in autosomal recessive retinitis pigmentosa. *Proceedings of the National Academy of Sciences,* 92**,** 10177-10181.

DRYJA, T. P., MCGEE, T. L., HAHN, L. B., COWLEY, G. S., OLSSON, J. E., REICHEL, E., SANDBERG, M. A. & BERSON, E. L. 1990a. Mutations within the Rhodopsin Gene in Patients with Autosomal Dominant Retinitis Pigmentosa. *New England Journal of Medicine,* 323**,** 1302-1307.

DRYJA, T. P., MCGEE, T. L., REICHEL, E., HAHN, L. B., COWLEY, G. S., YANDELL, D. W., SANDBERG, M. A. & BERSON, E. L. 1990b. A point mutation of the rhodopsin gene in one form of retinitis pigmentosa. *Nature,* 343**,** 364-366.

DULLA, K., AGUILA, M., LANE, A., JOVANOVIC, K., PARFITT, D. A., SCHULKENS, I., CHAN, H. L., SCHMIDT, I., BEUMER, W., VORTHOREN, L., COLLIN, R. W. J., GARANTO, A., DUIJKERS, L., BRUGULAT-PANES, A., SEMO, M., VUGLER, A. A., BIASUTTO, P., ADAMSON, P. & CHEETHAM, M. E. 2018. Splice-Modulating Oligonucleotide QR-110 Restores CEP290 mRNA and Function in Human c.2991+1655A>G LCA10 Models. *Mol Ther Nucleic Acids,* 12**,** 730-740.

DVIR, L., SROUR, G., ABU-RAS, R., MILLER, B., SHALEV, S. A. & BEN-YOSEF, T. 2010. Autosomal-recessive early-onset retinitis pigmentosa caused by a mutation in PDE6G, the gene encoding the gamma subunit of rod cGMP phosphodiesterase. *American journal of human genetics,* 87**,** 258-264.

EDWARDS, T. L., JOLLY, J. K., GROPPE, M., BARNARD, A. R., COTTRIALL, C. L., TOLMACHOVA, T., BLACK, G. C., WEBSTER, A. R., LOTERY, A. J., HOLDER, G. E., XUE, K., DOWNES, S. M., SIMUNOVIC, M. P., SEABRA, M. C. & MACLAREN, R. E. 2016. Visual Acuity after Retinal Gene Therapy for Choroideremia. *N Engl J Med,* 374**,** 1996-8.

ELLARD, S., BAPLE, E., CALLAWAY, A., BERRY, I., FORRESTER, N., TURNBULL, C. & MCMULLAN, D. 2020. ACGS Best Practice Guidelines for Variant Classification in Rare Disease 2020. *Retrieved from* *https://www.acgs.uk.com/media/11631/uk-practice-guidelines-for-variant-classification-v4-01-2020.pdf*.

ETZRODT, J., KRISHNA-K, K. & REDIES, C. 2009. Expression of classic cadherins and δ-protocadherins in the developing ferret retina. *BMC Neuroscience,* 10**,** 153.

FAHRENKAMP, D., HERRMANN, O., KOSCHMIEDER, S., BRÜMMENDORF, T. H. & SCHEMIONEK, M. 2017. Mtss1(CSC156) mutant mice fail to display efficient Mtss1 protein depletion. *Leukemia,* 31**,** 1017-1019.

FANG, L., HUANG, T. & TSILFIDIS, C. 2018. Immunopanning purification and culture of retinal ganglion cells from mouse. *Journal of Neuroscience Methods,* 303**,** 81-85.

FARRAR, G. J., CARRIGAN, M., DOCKERY, A., MILLINGTON-WARD, S., PALFI, A., CHADDERTON, N., HUMPHRIES, M., KIANG, A. S., KENNA, P. F. & HUMPHRIES, P. 2017. Toward an elucidation of the molecular genetics of inherited retinal degenerations. *Hum Mol Genet,* 26**,** R2-r11.

FARRAR, G. J., MILLINGTON-WARD, S., CHADDERTON, N., HUMPHRIES, P. & KENNA, P. F. 2012. Gene-based therapies for dominantly inherited retinopathies. *Gene Therapy,* 19**,** 137-144.

FAY, D. & SPENCER, A. 2006. Dominant mutations. *In: WormBook: The Online Review of C. elegans Biology [Internet]. Pasadena (CA): WormBook; 2005-2018.,* Available from: https://www.ncbi.nlm.nih.gov/books/NBK19699/.

FERENCHAK, K., DEITCH, I. & HUCKFELDT, R. 2021. Antisense Oligonucleotide Therapy for Ophthalmic Conditions. *Semin Ophthalmol,* 36**,** 452-457.

FERRER-COSTA, C., GELPÍ, J. L., ZAMAKOLA, L., PARRAGA, I., DE LA CRUZ, X. & OROZCO, M. 2005. PMUT: a web-based tool for the annotation of pathological mutations on proteins. *Bioinformatics,* 21**,** 3176-3178.

FINCKH, U., XU, S., KUMARAMANICKAVEL, G., SCHÜRMANN, M., MUKKADAN, J. K., FERNANDEZ, S. T., JOHN, S., WEBER, J. L., DENTON, M. J. & GAL, A. 1998. Homozygosity mapping of autosomal recessive retinitis pigmentosa locus (RP22) on chromosome 16p12.1-p12.3. *Genomics,* 48**,** 341-5.

FIORENTINO, A., YU, J., ARNO, G., PONTIKOS, N., HALFORD, S., BROADGATE, S., MICHAELIDES, M., CARSS, K. J., RAYMOND, F. L., CHEETHAM, M. E., WEBSTER, A. R., DOWNES, S. M. & HARDCASTLE, A. J. 2018. Novel homozygous splicing mutations in ARL2BP cause autosomal recessive retinitis pigmentosa. *Mol Vis,* 24**,** 603-612.

FLYNN, E., UEDA, K., AURAN, E., SULLIVAN, J. M. & SPARROW, J. R. 2014. Fundus Autofluorescence and Photoreceptor Cell Rosettes in Mouse Models. *Investigative Ophthalmology & Visual Science,* 55**,** 5643-5652.

FOSTER, R. G., HUGHES, S. & PEIRSON, S. N. 2020. Circadian Photoentrainment in Mice and Humans. *Biology,* 9**,** 180.

FUJINAMI, K., LOIS, N., MUKHERJEE, R., MCBAIN, V. A., TSUNODA, K., TSUBOTA, K., STONE, E. M., FITZKE, F. W., BUNCE, C., MOORE, A. T., WEBSTER, A. R. & MICHAELIDES, M. 2013a. A Longitudinal Study of Stargardt Disease: Quantitative Assessment of Fundus Autofluorescence, Progression, and Genotype Correlations. *Investigative Ophthalmology & Visual Science,* 54**,** 8181-8190.

FUJINAMI, K., SERGOUNIOTIS, P. I., DAVIDSON, A. E., WRIGHT, G., CHANA, R. K., TSUNODA, K., TSUBOTA, K., EGAN, C. A., ROBSON, A. G., MOORE, A. T., HOLDER, G. E., MICHAELIDES, M. & WEBSTER, A. R. 2013b. Clinical and Molecular Analysis of Stargardt Disease With Preserved Foveal Structure and Function. *American Journal of Ophthalmology,* 156**,** 487-501.e1.

GABRIEL, L. A., PEACHEY, N. S. & SUNNESS, J. S. 2012. Retinal Function Testing and Genetic Disease. *Genetic Diseases of the Eye***,** 343.

GAJ, T., GERSBACH, C. A. & BARBAS, C. F., 3RD 2013. ZFN, TALEN, and CRISPR/Cas-based methods for genome engineering. *Trends Biotechnol,* 31**,** 397-405.

GAL, A., LI, Y., THOMPSON, D. A., WEIR, J., ORTH, U., JACOBSON, S. G., APFELSTEDT-SYLLA, E. & VOLLRATH, D. 2000. Mutations in MERTK, the human orthologue of the RCS rat retinal dystrophy gene, cause retinitis pigmentosa. *Nat Genet,* 26**,** 270-1.

GALVIN, O., CHI, G., BRADY, L., HIPPERT, C., RUBIDO, M. D. V., DALY, A. & MICHAELIDES, M. 2020. The Impact of Inherited Retinal Diseases in the Republic of Ireland (ROI) and the United Kingdom (UK) from a Cost-of-Illness Perspective. *Clinical Ophthalmology (Auckland, NZ),* 14**,** 707.

GANAKAMMAL, S. R. & ALEXOV, E. 2019. Evaluation of performance of leading algorithms for variant pathogenicity predictions and designing a combinatory predictor method: application to Rett syndrome variants. *PeerJ,* 7**,** e8106-e8106.

GARANTO, A., CHUNG, D. C., DUIJKERS, L., CORRAL-SERRANO, J. C., MESSCHAERT, M., XIAO, R., BENNETT, J., VANDENBERGHE, L. H. & COLLIN, R. W. 2016. In vitro and in vivo rescue of aberrant splicing in CEP290-associated LCA by antisense oligonucleotide delivery. *Hum Mol Genet,* 25**,** 2552-2563.

GARANTO, A., RIERA, M., POMARES, E., PERMANYER, J., DE CASTRO-MIRÓ, M., SAVA, F., ABRIL, J. F., MARFANY, G. & GONZÀLEZ-DUARTE, R. 2011. High transcriptional complexity of the retinitis pigmentosa CERKL gene in human and mouse. *Invest Ophthalmol Vis Sci,* 52**,** 5202-14.

GARCÍA BOHÓRQUEZ, B., ALLER, E., RODRÍGUEZ MUÑOZ, A., JAIJO, T., GARCÍA GARCÍA, G. & MILLÁN, J. M. 2021. Updating the Genetic Landscape of Inherited Retinal Dystrophies. *Frontiers in Cell and Developmental Biology,* 9.

GEORGIOU, M., FUJINAMI, K. & MICHAELIDES, M. 2021. Inherited retinal diseases: Therapeutics, clinical trials and end points—A review. *Clinical & Experimental Ophthalmology,* 49**,** 270-288.

GIBSON, F., WALSH, J., MBURU, P., VARELA, A., BROWN, K. A., ANTONIO, M., BEISEL, K. W., STEEL, K. P. & BROWN, S. D. M. 1995. A type VII myosin encoded by the mouse deafness gene shaker-1. *Nature,* 374**,** 62-64.

GLASSMANN, A., MOLLY, S., SURCHEV, L., NAZWAR, T. A., HOLST, M., HARTMANN, W., BAADER, S. L., OBERDICK, J., PIETSCH, T. & SCHILLING, K. 2007. Developmental expression and differentiation-related neuron-specific splicing of metastasis suppressor 1 (Mtss1) in normal and transformed cerebellar cells. *BMC Dev Biol,* 7**,** 111.

GLUSMAN, G., CABALLERO, J., MAULDIN, D. E., HOOD, L. & ROACH, J. C. 2011. Kaviar: an accessible system for testing SNV novelty. *Bioinformatics,* 27**,** 3216-3217.

GOLDBERG, A. F. X., MORITZ, O. L. & WILLIAMS, D. S. 2016. Molecular basis for photoreceptor outer segment architecture. *Progress in retinal and eye research,* 55**,** 52-81.

GONZALEZ-QUEVEDO, R., SHOFFER, M., HORNG, L. & ORO, A. E. 2005. Receptor tyrosine phosphatase-dependent cytoskeletal remodeling by the hedgehog-responsive gene MIM/BEG4. *J Cell Biol,* 168**,** 453-63.

GRAHAM, T. R. & KOZLOV, M. M. 2010. Interplay of proteins and lipids in generating membrane curvature. *Current Opinion in Cell Biology,* 22**,** 430-436.

GREENWALD, D. L., CASHMAN, S. M. & KUMAR-SINGH, R. 2010. Engineered zinc finger nuclease-mediated homologous recombination of the human rhodopsin gene. *Invest Ophthalmol Vis Sci,* 51**,** 6374-80.

GUAN, Y., ZHU, Q., HUANG, D., ZHAO, S., JAN LO, L. & PENG, J. 2015. An equation to estimate the difference between theoretically predicted and SDS PAGE-displayed molecular weights for an acidic peptide. *Scientific Reports,* 5**,** 13370.

GUREVICH, V. V., HANSON, S. M., SONG, X., VISHNIVETSKIY, S. A. & GUREVICH, E. V. 2011. The functional cycle of visual arrestins in photoreceptor cells. *Progress in retinal and eye research,* 30**,** 405-430.

HACKAM, A. S., QIAN, J., LIU, D., GUNATILAKA, T., FARKAS, R. H., CHOWERS, I., KAGEYAMA, M., PARMIGIANI, G. & ZACK, D. J. 2004. Comparative gene expression analysis of murine retina and brain. *Molecular Vision,* 10**,** 637-649.

HADDAD, S., CHEN, C. A., SANTANGELO, S. L. & SEDDON, J. M. 2006. The Genetics of Age-Related Macular Degeneration: A Review of Progress to Date. *Survey of Ophthalmology,* 51**,** 316-363.

HALE, I. L., FISHER, S. K. & MATSUMOTO, B. 1996. The actin network in the ciliary stalk of photoreceptors functions in the generation of new outer segment discs. *J Comp Neurol,* 376**,** 128-42.

HAMEED, A., KHALIQ, S., ISMAIL, M., ANWAR, K., MEHDI, S. Q., BESSANT, D., PAYNE, A. M. & BHATTACHARYA, S. S. 2001. A new locus for autosomal recessive RP (RP29) mapping to chromosome 4q32-q34 in a Pakistani family. *Invest Ophthalmol Vis Sci,* 42**,** 1436-8.

HARTONG, D. T., BERSON, E. L. & DRYJA, T. P. 2006. Retinitis pigmentosa. *The Lancet,* 368**,** 1795-1809.

HEE, M. R., IZATT, J. A., SWANSON, E. A., HUANG, D., SCHUMAN, J. S., LIN, C. P., PULIAFITO, C. A. & FUJIMOTO, J. G. 1995. Optical Coherence Tomography of the Human Retina. *Archives of Ophthalmology,* 113**,** 325-332.

HEKSELMAN, I. & YEGER-LOTEM, E. 2020. Mechanisms of tissue and cell-type specificity in heritable traits and diseases. *Nature Reviews Genetics,* 21**,** 137-150.

HENDERSON, R. H. 2020. Inherited retinal dystrophies. *Paediatrics and Child Health,* 30**,** 19-27.

HERMAN, M. M., PERENTES, E., KATSETOS, C. D., DARCEL, F., FRANKFURTER, A., COLLINS, V. P., DONOSO, L. A., ENG, L. F., MARANGOS, P. J., WIECHMANN, A. F. & ET AL. 1989. Neuroblastic differentiation potential of the human retinoblastoma cell lines Y-79 and WERI-Rb1 maintained in an organ culture system. An immunohistochemical, electron microscopic, and biochemical study. *The American journal of pathology,* 134**,** 115-132.

HIGGS, H. N. & POLLARD, T. D. 2001. Regulation of actin filament network formation through ARP2/3 complex: activation by a diverse array of proteins. *Annu Rev Biochem,* 70**,** 649-76.

HILDEBRAND, G. D. & FIELDER, A. R. 2011. Anatomy and physiology of the retina. *Pediatric retina.* Springer.

HINKLE, J. W., MAHMOUDZADEH, R. & KURIYAN, A. E. 2021. Cell-based therapies for retinal diseases: a review of clinical trials and direct to consumer "cell therapy" clinics. *Stem Cell Research & Therapy,* 12**,** 538.

HOLT, R., BROWN, L., BROADGATE, S., BUTLER, R., JAGANNATH, A., DOWNES, S., PEIRSON, S. & HALFORD, S. 2015. Identification of rod- and cone-specific expression signatures to identify candidate genes for retinal disease. *Experimental Eye Research,* 132**,** 161-173.

HOSUR, V., LOW, B. E., LI, D., STAFFORD, G. A., KOHAR, V., SHULTZ, L. D. & WILES, M. V. 2020. Genes adapt to outsmart gene-targeting strategies in mutant mouse strains by skipping exons to reinitiate transcription and translation. *Genome Biology,* 21**,** 168.

HSU, P. D., SCOTT, D. A., WEINSTEIN, J. A., RAN, F. A., KONERMANN, S., AGARWALA, V., LI, Y., FINE, E. J., WU, X., SHALEM, O., CRADICK, T. J., MARRAFFINI, L. A., BAO, G. & ZHANG, F. 2013. DNA targeting specificity of RNA-guided Cas9 nucleases. *Nat Biotechnol,* 31**,** 827-32.

HU, J., WANG, F., YUAN, Y., ZHU, X., WANG, Y., ZHANG, Y., KOU, Z., WANG, S. & GAO, S. 2010. Novel Importin-α Family Member Kpna7 Is Required for Normal Fertility and Fecundity in the Mouse*. *Journal of Biological Chemistry,* 285**,** 33113-33122.

HUANG, H., CHEN, Y., CHEN, H., MA, Y., CHIANG, P.-W., ZHONG, J., LIU, X., ASAN, WU, J., SU, Y., LI, X., DENG, J., HUANG, Y., ZHANG, X., LI, Y., FAN, N., WANG, Y., TANG, L., SHEN, J., CHEN, M., ZHANG, X., TE, D., BANERJEE, S., LIU, H., QI, M. & YI, X. 2018. Systematic evaluation of a targeted gene capture sequencing panel for molecular diagnosis of retinitis pigmentosa. *PLOS ONE,* 13**,** e0185237.

HUANG, X., ACARÓN LEDESMA, H. & WEI, W. 2020. Chapter 9 - Synapse formation in the developing vertebrate retina. *In:* RUBENSTEIN, J., RAKIC, P., CHEN, B., KWAN, K. Y., CLINE, H. T. & CARDIN, J. (eds.) *Synapse Development and Maturation.* Academic Press.

HWANG, Y. H., KIM, S.-W., KIM, Y. Y., NA, J. H., KIM, H. K. & SOHN, Y. H. 2012. Optic Nerve Head, Retinal Nerve Fiber Layer, and Macular Thickness Measurements in Young Patients with Retinitis Pigmentosa. *Current Eye Research,* 37**,** 914-920.

IAROSSI, G., MARINO, V., MALTESE, P. E., COLOMBO, L., D'ESPOSITO, F., MANARA, E., DHULI, K., MODARELLI, A. M., CENNAMO, G., MAGLI, A., DELL'ORCO, D. & BERTELLI, M. 2021. Expanding the Clinical and Genetic Spectrum of RAB28-Related Cone-Rod Dystrophy: Pathogenicity of Novel Variants in Italian Families. *International Journal of Molecular Sciences,* 22**,** 381.

IMAMOTO, Y. & SHICHIDA, Y. 2014. Cone visual pigments. *Biochimica et Biophysica Acta (BBA) - Bioenergetics,* 1837**,** 664-673.

INTERNATIONAL HUMAN GENOME SEQUENCING, C. 2004. Finishing the euchromatic sequence of the human genome. *Nature,* 431**,** 931-945.

ISHIKAWA, K., NAGASE, T., NAKAJIMA, D., SEKI, N., OHIRA, M., MIYAJIMA, N., TANAKA, A., KOTANI, H., NOMURA, N. & OHARA, O. 1997. Prediction of the coding sequences of unidentified human genes. VIII. 78 new cDNA clones from brain which code for large proteins in vitro. *DNA Res,* 4**,** 307-13.

ITAN, Y., SHANG, L., BOISSON, B., CIANCANELLI, M. J., MARKLE, J. G., MARTINEZ-BARRICARTE, R., SCOTT, E., SHAH, I., STENSON, P. D., GLEESON, J., COOPER, D. N., QUINTANA-MURCI, L., ZHANG, S.-Y., ABEL, L. & CASANOVA, J.-L. 2016. The mutation significance cutoff: gene-level thresholds for variant predictions. *Nature Methods,* 13**,** 109.

JACOBSON, S. G., CIDECIYAN, A. V., ROMAN, A. J., SUMAROKA, A., SCHWARTZ, S. B., HEON, E. & HAUSWIRTH, W. W. 2015. Improvement and decline in vision with gene therapy in childhood blindness. *New England Journal of Medicine,* 372**,** 1920-1926.

JAFFE, G. J. & CAPRIOLI, J. 2004. Optical coherence tomography to detect and manage retinal disease and glaucoma. *Am J Ophthalmol,* 137**,** 156-69.

JAMSHIDI, F., PLACE, E. M., MEHROTRA, S., NAVARRO-GOMEZ, D., MAHER, M., BRANHAM, K. E., VALKANAS, E., CHERRY, T. J., LEK, M., MACARTHUR, D., PIERCE, E. A. & BUJAKOWSKA, K. M. 2019. Contribution of noncoding pathogenic variants to RPGRIP1-mediated inherited retinal degeneration. *Genetics in medicine : official journal of the American College of Medical Genetics,* 21**,** 694-704.

JARRETT, S. G., LEWIN, A. S. & BOULTON, M. E. 2010. The importance of mitochondria in age-related and inherited eye disorders. *Ophthalmic Res,* 44**,** 179-90.

JEON, C. J., STRETTOI, E. & MASLAND, R. H. 1998. The major cell populations of the mouse retina. *The Journal of neuroscience : the official journal of the Society for Neuroscience,* 18**,** 8936-8946.

JIMENO, D., FEINER, L., LILLO, C., TEOFILO, K., GOLDSTEIN, L. S., PIERCE, E. A. & WILLIAMS, D. S. 2006. Analysis of kinesin-2 function in photoreceptor cells using synchronous Cre-loxP knockout of Kif3a with RHO-Cre. *Invest Ophthalmol Vis Sci,* 47**,** 5039-46.

JUNGE, H. J., YANG, S., BURTON, J. B., PAES, K., SHU, X., FRENCH, D. M., COSTA, M., RICE, D. S. & YE, W. 2009. TSPAN12 Regulates Retinal Vascular Development by Promoting Norrin- but Not Wnt-Induced FZD4/β-Catenin Signaling. *Cell,* 139**,** 299-311.

KAJIWARA, K., BERSON, E. L. & DRYJA, T. P. 1994. Digenic retinitis pigmentosa due to mutations at the unlinked peripherin/RDS and ROM1 loci. *Science,* 264**,** 1604-8.

KANNABIRAN, C., SINGH, H. P. & JALALI, S. 2012. Mapping of locus for autosomal dominant retinitis pigmentosa on chromosome 6q23. *Human Genetics,* 131**,** 717-723.

KATAGIRI, S., AKAHORI, M., SERGEEV, Y., YOSHITAKE, K., IKEO, K., FURUNO, M., HAYASHI, T., KONDO, M., UENO, S., TSUNODA, K., SHINODA, K., KUNIYOSHI, K., TSURUSAKI, Y., MATSUMOTO, N., TSUNEOKA, H. & IWATA, T. 2014. Whole exome analysis identifies frequent CNGA1 mutations in Japanese population with autosomal recessive retinitis pigmentosa. *PloS one,* 9**,** e108721-e108721.

KAWABATA GALBRAITH, K., FUJISHIMA, K., MIZUNO, H., LEE, S. J., UEMURA, T., SAKIMURA, K., MISHINA, M., WATANABE, N. & KENGAKU, M. 2018. MTSS1 Regulation of Actin-Nucleating Formin DAAM1 in Dendritic Filopodia Determines Final Dendritic Configuration of Purkinje Cells. *Cell Rep,* 24**,** 95-106.e9.

KELLEY, J. B., TALLEY, A. M., SPENCER, A., GIOELI, D. & PASCHAL, B. M. 2010. Karyopherin alpha7 (KPNA7), a divergent member of the importin alpha family of nuclear import receptors. *BMC Cell Biol,* 11**,** 63.

KENNAN, A., AHERNE, A., PALFI, A., HUMPHRIES, M., MCKEE, A., STITT, A., SIMPSON, D. A. C., DEMTRODER, K., ORNTOFT, T., AYUSO, C., KENNA, P. F., FARRAR, G. J. & HUMPHRIES, P. 2002. Identification of an IMPDH1 mutation in autosomal dominant retinitis pigmentosa (RP10) revealed following comparative microarray analysis of transcripts derived from retinas of wild-type and Rho-/- mice. *Human Molecular Genetics,* 11**,** 547-558.

KENT, W. J., SUGNET, C. W., FUREY, T. S., ROSKIN, K. M., PRINGLE, T. H., ZAHLER, A. M. & HAUSSLER, D. 2002. The human genome browser at UCSC. *Genome Res,* 12**,** 996-1006.

KHAN, M., FADAIE, Z., CORNELIS, S. S., CREMERS, F. P. M. & ROOSING, S. 2019. Identification and Analysis of Genes Associated with Inherited Retinal Diseases. *In:* WEBER, B. H. F. & LANGMANN, T. (eds.) *Retinal Degeneration: Methods and Protocols.* New York, NY: Springer New York.

KIM, J. W., YANG, H. J., BROOKS, M. J., ZELINGER, L., KARAKULAH, G., GOTOH, N., BOLEDA, A., GIESER, L., GIUSTE, F., WHITAKER, D. T., WALTON, A., VILLASMIL, R., BARB, J. J., MUNSON, P. J., KAYA, K. D., CHAITANKAR, V., COGLIATI, T. & SWAROOP, A. 2016. NRL-Regulated Transcriptome Dynamics of Developing Rod Photoreceptors. *Cell Rep,* 17**,** 2460-2473.

KIRCHER, M., WITTEN, D. M., JAIN, P., O'ROAK, B. J., COOPER, G. M. & SHENDURE, J. 2014. A general framework for estimating the relative pathogenicity of human genetic variants. *Nature Genetics,* 46**,** 310-315.

KÖHLER, S., DOELKEN, S. C., MUNGALL, C. J., BAUER, S., FIRTH, H. V., BAILLEUL-FORESTIER, I., BLACK, G. C. M., BROWN, D. L., BRUDNO, M., CAMPBELL, J., FITZPATRICK, D. R., EPPIG, J. T., JACKSON, A. P., FRESON, K., GIRDEA, M., HELBIG, I., HURST, J. A., JÄHN, J., JACKSON, L. G., KELLY, A. M., LEDBETTER, D. H., MANSOUR, S., MARTIN, C. L., MOSS, C., MUMFORD, A., OUWEHAND, W. H., PARK, S.-M., RIGGS, E. R., SCOTT, R. H., SISODIYA, S., VOOREN, S. V., WAPNER, R. J., WILKIE, A. O. M., WRIGHT, C. F., VULTO-VAN SILFHOUT, A. T., LEEUW, N. D., DE VRIES, B. B. A., WASHINGTHON, N. L., SMITH, C. L., WESTERFIELD, M., SCHOFIELD, P., RUEF, B. J., GKOUTOS, G. V., HAENDEL, M., SMEDLEY, D., LEWIS, S. E. & ROBINSON, P. N. 2013. The Human Phenotype Ontology project: linking molecular biology and disease through phenotype data. *Nucleic Acids Research,* 42**,** D966-D974.

KOLB, H. 1995. *In:* KOLB, H., FERNANDEZ, E. & NELSON, R. (eds.) *Webvision: The Organization of the Retina and Visual System.* Salt Lake City (UT): University of Utah Health Sciences Center

Copyright: © 2020 Webvision .

KRÄMER, F., WHITE, K., PAULEIKHOFF, D., GEHRIG, A., PASSMORE, L., RIVERA, A., RUDOLPH, G., KELLNER, U., ANDRASSI, M., LORENZ, B., ROHRSCHNEIDER, K., BLANKENAGEL, A., JURKLIES, B., SCHILLING, H., SCHÜTT, F., HOLZ, F. G. & WEBER, B. H. F. 2000. Mutations in the VMD2 gene are associated with juvenile-onset vitelliform macular dystrophy (Best disease) and adult vitelliform macular dystrophy but not age-related macular degeneration. *European Journal of Human Genetics,* 8**,** 286-292.

KUMAR, N., ZHAO, P., TOMAR, A., GALEA, C. A. & KHURANA, S. 2004. Association of villin with phosphatidylinositol 4,5-bisphosphate regulates the actin cytoskeleton. *J Biol Chem,* 279**,** 3096-110.

KUMAR, P., HENIKOFF, S. & NG, P. C. 2009. Predicting the effects of coding non-synonymous variants on protein function using the SIFT algorithm. *Nature Protocols,* 4**,** 1073-1081.

LAMB, T. D. & PUGH, E. N., JR 2006. Phototransduction, Dark Adaptation, and Rhodopsin Regeneration The Proctor Lecture. *Investigative Ophthalmology & Visual Science,* 47**,** 5138-5152.

LATASIEWICZ, M., SALVETTI, A. P. & MACLAREN, R. E. 2017. A novel mutation in the dominantly inherited TOPORS gene supports haploinsufficiency as the mechanism of retinitis pigmentosa. *Ophthalmic Genetics,* 38**,** 562-566.

LEE, S. H., KERFF, F., CHEREAU, D., FERRON, F., KLUG, A. & DOMINGUEZ, R. 2007. Structural basis for the actin-binding function of missing-in-metastasis. *Structure (London, England : 1993),* 15**,** 145-155.

LEE, Y. G., MACOSKA, J. A., KORENCHUK, S. & PIENTA, K. J. 2002. MIM, a potential metastasis suppressor gene in bladder cancer. *Neoplasia,* 4**,** 291-4.

LENGSFELD, A. M., LÖW, I., WIELAND, T., DANCKER, P. & HASSELBACH, W. 1974. Interaction of Phalloidin with Actin. *Proceedings of the National Academy of Sciences,* 71**,** 2803-2807.

LÉVEILLARD, T., MOHAND-SAÏD, S., LORENTZ, O., HICKS, D., FINTZ, A.-C., CLÉRIN, E., SIMONUTTI, M., FORSTER, V., CAVUSOGLU, N., CHALMEL, F., DOLLÉ, P., POCH, O., LAMBROU, G. & SAHEL, J.-A. 2004. Identification and characterization of rod-derived cone viability factor. *Nature Genetics,* 36**,** 755-759.

LEVINE, F. 2017. 1 - Basic Genetic Principles. *In:* POLIN, R. A., ABMAN, S. H., ROWITCH, D. H., BENITZ, W. E. & FOX, W. W. (eds.) *Fetal and Neonatal Physiology (Fifth Edition).* Elsevier.

LI, Z.-Y., POSSIN, D. E. & MILAM, A. H. 1995. Histopathology of Bone Spicule Pigmentation in Retinitis Pigmentosa. *Ophthalmology,* 102**,** 805-816.

LIM, L. S., MITCHELL, P., SEDDON, J. M., HOLZ, F. G. & WONG, T. Y. 2012. Age-related macular degeneration. *The Lancet,* 379**,** 1728-1738.

LIN, J., LIU, J., WANG, Y., ZHU, J., ZHOU, K., SMITH, N. & ZHAN, X. 2005. Differential regulation of cortactin and N-WASP-mediated actin polymerization by missing in metastasis (MIM) protein. *Oncogene,* 24**,** 2059-66.

LIN, Y.-C., BOONE, M., MEURIS, L., LEMMENS, I., VAN ROY, N., SOETE, A., REUMERS, J., MOISSE, M., PLAISANCE, S., DRMANAC, R., CHEN, J., SPELEMAN, F., LAMBRECHTS, D., VAN DE PEER, Y., TAVERNIER, J. & CALLEWAERT, N. 2014. Genome dynamics of the human embryonic kidney 293 lineage in response to cell biology manipulations. *Nature Communications,* 5**,** 4767.

LIU, G., LIU, X., LI, H., DU, Q. & WANG, F. 2016. Optical Coherence Tomographic Analysis of Retina in Retinitis Pigmentosa Patients. *Ophthalmic Res,* 56**,** 111-22.

LIU, Q., ZHOU, J., DAIGER, S. P., FARBER, D. B., HECKENLIVELY, J. R., SMITH, J. E., SULLIVAN, L. S., ZUO, J., MILAM, A. H. & PIERCE, E. A. 2002. Identification and subcellular localization of the RP1 protein in human and mouse photoreceptors. *Invest Ophthalmol Vis Sci,* 43**,** 22-32.

LIU, Y., GONZÀLEZ-PORTA, M., SANTOS, S., BRAZMA, A., MARIONI, J. C., AEBERSOLD, R., VENKITARAMAN, A. R. & WICKRAMASINGHE, V. O. 2017. Impact of Alternative Splicing on the Human Proteome. *Cell Rep,* 20**,** 1229-1241.

LOBERG, R. D., NEELEY, C. K., ADAM-DAY, L. L., FRIDMAN, Y., ST JOHN, L. N., NIXDORF, S., JACKSON, P., KALIKIN, L. M. & PIENTA, K. J. 2005. Differential expression analysis of MIM (MTSS1) splice variants and a functional role of MIM in prostate cancer cell biology. *Int J Oncol,* 26**,** 1699-705.

LONDON, A., BENHAR, I. & SCHWARTZ, M. 2013. The retina as a window to the brain-from eye research to CNS disorders. *Nat Rev Neurol,* 9**,** 44-53.

LUKOWSKI, S. W., LO, C. Y., SHAROV, A. A., NGUYEN, Q., FANG, L., HUNG, S. S., ZHU, L., ZHANG, T., GRÜNERT, U., NGUYEN, T., SENABOUTH, A., JABBARI, J. S., WELBY, E., SOWDEN, J. C., WAUGH, H. S., MACKEY, A., POLLOCK, G., LAMB, T. D., WANG, P. Y., HEWITT, A. W., GILLIES, M. C., POWELL, J. E. & WONG, R. C. 2019. A single-cell transcriptome atlas of the adult human retina. *Embo j,* 38**,** e100811.

MACKAY, D. S., HENDERSON, R. H., SERGOUNIOTIS, P. I., LI, Z., MORADI, P., HOLDER, G. E., WASEEM, N., BHATTACHARYA, S. S., ALDAHMESH, M. A., ALKURAYA, F. S., MEYER, B., WEBSTER, A. R. & MOORE, A. T. 2010. Novel mutations in MERTK associated with childhood onset rod-cone dystrophy. *Mol Vis,* 16**,** 369-77.

MACLAREN, R. E., GROPPE, M., BARNARD, A. R., COTTRIALL, C. L., TOLMACHOVA, T., SEYMOUR, L., CLARK, K. R., DURING, M. J., CREMERS, F. P. M., BLACK, G. C. M., LOTERY, A. J., DOWNES, S. M., WEBSTER, A. R. & SEABRA, M. C. 2014. Retinal gene therapy in patients with choroideremia: initial findings from a phase 1/2 clinical trial. *The Lancet,* 383**,** 1129-1137.

MAEDER, M. L., STEFANIDAKIS, M., WILSON, C. J., BARAL, R., BARRERA, L. A., BOUNOUTAS, G. S., BUMCROT, D., CHAO, H., CIULLA, D. M., DASILVA, J. A., DASS, A., DHANAPAL, V., FENNELL, T. J., FRIEDLAND, A. E., GIANNOUKOS, G., GLOSKOWSKI, S. W., GLUCKSMANN, A., GOTTA, G. M., JAYARAM, H., HASKETT, S. J., HOPKINS, B., HORNG, J. E., JOSHI, S., MARCO, E., MEPANI, R., REYON, D., TA, T., TABBAA, D. G., SAMUELSSON, S. J., SHEN, S., SKOR, M. N., STETKIEWICZ, P., WANG, T., YUDKOFF, C., MYER, V. E., ALBRIGHT, C. F. & JIANG, H. 2019. Development of a

gene-editing approach to restore vision loss in Leber congenital amaurosis type 10. *Nature Medicine,* 25**,** 229-233.

MARSZALEK, J. R., LIU, X., ROBERTS, E. A., CHUI, D., MARTH, J. D., WILLIAMS, D. S. & GOLDSTEIN, L. S. 2000. Genetic evidence for selective transport of opsin and arrestin by kinesin-II in mammalian photoreceptors. *Cell,* 102**,** 175-87.

MARTÍNEZ MIR, A., PALOMA, E., ALLIKMETS, R., AYUSO, C., RÍO, T. D., DEAN, M., VILAGELIU, L., GONZÀLEZ-DUARTE, R. & BALCELLS, S. 1998. Retinitis pigmentosa caused by a homozygous mutation in the Stargardt disease gene ABCR.

MATTAPALLIL, M. J., WAWROUSEK, E. F., CHAN, C. C., ZHAO, H., ROYCHOUDHURY, J., FERGUSON, T. A. & CASPI, R. R. 2012. The Rd8 mutation of the Crb1 gene is present in vendor lines of C57BL/6N mice and embryonic stem cells, and confounds ocular induced mutant phenotypes. *Invest Ophthalmol Vis Sci,* 53**,** 2921-7.

MATTILA, P. K., PYKÄLÄINEN, A., SAARIKANGAS, J., PAAVILAINEN, V. O., VIHINEN, H., JOKITALO, E. & LAPPALAINEN, P. 2007. Missing-in-metastasis and IRSp53 deform PI(4,5)P2-rich membranes by an inverse BAR domain-like mechanism. *J Cell Biol,* 176**,** 953-64.

MATTILA, P. K., SALMINEN, M., YAMASHIRO, T. & LAPPALAINEN, P. 2003. Mouse MIM, a tissue-specific regulator of cytoskeletal dynamics, interacts with ATP-actin monomers through its C-terminal WH2 domain. *J Biol Chem,* 278**,** 8452-9.

MAW, M. A., CORBEIL, D., KOCH, J., HELLWIG, A., WILSON-WHEELER, J. C., BRIDGES, R. J., KUMARAMANICKAVEL, G., JOHN, S., NANCARROW, D., RÖPER, K., WEIGMANN, A., HUTTNER, W. B. & DENTON, M. J. 2000. A frameshift mutation in prominin (mouse)-like 1 causes human retinal degeneration. *Human Molecular Genetics,* 9**,** 27-34.

MAZZILLI, J. L., SNOOK, J. D., SIMMONS, K., DOMOZHIROV, A. Y., GARCIA, C. A., WETSEL, R. A., ZSIGMOND, E. M. & WESTENSKOW, P. D. 2020. A Preclinical Safety Study of Human Embryonic Stem Cell-Derived Retinal Pigment Epithelial Cells for Macular Degeneration. *J Ocul Pharmacol Ther,* 36**,** 65-69.

MCCARTHY, J. J. & MENDELSOHN, B. A. 2016. Interpreting the Pathogenicity of Genetic Variants. *Precision Medicine: A Guide to Genomics in Clinical Practice.* New York, NY: McGraw-Hill Education.

MCFALL, R. C., SERY, T. W. & MAKADON, M. 1977. Characterization of a new continuous cell line derived from a human retinoblastoma. *Cancer Res,* 37**,** 1003-10.

MÉJÉCASE, C., LAURENT-CORIAT, C., MAYER, C., POCH, O., MOHAND-SAÏD, S., PRÉVOT, C., ANTONIO, A., BOYARD, F., CONDROYER, C., MICHIELS, C., BLANCHARD, S., LETEXIER, M., SARAIVA, J. P., SAHEL, J. A., AUDO, I. & ZEITZ, C. 2016. Identification of a Novel Homozygous Nonsense Mutation Confirms the Implication of GNAT1 in Rod-Cone Dystrophy. *PLoS One,* 11**,** e0168271.

MELLOUGH, C. B., STEEL, D. H. W. & LAKO, M. 2009. Genetic Basis of Inherited Macular Dystrophies and Implications for Stem Cell Therapy. *STEM CELLS,* 27**,** 2833-2845.

MENON, M., MOHAMMADI, S., DAVILA-VELDERRAIN, J., GOODS, B. A., CADWELL, T. D., XING, Y., STEMMER-RACHAMIMOV, A., SHALEK, A. K., LOVE, J. C., KELLIS, M. & HAFLER, B. P. 2019. Single-cell transcriptomic atlas of the human retina identifies cell types associated with age-related macular degeneration. *Nat Commun,* 10**,** 4902.

MINKEVICIENE, R., HLUSHCHENKO, I., VIRENQUE, A., LAHTI, L., KHANAL, P., RAURAMAA, T., KOISTINEN, A., LEINONEN, V., NOE, F. M. & HOTULAINEN, P. 2019. MIM-Deficient Mice Exhibit Anatomical Changes in Dendritic Spines, Cortex Volume and Brain Ventricles, and Functional Changes in Motor Coordination and Learning. *Frontiers in Molecular Neuroscience,* 12.

MOLDAY, R. S. & MORITZ, O. L. 2015. Photoreceptors at a glance. *J Cell Sci,* 128**,** 4039-45.

MORDES, D., LUO, X., KAR, A., KUO, D., XU, L., FUSHIMI, K., YU, G., STERNBERG, P., JR. & WU, J. Y. 2006. Pre-mRNA splicing and retinitis pigmentosa. *Molecular vision,* 12**,** 1259-1271.

MORIMURA, H., FISHMAN, G. A., GROVER, S. A., FULTON, A. B., BERSON, E. L. & DRYJA, T. P. 1998. Mutations in the RPE65 gene in patients with autosomal recessive retinitis pigmentosa or leber congenital amaurosis. *Proc Natl Acad Sci U S A,* 95**,** 3088-93.

MOTTA, F. L., MARTIN, R. P., PORTO, F. B. O., WOHLER, E. S., RESENDE, R. G., GOMES, C. P., PESQUERO, J. B. & SALLUM, J. M. F. 2019. Pathogenicity Reclasssification of RPE65 Missense Variants Related to Leber Congenital Amaurosis and Early-Onset Retinal Dystrophy. *Genes,* 11**,** 24.

MÜLLER, T., HESS, M. W., SCHIEFERMEIER, N., PFALLER, K., EBNER, H. L., HEINZ-ERIAN, P., PONSTINGL, H., PARTSCH, J., RÖLLINGHOFF, B., KÖHLER, H., BERGER, T., LENHARTZ, H., SCHLENCK, B., HOUWEN, R. J., TAYLOR, C. J., ZOLLER, H., LECHNER, S., GOULET, O., UTERMANN, G., RUEMMELE, F. M., HUBER, L. A. & JANECKE, A. R. 2008. MYO5B mutations cause microvillus inclusion disease and disrupt epithelial cell polarity. *Nature Genetics,* 40**,** 1163-1165.

MURTHY, R. K., HAJI, S., SAMBHAV, K., GROVER, S. & CHALAM, K. V. 2016. Clinical applications of spectral domain optical coherence tomography in retinal diseases. *Biomedical Journal,* 39**,** 107-120.

NA, K.-H., KIM, H. J., KIM, K. H., HAN, S., KIM, P., HANN, H. J. & AHN, H. S. 2017. Prevalence, Age at Diagnosis, Mortality, and Cause of Death in Retinitis Pigmentosa in Korea—A Nationwide Population-based Study. *American Journal of Ophthalmology,* 176**,** 157-165.

NAKAZAWA, M., WADA, Y. & TAMAI, M. 1998. Arrestin Gene Mutations in Autosomal Recessive Retinitis Pigmentosa. *Archives of Ophthalmology,* 116**,** 498-501.

NANGIA, V., JONAS, J. B., KHARE, A. & SINHA, A. 2012. Prevalence of retinitis pigmentosa in India: the Central India Eye and Medical Study. *Acta Ophthalmologica,* 90**,** e649-e650.

NARAYAN, D. S., WOOD, J. P., CHIDLOW, G. & CASSON, R. J. 2016. A review of the mechanisms of cone degeneration in retinitis pigmentosa. *Acta Ophthalmol,* 94**,** 748-754.

NATHANS, J., PIANTANIDA, T. P., EDDY, R. L., SHOWS, T. B. & HOGNESS, D. S. 1986a. Molecular genetics of inherited variation in human color vision. *Science,* 232**,** 203-210.

NATHANS, J., THOMAS, D. & HOGNESS, D. 1986b. Molecular genetics of human color vision: the genes encoding blue, green, and red pigments. *Science,* 232**,** 193-202.

NEMET, I., TIAN, G. & IMANISHI, Y. 2014. Submembrane Assembly and Renewal of Rod Photoreceptor cGMP-Gated Channel: Insight into the Actin-Dependent Process of Outer Segment Morphogenesis. *The Journal of Neuroscience,* 34**,** 8164.

NIKOPOULOS, K., GILISSEN, C., HOISCHEN, A., ERIK VAN NOUHUYS, C., BOONSTRA, F. N., BLOKLAND, E. A. W., ARTS, P., WIESKAMP, N., STROM, T. M., AYUSO, C., TILANUS, M. A. D., BOUWHUIS, S., MUKHOPADHYAY, A., SCHEFFER, H., HOEFSLOOT, L. H., VELTMAN, J. A., CREMERS, F. P. M. & COLLIN, R. W. J. 2010. Next-Generation Sequencing of a 40 Mb Linkage Interval Reveals

TSPAN12 Mutations in Patients with Familial Exudative Vitreoretinopathy. *The American Journal of Human Genetics,* 86**,** 240-247.

NIXDORF, S., GRIMM, M.-O., LOBERG, R., MARREIROS, A., RUSSELL, P. J., PIENTA, K. J. & JACKSON, P. 2004. Expression and regulation of MIM (Missing In Metastasis), a novel putative metastasis suppressor gene, and MIM-B, in bladder cancer cell lines. *Cancer Letters,* 215**,** 209-220.

NOAILLES, A., MANEU, V., CAMPELLO, L., GÓMEZ-VICENTE, V., LAX, P. & CUENCA, N. 2016. Persistent inflammatory state after photoreceptor loss in an animal model of retinal degeneration. *Scientific Reports,* 6**,** 33356.

NUSSBAUM, R. L., LEWIS, R. A., LESKO, J. G. & FERRELL, R. 1985. Choroideremia is linked to the restriction fragment length polymorphism DXYS1 at XQ13-21. *American journal of human genetics,* 37**,** 473-481.

OOSTDYK, L. T., MCCONNELL, M. J. & PASCHAL, B. M. 2019. Characterization of the Importin-β binding domain in nuclear import receptor KPNA7. *Biochemical Journal,* 476**,** 3413-3434.

OSHIKAWA, M., TSUTSUI, C., IKEGAMI, T., FUCHIDA, Y., MATSUBARA, M., TOYAMA, S., USAMI, R., OHTOKO, K. & KATO, S. 2011. Full-Length Transcriptome Analysis of Human Retina-Derived Cell Lines ARPE-19 and Y79 Using the Vector-Capping Method. *Investigative Ophthalmology & Visual Science,* 52**,** 6662-6670.

OTA, T., SUZUKI, Y., NISHIKAWA, T., OTSUKI, T., SUGIYAMA, T., IRIE, R., WAKAMATSU, A., HAYASHI, K., SATO, H., NAGAI, K., KIMURA, K., MAKITA, H., SEKINE, M., OBAYASHI, M., NISHI, T., SHIBAHARA, T., TANAKA, T., ISHII, S., YAMAMOTO, J.-I., SAITO, K., KAWAI, Y., ISONO, Y., NAKAMURA, Y., NAGAHARI, K., MURAKAMI, K., YASUDA, T., IWAYANAGI, T., WAGATSUMA, M., SHIRATORI, A., SUDO, H., HOSOIRI, T., KAKU, Y., KODAIRA, H., KONDO, H., SUGAWARA, M., TAKAHASHI, M., KANDA, K., YOKOI, T., FURUYA, T., KIKKAWA, E., OMURA, Y., ABE, K., KAMIHARA, K., KATSUTA, N., SATO, K., TANIKAWA, M., YAMAZAKI, M., NINOMIYA, K., ISHIBASHI, T., YAMASHITA, H., MURAKAWA, K., FUJIMORI, K., TANAI, H., KIMATA, M., WATANABE, M., HIRAOKA, S., CHIBA, Y., ISHIDA, S., ONO, Y., TAKIGUCHI, S., WATANABE, S., YOSIDA, M., HOTUTA, T., KUSANO, J., KANEHORI, K., TAKAHASHI-FUJII, A., HARA, H., TANASE, T.-O., NOMURA, Y., TOGIYA, S., KOMAI, F., HARA, R., TAKEUCHI, K., ARITA, M., IMOSE, N., MUSASHINO, K., YUUKI, H., OSHIMA, A., SASAKI, N., AOTSUKA, S., YOSHIKAWA, Y., MATSUNAWA, H., ICHIHARA, T., SHIOHATA, N., SANO, S., MORIYA, S., MOMIYAMA, H., SATOH, N., TAKAMI, S., TERASHIMA, Y., SUZUKI, O., NAKAGAWA, S., SENOH, A., MIZOGUCHI, H., GOTO, Y., SHIMIZU, F., WAKEBE, H., HISHIGAKI, H., WATANABE, T., SUGIYAMA, A., et al. 2004. Complete sequencing and characterization of 21,243 full-length human cDNAs. *Nature Genetics,* 36**,** 40-45.

PACIORKOWSKI, A. R., WEISENBERG, J., KELLEY, J. B., SPENCER, A., TUTTLE, E., GHONEIM, D., THIO, L. L., CHRISTIAN, S. L., DOBYNS, W. B. & PASCHAL, B. M. 2014. Autosomal recessive mutations in nuclear transport factor KPNA7 are associated with infantile spasms and cerebellar malformation. *Eur J Hum Genet,* 22**,** 587-93.

PADNICK-SILVER, L., DERWENT, J. J. K., GIULIANO, E., NARFSTRÖM, K. & LINSENMEIER, R. A. 2006. Retinal Oxygenation and Oxygen Metabolism in Abyssinian Cats with a Hereditary Retinal Degeneration. *Investigative Ophthalmology & Visual Science,* 47**,** 3683-3689.

PALCZEWSKI, K. 2006. G Protein–Coupled Receptor Rhodopsin. *Annual Review of Biochemistry,* 75**,** 743-767.

PAN, Q., SHAI, O., LEE, L. J., FREY, B. J. & BLENCOWE, B. J. 2008. Deep surveying of alternative splicing complexity in the human transcriptome by high-throughput sequencing. *Nat Genet,* 40**,** 1413-5.

PAN, W. W., WUBBEN, T. J. & BESIRLI, C. G. 2021. Photoreceptor metabolic reprogramming: current understanding and therapeutic implications. *Commun Biol,* 4**,** 245.

PARFITT, D. A., LANE, A., RAMSDEN, C. M., CARR, A. F., MUNRO, P. M., JOVANOVIC, K., SCHWARZ, N., KANUGA, N., MUTHIAH, M. N., HULL, S., GALLO, J. M., DA CRUZ, L., MOORE, A. T., HARDCASTLE, A. J., COFFEY, P. J. & CHEETHAM, M. E. 2016. Identification and Correction of Mechanisms Underlying Inherited Blindness in Human iPSC-Derived Optic Cups. *Cell Stem Cell,* 18**,** 769-781.

PARINOT, C. & NANDROT, E. F. A Comprehensive Review of Mutations in the MERTK Proto-Oncogene. *In:* BOWES RICKMAN, C., LAVAIL, M. M., ANDERSON, R. E., GRIMM, C., HOLLYFIELD, J. & ASH, J., eds. Retinal Degenerative Diseases, 2016// 2016 Cham. Springer International Publishing, 259-265.

PARK, Y. H., SNOOK, J. D., ZHUANG, I., SHEN, G. & FRANKFORT, B. J. 2020. Optimized culture of retinal ganglion cells and amacrine cells from adult mice. *PLOS ONE,* 15**,** e0242426.

PAUNOLA, E., MATTILA, P. K. & LAPPALAINEN, P. 2002. WH2 domain: a small, versatile adapter for actin monomers. *FEBS Lett,* 513**,** 92-7.

PAZOUR, G. J., BAKER, S. A., DEANE, J. A., COLE, D. G., DICKERT, B. L., ROSENBAUM, J. L., WITMAN, G. B. & BESHARSE, J. C. 2002. The intraflagellar transport protein, IFT88, is essential for vertebrate photoreceptor assembly and maintenance. *J Cell Biol,* 157**,** 103-13.

PEARRING, J. N., SALINAS, R. Y., BAKER, S. A. & ARSHAVSKY, V. Y. 2013. Protein sorting, targeting and trafficking in photoreceptor cells. *Progress in Retinal and Eye Research,* 36**,** 24-51.

PEDDLE, C. F. & MACLAREN, R. E. 2017. The Application of CRISPR/Cas9 for the Treatment of Retinal Diseases. *Yale J Biol Med,* 90**,** 533-541.

PENN, J. S., LI, S. & NAASH, M. I. 2000. Ambient hypoxia reverses retinal vascular attenuation in a transgenic mouse model of autosomal dominant retinitis pigmentosa. *Investigative Ophthalmology and Visual Science,* 41**,** 4007-4013.

PETER, B. J., KENT, H. M., MILLS, I. G., VALLIS, Y., BUTLER, P. J., EVANS, P. R. & MCMAHON, H. T. 2004. BAR domains as sensors of membrane curvature: the amphiphysin BAR structure. *Science,* 303**,** 495-9.

PETRUKHIN, K., KOISTI, M. J., BAKALL, B., LI, W., XIE, G., MARKNELL, T., SANDGREN, O., FORSMAN, K., HOLMGREN, G. & ANDREASSON, S. 1998. Identification of the gene responsible for Best macular dystrophy. *Nature genetics,* 19**,** 241-247.

PETRUS-REURER, S., KUMAR, P., PADRELL SÁNCHEZ, S., ARONSSON, M., ANDRÉ, H., BARTUMA, H., PLAZA REYES, A., NANDROT, E. F., KVANTA, A. & LANNER, F. 2020. Preclinical safety studies of human embryonic stem cell-derived retinal pigment epithelial cells for the treatment of age-related macular degeneration. *Stem Cells Transl Med,* 9**,** 936-953.

PIAO, L., NAKAGAWA, H., UEDA, K., CHUNG, S., KASHIWAYA, K., EGUCHI, H., OHIGASHI, H., ISHIKAWA, O., DAIGO, Y., MATSUDA, K. & NAKAMURA, Y. 2011. C12orf48, termed PARP-1 binding protein, enhances poly(ADP-ribose) polymerase-1 (PARP-1) activity and protects pancreatic cancer cells from DNA damage. *Genes Chromosomes Cancer,* 50**,** 13-24.

PIRES, D. E. V., BLUNDELL, T. L. & ASCHER, D. B. 2016. mCSM-lig: quantifying the effects of mutations on protein-small molecule affinity in genetic disease and emergence of drug resistance. *Scientific Reports,* 6**,** 29575.

POLYAK, S. L. 1941. The retina. . *Chicago: University of Chicago Press*.

PONTIKOS, N., ARNO, G., JURKUTE, N., SCHIFF, E., BA-ABBAD, R., MALKA, S., GIMENEZ, A., GEORGIOU, M., WRIGHT, G., ARMENGOL, M., KNIGHT, H., KATZ, M., MOOSAJEE, M., YU-WAI-MAN, P., MOORE, A. T., MICHAELIDES, M., WEBSTER, A. R. & MAHROO, O. A. 2020. Genetic Basis of Inherited Retinal Disease in a Molecularly Characterized Cohort of More Than 3000 Families from the United Kingdom. *Ophthalmology,* 127**,** 1384-1394.

POPOVA, E. Y., SALZBERG, A. C., YANG, C., ZHANG, S. S. & BARNSTABLE, C. J. 2017. Identification and prediction of alternative transcription start sites that generate rod photoreceptor-specific transcripts from ubiquitously expressed genes. *PLoS One,* 12**,** e0179230.

POULTER, J. A., ALI, M., GILMOUR, D. F., RICE, A., KONDO, H., HAYASHI, K., MACKEY, D. A., KEARNS, L. S., RUDDLE, J. B., CRAIG, J. E., PIERCE, E. A., DOWNEY, L. M., MOHAMED, M. D., MARKHAM, A. F., INGLEHEARN, C. F. & TOOMES, C. 2010. Mutations in TSPAN12 Cause Autosomal-Dominant Familial Exudative Vitreoretinopathy. *The American Journal of Human Genetics,* 86**,** 248-253.

PRITCHETT-CORNING, K. R., CLIFFORD, C. B., ELDER, B. J. & VEZINA, M. 2012. Retinal Lesions and Other Potential Confounders of Ocular Research in Inbred Mice. *Investigative Ophthalmology & Visual Science,* 53**,** 3764-3765.

PROVENCIO, I., JIANG, G., DE GRIP, W. J., HAYES, W. P. & ROLLAG, M. D. 1998. Melanopsin: An opsin in melanophores, brain, and eye. *Proceedings of the National Academy of Sciences,* 95**,** 340-345.

PROVENCIO, I., RODRIGUEZ, I. R., JIANG, G., HAYES, W. P., MOREIRA, E. F. & ROLLAG, M. D. 2000. A Novel Human Opsin in the Inner Retina. *The Journal of Neuroscience,* 20**,** 600-605.

PUNZO, C., KORNACKER, K. & CEPKO, C. L. 2009. Stimulation of the insulin/mTOR pathway delays cone death in a mouse model of retinitis pigmentosa. *Nature neuroscience,* 12**,** 44-52.

QIAN, X., WANG, J., WANG, M., IGELMAN, A. D., JONES, K. D., LI, Y., WANG, K., GOETZ, K. E., BIRCH, D. G., YANG, P., PENNESI, M. E. & CHEN, R. 2021. Identification of Deep-Intronic Splice Mutations in a Large Cohort of Patients With Inherited Retinal Diseases. *Frontiers in genetics,* 12**,** 647400-647400.

QUINN, J., MUSA, A., KANTOR, A., MCCLEMENTS, M. E., CEHAJIC-KAPETANOVIC, J., MACLAREN, R. E. & XUE, K. 2021. Genome-Editing Strategies for Treating Human Retinal Degenerations. *Human Gene Therapy,* 32**,** 247-259.

RAHMAN, N., GEORGIOU, M., KHAN, K. N. & MICHAELIDES, M. 2020. Macular dystrophies: clinical and imaging features, molecular genetics and therapeutic options. *The British journal of ophthalmology,* 104**,** 451-460.

RAMBHATLA, L., CHIU, C. P., GLICKMAN, R. D. & ROWE-RENDLEMAN, C. 2002. In vitro differentiation capacity of telomerase immortalized human RPE cells. *Invest Ophthalmol Vis Sci,* 43**,** 1622-30.

RAMKUMAR, H. L., GUDISEVA, H. V., KISHABA, K. T., SUK, J. J., VERMA, R., TADIMETI, K., THORSON, J. A. & AYYAGARI, R. 2017. A Report on Molecular Diagnostic Testing for Inherited Retinal Dystrophies by Targeted Genetic Analyses. *Genetic testing and molecular biomarkers,* 21**,** 66-73.

RAY, T. A., COCHRAN, K., KOZLOWSKI, C., WANG, J., ALEXANDER, G., CADY, M. A., SPENCER, W. J., RUZYCKI, P. A., CLARK, B. S., LAEREMANS, A., HE, M. X., WANG, X., PARK, E., HAO, Y., IANNACCONE, A., HU, G., FEDRIGO, O., SKIBA, N. P., ARSHAVSKY, V. Y. & KAY, J. N. 2020. Comprehensive identification of mRNA isoforms reveals the diversity of neural cell-surface molecules with roles in retinal development and disease. *Nat Commun,* 11**,** 3328.

REID, T. W., ALBERT, D. M., RABSON, A. S., RUSSELL, P., CRAFT, J., CHU, E. W., TRALKA, T. S. & WILCOX, J. L. 1974. Characteristics of an established cell line of retinoblastoma. *J Natl Cancer Inst,* 53**,** 347-60.

RICHARDS, S., AZIZ, N., BALE, S., BICK, D., DAS, S., GASTIER-FOSTER, J., GRODY, W. W., HEGDE, M., LYON, E., SPECTOR, E., VOELKERDING, K. & REHM, H. L. 2015. Standards and guidelines for the interpretation of sequence variants: a joint consensus recommendation of the American College of Medical Genetics and Genomics and the Association for Molecular Pathology. *Genetics in Medicine,* 17**,** 405-424.

RIEMANN, C. D., BANIN, E., BARAK, A., BOYER, D. S., EHRLICH, R., JAOUNI, T., MCDONALD, R., TELANDER, D., KEANE, M., ACKERT, J., FERGUSON, M. D., SHABAT, A. B.-., MONES, J., ANGELINI, D., HOGGE, G. S. & REUBINOFF, B. 2020. Phase I/IIa Clinical Trial of Human Embryonic Stem Cell (hESC)-Derived Retinal Pigmented Epithelium (RPE, OpRegen) Transplantation in Advanced Dry Form Age-Related Macular Degeneration (AMD): Interim Results. *Investigative Ophthalmology & Visual Science,* 61**,** 865-865.

RINALDI, C. & WOOD, M. J. A. 2018. Antisense oligonucleotides: the next frontier for treatment of neurological disorders. *Nature Reviews Neurology,* 14**,** 9-21.

RIPPS, H. 2002. Cell death in retinitis pigmentosa: gap junctions and the 'bystander' effect. *Exp Eye Res,* 74**,** 327-36.

ROBSON, J. G., SASZIK, S. M., AHMED, J. & FRISHMAN, L. J. 2003. Rod and cone contributions to the a-wave of the electroretinogram of the macaque. *The Journal of physiology,* 547**,** 509-530.

RODIECK, R. W. 1998. *The first steps in seeing*, Sinauer Associates Sunderland, MA.

ROOSING, S., ROHRSCHNEIDER, K., BERYOZKIN, A., SHARON, D., WEISSCHUH, N., STALLER, J., KOHL, S., ZELINGER, L., PETERS, T. A., NEVELING, K., STROM, T. M., VAN DEN BORN, L. I., HOYNG, C. B., KLAVER, C. C., ROEPMAN, R., WISSINGER, B., BANIN, E., CREMERS, F. P. & DEN HOLLANDER, A. I. 2013. Mutations in RAB28, encoding a farnesylated small GTPase, are associated with autosomal-recessive cone-rod dystrophy. *Am J Hum Genet,* 93**,** 110-7.

ROSENFELD, P. J., COWLEY, G. S., MCGEE, T. L., SANDBERG, M. A., BERSON, E. L. & DRYJA, T. P. 1992. A Null mutation in the rhodopsin gene causes rod photoreceptor dysfunction and autosomal recessive retinitis pigmentosa. *Nature Genetics,* 1**,** 209-213.

RUIZ, A., KUEHN, M. H., ANDORF, J. L., STONE, E., HAGEMAN, G. S. & BOK, D. 2001. Genomic Organization and Mutation Analysis of the Gene Encoding Lecithin Retinol Acyltransferase in Human Retinal Pigment Epithelium. *Investigative Ophthalmology & Visual Science,* 42**,** 31-37.

RUSSELL, S., BENNETT, J., WELLMAN, J. A., CHUNG, D. C., YU, Z.-F., TILLMAN, A., WITTES, J., PAPPAS, J., ELCI, O., MCCAGUE, S., CROSS, D., MARSHALL, K. A., WALSHIRE, J., KEHOE, T. L., REICHERT, H., DAVIS, M., RAFFINI, L., GEORGE, L. A., HUDSON, F. P., DINGFIELD, L., ZHU, X., HALLER, J. A., SOHN, E. H., MAHAJAN, V. B., PFEIFER, W., WECKMANN, M., JOHNSON, C., GEWAILY, D., DRACK, A., STONE, E., WACHTEL, K., SIMONELLI, F., LEROY, B. P., WRIGHT, J. F., HIGH, K. A. & MAGUIRE, A. M. 2017. Efficacy and safety of voretigene neparvovec (AAV2-hRPE65v2) in

patients with RPE65-mediated inherited retinal dystrophy: a randomised, controlled, open-label, phase 3 trial. *The Lancet,* 390**,** 849-860.

SAARIKANGAS, J., KOURDOUGLI, N., SENJU, Y., CHAZAL, G., SEGERSTRALE, M., MINKEVICIENE, R., KUURNE, J., MATTILA, P. K., GARRETT, L., HOLTER, S. M., BECKER, L., RACZ, I., HANS, W., KLOPSTOCK, T., WURST, W., ZIMMER, A., FUCHS, H., GAILUS-DURNER, V., HRABE DE ANGELIS, M., VON OSSOWSKI, L., TAIRA, T., LAPPALAINEN, P., RIVERA, C. & HOTULAINEN, P. 2015. MIM-Induced Membrane Bending Promotes Dendritic Spine Initiation. *Dev Cell,* 33**,** 644-59.

SAARIKANGAS, J., MATTILA, P. K., VARJOSALO, M., BOVELLAN, M., HAKANEN, J., CALZADA-WACK, J., TOST, M., JENNEN, L., RATHKOLB, B., HANS, W., HORSCH, M., HYVÖNEN, M. E., PERÄLÄ, N., FUCHS, H., GAILUS-DURNER, V., ESPOSITO, I., WOLF, E., DE ANGELIS, M. H., FRILANDER, M. J., SAVILAHTI, H., SARIOLA, H., SAINIO, K., LEHTONEN, S., TAIPALE, J., SALMINEN, M. & LAPPALAINEN, P. 2011. Missing-in-metastasis MIM/MTSS1 promotes actin assembly at intercellular junctions and is required for integrity of kidney epithelia. *J Cell Sci,* 124**,** 1245-55.

SAISHIN, Y., ISHIKAWA, R., UGAWA, S., GUO, W., UEDA, T., MORIMURA, H., KOHAMA, K., SHIMIZU, H., TANO, Y. & SHIMADA, S. 2000. Retinal fascin: Functional nature, subcellular distribution, and chromosomal localization. *Investigative Ophthalmology and Visual Science,* 41**,** 2087-2095.

SALE, W. S., BESHARSE, J. C. & PIPERNO, G. 1988. Distribution of acetylated α-tubulin in retina and in in vitro—assembled microtubules. *Cell Motility,* 9**,** 243-253.

SANGER, F., NICKLEN, S. & COULSON, A. R. 1977. DNA sequencing with chain-terminating inhibitors. *Proc Natl Acad Sci U S A,* 74**,** 5463-7.

SANJURJO-SORIANO, C. & KALATZIS, V. 2018. Guiding Lights in Genome Editing for Inherited Retinal Disorders: Implications for Gene and Cell Therapy. *Neural Plast,* 2018**,** 5056279.

SARIC, A., FREEMAN, S. A., WILLIAMSON, C. D., JARNIK, M., GUARDIA, C. M., FERNANDOPULLE, M. S., GERSHLICK, D. C. & BONIFACINO, J. S. 2021. SNX19 restricts endolysosome motility through contacts with the endoplasmic reticulum. *Nature Communications,* 12**,** 4552.

SCHACHAT, A. P., WILKINSON, C. P., HINTON, D. R., WIEDEMANN, P., FREUND, K. B. & SARRAF, D. 2017. *Ryan's retina e-book*, Elsevier Health Sciences.

SCHIERLING, B., DANNEMANN, N., GABSALILOW, L., WENDE, W., CATHOMEN, T. & PINGOUD, A. 2012. A novel zinc-finger nuclease platform with a sequence-specific cleavage module. *Nucleic Acids Res,* 40**,** 2623-38.

SCHULZ, H. L., GRASSMANN, F., KELLNER, U., SPITAL, G., RÜTHER, K., JÄGLE, H., HUFENDIEK, K., RATING, P., HUCHZERMEYER, C., BAIER, M. J., WEBER, B. H. F. & STÖHR, H. 2017. Mutation Spectrum of the ABCA4 Gene in 335 Stargardt Disease Patients From a Multicenter German Cohort—Impact of Selected Deep Intronic Variants and Common SNPs. *Investigative Ophthalmology & Visual Science,* 58**,** 394-403.

SCHWARTZ, S. D., REGILLO, C. D., LAM, B. L., ELIOTT, D., ROSENFELD, P. J., GREGORI, N. Z., HUBSCHMAN, J. P., DAVIS, J. L., HEILWELL, G., SPIRN, M., MAGUIRE, J., GAY, R., BATEMAN, J., OSTRICK, R. M., MORRIS, D., VINCENT, M., ANGLADE, E., DEL PRIORE, L. V. & LANZA, R. 2015. Human embryonic stem cell-derived retinal pigment epithelium in patients with age-related macular degeneration and Stargardt's macular dystrophy: follow-up of two open-label phase 1/2 studies. *Lancet,* 385**,** 509-16.

SCHWARZ, J. M., RÖDELSPERGER, C., SCHUELKE, M. & SEELOW, D. 2010. MutationTaster evaluates disease-causing potential of sequence alterations. *Nature Methods,* 7**,** 575-576.

SCHWARZE, K., BUCHANAN, J., TAYLOR, J. C. & WORDSWORTH, S. 2018. Are whole-exome and whole-genome sequencing approaches cost-effective? A systematic review of the literature. *Genetics in Medicine,* 20**,** 1122-1130.

SCOLES, D. R., MINIKEL, E. V. & PULST, S. M. 2019. Antisense oligonucleotides: A primer. *Neurol Genet,* 5**,** e323.

SCOTTO-LAVINO, E., DU, G. & FROHMAN, M. A. 2006. 5' end cDNA amplification using classic RACE. *Nat Protoc,* 1**,** 2555-62.

SHARMA, A. & JAGANATHAN, B. G. 2021. Stem Cell Therapy for Retinal Degeneration: The Evidence to Date. *Biologics : targets & therapy,* 15**,** 299-306.

SHARON, D., BLACKSHAW, S., CEPKO, C. L. & DRYJA, T. P. 2002. Profile of the genes expressed in the human peripheral retina, macula, and retinal pigment epithelium determined through serial analysis of gene expression (SAGE). *Proc Natl Acad Sci U S A,* 99**,** 315-20.

SHARON, D., SANDBERG, M. A., RABE, V. W., STILLBERGER, M., DRYJA, T. P. & BERSON, E. L. 2003. RP2 and RPGR Mutations and Clinical Correlations in Patients with X-Linked Retinitis Pigmentosa. *The American Journal of Human Genetics,* 73**,** 1131-1146.

SHAW, G., MORSE, S., ARARAT, M. & GRAHAM, F. L. 2002. Preferential transformation of human neuronal cells by human adenoviruses and the origin of HEK 293 cells. *The FASEB Journal,* 16**,** 869-871.

SHEN, J., YANG, X., DONG, A., PETTERS, R. M., PENG, Y.-W., WONG, F. & CAMPOCHIARO, P. A. 2005. Oxidative damage is a potential cause of cone cell death in retinitis pigmentosa. *Journal of Cellular Physiology,* 203**,** 457-464.

SIMON, M. M., GREENAWAY, S., WHITE, J. K., FUCHS, H., GAILUS-DURNER, V., WELLS, S., SORG, T., WONG, K., BEDU, E., CARTWRIGHT, E. J., DACQUIN, R., DJEBALI, S., ESTABEL, J., GRAW, J., INGHAM, N. J., JACKSON, I. J., LENGELING, A., MANDILLO, S., MARVEL, J., MEZIANE, H., PREITNER, F., PUK, O., ROUX, M., ADAMS, D. J., ATKINS, S., AYADI, A., BECKER, L., BLAKE, A., BROOKER, D., CATER, H., CHAMPY, M.-F., COMBE, R., DANECEK, P., DI FENZA, A., GATES, H., GERDIN, A.-K., GOLINI, E., HANCOCK, J. M., HANS, W., HÖLTER, S. M., HOUGH, T., JURDIC, P., KEANE, T. M., MORGAN, H., MÜLLER, W., NEFF, F., NICHOLSON, G., PASCHE, B., ROBERSON, L.-A., ROZMAN, J., SANDERSON, M., SANTOS, L., SELLOUM, M., SHANNON, C., SOUTHWELL, A., TOCCHINI-VALENTINI, G. P., VANCOLLIE, V. E., WESTERBERG, H., WURST, W., ZI, M., YALCIN, B., RAMIREZ-SOLIS, R., STEEL, K. P., MALLON, A.-M., DE ANGELIS, M. H., HERAULT, Y. & BROWN, S. D. M. 2013. A comparative phenotypic and genomic analysis of C57BL/6J and C57BL/6N mouse strains. *Genome biology,* 14**,** R82-R82.

SISTIG, T., LANG, F., WROBEL, S., BAADER, S. L., SCHILLING, K. & EIBERGER, B. 2017. Mtss1 promotes maturation and maintenance of cerebellar neurons via splice variant-specific effects. *Brain Struct Funct,* 222**,** 2787-2805.

SJOSTRAND, F. S. 1959. Fine Structure of Cytoplasm: The Organization of Membranous Layers. *Reviews of Modern Physics,* 31**,** 301-318.

SMITH, A. J., CARTER, S. P. & KENNEDY, B. N. 2017. Genome editing: the breakthrough technology for inherited retinal disease? *Expert Opinion on Biological Therapy,* 17**,** 1245-1254.

SMITH, R. S., RODERICK, T. H. & SUNDBERG, J. P. 1994. Microphthalmia and associated abnormalities in inbred black mice. *Lab Anim Sci,* 44**,** 551-60.

SPARROW, J. R., GREGORY-ROBERTS, E., YAMAMOTO, K., BLONSKA, A., GHOSH, S. K., UEDA, K. & ZHOU, J. 2012. The bisretinoids of retinal pigment epithelium. *Progress in Retinal and Eye Research,* 31**,** 121-135.

SPENCER, W. J., LEWIS, T. R., PHAN, S., CADY, M. A., SEREBROVSKAYA, E. O., SCHNEIDER, N. F., KIM, K.-Y., CAMERON, L. A., SKIBA, N. P., ELLISMAN, M. H. & ARSHAVSKY, V. Y. 2019. Photoreceptor disc membranes are formed through an Arp2/3-dependent lamellipodium-like mechanism. *Proceedings of the National Academy of Sciences,* 116**,** 27043.

STEPHENSON, M. L. & ZAMECNIK, P. C. 1978. Inhibition of Rous sarcoma viral RNA translation by a specific oligodeoxyribonucleotide. *Proceedings of the National Academy of Sciences of the United States of America,* 75**,** 285-288.

STRAND_NGS. 2021. *Storage and Computation Requirements.* [Online]. [Accessed Vistied on October 20, 2021].

STRAUSS, O. 2005. The retinal pigment epithelium in visual function. *Physiological reviews,* 85**,** 845-881.

STRAUSS, O. 2011. The Retinal Pigment Epithelium. *In: Kolb H, Fernandez E, Nelson R, editors. Webvision: The Organization of the Retina and Visual System [Internet]. Salt Lake City (UT): University of Utah Health Sciences Center; 1995-. Available from: https://www.ncbi.nlm.nih.gov/books/NBK54392/*.

STROM, S. P., CLARK, M. J., MARTINEZ, A., GARCIA, S., ABELAZEEM, A. A., MATYNIA, A., PARIKH, S., SULLIVAN, L. S., BOWNE, S. J., DAIGER, S. P. & GORIN, M. B. 2016. De Novo Occurrence of a Variant in ARL3 and Apparent Autosomal Dominant Transmission of Retinitis Pigmentosa. *PLoS One,* 11**,** e0150944.

SUETSUGU, S., MURAYAMA, K., SAKAMOTO, A., HANAWA-SUETSUGU, K., SETO, A., OIKAWA, T., MISHIMA, C., SHIROUZU, M., TAKENAWA, T. & YOKOYAMA, S. 2006. The RAC binding domain/IRSp53-MIM homology domain of IRSp53 induces RAC-dependent membrane deformation. *J Biol Chem,* 281**,** 35347-58.

SURGUCHEVA, I., NINKINA, N., BUCHMAN, V. L., GRASING, K. & SURGUCHOV, A. 2005. Protein aggregation in retinal cells and approaches to cell protection. *Cell Mol Neurobiol,* 25**,** 1051-66.

SUZUKI, K., TSUNEKAWA, Y., HERNANDEZ-BENITEZ, R., WU, J., ZHU, J., KIM, E. J., HATANAKA, F., YAMAMOTO, M., ARAOKA, T., LI, Z., KURITA, M., HISHIDA, T., LI, M., AIZAWA, E., GUO, S., CHEN, S., GOEBL, A., SOLIGALLA, R. D., QU, J., JIANG, T., FU, X., JAFARI, M., ESTEBAN, C. R., BERGGREN, W. T., LAJARA, J., NUÑEZ-DELICADO, E., GUILLEN, P., CAMPISTOL, J. M., MATSUZAKI, F., LIU, G. H., MAGISTRETTI, P., ZHANG, K., CALLAWAY, E. M., ZHANG, K. & BELMONTE, J. C. 2016. In vivo genome editing via CRISPR/Cas9 mediated homology-independent targeted integration. *Nature,* 540**,** 144-149.

SZAMIER, R. B. 1981. Ultrastructure of the preretinal membrane in retinitis pigmentosa. *Investigative Ophthalmology and Visual Science,* 21**,** 227-236.

TANACKOVIC, G., RANSIJN, A., THIBAULT, P., ABOU ELELA, S., KLINCK, R., BERSON, E. L., CHABOT, B. & RIVOLTA, C. 2011. PRPF mutations are associated with generalized defects in spliceosome formation and pre-mRNA splicing in patients with retinitis pigmentosa. *Human Molecular Genetics,* 20**,** 2116-2130.

TERAKITA, A. 2005. The opsins. *Genome Biology,* 6**,** 213.

TESTA, F., MAGUIRE, A. M., ROSSI, S., PIERCE, E. A., MELILLO, P., MARSHALL, K., BANFI, S., SURACE, E. M., SUN, J., ACERRA, C., WRIGHT, J. F., WELLMAN, J., HIGH, K. A., AURICCHIO, A., BENNETT, J. & SIMONELLI, F. 2013. Three-year follow-up after unilateral subretinal delivery of adeno-associated virus in patients with Leber congenital Amaurosis type 2. *Ophthalmology,* 120**,** 1283-1291.

TRAVIS, G. H., BRENNAN, M. B., DANIELSON, P. E., KOZAK, C. A. & SUTCLIFFE, J. G. 1989. Identification of a photoreceptor-specific mRNA encoded by the gene responsible for retinal degeneration slow (rds). *Nature,* 338**,** 70-73.

TSANG, S. H., TSUI, I., CHOU, C. L., ZERNANT, J., HAAMER, E., IRANMANESH, R., TOSI, J. & ALLIKMETS, R. 2008. A novel mutation and phenotypes in phosphodiesterase 6 deficiency. *American journal of ophthalmology,* 146**,** 780-788.

TU, H. Y., WATANABE, T., SHIRAI, H., YAMASAKI, S., KINOSHITA, M., MATSUSHITA, K., HASHIGUCHI, T., ONOE, H., MATSUYAMA, T., KUWAHARA, A., KISHINO, A., KIMURA, T., EIRAKU, M., SUZUMA, K., KITAOKA, T., TAKAHASHI, M. & MANDAI, M. 2019. Medium- to long-term survival and functional examination of human iPSC-derived retinas in rat and primate models of retinal degeneration. *EBioMedicine,* 39**,** 562-574.

VAN DER VELDE, K. J., DE BOER, E. N., VAN DIEMEN, C. C., SIKKEMA-RADDATZ, B., ABBOTT, K. M., KNOPPERTS, A., FRANKE, L., SIJMONS, R. H., DE KONING, T. J., WIJMENGA, C., SINKE, R. J. & SWERTZ, M. A. 2017. GAVIN: Gene-Aware Variant INterpretation for medical sequencing. *Genome Biol,* 18**,** 6.

VAUGHAN, D. K. & FISHER, S. K. 1987. The distribution of F-actin in cells isolated from vertebrate retinas. *Experimental Eye Research,* 44**,** 393-406.

VAUGHAN, D. K. & FISHER, S. K. 1989. Cytochalasin D disrupts outer segment disc morphogenesis in situ in rabbit retina. *Investigative Ophthalmology & Visual Science,* 30**,** 339-342.

VÁZQUEZ-DOMÍNGUEZ, I., GARANTO, A. & COLLIN, R. W. 2019. Molecular Therapies for Inherited Retinal Diseases—Current Standing, Opportunities and Challenges. *Genes,* 10**,** 654.

VEITIA, R. A., CABURET, S. & BIRCHLER, J. A. 2018. Mechanisms of Mendelian dominance. *Clin Genet,* 93**,** 419-428.

VELERI, S., LAZAR, C. H., CHANG, B., SIEVING, P. A., BANIN, E. & SWAROOP, A. 2015. Biology and therapy of inherited retinal degenerative disease: insights from mouse models. *Dis Model Mech,* 8**,** 109-29.

VERBAKEL, S. K., VAN HUET, R. A. C., BOON, C. J. F., DEN HOLLANDER, A. I., COLLIN, R. W. J., KLAVER, C. C. W., HOYNG, C. B., ROEPMAN, R. & KLEVERING, B. J. 2018. Non-syndromic retinitis pigmentosa. *Progress in Retinal and Eye Research,* 66**,** 157-186.

VIGNAL, A., MILAN, D., SANCRISTOBAL, M. & EGGEN, A. 2002. A review on SNP and other types of molecular markers and their use in animal genetics. *Genet Sel Evol,* 34**,** 275-305.

VITRAVENE STUDY GROUP 2002. A randomized controlled clinical trial of intravitreous fomivirsen for treatment of newly diagnosed peripheral cytomegalovirus retinitis in patients with AIDS. *Am J Ophthalmol,* 133**,** 467-74.

VOLLAND, S., ESTEVE-RUDD, J., HOO, J., YEE, C. & WILLIAMS, D. S. 2015. A comparison of some organizational characteristics of the mouse central retina and the human macula. *PloS one,* 10**,** e0125631-e0125631.

VON RÜCKMANN, A., FITZKE, F. W. & BIRD, A. C. 1995. Distribution of fundus autofluorescence with a scanning laser ophthalmoscope. *Br J Ophthalmol,* 79**,** 407-12.

WADA, Y., ABE, T., TAKESHITA, T., SATO, H., YANASHIMA, K. & TAMAI, M. 2001. Mutation of human retinal fascin gene (FSCN2) causes autosomal dominant retinitis pigmentosa. *Invest Ophthalmol Vis Sci,* 42**,** 2395-400.

WANG, E. T., SANDBERG, R., LUO, S., KHREBTUKOVA, I., ZHANG, L., MAYR, C., KINGSMORE, S. F., SCHROTH, G. P. & BURGE, C. B. 2008. Alternative isoform regulation in human tissue transcriptomes. *Nature,* 456**,** 470-6.

WANG, F., WANG, H., TUAN, H. F., NGUYEN, D. H., SUN, V., KESER, V., BOWNE, S. J., SULLIVAN, L. S., LUO, H., ZHAO, L., WANG, X., ZANEVELD, J. E., SALVO, J. S., SIDDIQUI, S., MAO, L., WHEATON, D. K., BIRCH, D. G., BRANHAM, K. E., HECKENLIVELY, J. R., WEN, C., FLAGG, K., FERREYRA, H., PEI, J., KHAN, A., REN, H., WANG, K., LOPEZ, I., QAMAR, R., ZENTENO, J. C., AYALA-RAMIREZ, R., BUENTELLO-VOLANTE, B., FU, Q., SIMPSON, D. A., LI, Y., SUI, R., SILVESTRI, G., DAIGER, S. P., KOENEKOOP, R. K., ZHANG, K. & CHEN, R. 2014. Next generation sequencing-based molecular diagnosis of retinitis pigmentosa: identification of a novel genotype-phenotype correlation and clinical refinements. *Hum Genet,* 133**,** 331-45.

WANG, S. T., CHEN, L. L., ZHANG, P., WANG, X. B., SUN, Y., MA, L. X., LIU, Q. & ZHOU, G. M. 2019. Transplantation of Retinal Progenitor Cells from Optic Cup-Like Structures Differentiated from Human Embryonic Stem Cells In Vitro and In Vivo Generation of Retinal Ganglion-Like Cells. *Stem Cells Dev,* 28**,** 258-267.

WANG, Z., GAO, F., ZHANG, M., ZHENG, Y., ZHANG, F., XU, L., CAO, L. & HE, W. 2020. Intravitreal Injection of Human Retinal Progenitor Cells for Treatment of Retinal Degeneration. *Med Sci Monit,* 26**,** e921184.

WEIL, D., BLANCHARD, S., KAPLAN, J., GUILFORD, P., GIBSON, F., WALSH, J., MBURU, P., VARELA, A., LEVILLIERS, J., WESTON, M. D. & ET AL. 1995. Defective myosin VIIA gene responsible for Usher syndrome type 1B. *Nature,* 374**,** 60-1.

WEISZ HUBSHMAN, M., BROEKMAN, S., VAN WIJK, E., CREMERS, F., ABU-DIAB, A., KHATEB, S., TZUR, S., LAGOVSKY, I., SMIRIN-YOSEF, P., SHARON, D., HAER-WIGMAN, L., BANIN, E., BASEL-VANAGAITE, L. & DE VRIEZE, E. 2017. Whole-exome sequencing reveals POC5 as a novel gene associated with autosomal recessive retinitis pigmentosa. *Human Molecular Genetics,* 27**,** 614-624.

WEISZ HUBSHMAN, M., BROEKMAN, S., VAN WIJK, E., CREMERS, F., ABU-DIAB, A., KHATEB, S., TZUR, S., LAGOVSKY, I., SMIRIN-YOSEF, P., SHARON, D., HAER-WIGMAN, L., BANIN, E., BASEL-VANAGAITE, L. & DE VRIEZE, E. 2018. Whole-exome sequencing reveals POC5 as a novel gene associated with autosomal recessive retinitis pigmentosa. *Hum Mol Genet,* 27**,** 614-624.

WELCH, M. D. & MULLINS, R. D. 2002. Cellular Control of Actin Nucleation. *Annual Review of Cell and Developmental Biology,* 18**,** 247-288.

WERDICH, X. Q., PLACE, E. M. & PIERCE, E. A. 2014. Systemic Diseases Associated with Retinal Dystrophies. *Seminars in Ophthalmology,* 29**,** 319-328.

WESTENENG-VAN HAAFTEN, S. C., BOON, C. J. F., CREMERS, F. P. M., HOEFSLOOT, L. H., DEN HOLLANDER, A. I. & HOYNG, C. B. 2012. Clinical and Genetic Characteristics of Late-onset Stargardt's Disease. *Ophthalmology,* 119**,** 1199-1210.

WILLIAMS, D. S., LINBERG, K. A., VAUGHAN, D. K., FARISS, R. N. & FISHER, S. K. 1988. Disruption of microfilament organization and deregulation of disk membrane morphogenesis by cytochalasin D in rod and cone photoreceptors. *J Comp Neurol,* 272**,** 161-76.

WILSON, J. H. & WENSEL, T. G. 2003. The nature of dominant mutations of rhodopsin and implications for gene therapy. *Molecular Neurobiology,* 28**,** 149-158.

WOODINGS, J. A., SHARP, S. J. & MACHESKY, L. M. 2003. MIM-B, a putative metastasis suppressor protein, binds to actin and to protein tyrosine phosphatase delta. *Biochem J,* 371**,** 463-71.

XI, Q., PAUER, G. J. T., MARMORSTEIN, A. D., CRABB, J. W. & HAGSTROM, S. A. 2005. Tubby-like Protein 1 (TULP1) Interacts with F-actin in Photoreceptor Cells. *Investigative Ophthalmology & Visual Science,* 46**,** 4754-4761.

XIE, F., YE, L., TA, M., ZHANG, L. & JIANG, W. G. 2011. MTSS1: a multifunctional protein and its role in cancer invasion and metastasis. *Front Biosci (Schol Ed),* 3**,** 621-31.

XU, M., YANG, L., WANG, F., LI, H., WANG, X., WANG, W., GE, Z., WANG, K., ZHAO, L., LI, H., LI, Y., SUI, R. & CHEN, R. 2015. Mutations in human IFT140 cause non-syndromic retinal degeneration. *Hum Genet,* 134**,** 1069-78.

XUE, K., JOLLY, J. K., BARNARD, A. R., RUDENKO, A., SALVETTI, A. P., PATRÍCIO, M. I., EDWARDS, T. L., GROPPE, M., ORLANS, H. O., TOLMACHOVA, T., BLACK, G. C., WEBSTER, A. R., LOTERY, A. J., HOLDER, G. E., DOWNES, S. M., SEABRA, M. C. & MACLAREN, R. E. 2018. Beneficial effects on vision in patients undergoing retinal gene therapy for choroideremia. *Nature Medicine,* 24**,** 1507-1512.

XUE, K. & MACLAREN, R. E. 2020. Antisense oligonucleotide therapeutics in clinical trials for the treatment of inherited retinal diseases. *Expert Opin Investig Drugs,* 29**,** 1163-1170.

YAMAGATA, M. & SANES, J. R. 2010. Synaptic localization and function of Sidekick recognition molecules require MAGI scaffolding proteins. *Journal of Neuroscience,* 30**,** 3579-3588.

YAMAGISHI, A., MASUDA, M., OHKI, T., ONISHI, H. & MOCHIZUKI, N. 2004. A novel actin bundling/filopodium-forming domain conserved in insulin receptor tyrosine kinase substrate p53 and missing in metastasis protein. *J Biol Chem,* 279**,** 14929-36.

YAN, T., ZHANG, A., SHI, F., CHANG, F., MEI, J., LIU, Y. & ZHU, Y. 2018. Integrin αvβ3–associated DAAM1 is essential for collagen-induced invadopodia extension and cell haptotaxis in breast cancer cells. *Journal of Biological Chemistry,* 293**,** 10172-10185.

YANG, X., CHUNG, J.-Y., RAI, U. & ESUMI, N. 2018. Cadherins in the retinal pigment epithelium (RPE) revisited: P-cadherin is the highly dominant cadherin expressed in human and mouse RPE in vivo. *PloS one,* 13**,** e0191279-e0191279.

YANG, Z., CHEN, Y., LILLO, C., CHIEN, J., YU, Z., MICHAELIDES, M., KLEIN, M., HOWES, K. A., LI, Y., KAMINOH, Y., CHEN, H., ZHAO, C., CHEN, Y., AL-SHEIKH, Y. T., KARAN, G., CORBEIL, D., ESCHER, P., KAMAYA, S., LI, C., JOHNSON, S., FREDERICK, J. M., ZHAO, Y., WANG, C., CAMERON, D. J., HUTTNER, W. B., SCHORDERET, D. F., MUNIER, F. L., MOORE, A. T., BIRCH, D. G., BAEHR, W., HUNT, D. M., WILLIAMS, D. S. & ZHANG, K. 2008. Mutant prominin 1 found in patients with macular degeneration disrupts photoreceptor disk morphogenesis in mice. *The Journal of Clinical Investigation,* 118**,** 2908-2916.

YARAR, D., D'ALESSIO, J. A., JENG, R. L. & WELCH, M. D. 2002. Motility determinants in WASP family proteins. *Molecular biology of the cell,* 13**,** 4045-4059.

YARDLEY, J., LEROY, B. P., HART-HOLDEN, N., LAFAUT, B. A., LOEYS, B., MESSIAEN, L. M., PERVEEN, R., REDDY, M. A., BHATTACHARYA, S. S., TRABOULSI, E., BARALLE, D., DE LAEY, J.-J., PUECH, B., KESTELYN, P., MOORE, A. T., MANSON, F. D. C. & BLACK, G. C. M. 2004. Mutations of VMD2 Splicing Regulators Cause Nanophthalmos and Autosomal Dominant Vitreoretinochoroidopathy (ADVIRC). *Investigative Ophthalmology & Visual Science,* 45**,** 3683-3689.

YATES, A., AKANNI, W., AMODE, M. R., BARRELL, D., BILLIS, K., CARVALHO-SILVA, D., CUMMINS, C., CLAPHAM, P., FITZGERALD, S., GIL, L., GIRÓN, C. G., GORDON, L., HOURLIER, T., HUNT, S. E., JANACEK, S. H., JOHNSON, N., JUETTEMANN, T., KEENAN, S., LAVIDAS, I., MARTIN, F. J., MAUREL, T., MCLAREN, W., MURPHY, D. N., NAG, R., NUHN, M., PARKER, A., PATRICIO, M., PIGNATELLI, M., RAHTZ, M., RIAT, H. S., SHEPPARD, D., TAYLOR, K., THORMANN, A., VULLO, A., WILDER, S. P., ZADISSA, A., BIRNEY, E., HARROW, J., MUFFATO, M., PERRY, E., RUFFIER, M., SPUDICH, G., TREVANION, S. J., CUNNINGHAM, F., AKEN, B. L., ZERBINO, D. R. & FLICEK, P. 2015. Ensembl 2016. *Nucleic Acids Research,* 44**,** D710-D716.

YI, Z., OUYANG, J., SUN, W., LI, S., XIAO, X. & ZHANG, Q. 2020. Comparative exome sequencing reveals novel candidate genes for retinitis pigmentosa. *EBioMedicine,* 56**,** 102792.

YIOTI, G., STEFANIOTOU, M., ZIAVROU, I., KOTSIS, K. & HYPHANTIS, T. 2017. Illness Perceptions, Psychiatric Manifestations, and Quality of Life in Patients with Inherited Retinal Dystrophies. *Seminars in Ophthalmology,* 32**,** 428-437.

YOSHIDA, N., IKEDA, Y., NOTOMI, S., ISHIKAWA, K., MURAKAMI, Y., HISATOMI, T., ENAIDA, H. & ISHIBASHI, T. 2013. Clinical evidence of sustained chronic inflammatory reaction in retinitis pigmentosa. *Ophthalmology,* 120**,** 100-5.

YOUNG, R. W. 1967. The renewal of photoreceptor cell outer segments. *The Journal of cell biology,* 33**,** 61-72.

YU, D., ZHAN, X. H., NIU, S., MIKHAILENKO, I., STRICKLAND, D. K., ZHU, J., CAO, M. & ZHAN, X. 2011. Murine missing in metastasis (MIM) mediates cell polarity and regulates the motility response to growth factors. *PLoS One,* 6**,** e20845.

YU, J., LIN, S., WANG, M., LIANG, L., ZOU, Z., ZHOU, X., WANG, M., CHEN, P. & WANG, Y. 2016. Metastasis suppressor 1 regulates neurite outgrowth in primary neuron cultures. *Neuroscience,* 333**,** 123-31.

ZHANG, J., WANG, C., SHEN, Y., CHEN, N., WANG, L., LIANG, L., GUO, T., YIN, X., MA, Z., ZHANG, B. & YANG, L. 2016. A mutation in ADIPOR1 causes nonsyndromic autosomal dominant retinitis pigmentosa. *Hum Genet,* 135**,** 1375-1387.

ZHANG, J., YAO, Y., HE, H. & SHEN, J. 2020. Clinical Interpretation of Sequence Variants. *Current protocols in human genetics,* 106**,** e98-e98.

ZHANG, K., KNIAZEVA, M., HAN, M., LI, W., YU, Z., YANG, Z., LI, Y., METZKER, M. L., ALLIKMETS, R., ZACK, D. J., KAKUK, L. E., LAGALI, P. S., WONG, P. W., MACDONALD, I. M., SIEVING, P. A., FIGUEROA, D. J., AUSTIN, C. P., GOULD, R. J., AYYAGARI, R. & PETRUKHIN, K. 2001. A 5-bp deletion in ELOVL4 is associated with two related forms of autosomal dominant macular dystrophy. *Nature Genetics,* 27**,** 89-93.

ZHANG, Q., ZULFIQAR, F., XIAO, X., RIAZUDDIN, S. A., AHMAD, Z., CARUSO, R., MACDONALD, I., SIEVING, P., RIAZUDDIN, S. & HEJTMANCIK, J. F. 2007. Severe retinitis pigmentosa mapped to 4p15 and associated with a novel mutation in the PROM1 gene. *Human Genetics,* 122**,** 293-299.

ZHAO, H., PYKÄLÄINEN, A. & LAPPALAINEN, P. 2011. I-BAR domain proteins: linking actin and plasma membrane dynamics. *Current Opinion in Cell Biology,* 23**,** 14-21.

ZHOU, R. & CASPI, R. R. 2010. Ocular immune privilege. *F1000 biology reports,* 2**,** 3.

ZHOU, W., LIU, X., VAN WIJNBERGEN, J. W. M., YUAN, L., LIU, Y., ZHANG, C. & JIA, W. 2020. Identification of PIEZO1 as a potential prognostic marker in gliomas. *Sci Rep,* 10**,** 16121.

ZHOU, Y., LI, S., HUANG, L., YANG, Y., ZHANG, L., YANG, M., LIU, W., RAMASAMY, K., JIANG, Z., SUNDARESAN, P., ZHU, X. & YANG, Z. 2018. A splicing mutation in aryl hydrocarbon receptor associated with retinitis pigmentosa. *Hum Mol Genet,* 27**,** 2563-2572.

ZHU, D., XIE, M., GADEMANN, F., CAO, J., WANG, P., GUO, Y., ZHANG, L., SU, T., ZHANG, J. & CHEN, J. 2020. Protective effects of human iPS-derived retinal pigmented epithelial cells on retinal degenerative disease. *Stem Cell Res Ther,* 11**,** 98.

ZHU, J., CHEN, G., ZHU, S., LI, S., WEN, Z., BIN, L., ZHENG, Y. & SHI, L. 2016. Identification of Tissue-Specific Protein-Coding and Noncoding Transcripts across 14 Human Tissues Using RNA-seq. *Scientific Reports,* 6**,** 28400.

ZHU, J., MING, C., FU, X., DUAN, Y., HOANG, D. A., RUTGARD, J., ZHANG, R., WANG, W., HOU, R., ZHANG, D., ZHANG, E., ZHANG, C., HAO, X., XIONG, W. & ZHANG, K. 2017. Gene and mutation independent therapy via CRISPR-Cas9 mediated cellular reprogramming in rod photoreceptors. *Cell Res,* 27**,** 830-833.

ZHU, Y. Y., MACHLEDER, E. M., CHENCHIK, A., LI, R. & SIEBERT, P. D. 2001. Reverse transcriptase template switching: a SMART approach for full-length cDNA library construction. *Biotechniques,* 30**,** 892-7.

Appendices

Appendix A: List of genes on RP 111 Gene panel (RP and RP-associated genes) used in standard NHS genetic testing

ABCA4	*CLRN1*	*GUCA1B*	*OFD1*	*RD3*	*SPATA7*
ABHD12	*CNGA1*	*GUCY2D*	*OTX2*	*RDH5*	*TOPORS*
ADAM9	*CNGA3*	*IDH3B*	*PDE6A*	*RDH12*	*TRPM1*
AIPL1	*CNGB1*	*IMPDH1*	*PDE6B*	*RGR*	*TSPAN12*
ARL6	*CNGB3*	*IMPG2*	*PDE6C*	*RHO*	*TTC8*
BBS1	*CRB1*	*IQCB1*	*PDE6G*	*RIMS1*	*TTPA*
BEST1	*CRX*	*KCNJ13*	*PDE6H*	*RLBP1*	*TULP1*
C1QTNF5	*CYP4V2*	*KCNV2*	*PITPNM3*	*ROM1*	*UNC119*
C2ORF71	*DHDDS*	*KLHL7*	*POC1B*	*RP1*	*USH2A*
C8ORF37	*EYS*	*LCA5*	*PRCD*	*RP2*	*WDR19*
CA4	*FAM161A*	*LRAT*	*PROM1*	*RP9*	*ZNF513*
CABP4	*FLVCR1*	*LRIT3*	*PRPF3*	*RPE65*	
CACNA1F	*FSCN2*	*LRP5*	*PRPF31*	*RPGR*	
CACNA2D4	*FZD4*	*MAK*	*PRPF6*	*RPGRIP1*	
CAPN5	*GNAT1*	*MERTK*	*PRPF8*	*RPGRIP1L*	
CC2D2A	*GNPTG*	*NDP*	*PRPH2*	*RS1*	
CDHR1	*GPR179*	*NMNAT1*	*RAB28*	*SAG*	
CEP290	*GRK1*	*NR2E3*	*RAX2*	*SEMA4A*	
CERKL	*GRM6*	*NRL*	*RBP3*	*SLC24A1*	
CHM	*GUCA1A*	*NYX*	*RBP4*	*SNRNP200*	

Appendix B: Primers used for segregation analysis

Family 3004 - Primers

GENE SYMBOL	Forward (5' – 3')	Reverse (5' – 3')
ACSL1	GGAGTTCTTAATCTGGGCTG	CACCATATCTTCGAGGATAGC
ADAM33	GCCCCAAGAGTTTCTGATCT	CTTGGTAGTGGCAATGATCC
ADARB1	GTTGCACTCCTTCGTCAGTT	TTTGATAGCCACAGAGCAGC
ANKRD30BL	GTTCTGCTCAGCTGCCTAAA	CTGGTACCTCTTCTTCGCAT
ARPP21	GACCTCCCATTGACTCCTGA	TCTGTGACTATGTGTGTGCC
BFSP2	GTCTCCATAACTGGCAAGGT	TATGTGAGAGGAAGTCTGGG
BPHL	GTCAAGCACCTACCACTGTT	TCTCTTCCGTGGTACCCTAA
C2orf16	GAAGACATCACAGTCCCTCT	CTGTGATGGCTTCTCTCTGA
C4BPA	GATGCTGTGTCCCAAGGTAT	GAGTCACTTGAAACCAGGAG
CCDC103	GACTGAGCAAGTGTCTGACA	TGGAGGCAGAAACCTATCTC
DOK1	GAGGGAGTACAACGGAAGAA	TCTGGCTTCTGCTGGTTCTA
FOXP2	GTTGAGATTGGCTGCTTCCT	TGATGTGCTTAGGGAATCGC
FPR1	GTGTAAGGGACAGTGGTGAG	TGGCAAAGTGGAGGTGAAAC
GTDC1	GTTCTGCTTCTGTGCCTTGA	CAGGCTCTTGAGAAGACATC
HCLS1	GTCCTCCATTGATTCCTCCT	CAGCCTGATGATCCTGCATA
HRC	GATGAAGGAGAAGAGGAGGA	TCCTCATCTTCTTCCTCGTC
KIF16B	GCACACAGAGGACAGATCTT	ATGAAGGCAGAGCACATCTC
KPNA7	GGATGATGGCTAGAGTAGGT	CTCTGACAACACATCGAAGC
LARGE1	GTGGCCTAAGCATCACATCT	TGCCATGAGCCTGACATAGA
M1AP	GGATGGCTCTAATTCCCAGT	ATTCATGCAGGAAGTCCCTC
NACC1	GTACAGCATGATGAACGTCG	GTATCAGCTCCTCCATCTCA
NDUFAF5	GACGTTTCAGAGGCCATAGA	GGAGAGAAAGAGTGCCATGA

OSTC	GCCAACATGGTGAAAACCTG	ATGCCACTCAACATCATTGG
PARPBP	GTTCGGTGGATTGGGTGTAT	ACAATACCCAGCTCAGCTTC
PCDHB10	GGTATGGGCAGAAGATGTAG	TTGTCCGCGTTGATGGAGAC
PCDHB14	GTGCTGCTCTCTGACGTCAA	AGAAGAGGAAGAGCGACGAC
SAXO2	GTCACTGGATAGGACCTTAT	TTTGGATGGGATTGTGGGTC
SCAF11	GGATCAGGCCCAGAGTTTAT	CCAGATCTCATTCTAGGTCC
SEC23IP	GGTCTCGAGCTATCCTTCCA	TACAGCCAAGTTGCTCTCAC
SKIV2L2	GGGCATATGTGTGTGCATGT	TTCACTACCTCAAACCGTGC
SLC22A13	TGAAGGACACCACACAGTCA	AACACAGGAAGCACCAGTGC
SPRR2A	GCTTCTCTCTCTGGAGGATT	GCAGATTACTGGCTAAGGAG
TMEM82	GCCCTCATCAACCAGGACTT	GATCTCCTGCTCATCCTTCA
TUBGCP6	GGAGAATGTGTCAGATGTGG	AGCCACCCTACTCTGACCTA
USF3	GTATGTCCCTGATGAGCAGA	TGCCCTGAACAAGATTCCTC
VENTX	GAATCGAAGGCAATTAGGCG	ACGAAGACACAGCTGAGGAAC

Family 3013 - Primers

GENE SYMBOL	Forward (5' – 3')	Reverse (5' – 3')
BBS9	GCCACTCCTGAAGATTGTTG	AAATTCAGCTGCACCAGTGC
CIT	GTTCTGGGATACATGTGCAG	GATTAGTGGGTAGGTCAGAG
CRYAB	GCATTTGGTCTCACCTAAGG	CTAAAATCCTTGGAGCCCTC
FAT4	GTTAGTGTTGGACCATCAGG	CACTATCTGGGTCAGTTGCT
KIN	GGCAACTGGAACTGGAGAAA	AGAGCAAGACTCCATCTCCA
MYO5B	GTGTTGTGGGCCTTGTCTAA	GAATGTAAGGTCTCCCAGCA
MYO9A	GCATGTTTCCTTCAGTGACT	CTACCCAGTCTAACTAATGC
PABPC4L	GCGCTGGACACAATGAACTT	CACTGGAATCTGTCATCACC
PIEZO1	GATGTTCAACCAGAATGTGG	TTGGCATAGATGTCCTCCAC
REG1B	GGAGGAGGAATTCGGACATT	AGGATCAGAAGGAGTGTAGC
SEC24D	GGGAACCACACTCATACTTG	AGCCTTCCCTCTATGTGATG
SET	GAGACCTCAGGTGAGAGCAG	CTTAGCCATTTCCAAGACCC
SLC22A13	GTTTGTGATCGGAAGCACCT	CCATTACTCCTAGATGCCAC
TRPM4	GTGTTCTGAGGGTGTCGGAA	GATGTGTCCCAGCTGTTTCA
URAD	GGTCCAGGACTTGTTAGAGG	GAATTGAAGCAGTGAGCTGG

Family 3027 - Primers

GENE SYMBOL	Forward primer (5' – 3')	Reverse primer (5' – 3')
CACNA1E	GACTAGAGCAGCCCATCTTG	TCACACACACATCAAGCTGC
CCDC80	GAGATGATCAGAGATGAGGG	CTTCTGCCTGATCTTCTCGA
DNTTIP2	GCAACTAGAAGAACCAGGAG	GTTGGCTTTCATCACTGCTG
DOPEY1	GGACAACTTGAGTTACGAAG	GTCATGAAGAGTGTGTGTGG
FAT1	GTTGCCATCTGTGGAGATTG	GAGCTCTTCATCCCACAAAG
GALNT5	GGTCACTGCATTTATAGCCA	TATTGCATCAGCAGACTCTG
GATA6	GACTTGCTGCTGTTCACTGA	GTCTCATCCGTGGAAAGGAA
HSP90AB1	GCTGGAATTAGGCTTGACAA	AAGCCATGTGAGACTTGACC
HSPA9	GGAACCCAAGTACGAAATGG	GATTCTCACCACCCACAGTT
KHDC1	GGAAGAGATACCGGGATTGT	TGAGCATAAGAGGTGAGAGG
KIF5B	GGAAGAGACAGTGGTAAGAA	GTACCTGTTTGTGCACTTTAG
LPA	GTATGTCCATCTGCCTGCTA	AGCCTGAGACATTCTACCCA
MED16	GACAGAAAGGTACAGACGCT	TGCTGGCACTTTACTGACCA
MTSS1	GATTTGCCAGTCCCAACAGT	GAATGGAGGAAGTCAGGCTA
PIGZ	GTGGGCATAGAGTATGAAGT	CATCTACCCAGACATGCTAC
POLH	GGGAACACTCTGAAGGAGAA	TCAATGTCCCACTGTCCCTA
PRKCDB	GATCAGTGCTGTGTCCGTCA	CTTGTAACTGCCTTCCCACA
HTD2	GTGCTGAAGATGTTCCCACT	CAGGATTTGGAAGCTTCTGG
SENP1	GCTAGGCCTGAGTGTCTATT	CACTACCCTCTGTGTGTTCT
TRAF3IP1	GGTGAATTCCAAGTCGCACA	AGACCACCACAAACTCTTGC
TRMT1	GGGATATCAGCTTACCGAGG	GTGATCACAGCACATCTGGT
ZNF451	GATGGATGAGGTAGAAGGTG	CACGGCAACCACAAGTTAAC

Family 3032

GENE SYMBOL	Forward primer (5’ – 3’)	Reverse primer (5’ – 3’)
CD4	GGGTGCAGGTTGTTAAGTCA	CACAACCCACCTCACTTCAT
MYH11	GACATCAGGAGTTGGAGACA	AAGGACAGTGGGTCAAGAGA
PABPN1	GCGTGTTGATTGACAGGCAG	AACAACACTAGGCAACCGTG
TMEM245	GAGGAGAACCTAGGTACGTT	CATTCACACAGTCAGCCTCT
CCAR1	GTCTGAGTCATTGCAGGAAG	AGTTGAGATTGTGCCACTGC
DNMBP	GGAAAGTTCTGTCTGTTCTG	TGTACAGACACAGGTCCTAC
ENAM	GAAGATCCTCCTAAAGCAGA	GGACTGGCATATAACCCTCA
EPB41L3	GCATTTGCTAACTCAGTGGT	CCCAGCTCTCAATATCTAGG
FOXK1	GATGCGTGATGTCTCGGAAA	TGCTGTGAGGTTACGATGGA
FRMD3	GAACTTATGGTACAGGGTCT	TGAGCAACCCAGCATGTAGA
GALNT9	GGTGTGTGGCATGTGTGTAA	CTCCACTGAGAACAAGCGTA
OR1E2	GACAGAGCATGATGGGACAA	GCAGAGCAGACATATCACAG
PLCE1	GTGGGACGAATGGGTGATTA	CATAGCTACTGCTTCCTGGA
SERPINA10	GGAACGAGAAGACGAGAAGT	TGAATGAATCAGCCAGGCAC
SPON2	GATGAATGCACACGTTGGTG	CAATCTCCTGGAGCAGCAAT
TLL2	GTTTGTGGGCTGGAGATGAA	TGTCCGGGCACAATTCACTA

Appendix C: Primers used for gene expression and 5' RACE

1. **Primers for gene expression**

GENE	Primer ID	Forward 5' – 3')	Reverse (5' – 3')
KPNA7	Exon 1_5	GTACCGAGGCAAAGATGTGT	TGGGTGAAATCAAGGCTAGG
	Exon 2_6	GGCCAAGAAAGATGAACAGA	GGCACAGATTCGACAAGGTC
	Exon 8_10	GAGCCACTGGTGAATCTGCT	TGGTCTATGACTTGGCTCAG
PARPBP	Exon 2_6	GGCGTGCTCTTTGTAACTCT	TGGTGGTGCATATCCTTTCC
	Start_Stop	ATGGCTGTGTTTAATCAGAAG	TTATAGTCTAAAAAACTGAGTT
MYO5B	Exon37_39	GAGCATTCAGGGTCTATCTG	AATAGCAGTTGCTGAGGGTC
PIEZO1	Exon40_45	GAAGAGGGGGAGGAAGAGAA	AGATGATGGCGATGAGGAAG
MTSS1	Start_Stop	ATGGAGGCTGTGATTGAGAAGG	CTAAGAAAAGCGAGGGGCTGAG
	Exon 2_8	GAGCTATCCAGTTTGGGAAG	ATCGGCCACGTTCTTCAATC
	Exon 6_8	AAGAAGTCCTCGGATACGCT	ATCGGCCACGTTCTTCAATC
	Exon 11_Intron 11	GAACAGTGTCAACAGCAGTG	CACTTATAGCACCTCTCCCT
	Exon 11_13	GAACAGTGTCAACAGCAGTG	TCCGGTTCTCGCTTCTCTTT
	Exon4start_Stop	ATGTGCATGAGGCACAGAAG	CTAAGAAAAGCGAGGGGCTGAG
m*Mtss1*	Exon 2_6	GAGCTATCCAGTTTGGGAAG	TTGCCTTCTTCTGCAGCTTC
	Exon 8_11	GGTTCTGCACCTTCATCTCT	AGCTAGGGATCTGAGATGAC
	Intron 3_Exon4	CACTTGTTCCTTGTCCTGGA	CTGGAGAACTGCCTCAGCTT

2. Primers for Mtss1 5' RACE experiments and sequencing of 5' RACE products

1. m*Mtss1*_ GSP1_2R: 5' – GATTACGCCAAGCTTGCTGGGACTGTAGCTTTCCGGCTTT – 3'
2. m*Mtss1*_ GSP1_5R: 5' – GATTACGCCAAGCTTTGCGTGGTCCTTGTCCAGCTGGTTG – 3'
3. m*Mtss1* NGSP1_A1R: 5' – GATTACGCCAAGCTTTGTTTACACAGCCCATCACTCCCTC – 3'
4. M13_Forward: 5' – TGTAAAACGACGGCCAGT – 3'

5. M13_Reverse: 5’ – CAGGAAACAGCTATGACC – 3’

Appendix D: Summary of levels of expression of key candidate genes in the various retinal cell types as reported by scRNA-seq on the adult human retina

(Data extracted from Lukowski et al., 2019)

	Rods	**Cones**	**Bipolar**	**RGC**
MTSS1	1.0914	0.5105	0.6034	1.0279
PARPBP	0.0503	0.0026	0.0211	0.0462
MYO5B	1.0295	0.1505	0.2061	0.0073
PIEZO1	0.1206	0.0786	0.0076	0.0438
DNMBP	0.8040	0.2020	0.1626	0.0374
EPB41L3	0.2948	0.6961	2.4636	1.2668
PLCE1	0.8436	0.1301	0.3360	0.2043

Appendix E: List of antibodies used for immunohistochemistry and western immunoblot

Antibody	Host	Source/Product number	Concentration	
			IHC	WB
βactin	mouse	Thermo Fisher, AM4302 (clone AC-15)	n/a	1:20000
Brn3a	Goat	Santa Cruz, sc-31985	1:1000	n/a
CTTN	Mouse	Santa Cruz, sc-55579	n/a	n/a
DAAM1	Mouse	Santa Cruz, sc-100942	n/a	1:400
DAPI	n/a	Sigma, D9542	1:2000	n/a
GFP	Mouse	Sigma, G6539	n/a	1:1000
GAPDH	Mouse	Abcam, ab8245	n/a	1:10000
MTSS1 (N-terminal)	Rabbit	Novus Biologicals, NBP2-24717	1:100	1:1000
MTSS1 (C-terminal)	Rabbit	Novus Biologicals, NBP2-24716	1:100	1:1000
MTSS1-P549	Rabbit	Cell Signalling, 4385	N/A	1:1000
PARPBP	Rabbit	Novus Biologicals, NBP1-93969	1:200	n/a
Peanut Agglutinin (PNA) FITC	n/a	Sigma, L7381	1:100	n/a
Phalloidin-TRITC	n/a	Sigma, P1951	1:200	n/a
PKCα	Mouse	Abcam, ab11723	1:250	n/a

Rhodopsin (1D4)	Mouse	Gift, Mike Cheetham	1:1000	n/a
Synaptophysin	Mouse	Novus Biologicals, NBP1-47483	1:200	n/a
AlexaFluor 488-conjugated anti-Goat IgG	Donkey	Invitrogen, A11055	1:400	n/a
AlexaFluor 488-conjugated anti-mouse IgG	Donkey	Invitrogen, A21202	1:400	n/a
AlexaFluor 488-conjugated anti-rabbit IgG	Donkey	Invitrogen, A21206	1:400	n/a
AlexaFluor 568-conjugated anti-rabbit IgG	Donkey	Invitrogen, A10042	1:400	n/a
AlexaFluor 647-conjugated anti-mouse IgG	Donkey	Invitrogen, A31571	1:400	n/a
AlexaFluor 568-conjugated anti-rabbit IgG	Goat	Invitrogen, A11011	1:400	n/a
AlexaFluor 647-conjugated anti-mouse IgG	Goat	Invitrogen, A21235	1:400	n/a
HRP-conjugated anti-mouse IgG	Donkey	Abcam, ab98799	n/a	1:10000
HRP-conjugated anti-rabbit IgG	Donkey	Abcam, ab16284	n/a	1:3000

Appendix F: Antibody validation information

Antibody	Application/validation information	References
MTSS1 (NBP2-24716)	Band of expected size detected by WB on human, moue and rat testis lysates but absent in sample treated with immunizing peptide. Validated in peer-reviewed publication for WB and IHC.	Product supplier's website: https://www.novusbio.com/NBP2-24716 PMID:29972794
MTSS1 (NBP2-24716)	Band of expected size detected by WB on human, moue and rat testis lysates but absent in pre-immune serum. *Not validated in peer-reviewed publications.*	Product supplier's website: https://www.novusbio.com/NBP2-24717
MTSS1 (P549)	Validated by peer-reviewed publications for WB.	PMID: 32373113 / PMID: 30250603 / PMID: 23383207
PARPBP (NBP1-93969)	Validated for IHC/ICC/IF. Antibody verified on a Protein Array containing target protein plus 383 other non-specific proteins. *Not validated in peer-reviewed publications.*	Product supplier's website: https://www.fishersci.com/shop/products/anti-c12orf48-polyclonal-novus-biologicals/NBP193969
DAAM1 (sc-100942)	Validated in peer-reviewed publications for WB and IF.	PMID: 31114334 / PMID: 30150563

Appendix G: IRD patients with variants in *MTSS1* from Genomics England rare disease programme database

Variant	Change	gnomAD	CADD	Phenotype	Penetrance	Segregation
8-124568433-C-A	p.Leu188Phe	0	24	Rod-cone dystrophy	complete	Dominant
8-124553428-A-G	p.Ile611Thr	6.58E-06	24.5	Rod-cone dystrophy	complete	Dominant
8-124568422-C-T	p.Arg192His	0	27.8	Rod-cone dystrophy	complete	Dominant
8-124727876-C-T	(ENST00000518547.6):c.72+8G>A	0	17.53	Rod-cone dystrophy	complete	Dominant
8-124558750-G-A	p.Ser372Leu	6.57E-06	22.4	Inherited Macular dystrophy	complete	Dominant
8-124556380-T-C	p.Asp419Gly	0	32	Inherited Macular dystrophy	complete	Dominant
8-124555864-G-A	p.Ala482Val	0	20.9	Developmental macular and foveal dystrophy	complete	Dominant